Evaluation of an Oxygen Injection Technology for In-Situ Hydrocarbon Bioremediation in a Fractured Bedrock Environment

by

Karen D. Greer

A thesis
presented to the University of Waterloo
in fulfillment of the
thesis requirement for the degree of

Master of Science
in
Earth Sciences

Waterloo, Ontario, Canada, 2009

Authors Declaration

I hereby declare that I am the sole author of this thesis. This is a true copy of the thesis, including any required final revisions, as accepted by my examiners.

I understand that my thesis may be made electronically available to the public.

Abstract

Oxygen has been shown to be an effective addition of enhancing the bioremediation of petroleum hydrocarbon contamination in porous media; however, the ability to effectively deliver oxygen to petroleum hydrocarbon contaminated groundwater has proven difficult.

A field and numerical modelling study was completed at a former gas station in southern Ontario, to assess the delivery of oxygen into groundwater in a fractured limestone aquifer that had been contaminated with petroleum hydrocarbons.

A field investigation was completed to characterize the bedrock aquifer and the groundwater flow system. Several hydraulically active fracture zones were identified and characterized.

To evaluate how dissolved oxygen would behave in this type of groundwater environment, an injection test was completed using iTi's gPro® oxygen injection technology. About 1000 L of water containing dissolved oxygen at ~ 30 mg/L and a bromide tracer was injected over ~ 90 minutes and monitored for ~ 10 days in the injection well and in a multilevel monitoring well located 3 metres down-gradient. The oxygen concentration rose rapidly within the injection well and at two of the down-gradient monitor intervals which were aligned with the injection well via major fractures. Concentration tailing persisted in the injection well for several days following injection. The effects of biodegradation were not assessed as part of this investigation.

A three-dimensional numerical model for groundwater flow and advective-dispersive transport within a discretely-fractured porous medium was calibrated to the field conditions. The simulated injection test demonstrated that oxygen rapidly filled the porous matrix surrounding the injection well and filled the local intersecting fractures.

Following injection, the oxygenated groundwater in the local fractures was rapidly flushed by the natural groundwater flow, with oxygen arrivals appearing as sharp pulses in the fracture-associated breakthrough curves in the monitor well. Back diffusion of oxygen from the porous matrix into the injection well was accurately reproduced by the model.

Media properties (fracture apertures, hydraulic gradient and hydraulic conductivity) were varied to assess the sensitivity of the model and to evaluate the effectiveness of the remediation technology under different conditions. The sensitivity runs demonstrated that the distribution of oxygen within the system could be significantly different with varying degrees of advective transport within the fractures and diffusion into the rock matrix which depends on the physical properties and hydrogeological conditions.

Predictive simulations were then run with two different injection scenarios: a continuous injection for 1 week and a cyclic injection scenario (injection every 2 days). The same mass of oxygen was delivered in each simulation (~3 kg). The results demonstrated that the delivery of oxygen into the system (continuous or cyclic) could affect the advective transport of oxygen through the fractures and the diffusion of oxygen into the matrix. The continuous injection resulted in a maximum zone of influence (down-gradient and in the transverse direction) while maintaining high levels of oxygen within the matrix. On the other hand the cycle injection provided a more continuous supply of oxygen over time to the system. The zone of influence was reduced but diffusion into the matrix along the fractures increased, creating a more uniform zone of increased oxygen concentrations around the injection well and along the fractures.

This study demonstrated that oxygen could effectively be delivered to a fractured bedrock system at levels potentially sufficient to enhance aerobic biodegradation. Additional areas requiring investigation include the behavior of oxygen during hydrocarbon biodegradation through field and modelling studies. Full scale implementation of the technology should then be considered to provide additional information with respect to the applicability of the technology to real world environments.

Acknowledgements

I would like to start by thanking my supervisor Dr. Jim Barker and my committee members Dr. John Molson, Dr. Neil Thomson and Ron Donaldson for their guidance and support throughout this process and for the patience while I completed my degree part time.

Thank you to the partners in this thesis inVentures Technologies Inc. (iTi), Aaron Archibald, John Archibald and Jim Begley for giving me the opportunity to use their technology and to Mac's Milk Convenience Stores for providing me with the field site to complete the thesis.

To all the staff and students at the University including Bob Ingleton, Marianne vanderGriendt, Shirley Chatten, Juliana Freitas, Pete Pehme, Claudia Nass and Sue Fisher that helped me in the field, lab and office staged of my thesis.

Thank you to WESA for allowing me to complete my degree while working for them full time, and to Ron Donaldson, Ian Macdonald and all the staff at WESA for your support understanding and encouragement throughout this process.

I wish to thank all my friends and family for all their encouragement and support and a very special thank you to my parents Ron and Judy Greer and my husband David Schaub, I could not have done this without them.

Finally, I would like to dedicate this thesis in memory of Shannon Wagner. We were each other's support and motivation throughout this process and I will carry this degree in memory of her forever.

Table of Contents

List of Figures viii
List of Tables x
1.0 Introduction 1
1.1 Petroleum Hydrocarbon Contamination and Remediation 1
1.1.1 Flow and Transport within Fracture Networks 3
1.1.2 Modelling Approaches for Fractured Media 5
1.2 Remediation Technology Selection and Design 6
1.2.1 The Selected Remediation Technology 7
1.3 Thesis Objectives 8
2.0 Site Background 10
2.1 Location and Description 10
2.2 Regional Geology and Hydrogeology 11
3.0 Methods 14
3.1 Initial Investigation 14
3.1.1 Bedrock Characterization 14
3.1.2 Hydraulic Testing 16
3.1.3 Multi Level Well Installation 19
3.1.4 Digital Borehole Imaging 22
3.1.5 Fracture Calculations 23
3.1.6 Tracer Testing 24
3.1.7 Cross Borehole Testing 24
3.2 Injection Testing 25
3.3 Modelling Approach 26
4.0 Field Results and Interpretation 30
4.1 Site Characterization 30
4.1.1 Hydraulic Testing 30
4.1.2 Groundwater Flow and Contaminant Distribution 31
4.1.3 Digital Borehole Imaging 34
4.1.4 Fracture Calculations 36
4.1.5 Tracer Testing 38
4.1.6 Cross Borehole Testing 39
4.2 Summary and Site Conceptual Model 42
4.3 gPro® Technology 43
4.4 Injection Test 45
4.4.1 Dissolved Oxygen Distribution 45
4.4.2 Tracer Distribution and Comparison 50
4.4.3 Summary 56
4.4.4 Hydrocarbon Concentrations and Distribution 57
4.4.5 Iron Concentrations and Distribution 57

5.0 Numerical Modelling 58
5.1 Introduction 58
5.2 Model Development 60
5.3 Base Case (Field-data) 67
5.4 Base Case (Best-Fit) Simulation 70
5.4.1 Flow Simulation 70
5.4.2 Transport Simulation 73
5.4.3 Thermal Simulation 81
5.5. Sensitivity Analysis 83
5.5.1 Random Fracture Network 89
6.1 Effectiveness of Oxygen Injection 95
6.2 Predictive Simulations 96
6.2.1 Simulation 1 – Continuous Injection 96
6.2.2 Simulation 2 – Cycle Injection 99
6.2.3 Simulation Summary 102
7.0 Summary and Conclusions 103
8.0 Recommendations 105
References 106
Appendices
Appendix A 112
Appendix B 116
Appendix C 143
Appendix D 148
Appendix E 151
Appendix F 154
Appendix G 158
Appendix H 185

List of Figures

Figure 2-1 – Site map with PHC (F1 + F2) groundwater plume delineated and study area defined. 13
Figure 3-1- Location of injection well TW2 and down-gradient monitoring well TW1.. 15
Figure 3-2 - Borehole logs for TW1 and TW2. 18
Figure 3-3 - Instrumentation of TW1 (monitor well) and TW2 (injection well). 20
Figure 3-4 - Configuration of the quadrilateral elements representing the porous matrix in the numerical model; concentrations are computed at each of the nodes (Molson & Frind, 2009). 27
Figure 3-5 - Geometric arrangement showing how 2D fractures are overlain onto the porous matrix (Molson and Frind, 2009). 28
Figure 4-1 - Borehole images showing a) porous matrix in Zone 1 b) highly fractured rock in Zone 1, c) and d) discrete fractures in Zone 2a. 35
Figure 4-2 - Site conceptual model showing injection well (TW2), the 7 monitoring points within the monitor well TW1, and the major fractures identified from the borehole logs and video. 37
Figure 4-3 - SF_6 tracer test breakthrough curves. 39
Figure 4-4 - Cross borehole test results of hydraulic head versus time showing response at: a) TW1-1 to TW1-4, and b) TW1-6 and TW1-7. 41
Figure 4-5 - gPro® unit photos. 44
Figure 4-6 - Oxygen concentrations at the injection well TW2. 46
Figure 4-7 - Breakthrough curves for oxygen at the down-gradient monitor points at: a) TW1-1, b) TW1-2, 3, 4, c) TW1-6, and d) TW1-7. Note different concentration scale for plot b). 50
Figure 4-8 - Normalized concentration (C/Co) breakthrough plots for oxygen and bromide in the injection well, TW2. 52
Figure 4-9 - Normalized concentration (C/Co) breakthrough plots for oxygen and bromide in a) TW1-1, b) TW1-2, c) TW1-3, d) TW1-4, e) TW1-6 and f) TW1-7. 55
Figure 5-1 - Site location map with PHC (F1 + F2) groundwater plume delineated and model area defined. 62
Figure 5-2 - Location of injection well TW2, down-gradient monitoring well TW1 and model domain. 63
Figure 5-3 - Perspective plot showing the 3D model grid. The system is assumed symmetric about the y = 0 face. 63
Figure 5-4 - Model layout and input parameters showing a) grid and flow boundary conditions and b) transport domain with monitoring points and fracture apertures identified. Fracture numbers are shown at left. 64
Figure 5-5 - Pressure curve comparison between observed and model-input injection pressures. 65
Figure 5-6 - Graphic showing layout of additional model monitoring points within the matrix (between fractures 2 and 3) and along fracture 2. 67
Figure 5-7 - Field case (un-calibrated) oxygen breakthrough curves a) observed and b) simulated. 68

Figure 5-8 - Hydraulic head distribution a) during injection (end of second injection period) and b) steady state following injection. 71
Figure 5-9 - Velocity vectors during injection within the matrix and the fractures. 72
Figure 5-10 - Radial velocity vectors along fracture 2 in the horizontal (xy) plane..... 73
Figure 5-11 - Calibrated base case oxygen breakthrough curves a) observed and b) simulated. 74
Figure 5-12 - Base Case oxygen breakthrough curves a) Simulated results at field observation points, b) matrix monitoring points and c) fracture monitoring points (see Figure 5-4 for monitor point locations). 76
Figure 5-13 - Base case simulated oxygen distribution after 0.077, 0.5, 1.0 and 5.0 days a) plan view (xz), b) concentration profiles at AA' and BB' and c) transverse distribution (yz) at AA' and BB'..... 79
Figure 5-14 - Base case simulated oxygen distribution at 10, 50, 125 and 200 days showing a) vertical section (xz plane), b) concentration profiles at AA' and BB' and c) transverse distribution (yz) at AA' and BB'. 80
Figure 5-15 - Observed and simulated temperature evolution in the injection well, showing simulated results for thermal conductivities of λ=2, 3.8 and 5 $Jm^{-1}s^{-1}{}^{\circ}C^{-1}$. 83
Figure 5-16 – Simulated oxygen distribution under homogeneous, non-fractured conditions (Scenario 1) after a) 0.077 days and b) 5.0 days..... 87
Figure 5-17 – Simulated oxygen distribution with 10 × higher diffusion coefficient (Scenario 2a) after a) 0.077 days and b) 5.0 days. 87
Figure 5-18 – Simulated oxygen distribution with 2 × larger fracture apertures (Scenario 3a) after a) 0.077 days and b) 5.0 days..... 88
Figure 5-19– Simulated oxygen distribution with low hydraulic conductivity of 1.0×10^{-8} m/s (Scenario 5) after a) 0.077 days and b) 5.0 days. 88
Figure 5-20 - Random fracture network, mean aperture of 100 μm..... 90
Figure 5- 21 - Simulated oxygen distribution assuming the base case conditions overlain by a random fracture network (Scenario 7) with: a) mean aperture 50 μm and b) mean aperture 100 μm..... 91
Figure 5-22 – Simulated oxygen distribution with low hydraulic conductivity and random fracture network (Scenario 7c) (mean aperture 100 μm) a) after 0.077 days and b) after 5.0 days. 93
Figure 6-1 – Continuous 7-day injection simulation showing oxygen distribution at 7, 50, 125 and 200 days in the a) vertical (xz) and b) transverse (yz) sections at vertical profile locations AA' and BB'. 98
Figure 6-2 – Cycle injection showing oxygen distribution at 10, 50, 126 and 200 days in the a) vertical (xz), and b) transverse (yz) sections at AA' and BB' (plot times correspond to the end of each injection cycle). 101

List of Tables

Table 4-1 - Hydraulic Testing Results..... 30
Table 4-2 - Groundwater Elevations 32
Table 5-1 - Base-case model input variables for the oxygen injection test. 66
Table 5-2 - Field and Model Variable Comparison (see Figure 5-4 for fracture positions). 72
Table 5-3 - Outline of sensitivity analyses performed with the model..... 84
Table 5-4 - Random fracture network statistics..... 89

1.0 Introduction

1.1 Petroleum Hydrocarbon Contamination and Remediation

Petroleum hydrocarbons are a major source of groundwater contamination across North America and around the world. The management and remediation of these types of contaminants is a widespread challenge. The rising costs and limitations of conventional methods for plume management and remediation have led to the development of a variety of in-situ remediation methods.

It is well known that the biodegradation of petroleum hydrocarbons, namely the BTEX compounds (benzene, toluene, ethylbenzene and xylenes), is most effective under aerobic groundwater conditions and is limited or less rapid under anoxic groundwater conditions (Landmeyer et al., 2003, Hutchins et al., 1991 and Lovley et al., 1988). Groundwater is described as being anoxic when dissolved oxygen (DO) concentrations are less than 0.3 mg O_2/L, dysoxic from 0.3 - 3.0 mg O_2/L and aerobic for concentrations greater than 3.0 mg O_2/L (Malard et al., 1999).

Oxygen addition has also been shown to be an effective approach to enhance the bioremediation of petroleum hydrocarbon groundwater contamination (Landmeyer et al., 2003, Johnston et al., 1998, Arnon et al., 2005). Studies completed by Chiang et al. (1989) concluded that a minimum 2 mg O_2/L was required for rapid biodegradation of BTX compounds. The study also noted that approximately 3 mg/L of DO was required to degrade 1 mg/L of hydrocarbons, depending on the compounds, based on a stoichiometric balanced equation (e.g., $C_6H_6 + 7.5O_2 \rightarrow 6CO_2 + 3\ H_2O$).

Numerous remedial strategies have been developed for use at petroleum hydrocarbon contaminated sites that work by removing the oxygen limiting factors to encourage efficient in-situ biodegradation. These remedial strategies have included the injection of oxygen using various methods and engineered technologies.

With the addition of oxygen to the system, other factors may limit bioremediation. The most common limiting factors are related to site conditions such as heterogeneities (especially low permeability layers), non-hydrocarbon oxygen demands, microbiological properties and the delivery of oxygen to localized contamination zones (Landmeyer et al., 2003).

Total oxygen demand has been shown to be a major factor with respect to the remediation efficiency of oxygen injection systems (Landmeyer et al., 2003, Chapman et al., 1998). In many cases, when oxygen was injected using a given technology, the injected water could be traced down-gradient, but the dissolved oxygen became undetectable. The lack of measurable dissolved oxygen down-gradient was attributed to the utilization of the oxygen along the flow path. Oxygen demands may be attributed to petroleum hydrocarbon contamination, non-BTEX organic contaminants, natural organic matter and reduced inorganic species (iron, manganese etc.) (Chapman et al., 1998).

It has also been shown that groundwater has very little oxygen reduction capacity compared to aquifer solids. An aquifer's natural oxygen demand creates challenges for in-situ treatment of contamination by chemical and/or microbial methods (Barcelona et al., 1991). Barcelona et al. (1991) showed it is difficult to overcome the reduction capacity of aquifer solids, therefore making the addition of oxygen to remediate aquifers difficult. Another issue relates to the “lag time” for the specific microorganisms required for bioremediation to acclimatize to oxygen-enhanced groundwater (Landmeyer et al., 2003).

The basis for the theory that oxygen addition will potentially enhance the bioremediation of certain groundwater contaminants is the presence of an indigenous microbial population capable of biodegrading the desired contaminant. If the microbial population is not present, or cannot be stimulated, then the concept of oxygen addition is not suitable for the application.

The stimulation of the indigenous microbial population (bacteria) and the changes to the environment detailed above are all dependent on the injected oxygen reaching the desired treatment area, and to ultimately reach the microorganisms and contaminants.

Several studies have been conducted looking at the effects of the physical properties of a system on the transport of oxygen. Landmeyer et al. (2003) showed that oxygen transport is enhanced in sediments with greater permeability and that delivery into less permeable units may be difficult. This is especially true of complex hydrological systems such as fractured bedrock environments. Arnon et al. (2005), for example, looked at the effects of oxygen addition in fractured bedrock environments and found that an increased groundwater flow rate (in factures) reduced biodegradation due to less contact time between the substrate and the microorganisms within the fractures.

Research into the injection of oxygen and its subsequent distribution within discrete fractures zones was not reported in the peer-reviewed literature; these issues therefore form the focus of this investigation. This study is the first to look in detail at the high-pressure injection of oxygenated water into fractured rock for the purpose of enhancing the aerobic biodegradation of petroleum hydrocarbons. This study is also the first found to use a discrete fracture model to simulate the behavior of oxygenated water in a fractured bedrock aquifer.

1.1.1 Flow and Transport within Fracture Networks

Due to the complex nature of fractured bedrock, the principles for flow and transport which are generally applied for porous media are not directly transferable to fractured media. To fully characterize and understand the distribution of a solute such as dissolved petroleum hydrocarbons within fractured rock, a detailed understanding is required of the contaminant, the rock characteristics and groundwater flow within the formation. Each of these factors has a direct influence on the effectiveness of contaminant remediation.

The key processes controlling solute transport in fractured rock include advection, dispersion, absorption, chemical reactions (including water-rock interaction), channeling and matrix diffusion (Kim et al., 2002); however the dominant solute transport mechanism is usually by advection though conductive fractures.

As a solute front travels through a fracture, a strong concentration gradient develops between the open fractures and the initially uncontaminated rock matrix. This gradient then drives diffusion of the solute into the rock matrix (Lipson et al., 2005 and Jardine et al., 1999). Matrix diffusion has been shown to be a significant process that controls contaminant transport in fractured bedrock and its importance increases as the residence time of the solute increases (Jardine et al., 1999). Studies have shown that even on small scales (tens of metres), matrix diffusion can be a dominant process in such environments even with a matrix porosity of less than 5% (Lapcevic et al., 1999 and Parker et al., 1994). Matrix porosity has been shown to be a factor that controls the rate of diffusion across the fracture walls, with higher porosity allowing for greater diffusion and vice versa. This is particularly true at slower groundwater velocities since with higher groundwater velocities there is less time available for the solute to be transferred (Jardine et al., 1999).

The forward diffusion of the solute into the matrix will continue until the solute storage capacity of the matrix has been reached or where the solute concentrations in the fracture are equal to those in the matrix (Lipson et al., 2005). This forward diffusion ceases when the solute source is removed from the fractures, reversing the concentration gradients which causes the solute to back-diffuse out of the matrix and into the groundwater in the fractures (Lipson et al., 2005). During tracer tests in fracture rock, the effects of matrix back-diffusion can often be seen as late-time tailing in breakthrough curves (Lapcevic et al., 1999). In cases of high matrix permeability, solute transport through the matrix has also been shown to occur by advection and dispersion processes (Grisak et al., 1980).

Over long time periods, solute diffusion may result in most of the solute being stored within the matrix and not in the fractures. The time required to remediate the aqueous phase contamination in fractured rock will therefore be determined based on the rate at which the contaminants can back-diffuse from the rock matrix (Lipson et al., 2005). This process also results in the rate of dissolved plume migration being significantly less than the rate of groundwater flow. Remediation efforts, such as enhanced in-situ biodegradation are therefore limited by the ability to effectively deliver the remediation agent to the entire system (fractures and matrix).

The characterization of the bedrock system therefore becomes a key factor when understanding the behavior of dissolved solutes and in designing effective site remediation strategies.

1.1.2 Modelling Approaches for Fractured Media

An additional challenge when characterizing fractured rock arises with respect to modelling the groundwater system and determining if the rock can be treated as an equivalent porous medium (EPM) or if a discrete fracture network (DFN) model is required. Past studies have shown that EPM models are applicable when the fracture network is dense and highly interconnected with negligible effects from the rock matrix or when the fracture network and the rock matrix allows for sufficient interaction to establish a local equilibrium (Berkowitz et al., 2002). In a situation where the rock matrix is an active part of the flow system and transport occurs both in the rock matrix and in the discrete fractures, the system can be defined as a dual-permeability model (Berkowitz et al., 2002). DFN models can allow for the fluid flow and solute transport within a discrete fracture to be accounted for explicitly (Berkowitz et al., 2002) with negligible advective transport within the matrix or incorporated on the level desired.

Analytical models (e.g. CRAFLUSH; Sudicky and Frind, 1982) were first developed to assess groundwater flow and solute transport in discrete fractures (Grisak et al. 1981, Tsang et al. 1981 and Sudicky and Frind, 1982). Multiple fractures were modelled as parallel plates with constant apertures with some solutions accounting for matrix diffusion. Flow and transport within each fracture was limited to one dimension. However, the parallel plate model is limited in representing flow within a complex DFN (Tsang, 1984) and therefore more sophisticated numerical models were subsequently developed for modelling two and three-dimensional flow and heat or solute transport in fractured media (e.g. Tsang et al. 1991, Molson and Frind, 1994, Therrien et al. 1996, Yang et al. 1996). Berkowitz et al. 2002) provides a more complete review of different modelling approaches.

These types of numerical DFN models have been applied in a variety of settings to model multi-dimensional flow and transport of heat, as well as various contaminants (e.g. Odling et al. 1997, MacQuarrie and Mayer, 2005, Gwo et al. 2005, Mundel et al. 2007, and Molson et al. 2007) and to help in the design of remedial measures (Eckert et al. 2002). To date, DFN models have not been applied to a detailed high concentration oxygen injection case, which will be the focus of this study.

1.2 Remediation Technology Selection and Design

The delivery of oxygen into the subsurface has been investigated through several different technologies including Oxygen Release Compounds (Landmeyer et al., 2001 and 2003, Schafer et al., 2006), diffusive oxygen release (Wilson et al., 2002, Azadpour-Keeley et al., 2006, Salanitro et al., 2000), air sparging (Johnston et al., 1998, Bass et al., 1997) and iSoc® (Mulica et al., 2004).

inVentures Technologies Inc. (iTi) has several different technologies under development for the in-situ remediation of hydrocarbon contamination including the iSoc® technology, the Low Pressure Gas Infusion (gPro® LP) and High Pressure Gas Infusion (gPro® HP) technologies. Configurations of the gPro® unit include systems for in-situ and ex-situ generation of oxygen and delivery, as well as in-situ and ex-situ water supplies. iTi's gPro® HP (gPro®) was selected to be evaluated for use in this thesis.

The gPro® technology has been developed to accommodate variable site-specific criteria, including site location (access to power and water supply), site conditions (geology, hydrogeology, type of contaminant, groundwater chemistry), as well as the volume of water available and the treatment objectives.

For this study, site conditions were a major factor in the selection of the gPro® technology. The fractured bedrock geology and hydrogeology was first assessed to determine if treated (oxygenated) water could be rapidly injected at high rates and pressures so treatment could occur within a reasonable time frame (hours), thus allowing all equipment to be rapidly removed from the site.

The contaminants of concern were also evaluated to insure that the selected gPro® technology was suitable for reaching the objectives. Groundwater chemistry, namely dissolved iron and manganese, was also assessed to determine if high concentrations would interfere with the operation of the gPro® system.

1.2.1 The Selected Remediation Technology

The HP gPro® Technology is a high rate gas in-fusion system that transfers gases (in this case oxygen) into and out of water. The system enables rapid gas transfer from the gas phase to the water phase and infuses high concentrations of dissolved gas into the water.

The in-situ Gi (gas infusion) remediation methodology involves the injection of oxygenated water into the local groundwater with the goal of enhancing and accelerating natural biodegradation processes.

The method is based on iTi's Gas inFusion™ (Gi) technology. Patented porous hydrophobic micro-hollow fibers (MHF) are utilized to dissolve oxygen into water under high pressure, creating supersaturated conditions. Using conventional gas infusion techniques, the supersaturated water would become unstable and oxygen would come out of solution quickly, as governed by Henry's Law. The Gi technology circumvents this problem through the MHF technology and allows for stable elevated concentrations of dissolved oxygen, which are essential for any biological treatment process. According to iTi's literature, the gPro® unit is capable of delivering between 26 and 68 mg/L of DO, depending on flow rates and pressures (iTi, 2007).

1.3 Thesis Objectives

The focus of this study was the delivery of oxygen into fractured bedrock. The main objectives for the thesis are as follows:

1- characterize the bedrock aquifer and create a site conceptual model;
2- evaluate the gPro® technology (in-situ or ex-situ) to field site conditions and design the remediation setup;
3- implement a pilot-scale remediation system using the selected technology; and
4- monitor and evaluate the effectiveness of oxygen delivery.

A three-dimensional numerical model for groundwater flow and advective-dispersive transport within a discretely-fractured porous medium was also developed and calibrated to the field conditions.

The model was used to validate the site conceptual model, to simulate the observed distribution of oxygen within the system and to assess the effectiveness of the oxygen delivery system within the fracture network and porous matrix. Finally the model was used to test the sensitivity of the model to key properties, in order to focus and/or optimize field investigations at other sites.

The research did not assess the implication of oxygen addition on hydrocarbon biodegradation. This was justified on the basis that during the field testing, little utilization of oxygen was noted within the system. The lack of utilization could be attributed to several factors (time scale etc.) but the reasons were not investigated. Thus in this study the delivery and transport of oxygen is considered to be under ideal (conservative) conditions.

2.0 Site Background

2.1 Location and Description

The site selected for this study was a former gas station located within a small rural community in southwestern Ontario. The site operated as a fuel dispensing operation from the early 1970's until the mid 1990's. Historical records for the area also indicate that there were numerous operations in the vicinity of the site that also used petroleum hydrocarbon products (such as home heating oil and motor oils). As a result, the groundwater plume may have multiple contributing sources of petroleum hydrocarbon compounds (PHCs) including BTEX and PHC F1 (C_6-C_{10}) to F4 (C_{34}-C_{50}) compounds.

Several on-site investigations have been completed by WESA Inc. (WESA) to delineate the groundwater contamination and assess remedial options. The groundwater contamination in the area is defined by dissolved concentrations of PHCs (BTEX, F1 (C_6-C_{10}) to F4 (C_{34}-C_{50})) above the legislated Ministry of the Environment (MOE) Site Condition Standards (SCS) (MOE, 2004) for potable groundwater (Figure 2-1). The groundwater analytical data used to contour the levels of contamination were collected from conventional groundwater monitoring wells (1.5 to 3 m screens) and therefore the concentrations are vertically integrated. The groundwater contamination on site is within the dolostone bedrock of the Guelph Formation.

As part of the remedial efforts at the site, WESA commissioned a vapour and groundwater extraction system to remediate high levels of PHC contamination near the source area and in the core of the plume (main site) in October 2006 (WESA, 2006). These systems were designed to address the core high-concentration contamination zone, but did not affect the lower level PHC contamination in the study area.

Based on the need to remediate the full extent of the groundwater contamination, other options were assessed and the objective of this thesis established.

To meet these objectives, the site was divided into two parts: the main study area that encompasses the site property including the zone of influence resulting from the remediation system, and a secondary study area north of the site along the main street (study area). The secondary study area is the focus of this thesis and was located to ensure the effects of the primary site remedial operations would not interfere with the results of this investigation.

2.2 Regional Geology and Hydrogeology

The regional Quaternary geology is characteristic of the Dundalk Till Plain physiographic region, a drumlinized gently undulating till plain extending across the area, and composed of silty sand to sandy silt (Chapman and Putnam, 1984). The geology in the vicinity of the site consists of 0.6 to 3 metres (m) of unsaturated silty sand to sandy silt overlying fractured dolostone of the Guelph Formation (WESA, 2006).

The Guelph Formation is distributed throughout southwestern Ontario between the Niagara and Bruce peninsulas. The formation was deposited in the middle and late Silurian during the Wenlock to Ludlow stages. The depositional environment during that time was reef and inter-reef and the deposited rock is described as fine to medium brown crystalline saccharoidal dolostone or dolomitic limestone that is richly fossiliferous. The depositional environment resulted in medium to thick bedded units with strong bedding plain features. The strata strikes to the northwest-southeast and dips to the southwest (Eyles et al., 1997). The lithological characteristics of the formation have been shown to be very regionally consistent (Brunton et al., 2007 and Eyles et al., 1997).

The origin of the bedrock jointing in the area is a matter of scientific debate, but studies have been conducted which correlate the orientation of the joints to the modern drainage features (Eyles et al., 1997). At the regional scale, the bedrock joints have been shown to be influenced by the trend of modern drainage networks (rivers).

The regional orientation of joints and river trends are within 20° (140° versus 180°, respectively), and past studies have concluded that these trends are consistent over both the regional and local scales (Eyles et al., 1997). Locally, the joints trend parallel to the river, located approximately 200 m south-east of the site with a strike consistent with the bedding plains towards the northwest-southeast and dipping to the southwest.

The Guelph Formation has been reported to range in thickness between 4 and 100 m. In the Cambridge and Guelph areas, the formation ranges between 15 and 22 m in thickness (Brunton et al., 2008). The Guelph Formation has a lower contact with the Eramosa Member of the Lockport Formation and with the Amabel Formation. The contact is gradational over the depositional area (OGS, 1992).

The top of the Guelph Formation has been significantly weathered, therefore creating an interfacial aquifer, with groundwater flowing along the bedrock surface and within the overburden units. Within the study area, the local overburden has been confirmed to be unsaturated, even with seasonal maximum highs in water levels with a groundwater elevation within the bedrock aquifer at approximately 3 metres (m) below ground surface (bgs) (WESA, 2007).

Below the upper portion of weathered bedrock, the bedrock is more competent, but extensively fractured (Eyles et al., 1997) with fractures corresponding to strong bedding plain features. The groundwater flow within the unit is predominantly horizontal and controlled by the bedding plain features. This regional bedrock aquifer is unconfined, with groundwater flow from the northwest towards the southeast (Brunton et al., 2008). Local groundwater flow directions are largely controlled by the river (located approximately 200 m south-east of the site) and are consistent with the regional flow.

Site-specific characterization of the bedrock was based on borehole drilling on site. The results of the drilling are provided as part of the site bedrock characterization presented in Section 3.1.

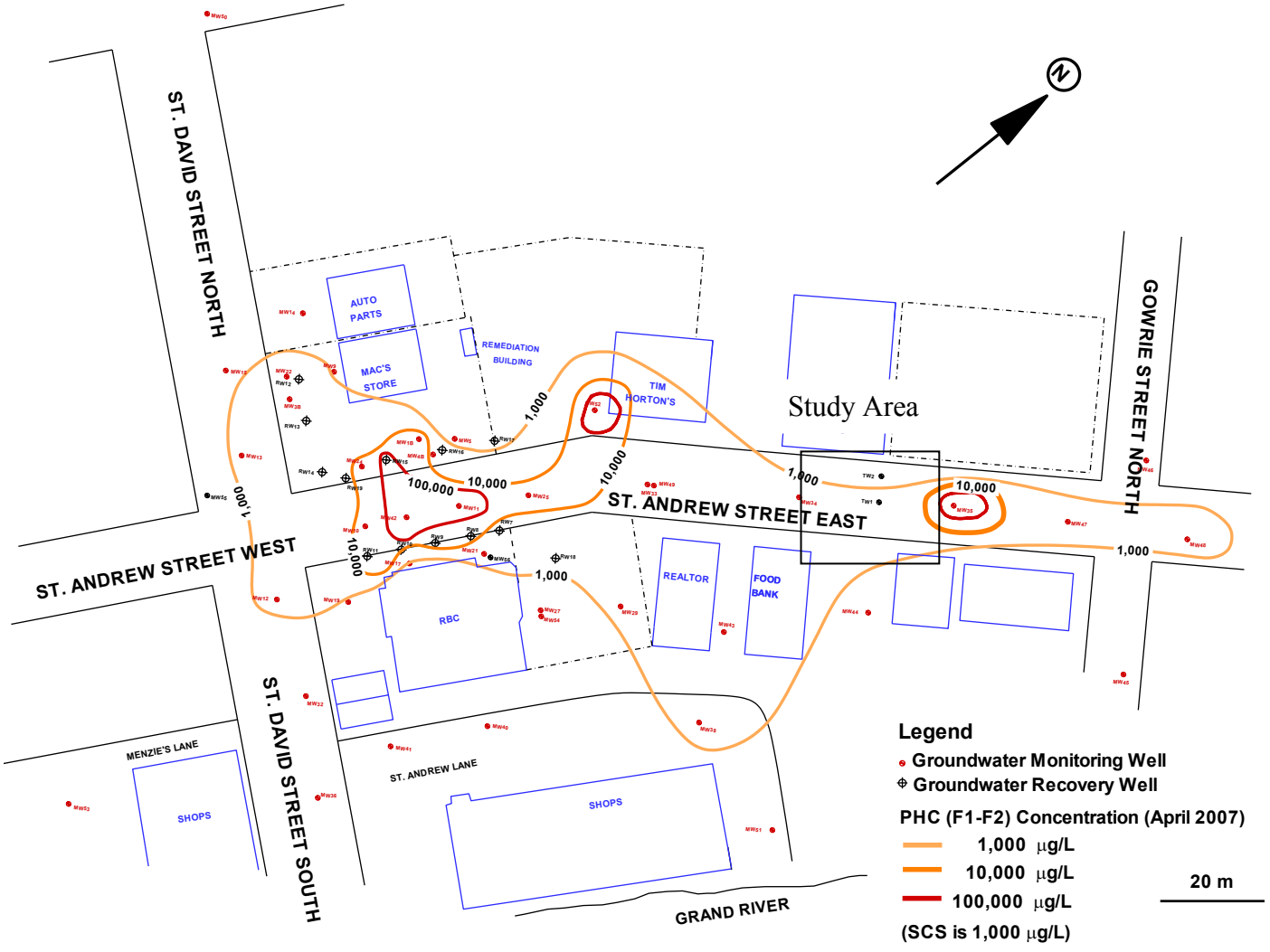

Figure 2-1 – Site map with PHC (F1 + F2) groundwater plume delineated and study area defined.

3.0 Methods

3.1 Initial Investigation

To characterize the bedrock and to establish a site conceptual model, a phased approach to the investigation was completed in which the results from each phase could be evaluated and used to design the following phase. The phases included borehole drilling and hydraulic testing (packer testing), multi-level well monitoring and sampling, digital borehole imaging, tracer testing and cross-borehole testing.

The methodology for each phase of the investigation is provided below.

3.1.1 Bedrock Characterization

The bedrock on site was first characterized through the drilling of two open-hole bedrock test wells (TW1 and TW2) (Figure 2-1). The wells were located 3 m apart along the direction of groundwater flow; TW2 was located up-gradient of TW1 within the road way (Figure 3-1). The wells were completed to a total depth of approximately 9 m bgs as determined based on the maximum depth of contamination detected in a multi-level monitoring well previously installed in the main study area (WESA, 2006). The test wells were located within the road and were positioned to avoid existing infrastructure such as gas and water mains.

The wells were drilled using air rotary drilling techniques by Aardvark Well Drilling of Guelph, Ontario. A 114 mm casing was advanced 30 cm into rock and grout was used to seal the annulus between the casing and the borehole wall.

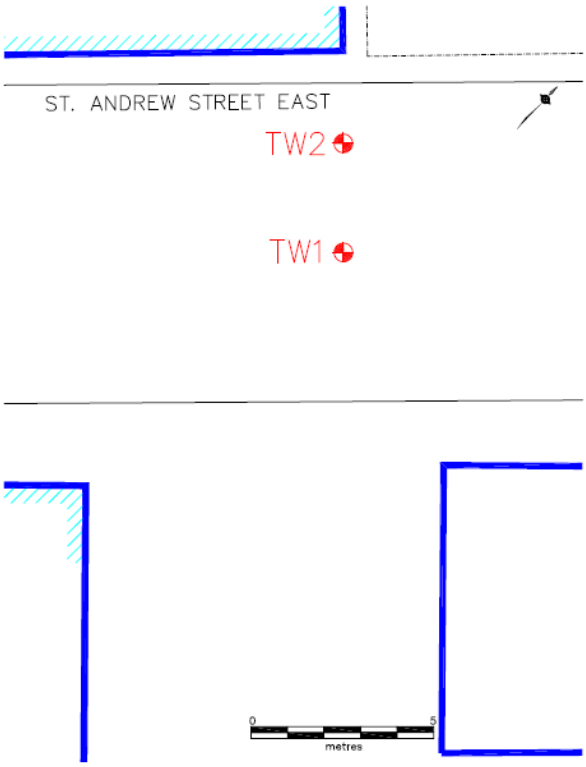

Figure 3-1- Location of injection well TW2 and down-gradient monitoring well TW1.

The wells were designed to insure a seal between the unconsolidated overburden and the bedrock across the overburden/bedrock interface. Following the installation of the casing, a 98.4 mm diameter hole was then drilled into the rock, to a total depth of approximately 9 m bgs.

During drilling, the characteristics of the bedrock were noted and are presented in the borehole well logs (Figure 3-2). Unconsolidated sand and gravel fill was noted from surface to the top of bedrock at ~ 2.20 m bgs. The bedrock was characterized as a highly fractured dolomitic limestone, light grey in colour. A highly fractured zone was observed which extended to ~ 3.0 m bgs, below which the competency of the bedrock increased with depth. Notable changes in the bedrock were observed at ~ 5.5 m bgs and at ~ 8.0 m bgs. At 5.5 m bgs, the colour of the bedrock changed to a darker shade of grey with increased competency and more discrete fractures with depth. The final change in the bedrock (~ 8.0 m bgs) again indicated the competency increase and fewer fractures were noted.

Major discrete fractures were noted along the depth of the boreholes and were determined to be dipping towards the southeast (down-gradient from TW2 to TW1 and towards the river) by approximately 10 cm over a 3 m distance.

3.1.2 Hydraulic Testing

Packer testing of each borehole was conducted to obtain direct measurements of the bulk transmissivity of the formation at 1 m intervals along the depth of the boreholes. The testing used an inflatable straddle packer system and a falling head injection test protocol (Richard et al., 2004). The testing method was selected based on the design of the system to function within a range of bulk rock transmissivities from 10^{-4} m^2/s to 10^{-11} m^2/s and the ability to test based on a one metre test section. The testing range and the testing interval allowed for detailed, depth discrete transmissivities to be obtained, the hydraulically active (highest permeability) zones to be identified and the vertical and horizontal groundwater flow gradients to be determined. Each one metre interval of the saturated open borehole bedrock well was tested and duplicate tests were performed every five tests, to insure quality control.

Based on the adopted methodology, discrete sections of each borehole were isolated using a pair of pneumatically inflated packers and then hydraulically tested. Water was injected under gravity flow through a manometer at the ground surface that was hydraulically connected via polyethylene tubing to the isolated zone in the borehole. Two different manometers were available depending on the relative permeability of the test interval: a large (4") diameter manometer for more permeable intervals, and a small (½") diameter manometer for less permeable intervals. The rate of decline of the water level in the manometer was monitored and recorded to obtain a measurement of the volumetric flow rate of the injected water. These data were used to estimate the hydraulic conductivity of the test interval. Bulk rock transmissivity was then calculated based on the estimated hydraulic conductivity and the length of the test interval. Water level measurements were recorded until the level had dropped below the manometer.

Down borehole pressure-transducer readings were also recorded and logged in the field to provide information on the static head in the injection interval.

Borehole TW1 was tested sequentially from bottom to top at one metre intervals to provide a continuous record of permeability/transmissivities with depth. Based on the results from TW1, key zones in TW2 were selected for testing.

The data analysis methodology was based on the Theim equation, modified for single well injection tests (Richard et al., 2004), using the following equations:

$$Q = \left(\frac{\Delta h \cdot T \cdot 2\pi}{\ln(r_e / r_w)} \right) \tag{1}$$

$$re = 2\left[\left(\frac{T}{S} \right) t \right]^{½} \tag{2}$$

where Q is the flow rate of water into the system (m^3/s) (calculated from the change in head vs time observed in the ½" and 4" manometer), Δh is the change in head ($H_{initial} - H_{static}$) (m), T is the transmissivity (to be calculated in m/s), r_e the radius of influence estimated from equation 2 (m), r_w the radius of the well (m), S is the storativity (estimated at 10^{-4} for preliminary calculations) and t is the total elapsed time of the test.

The storativity and transmissivity were first estimated (based on the dissipation of the packer inflation pulse) to calculate the radius of influence. Equation 1 was then solved for T.

The method assumes that Δh is constant and that S is equal to 10^{-4}. The constant head is valid where it is found to be significantly greater than the change in head used to calculate Q. A variation in S by a few orders of magnitude results in less than a factor of three change in T.

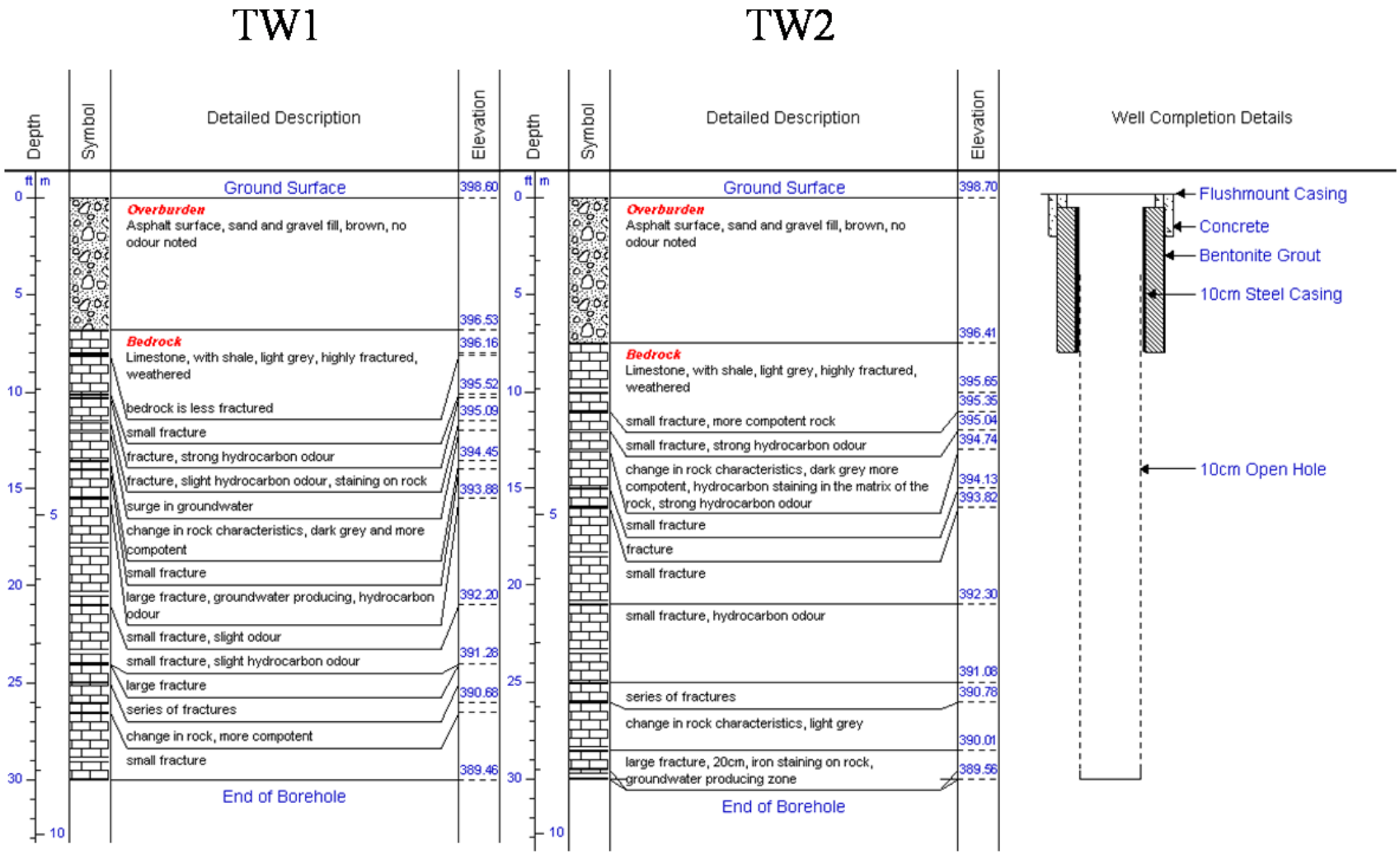

Figure 3-2 - Borehole logs for TW1 and TW2.

Based on the calculated transmissivity for each interval and a one metre interval length (b), the hydraulic conductivity of each interval was calculated using the following equation;

$$K = \frac{T}{b} \tag{3}$$

3.1.3 Multi Level Well Installation

Based on the hydraulically active zones in the rock as identified from the drilling and hydraulic testing, the down-gradient well (TW1) was instrumented with a Solinst CMT Multilevel monitoring system with seven isolated sampling intervals. The system consisted of a 43 mm diameter tube with seven isolated chambers, six in a pie shape around a center hexagonal chamber. With the exception of the bottom interval which is the center hexagonal chamber, an 8 cm hole was cut into each chamber at the desired depth and a 50 cm screen was fastened around each hole to create an isolated screened interval. A screen was placed around the bottom of the pipe for the final interval. The system was lowered into the borehole and alternating lifts of sand and bentonite were placed around each of the screen intervals to complete the isolated sampling interval at each depth. A minimum 30 cm of sand pack and bentonite seal was installed between each interval.

The sampling intervals were positioned to target the hydraulically active zones within the bedrock; TW1-1 to TW1-4 (3.5, 4.1, 4.7 and 5.3 m bgs) in the upper highly fractured zones and TW1-5 to TW1-7 (7.3, 7.9 and 9.0 m bgs) in the discretely fractured lower zones (Figure 3-3). The second test well (TW2) was left as an open bedrock hole to be used as an injection point for the planned technology evaluation (Figure 3-3).

Following the instrumentation of TW1, the water levels were measured in each of the seven zones and in TW2. The water levels were measured relative to the surveyed top of casing using a Solinst water level tape and the groundwater elevations were then calculated.

These data were used to calculate the vertical and horizontal gradients and to better characterize the flow of groundwater in the study area.

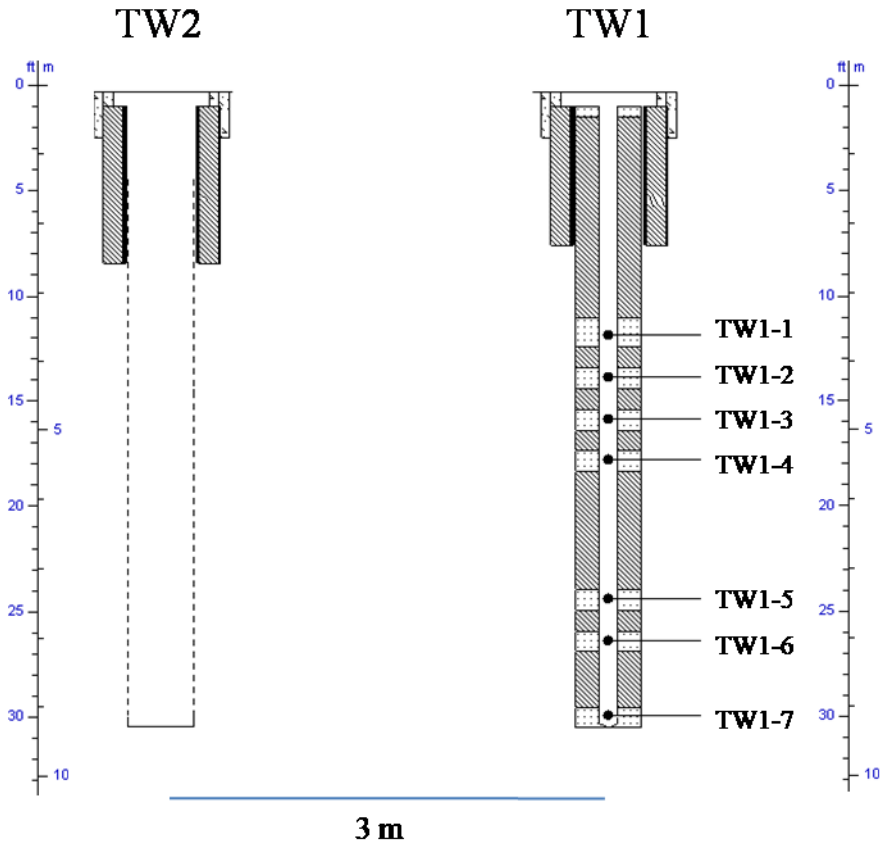

Figure 3-3 - Instrumentation of TW1 (monitor well) and TW2 (injection well).

The vertical and horizontal concentration distribution of BTEX and PHC parameters were determined through the sampling of each of the zones in TW1 and TW2 on several occasions (November 2006, April 2007 and April 2008).

Low flow sampling techniques, in accordance with the EPA low flow protocols (EPA, 1996) were used to sample the seven (7) ports in TW1. Dedicated low density polyethylene tubing was installed into each sampling port. Ports were purged using a peristaltic pump at surface. Flow rates were maintained between 0.1 and 0.5 L/min and a flow-through cell was used to monitor pH, conductivity and dissolved oxygen (DO). These parameters were monitored and the sample intervals pumped until the parameters stabilized within +/- 5% - 10% or within an absolute range (+/- 0.2 mg/L for DO). Stability was deemed attained when three consecutive readings fell within the criteria. The well was sampled once the parameters had stabilized to insure that the samples represented natural groundwater conditions within the formation. Purging and sampling equipment was decontaminated with distilled water between each well.

The pH and electrical conductivity measurements were determined using a Hanna Instruments HI-98129 pH/conductivity/TDS/C meter. DO measurements were made using an Orion Model 835 Dissolved Oxygen Meter.

Conventional purging and sampling techniques were used to obtain a sample from TW2. Water levels within the well were measured prior to sampling. The monitoring well was developed and sampled by purging a minimum of three well volumes using dedicated Waterra™ inertial lift foot valves and polyethylene tubing.

The wells were sampled for BTEX, PHC F1, F2 and F3 fractions, total and dissolved iron and manganese and biochemical oxygen demand (BOD). Iron, manganese and BOD were not sampled at each sampling event.

The groundwater samples for BTEX and PHC parameters were collected in triplicate, using clean 40-mL glass vials with Teflon septa, filled with no headspace, and preserved with 0.4 mL of 10% sodium azide and stored at 4°C until delivered to the lab for analyses. Analyses were performed by the University of Waterloo Organic Geochemistry Laboratory in accordance with the Canadian Council of Ministers of the Environment (CCME) standard methodology for petroleum hydrocarbons in groundwater (CCME,

2001) with modifications as outlined in Appendix A. Duplicate samples were collected for quality control and quality assurance purposes (QA/QC).

BOD samples were collected in clean 500 mL amber glass bottles with Teflon septa, filled with no headspace. No preservative was used. The samples were delivered to the University of Waterloo Organic Geochemistry Laboratory for analyses within 3 hours of collection. BOD analyses were completed in accordance with the Standard Method 5210 (Eaton et al., 1995) with modifications to optimize analysis of samples containing volatile organic contaminants (Chapman et al., 1998).

Dissolved and total iron and manganese samples were collected in 125 mL plastic bottles. Samples collected for dissolved metal analysis were field-filtered using a 0.45-µm in-line Waterra™ filter and preserved in the field with 0.5 mL of HNO_3. Samples collected for total metal analyses were not filtered or preserved in the field. All samples were stored at 4°C until delivered to the lab for analyses. The samples were analyzed by ALS Laboratories of Waterloo, Ontario in accordance with the United States Environmental Protection Agency's (EPA) methodology for "Determination of Trace Elements in Water and Wastes by Inductively Coupled Plasma-Mass Spectrometry" (EPA Method 200.8 ICP-MS).

3.1.4 Digital Borehole Imaging

Digital borehole imaging was completed using an R-CAM 1000 down hole camera manufactured by Laval Underground Surveyors, which generated a visual representation of the borehole walls in TW2. The images allowed for the identification of discrete fractures and fracture features, and allowed for better characterization of changes in rock properties such as competency and matrix porosity.

3.1.5 Fracture Calculations

Based on the results of the hydraulic testing and the digital borehole imaging, key fracture calculations were performed to determine the fracture spacing (2B), hydraulic fracture aperture (2b), and fracture velocity (ν_f).

The fracture frequency was determined by examining the borehole imaging outputs and counting the number of fractures per unit depth within the borehole.

Hydraulic fracture apertures (2b) were then calculated using the cubic law as derived by Snow et al. (1968) and as applied by Lapcevic et al. (1999) and Novakowski et al. (2006) as follows:

$$2b = \left(\frac{T \cdot 12\mu \cdot 2B}{\rho g} \right)^{1/3} \tag{4}$$

where 2b is the average hydraulic fracture aperture (m), T is the transmissivity from packer testing (m^2/s), μ is the viscosity of water at 20°C (10^{-3} kg/s-m), g is the gravitational constant (10 m/s^2), ρ is the density of water at 20°C (1000 kg/m^3) and 2B is the fracture spacing (m).

The fracture groundwater velocities were then calculated using the cubic law (Novakowski et al., 2006);

$$\nu = \frac{-(2b)^2}{12\mu} \rho g \nabla h \tag{5}$$

where ∇h is the hydraulic head gradient.

3.1.6 Tracer Testing

To confirm the hydrogeological properties of the aquifer and to identify and confirm flow paths between wells, a conservative tracer test was completed. The tracer test involved the injection of 500 L of water, spiked with 2470 µg/L sulfur hexafluoride (SF_6), into the up-gradient open bedrock well (TW2). SF_6 was selected as the tracer due to its conservative behavior in groundwater environments and has been shown to have similar breakthrough curves to bromide (Gamlin et al., 2001). Bromide was used as the tracer for the injection test on site, as detailed below.

Concentration breakthrough within the injection well and down-gradient wells (TW1-1 to TW1-7) was monitored over time. Water samples for SF_6 analysis were collected in duplicate, using 40 mL screw cap plastic containers fitted with Teflon-lined septa. The samples were stored at 4°C until delivered to the University of Waterloo Organic Geochemistry Laboratory for analysis. The samples were analysed using a method developed by the laboratory and described by Wilson et al. (1993).

3.1.7 Cross Borehole Testing

To evaluate the connectivity of fractures between the boreholes and to identify the most significant conductive fractures (Illman et al., 2007 and Paillet et al., 1993) a cross borehole hydraulic test was completed to determine the hydraulic connection between the up-gradient well (TW2) and the down-gradient monitoring points (TW1-1 to TW1-7).

The test involved the injection of water into TW2 (below 5.5 m bgs) at a rate of 5 L/min for approximately 90 minutes and the monitoring of the hydraulic head responses in the down-gradient monitoring points over time. The injection was completed within an isolated interval of the bedrock (below ~5.5 m bgs). The field testing conditions and set up (packer position, injection conditions etc.) were consistent with the injection test detailed in Section 2.2 below.

Water levels within the monitoring points were monitored during the injection and recovery periods.

3.2 Injection Testing

The oxygen injection test was designed based on the site conditions using the gPro® technology. The objective of the test was to evaluate the delivery of the oxygenated water into the bedrock formation and to evaluate the distribution of injected water and oxygen within the lower discrete fracture zone. The test interval in TW2, below 5.5 m bgs was isolated using packers to assess the conditions within the discrete fractured zone and to isolate the upper highly fractured rock. The effects of biodegradation, as a result of the addition of oxygen into the formation, were not assessed as part of this test.

Water was injected in two 500 L batches pre-mixed with sodium bromide (bromide) and treated using the gPro® technology prior to injection. The injection water was obtained from the on-site groundwater remediation system and was collected in a 500 L tank at an average concentration of 688 mg Br/L. The treated water exiting the gPro® was injected into the isolated zone (below 5.5 m bgs) in TW2 (injection well).

Bromide was selected as the tracer because it has been shown to behave conservatively with little matrix diffusion over short term time scales of less than 50 days (Jardine et al., 1999).

Dissolved oxygen (DO) and bromide concentrations were measured in TW2 during the injection to assess the temporal change in injection water. DO measurements were collected in the field through a flow-through cell using an Orion Model 835 Dissolved Oxygen Meter. Bromide concentrations were calculated based on millivolt (mV) readings collected in the field using an Orion Model 230A pH meter equipped with a Cole-Parmer 27502-04 bromide electrode.

DO and bromide concentrations in the injection well and in the down-gradient well were monitored until they were within the range of background concentrations between 1.3 and 7.3 mg/L (as measured in April 2007) after approximately 10 days. The sample frequency was adjusted throughout the test to provide a well-defined breakthrough curve. The low sampling rate was designed to minimize distribution to the flow system.

Samples were also collected prior to the start of the injection testing and throughout the monitoring period for BTEX, naphthalene, and iron analysis. The BTEX and naphthalene samples were collected and analyzed based on the methodology described in Section 2.1.3 above.

Iron samples were collected in duplicate, using 40 mL screw cap plastic containers fitted with Teflon-lined septa. The samples were stored at 4°C until delivered to the University of Waterloo Organic Geochemistry Laboratory for analysis. The samples were analysed in accordance with the Hach Company Method 8008 (FerroVer Method) for total iron analysis using a Hach DR/2400 Portable Spectrophotometer. The method was adapted from *Standard Methods for the Examination of Water and Waste Water*. The method concentration range is between 0.02 and 3.00 mg/L.

A Solinst Level Logger pressure transducer was placed in the injection well below the packer to monitor the performance of the packer and the water level (pressures) in the injection zone during injection.

3.3 Modelling Approach

The model chosen to simulate the oxygen injection test was the discrete fracture network model HEATFLOW/SMOKER (Molson et al, 1992; Molson and Frind, 2009). This model considers advective-dispersive transport of a dissolved phase component (or heat) within a porous matrix and/or a discrete fracture network.

The HEATFLOW/SMOKER model assumes transport is governed within the 3D porous matrix by the general advective-dispersive transport equation given by:

$$\frac{\partial}{\partial x_i}\left[D_{ij} \frac{\partial c}{\partial x_j} \right] - \nu_i \frac{\partial c}{\partial x_i} = \frac{\partial c}{\partial t} \qquad (6)$$

where x_i are the 3D spatial coordinates (x_i = x,y,z), c is the dissolved (aqueous phase) concentration (kg/m^3) (in this case oxygen), D_{ij} is the hydrodynamic dispersion coefficient (m^2/s), v_i is the average linear groundwater velocity (m/s) and t is time (s) (Figure 3-4).

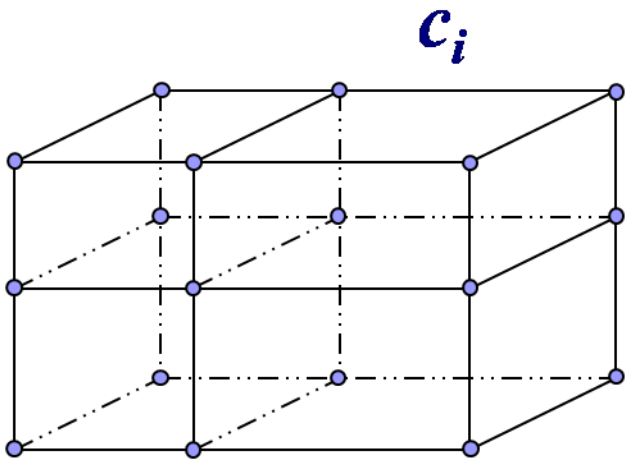

Figure 3-4 - Configuration of the quadrilateral elements representing the porous matrix in the numerical model; concentrations are computed at each of the nodes (Molson & Frind, 2009).

The dispersion coefficient D_{ij} in equation (6) includes mechanical dispersion and molecular diffusion (see Molson et al. 1992). Simplified to a 1D system, for example, D_{ij} can be defined as: $D_{ij} = \alpha_L v + D^*$ where α_L is the longitudinal dispersivity (m) and D^* is the molecular diffusion coefficient (m^2/s). The term D^* represents diffusion through the bulk porous medium, and is in turn defined as $D^* = D_o \cdot \tau$ where D_o is the diffusion coefficient in water (1.97 x 10^{-9} m^2/s; Wilk et al., 1955) and τ is the tortuosity factor (Freeze and Cherry, 1979; Aachib et al., 2004).

The HEATFLOW/SMOKER numerical model simulates transport in the fractures by solving a similar transport equation within 2D planar fractures according to:

$$\frac{\partial c'}{\partial t} + \frac{\partial (\nu_i c')}{\partial x_i} - \frac{\partial}{\partial x_i}\left(D_{ij} \frac{\partial c'}{\partial x_i} \right) - D_{ij}\left[\frac{\partial c'}{\partial z} \right]_{z=\pm b} = 0 \qquad (7)$$

where b is the half fracture aperture (m) and c' is the concentrations in the fracture (Figure 3-5). The last term on the l.h.s of (7) accounts for mass transfer across the fracture/matrix interface.

The fracture velocities are assumed governed by the cubic law defined as follows:

$$\nu = \frac{-(2b)^2}{12\mu} \rho g \nabla h \qquad (8)$$

where 2b is the fracture aperture (m), μ is the viscosity (10^{-3} kg/ms) and ρ the density (kg/m^3) of water, g is the gravitational constant (m/s^2) and ∇h is the hydraulic head gradient.

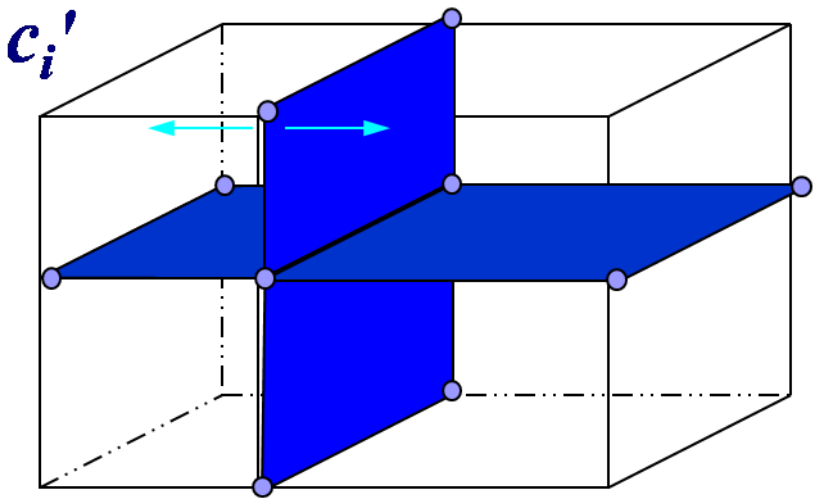

Figure 3-5 - Geometric arrangement showing how 2D fractures are overlain onto the porous matrix (Molson and Frind, 2009).

The HEATFLOW/SMOKER model solves the coupled equations 6-8 using the Galerkin finite element method. Model verification examples and model details are provided in Molson et al. (1992) and Molson and Frind, 2009.

4.0 Field Results and Interpretation

4.1 Site Characterization

4.1.1 Hydraulic Testing

Transmissivity and hydraulic conductivity values were calculated for each hydraulic test interval using the Theim equation methodology as described in Section 2.1.2 (Richard et al., 2004). Data used for each calculation included static hydraulic heads, selected pressure transducer readings and volumetric flow rates of the injection water. The results are summarized in Table 4-1 for each interval in the test wells and full results are provided in Appendix B.

Table 4-1 - Hydraulic Testing Results

Well	Interval	Depth (m)	Center Depth (m)	K (m/s)
TW1	1	8.0 - 9.0	8.5	4.00E-07
	2	7.0 - 8.0	7.5	5.00E-06
	3	5.3 - 6.3	5.8	2.00E-06
	4	4.3 - 5.3	4.8	1.00E-05
	5	3.3 - 4.3	3.8	1.00E-05
TW2	1	8.0 - 9.0	8.5	6.00E-07
	2	7.0- 8.0	7.5	7.00E-07
	3	6.4 - 7.4	6.9	2.00E-07
	4	5.4 - 6.4	5.9	1.00E-07
	5	4.4 - 5.4	4.9	3.00E-06
duplicate	5	4.4 - 5.4	4.9	4.00E-06
	6	3.4 - 4.4	3.9	1.00E-05
duplicate	6	3.4 - 4.4	3.9	1.00E-05

The bulk hydraulic conductivities of the fractured bedrock were found to range from 10^{-5} m/s to 10^{-7} m/s. Based on the results of the hydraulic packer testing, the rock can be divided into three zones given the calculated hydraulic conductivity. An upper zone

defined with an average hydraulic conductivity of 1.0 x 10^{-5} m/s extending from the top of rock (~2.0 m bgs) to ~5.5 m bgs, a second zone with an average hydraulic conductivity of 1.0 x 10^{-6} m/s (~5.5 to ~8.0 m bgs) and a lower zone (~8.0 to ~9.0 m bgs) with an average hydraulic conductivity of 1.0 x 10^{-7} m/s.

Throughout the hydraulic testing, duplicate tests were conducted every five intervals to test the reproducibility of the injection flow rates and the equipment assembly. Duplicate tests were reproducible within less than one third of an order of magnitude or a relative percent difference of 28.5%, indicating that both the manometer readings for the flow rate calculations and the equipment assembly were consistent during the on-site hydraulic testing.

4.1.2 Groundwater Flow and Contaminant Distribution

Following the instrumentation of TW1, the water levels in each of the seven zones (TW1-1 to TW1-7) and in TW2 were measured on several occasions (Table 4-2). April 2008 levels are considered most representative and were used to calculate the vertical and horizontal gradients and to better characterize the flow of groundwater in the study area.

The horizontal gradient recorded in April 2008 between TW2 and TW1-4 was 0.01. The static water level in the open borehole, TW2, was reported at 3.03 m bgs (395.63 m asl). The water levels in the isolated intervals of TW1 showed two distinct zones: an upper zone that extended from TW1-1 to TW1-4 with an average groundwater elevation at 2.91 m bgs (395.69 m asl), and a lower zone which extended from TW1-5 to TW1-7 with an average groundwater elevation of 7.53 m bgs (391.08 m asl).

Table 4-2 - Groundwater Elevations

Well Id	Total Well Depth (m.bgs)	Ground Elevation (m.asl)	Well Depth (m.asl)	Water Level (m.bgs)	Water Elevation (m.asl)	Water Level (m.bgs)	Water Elevation (m.asl)	Water Level (m.bgs)	Water Elevation (m.asl)	Water Level (m.bgs)	Water Elevation (m.asl)	Water Level (m.bgs)	Water Elevation (m.asl)	Water Level (m.bgs)	Water Elevation (m.asl)
				08-Nov-06		25-Apr-06		25-Apr-07		07-Nov-07		24-Jan-08		22-Apr-08	
TW1-1	3.5	398.6	395.1	3.01	395.59	3.00	395.60	3.00	395.60	dry	dry	3.05	395.55	2.90	395.70
TW1-2	4.1	398.6	394.5	3.00	395.60	3.00	395.60	3.00	395.60	3.89	394.71	3.03	395.57	2.89	395.71
TW1-3	4.7	398.6	393.9	3.02	395.58	3.05	395.55	3.05	395.55	3.88	394.72	3.03	395.57	2.93	395.67
TW1-4	5.3	398.6	393.3	3.02	395.58	3.10	395.50	3.10	395.50	3.88	394.72	3.60	395.00	2.91	395.69
TW1-5	7.32	398.6	391.28	dry	dry	dry	dry	7.35	391.25	dry	dry	7.77	390.83	dry	dry
TW1-6	7.9	398.6	390.7	7.51	391.09	7.75	390.85	7.75	390.85	7.93	390.67	7.50	391.10	7.46	391.14
TW1-7	9	398.6	389.6	7.81	390.79	8.06	390.54	8.06	390.54	8.36	390.24	7.91	390.69	7.59	391.01
TW2	9.05	398.7	389.65	3.10	395.60	3.07	395.63	3.07	395.63	3.92	394.78	3.16	395.54	3.03	395.67

The vertical gradient within the upper zone was neutral (as estimated between TW1-1 and TW1-4), while a strong vertical downward gradient (-1.75) was estimated between the upper zone and the lower zone, as measured between TW1-4 and TW1-6. There was also a weaker (-0.12) downward gradient measured between TW1-6 and TW1-7. Being an open hole across both zones, the water level in TW2 represents an equilibrated head between the two systems.

The vertical and horizontal concentration distribution of key chemical parameters was then determined through the sampling of each of the wells TW1-1 to TW1-7 and TW2 (Appendix C).

A limited amount of information is available about the contamination in the study area, and with the lack of historical information it is difficult to characterize the distribution of petroleum hydrocarbon contamination. It is assumed that some natural attenuation of the contamination has occurred, but the age and origin of the source is unknown.

The horizontal extent of the contamination was defined by WESA from the April 2007 monitoring and from sampling events that took place on site (WESA, 2007). The contamination zone is defined by concentrations of PHC (F1 + F2) above the MOE Table 2 Site Condition Standard of 1000 µg/L (MOE, 2005), and extends along St Andrew's Street East towards Gowrie Street, including TW1 and TW2 (Figure 2-1). The concentration of PHC (F1+F2) in TW1-1 was 1980 µg/L. The exact lateral delineation is uncertain due to the limited number of monitoring points. The April 2007 data were collected prior to any active remediation within the study area.

The vertical distribution of contaminants can be best represented by the concentrations of ethylbenzene in the TW1 well. The maximum concentration was reported in TW1-1 at 334 µg/L (above the SCS of 2.4 µg/L). Concentrations then decreased with depth in TW1-2, TW1-3 and TW1-4 at 6.41, 2.39 and 1.44 µg/L, respectively. Within the lower zones, concentrations at TW1-6 and TW1-7 were above the SCS at 3.6 and 2.49 µg/L, respectively. Based on the vertical distribution of contaminants within these wells, it can

be noted that contamination is concentrated within the upper zone but extends to the full depth of investigation. This suggests that some hydraulic connection exists between the upper and lower zones, up-gradient of TW2 and TW1.

Total and dissolved iron and manganese samples were collected in November 2006 to help in the technology assessment (Appendix C). The total iron concentrations ranged between 0.34 and 8.08 mg/L in TW1-3 and TW1-6. The results in the open bedrock well TW2 were 0.59 mg/L. A similar range was noted with the dissolved iron. A minimum concentration of 0.3 mg/L was reported in TW1-3 and TW1-4, the concentration dropped from 8.08 mg/L to 0.48 mg/L at TW1-6 between November 2006 and April 2007, a maximum concentration of 6.21 mg/L was noted in TW1-7 and a peak concentration of 0.39 mg/L was observed in TW2. Dissolved manganese concentrations showed a minimum concentration in TW1-2 at 0.019 mg/L and a maximum of 0.132 mg/L in TW1-1. Total manganese concentrations reflected similar concentrations with a minimum in TW1-2 of 0.015 mg/L and a maximum of 0.157 mg/L in TW1-2.

Dissolved oxygen (DO) analyses were completed to establish base line conditions on site. DO concentrations ranged from 1.6 mg/L in TW1-1 to 9.0 mg/L in TW1-2. The concentration in TW2 was 2.2 mg/L (Appendix C).

BOD samples were also collected to establish a baseline prior to the start of any remediation (oxygen addition) activity on site. The results ranged from a minimum in TW1-4 at 0.13 mg/L to a maximum in TW1-1 of 15.7 mg/L (Appendix C). The BOD results were not used as part of this thesis but were collected to establish baseline conditions.

4.1.3 Digital Borehole Imaging

Based on the results of the imaging, major changes within the rock were noted and the discrete fractures were identified. A distinct transition in the rock's appearance was noted at ~ 3.8 m bgs, dividing the upper zone identified during the hydraulic testing into two

zones, Zone 1 and Zone 2a. The average bulk hydraulic conductivity for both zones is 1.0 x 10^{-5} m/s but based on the imaging, two distinct rock characteristics were noted. Zone 1 was highly weathered with only a few discrete fractures. With increasing depth the competency of the rock increased and several more discrete fractures were identified. The discrete fractures within this sub-zone (Zone 2a) were identified at ~ 4.1, 4.7 and 5.2 m bgs. The characteristics of the rock seen in Zone 2a are consistent to a depth of ~ 8.0 m bgs, with discrete fractures also noted at ~ 5.95, 6.45, 7.29 and 7.47 m bgs.

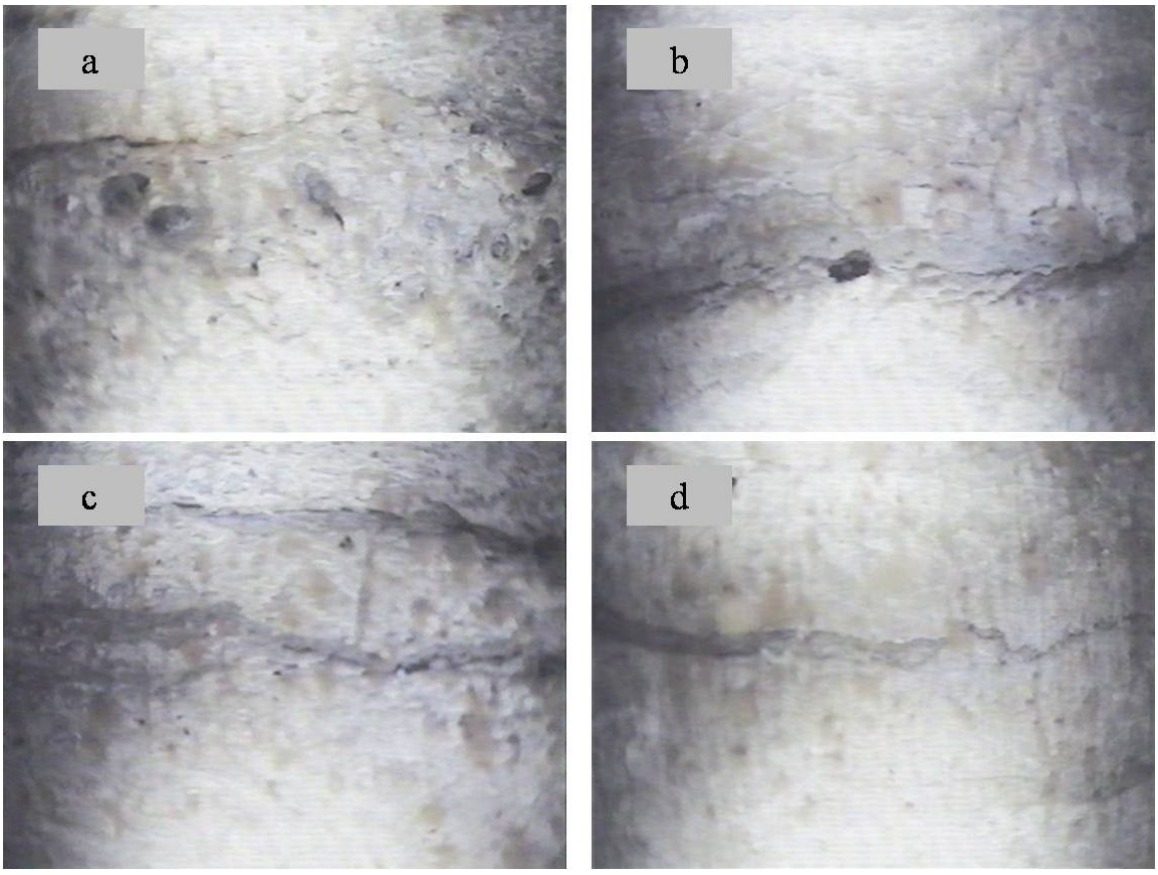

Figure 4-1 - Borehole images showing a) porous matrix in Zone 1 b) highly fractured rock in Zone 1, c) and d) discrete fractures in Zone 2a.

Based on the results of the hydraulic testing, a transition in the hydraulic conductivity of the rock (from an average hydraulic conductivity of 1.0 x 10^{-5} m/s to 1.0 x 10^{-6} m/s) was noted at ~ 5.5 m bgs. Therefore, Zone 2b was identified from ~ 5.5 to 8.0 m bgs. Below ~8.0 m bgs, a reduced fracture frequency and lower rock matrix porosity were noted (on

visual inspection). The change in rock characteristics is consistent with the change in hydraulic conductivity at that depth, as identified during the packer testing. Therefore a third zone (Zone 3) was identified below a depth of approximately 8.0 m bgs. Images showing features of the rock are provided in Figure 4-1.

The results of the investigation were compiled to create a site conceptual model as shown in Figure 4-2. The figure identifies the four zones within the rock (Zone 1, Zone 2a, Zone 2b and Zone 3) based on the rock characteristics and the hydraulic conductivity. The site conceptual model is summarized in Section 4.2 below.

4.1.4 Fracture Calculations

Given the properties of the bedrock determined through hydraulic testing and digital borehole imaging, the fracture spacing (2B), hydraulic fracture aperture (2b), and fracture velocity (ν_f) were determined for each of the major fractures within each of the identified zones.

Based on the highly weathered nature of the upper bedrock, the fracture frequency could not be determined for Zone 1. For the remainder of the borehole (~ 3.8 m bgs to ~9.0 m bgs), one fracture was present on average for each half meter of rock (2B = 0.5 m), based on images of the borehole wall.

Fractures identified within Zone 2a (fractures 5, 6 and 7) of the site conceptual model were calculated to have a fracture aperture of 183 μm and a fracture velocity of 1.37×10^{-3} m/s, based on the bulk hydraulic conductivity of 1.0×10^{-5} m/s and a fracture spacing of 0.5 m. Within Zone 2b the fracture apertures were calculated at 146 μm, with a fracture velocity of 8.7×10^{-4} m/s, based on a bulk hydraulic conductivity of 1.0×10^{-6} m/s and a fracture spacing of 0.5 m. The fractures identified in this zone are labeled numbers 1, 2, 3 and 4.

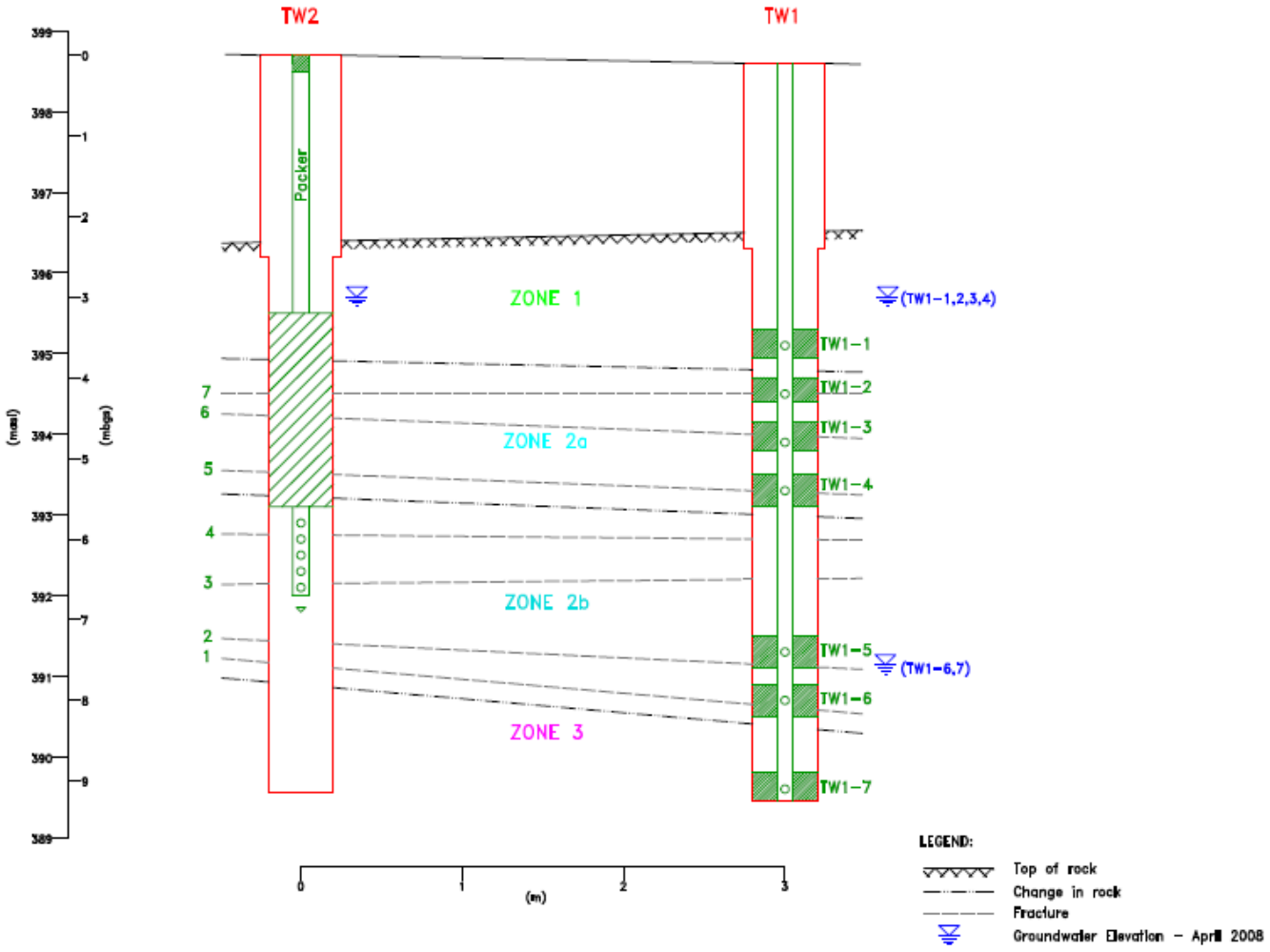

Figure 4-2 - Site conceptual model showing injection well (TW2), the 7 monitoring points within the monitor well TW1, and the major fractures identified from the borehole logs and video.

4.1.5 Tracer Testing

A conservative tracer test was completed to confirm the hydrogeological properties of the aquifer and to identify and confirm flow paths between wells TW1 and TW2. The initial concentration of SF_6 in the injected water was 2470 µg/L. The breakthrough of the tracer was measured in the down-gradient wells (TW1-1 to TW1-7) (Figures 4-3). The full tracer test data set is provided in Appendix D.

Tracer breakthrough was observed in three of the seven down-gradient monitoring points (TW1-2, -3 and -4) completed within Zone 2a. No response was noted in TW1-1 (Zone 1), TW1-6 (Zone 2b) or TW1-7 (Zone 3). It should be noted that the time of breakthrough of the maximum concentration in TW1 (TW1-2 to TW1-4) was not likely seen due to the sparse sampling frequency.

The results of the tracer test, however, did confirm a hydraulic connection between the injection well (TW2) and the monitoring points completed in Zone 2a down-gradient. Note that the injection well (TW2) and observation well (TW1) are only 3 m apart. No response was noted within the upper (TW1-1) or lower monitoring points (TW1-6 and TW1-7) completed in Zones 1, 2b and 3, respectively. The lack of response in the upper zone indicates that there is no direct vertical connection between the injection well and the down-gradient upper zone. Within the lower zones the lack of response could be attributed to the injection of the tracer into the entire open borehole as opposed to being injected into a discreetly isolated interval, as used for the cross borehole and injection tests detailed below. The open-hole tracer injection could potentially result in the injected tracer being preferentially transported through the discrete fractures and through the more highly conductive matrix of Zone 2a.

The results of the SF_6 tracer test confirmed a hydraulic connection between the two wells within Zone 2a and showed that the monitoring well network could also be used to monitor the effectiveness of the oxygen delivery technology within those zones.

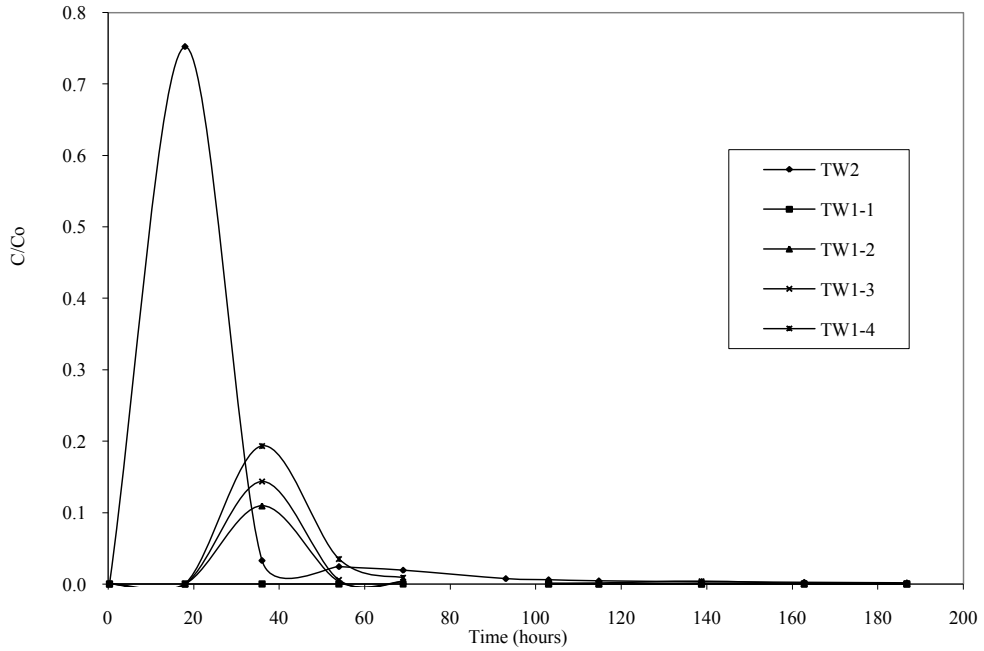

Figure 4-3 - SF_6 tracer test breakthrough curves.

4.1.6 Cross Borehole Testing

A cross borehole pressure test was also completed to characterize the connectivity of the fractures between boreholes. Day-Lewis et al. (2000) showed that, by examining the drawdown versus time graphs for two wells, the connectivity between them can be determined. During pumping or injection, the borehole intervals that are connected by a high permeability zone show similar drawdown responses. If the borehole intervals were not connected by a high hydraulic conductivity zone, the drawdown response would be different (Day-Lewis et al., 2000).

The hydraulic head response in each of the monitoring points was monitored and plotted versus time (Figure 4-4). Results of the test are detailed below. It should be noted that following the injection, the monitoring points began to recover, with the recovery being consistent with the injection results at each of the monitoring locations. Full results are provided in Appendix D.

No hydraulic response was noted in TW1-1, which was completed in the upper zone, Zone 1. The results confirm those of the tracer and injection test (below), which showed no direct hydraulic connection between the injection well (TW2) and TW-1 or between the lower zone (Zone 2a) and the upper zone (Zone 1).

Within the lower monitoring points (TW1-2, TW1-3 and TW1-4) that were completed within Zone 2a, the upper zone and above the packed-off interval in the injection well, respectively, an approximately 5 cm increase in water level was noted within the first 200 seconds following the start of the injection. Minor fluctuations were noted within these monitoring points over time but remained relatively constant throughout the injection. The results confirmed that these monitoring points were completed on discrete fractures within the bedrock (see conceptual model in Figure 4-2) and that the horizontal hydraulic connection is strong.

TW1-6 saw no hydraulic head response (< 2 cm). The results confirm that there is no direct hydraulic connection between the injection interval and the TW1-6 monitoring point and therefore this monitoring point is clearly not positioned directly in line with an interconnected discrete fracture (fracture 1, see Figure 4-2) but is likely offset from the fracture, based on the position identified from the down hole camera images.

The results of the cross-borehole test indicated that there is a strong hydraulic connection between the injection well (TW2) and TW1-7. The hydraulic head response was rapid (0.54 m in 390 seconds) and then stabilized, for a total increase of 0.73 m over the 90 min injection period. Based on these results, the connection is assumed to be a result of the injection pressure. The injection of water under pressure created a hydraulic connection that may not be present under natural flow conditions.

Overall, four main conclusions can be drawn: 1- a lack of hydraulic connection with the upper zone (Zone 1) was confirmed, 2- a strong hydraulic connection along the discrete fractures was noted within the system (TW1-2, 3 and 4), 3- the test confirmed that monitoring point TW1-6 must be offset from fracture 1 since there is no hydraulic

connection to the injection well, and 4- there was a strong hydraulic connection between the injection well (TW2) and the down-gradient monitoring point TW1-7 located in Zone 3.

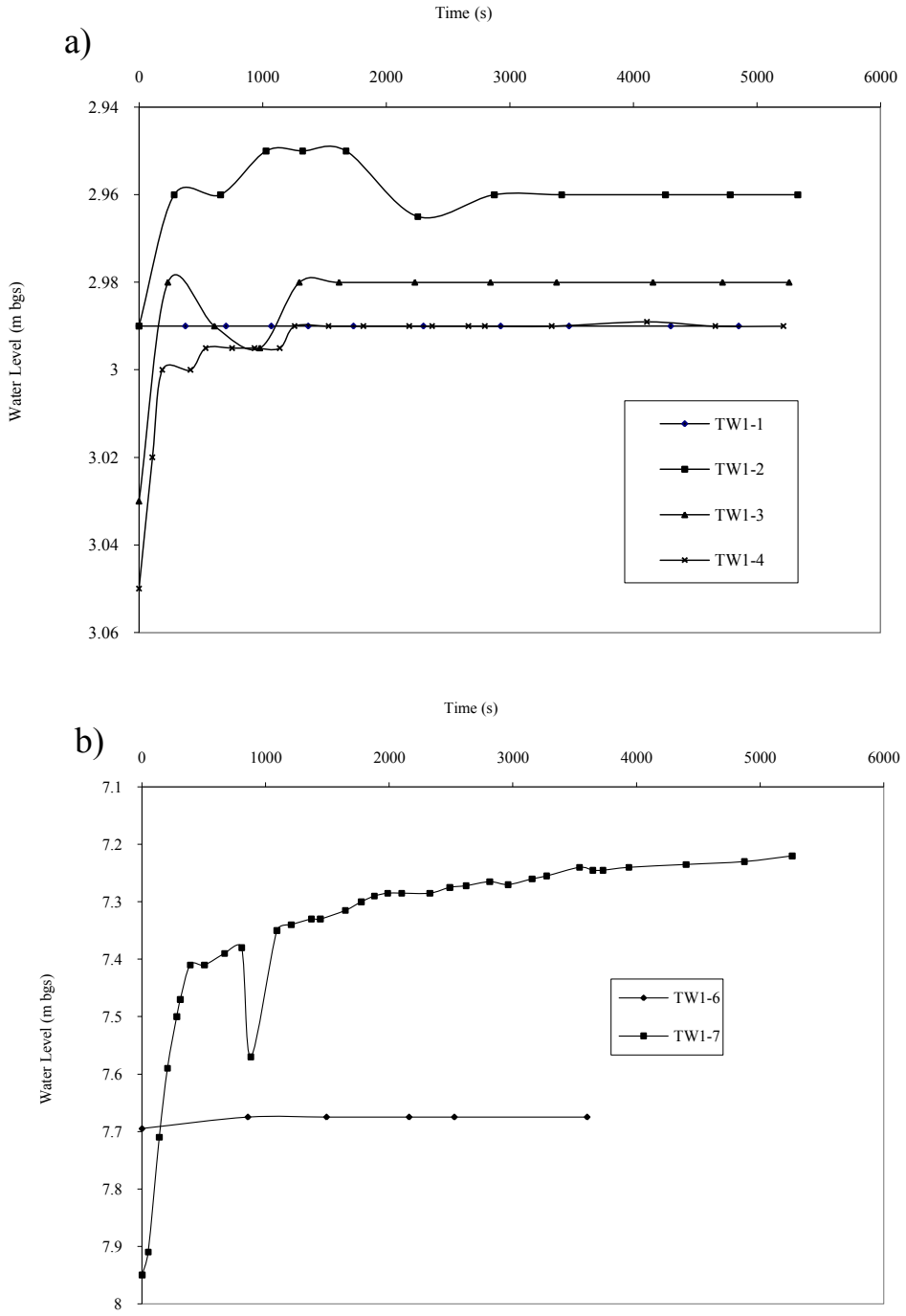

Figure 4-4 - Cross borehole test results of hydraulic head versus time showing response at: a) TW1-1 to TW1-4, and b) TW1-6 and TW1-7.

4.2 Summary and Site Conceptual Model

Based on this investigation, a site conceptual model was developed which is presented in Figure 4-2 and summarized below. The rock has been divided into four distinct units:

Zone 1 - Extends from the top of rock (2.0 m) to ~ 3.8 m bgs, has an average bulk hydraulic conductivity of 1.0 x 10^{-5} m/s and is highly weathered. There is no direct hydraulic connection between the injection well and Zone 1 down-gradient (as seen in TW1-1) or with the lower zone (Zone 2a).

Zone 2a – Extends between ~3.8 and 5.5 m bgs, has an average bulk hydraulic conductivity of 1.0 x 10^{-5} m/s, contains discrete fractures at ~4.1, 4.7 and 5.2 m bgs (fractures 5, 6 and 7). The hydraulic fracture apertures within this unit were calculated to be 183 μm with groundwater velocities of 1.37 x 10^{-3} m/s. A strong hydraulic connection was confirmed across the unit based on the response between the injection well (TW2) and the down-gradient monitoring points completed in this unit (TW1-2, 3 and 4). The results were consistent from the initial tracer testing and cross borehole testing.

Zone 2b – Extends between ~5.5 and 8.0 m bgs, has an average bulk hydraulic conductivity of 1.0 x 10^{-6} m/s, contains discrete fractures at ~ 5.95, 6.45, 7.29 and 7.47 m bgs (1, 2, 3, and 4). The hydraulic fracture apertures within this unit were calculated to be 146 μm with groundwater velocities of 8.7 x 10^{-4} m/s. Limited down-gradient monitoring data were available within this unit. Monitoring point TW1-5 was completed within this unit but was found to be dry for the duration of the investigation. The monitoring point was suspected to have been damaged during installation. TW1-6 was also completed within this unit. The results of the cross borehole test indicated that the monitoring point was off-set from a discrete fracture and therefore does not provide direct evidence as to the behavior of Zone 2b.

Zone 3 – Extends between ~8.0 m and the bottom of the borehole (~9.0 m bgs), and has an average bulk hydraulic conductivity of 1.0 x 10^{-7} m/s. No discreet fractures were noted

within this zone at the depths investigated. Based on the results of the cross borehole testing, a strong hydraulic connection was noted between the injection well (TW2) and the down-gradient monitoring point (TW1-7) located within this zone. The hydraulic connection was a result of the injection under pressure and would not exist under natural conditions.

The groundwater levels within the upper zones (Zones 1 and 2a) are on average approximately 3.03 m bgs (395.63 m asl) whereas the lower zones (Zones 2b and 3) have an average groundwater elevation of 7.53 m bgs (391.08 m asl). The water levels on site confirm two potential flow systems. The injection well (TW2) is completed across both systems whereas the down-gradient monitoring points are isolated monitoring points with TW1-1 to TW1-4 (Zones 1 and 2a) in the upper system and TW1-6 and TW1-7 (Zones 2b and 3) in the lower system.

Contamination within the rock is concentrated within the upper two zones, but due to the strong downward gradients and apparent connectivity, some contamination has also entered Zones 2b and 3 (see analytical parameter table in Appendix C).

Based on work completed on site by WESA (WESA, 2006) the matrix porosity was assumed to be 0.15, which falls within the range of the regional aquifer of 0.11 to 0.17 (Novakowski et al., 1994). The hydraulic conductivity of the rock matrix is 1.0×10^{-7} m/s.

4.3 gPro® Technology

iTi's High Pressure Gas Infusion Technology (gPro®) was selected for evaluation in this study. An ex-situ system was selected over an in-situ version of the technology due to the high iron concentrations in the groundwater. There was concern that the high iron would interfere with the operation of the system causing the internal membranes to become plugged if excess iron precipitated in the presence of oxygen. Treated water from the

groundwater remediation system on the main site was therefore selected as the water supply. The groundwater from the remediation system is consistent in chemistry with the groundwater on site (see effluent sample in Table 4-3) but has been treated through an air stripper to remove the hydrocarbon contamination. Through the remediation process, the iron precipitates out of the water and thus the iron concentrations in the treated water (Table 4-4) are significantly lower than in the natural groundwater and therefore would not interfere with the operation of the technology.

In addition, a mobile unit was constructed to fit into the back of a cargo van to facilitate moving on and off the site (Figure 4-5). The system design involved a 500 L holding tank with the discharge piped to the gPro® unit. Discharge from the gPro® unit was attached to the top of a down-hole set-up that included an inflatable packer and sampling port. The system was closed from the discharge of the tank to the open bedrock hole below the sealed packer. A generator was used to power the gPro® unit and flow rates were set using the discharge valve from the tank and the regulator on the gPro® unit. The gPro® unit was operated in accordance with a Mobile Certificate of Approval (air) issued by the Ministry of the Environment.

Figure 4-5 - gPro® unit photos.

4.4 Injection Test

During the injection test, the treated water exiting the gPro®, with an average dissolved oxygen concentration (measured in the well) of 26.4 mg/L, was injected into TW2 (the open bedrock well) at a rate of approximately 11 L/min for 44.2 minutes, then stopped for 29 minutes (to refill the tank) and then injected at 10.6 L/min for 37.8 minutes, for a total injection volume of 884 L. Dissolved oxygen (DO) and bromide concentrations were measured in TW2 as often as possible and at least every 5 minutes during injection.

TW2 continued to be monitored for 212 hours (8.8 days) until oxygen and bromine concentrations had returned to background levels (~5.2 mgO_2/L, and not detected, respectively). Concentrations of oxygen, bromide and iron at TW1 (all seven monitoring ports) were sampled as often as possible to generate the breakthrough curves. Sampling started 40 minutes after the start of the injection and continued for 212 hours. The observed distribution of oxygen and the conservative bromide tracer results from the injection test are provided below. Tabulated results are provided in Appendix E.

The pressure in the injection interval during injection, as monitored by the pressure transducer, reported an increase to ~ 50 m of head above the static level of ~ 4 m. This increase was noted during the first injection period, returned to static between the two injections, and then increased again during the second injection period before returning to static conditions for the remainder of the test.

4.4.1 Dissolved Oxygen Distribution

Breakthrough curves (concentration over time) were developed for oxygen at each monitoring point and the observations and interpretation at each of the monitoring points are provided below.

TW2- Within the injection well, the oxygen concentrations reached their maximum at the time of injection and decreased exponentially to 20% of the peak injection concentration after 44.25 hours, decreasing to less than 10% over the remainder of the monitoring period (212 hours) (Figure 4-6).

The shape of the breakthrough curve, characterized by sharp peaks and a diffusive-like tail, is consistent with that seen at another fractured bedrock site within a similar dolostone unit (Novakowski et al., 1995). The shape suggests that a significant amount of oxygen has entered the matrix around the injection well, assumed to be a result of advective transport due to the pressure gradients during injection. The diffusive-like tail noted on the breakthrough curves is a result of the back diffusion of the oxygen from the matrix. It should also be noted, however, that the migration of oxygen into the matrix is limited by the short injection time and possibly due to some loss of the injection pulse into the fractures.

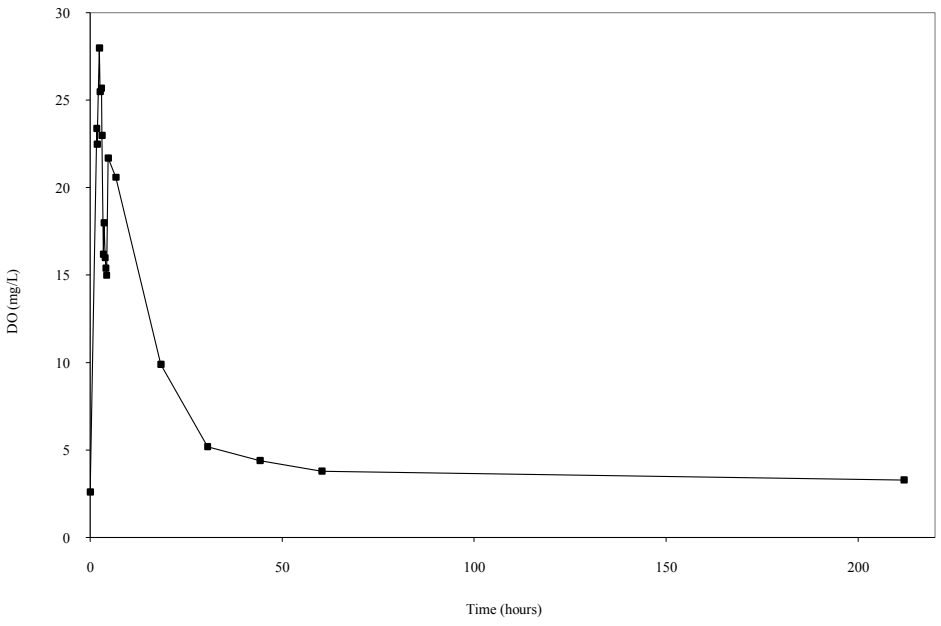

Figure 4-6 - Oxygen concentrations at the injection well TW2.

TW1-1 is located in the highly weathered and fractured Zone 1, above the injection zone. Oxygen concentrations rarely rose above background (1.8 mg/L); highest concentrations

were noted at or after 30 hours (4.8 mg/L) and again at 212 hours (4.7 mg/L) (Figure 4-7a).

The results indicate that there is no direct connection via a discrete fracture between the lower zone (injection zone) and the upper zone (Zone 1), consistent with the results of the initial tracer testing and cross borehole testing. The appearance of oxygen within this monitoring point at later times could indicate that there is a vertical component of flow between Zone 2a and the upper zone (Zone 1) despite the lack of hydraulic connection noted with the cross borehole test between these intervals.

TW1-2, 3 and 4 are completed in fractures within the upper discrete fracture network zone (Zone 2a) and above the injection zone in TW2. Based on their rapid response, it can be suggested that the oxygen pulses propagated rapidly through the fractures to these monitoring points 3 m down-gradient from the injection well. The breakthrough curves at each of these monitoring points are similar and mirrored those of the injected pulses (Figure 4-7 b). The concentrations of oxygen reached approximately 20 mg/L (8 to 22 mg/L) after approximately 2 hours in TW1-2 and TW1-3. At each of the monitoring points, the oxygen concentrations remained above background after 212 hours with a 70% reduction in concentration after the first 18 hours (Figure 4-7 b).

The rapid breakthrough of oxygen at these down-gradient monitor locations suggests the injection water had moved through the fractures by advective transport. In previous studies within fractured rock, peak tracer concentration arrival times and breakthrough curve shapes were found to change depending on the diffusion coefficient and on the distance of the monitoring point from the injection point (Novakowski et al., 1994 and 1995).

TW1-6 – A peak oxygen concentration of approximately 3 mg/L was reached after 4.5 hours. Concentrations remained above background levels for over 212 hours. The bulk of the oxygen was removed after 61 hours (Figure 4-7 c).

Based on the initial testing completed on site, this monitoring point was concluded to be located approximately 0.2 m from fracture 1 within Zone 2b (Figure 4-2). Because of its muted response, the shape of the breakthrough curve at TW1-6 is likely the result of diffusive transport within the matrix and not from direct transport within the fractures, as was seen in the monitoring points detailed above (TW1-2, TW1-3 and TW1-4). The response at TW1-6 can be explained by assuming that the injection pulse had migrated through the nearby fracture which was off-set by 0.2 m from TW1-6. From the fracture, the oxygen was transported by diffusion into the matrix, eventually reaching the monitor point.

TW1-7 – This monitoring point is within the lower aquifer zone (Zone 3). Oxygen concentrations at this monitoring point increased slightly over time, with a peak concentration of 3.7 mg/L (background of 0.11 mg/L) after 31 hours and remained slightly above background throughout the remaining monitoring period (Figure 4-7 d). The oxygen breakthrough at this location is consistent with the diffusion of oxygen through the matrix and into the monitoring point over time.

a)

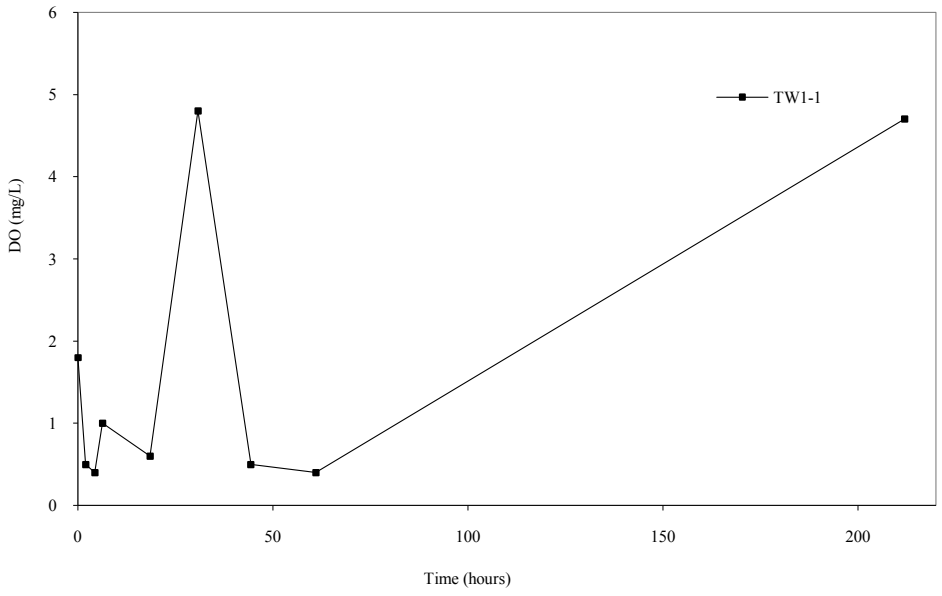

b)

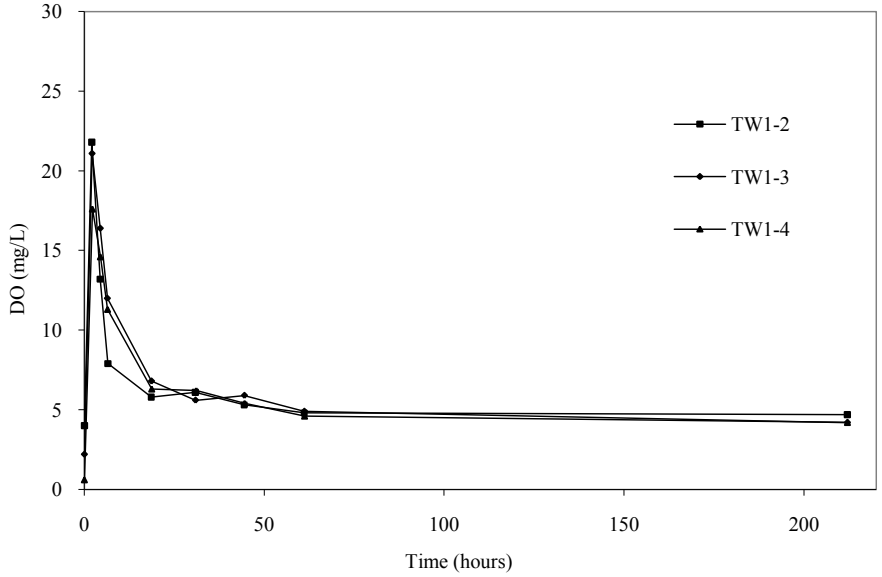
30
25
20
15
10
5
0
DO (mg/L)
0
50
100
150
200
Time (hours)
TW1-2
TW1-3
TW1-4

c)

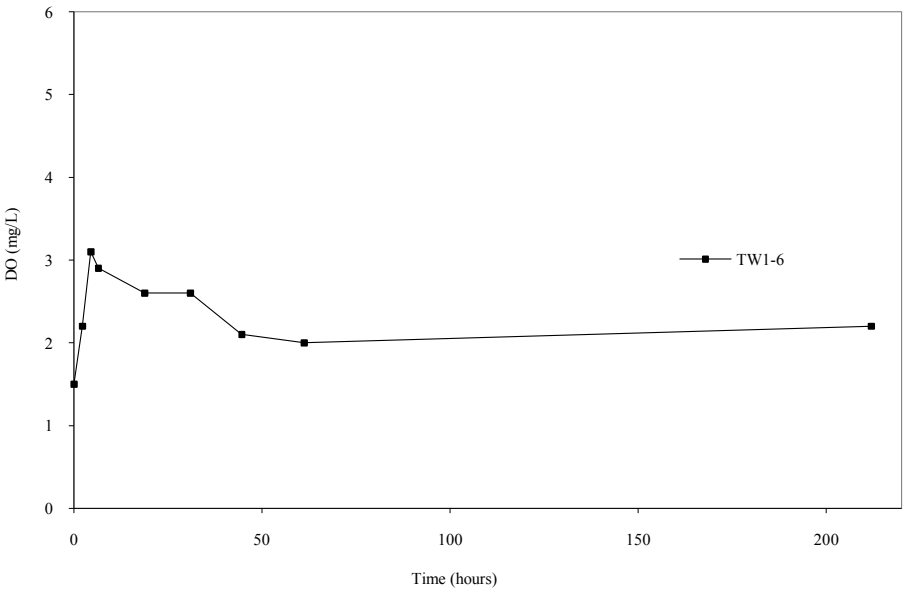
6
5
4
3
2
1
0
DO (mg/L)
0
50
100
150
200
Time (hours)
TW1-6

d)

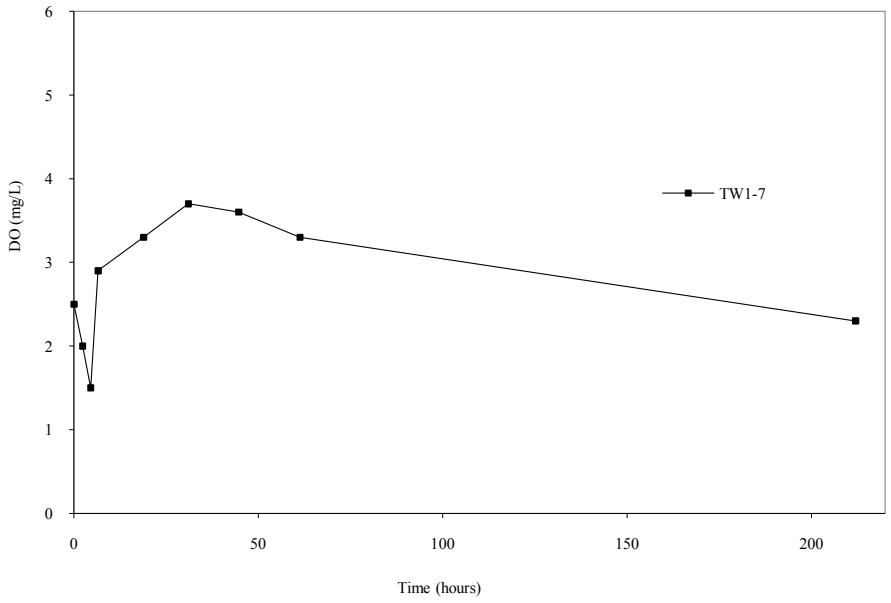

Figure 4-7 - Breakthrough curves for oxygen at the down-gradient monitor points at: a) TW1-1, b) TW1-2, 3, 4, c) TW1-6, and d) TW1-7. Note different concentration scale for plot b).

4.4.2 Tracer Distribution and Comparison

Bromide tracer breakthrough results were plotted as normalized concentrations (C/Co) versus time and were compared to oxygen concentrations. Results from the bromide breakthrough and the comparison at each monitoring point are detailed below.

In the injection well (TW2), the concentrations of oxygen and bromide followed similar initial trends (Figure 4-8). The concentrations peaked at the time of injection and decreased exponentially for the remainder of the monitoring period (212 hours). Over time the bromide concentrations decrease more rapidly to background conditions compared to, therefore a variation in the breakthrough curve tails can be noted (lack of diffusive tail on the bromide breakthrough curve). The variation in the breakthrough

curve tails confirms the transport of oxygen into the matrix and the resulting back diffusion over time.

Within TW1-1 (Figure 4-9a) bromide concentrations peaked after 2.6 hours (22 mg/L) and remained above background concentrations until after 44 hours before returning to background conditions. The bromide trends did not follow those of oxygen at later times with the oxygen concentration continuing to increase over time. The transport of bromide at this location confirms a vertical connection between Zone 1 and Zone 2a (initial transport of bromide and oxygen into Zone 1) and indicates that a portion of the transport is due to matrix diffusion with the oxygen concentrations increasing with time, but the bromide returns to background.

At monitoring points TW1-2, 3 and 4, bromide concentrations also reached a normalized concentration (C/Co) of ~1.0 after approximately 2 hours but the C/Co value for oxygen only reached 0.78, also after 2 hours. At each of the monitoring points, bromide concentrations returned to within the range of background concentrations (C/Co ~ 0.18) approximately 44 hours after injection. The rapid breakthrough of bromide at these down-gradient monitor locations confirms advective-dominated transport through the fractures (Figure 4-9a-d). The lack of diffusive tails noted with the bromide curves confirms the transport of oxygen into the matrix and resulting back diffusion.

The breakthrough curves for oxygen and bromide at TW1-6 are similar in shape but not magnitude (Figure 4-9e). The normalized (C/Co) concentration for oxygen is greater than that of bromide (peak concentrations of oxygen of C/Co = 0.14 after 1.42 hours versus C/Co = 0.08 after 4.5 hours). Concentrations remained above background levels for over 212 hours.

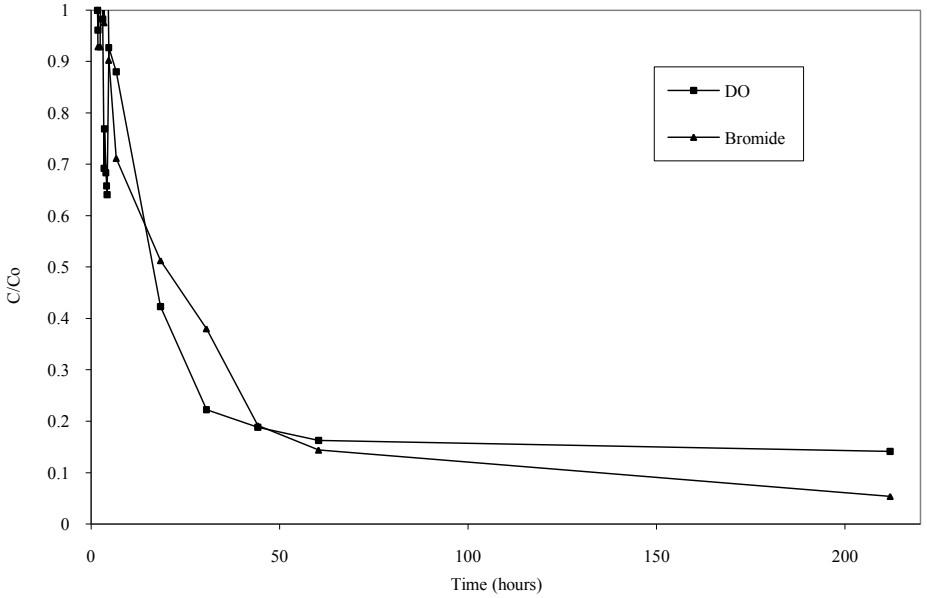

Figure 4-8 - Normalized concentration (C/Co) breakthrough plots for oxygen and bromide in the injection well, TW2.

The maximum normalized concentration of bromide measured at TW1-6 was 6 % less than that of oxygen and concentrations returned to background levels within 50 hours of injection while increased concentrations of oxygen persisted. Bromide concentrations returned to background levels quickly due the natural up-gradient water being flushed through the fractures (under natural groundwater flow gradients). These results confirm that the dissolved solutes were transported by advection through a nearby fracture and that oxygen transport into the monitoring point was a result of matrix diffusion.

The breakthrough curves for oxygen and bromide at TW1-7 are very different in shape and magnitude (Figure 4-9f). A peak normalized bromide concentration of C/Co = 0.48 was observed at about 61 hours. Oxygen concentrations above background were minimal with a peak of C/Co = 0.16 after 31 hours (background of C/Co = 0.11) and remained slightly above background throughout the remaining monitoring period.

The bromide breakthrough suggests that the transport was not dominated by diffusion but by advective transport through the matrix. This can be confirmed with direct hydraulic

connection noted between the injection well and TW1-7 from the cross borehole testing. The variation between the oxygen and bromide breakthrough curves could be attributed to the diffusion of oxygen into the matrix along the flow path or might be evidence of oxygen utilization within the system.

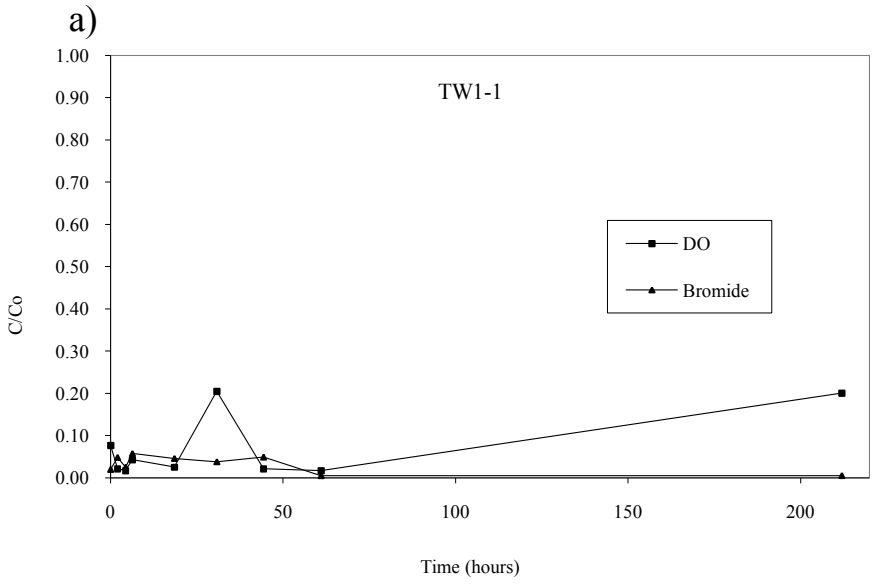

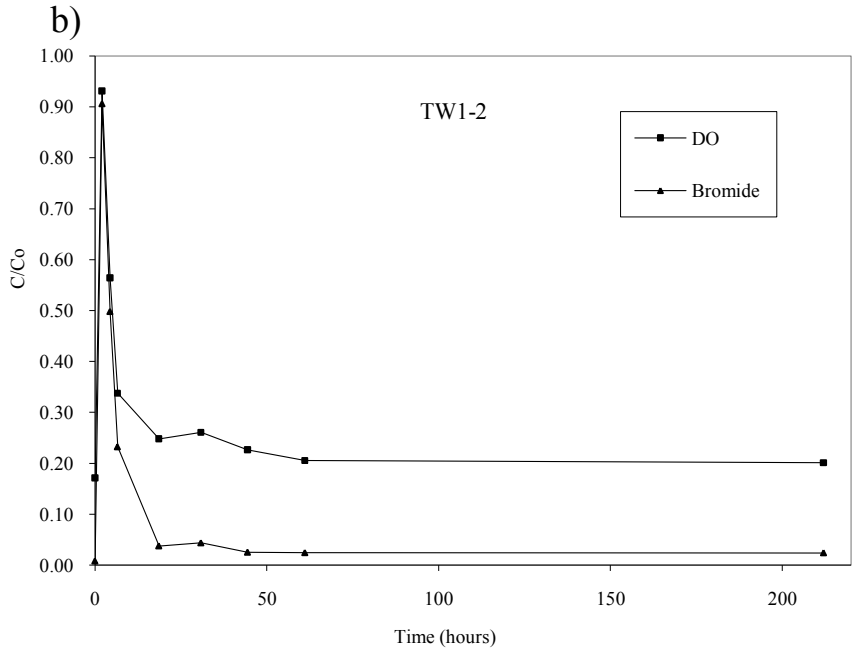

c)

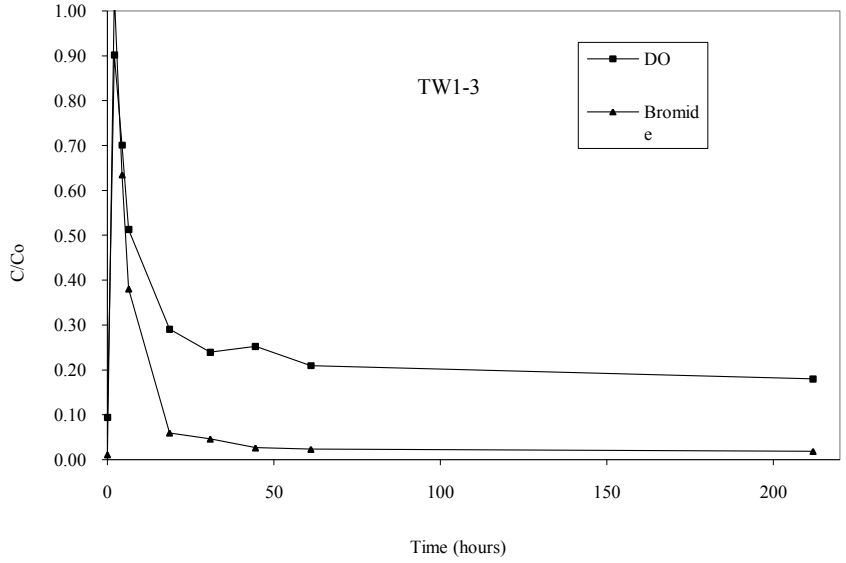
TW1-3
DO
Bromide
C/Co
Time (hours)
1.00
0.90
0.80
0.70
0.60
0.50
0.40
0.30
0.20
0.10
0.00
0
50
100
150
200

d)

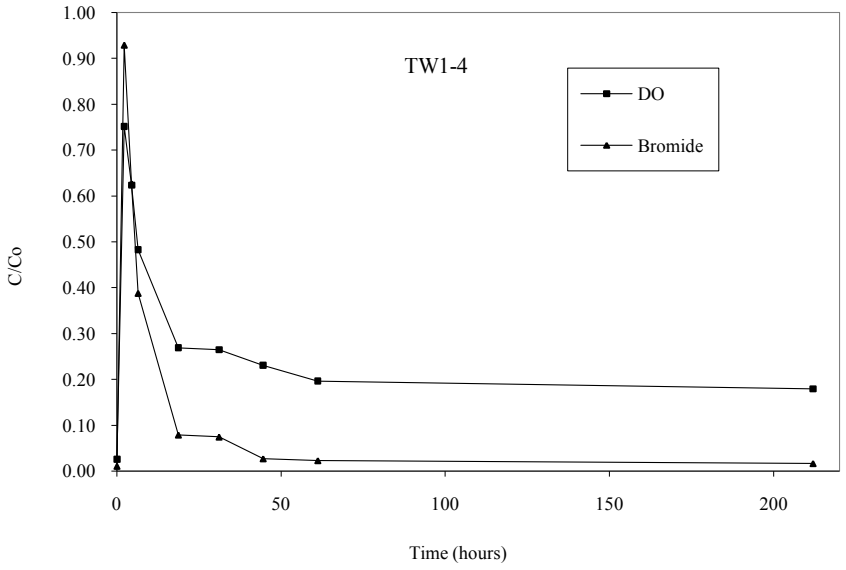
TW1-4
DO
Bromide
C/Co
Time (hours)
1.00
0.90
0.80
0.70
0.60
0.50
0.40
0.30
0.20
0.10
0.00
0
50
100
150
200

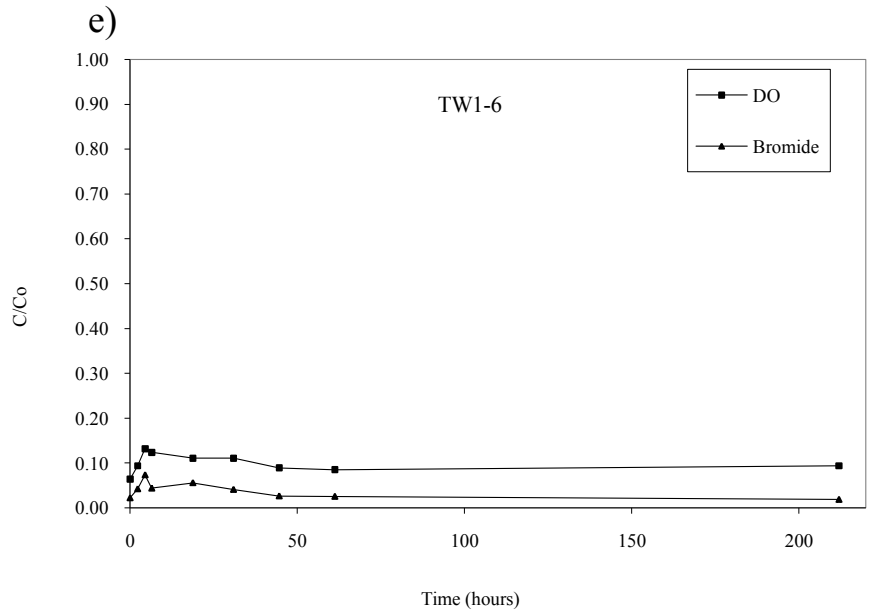

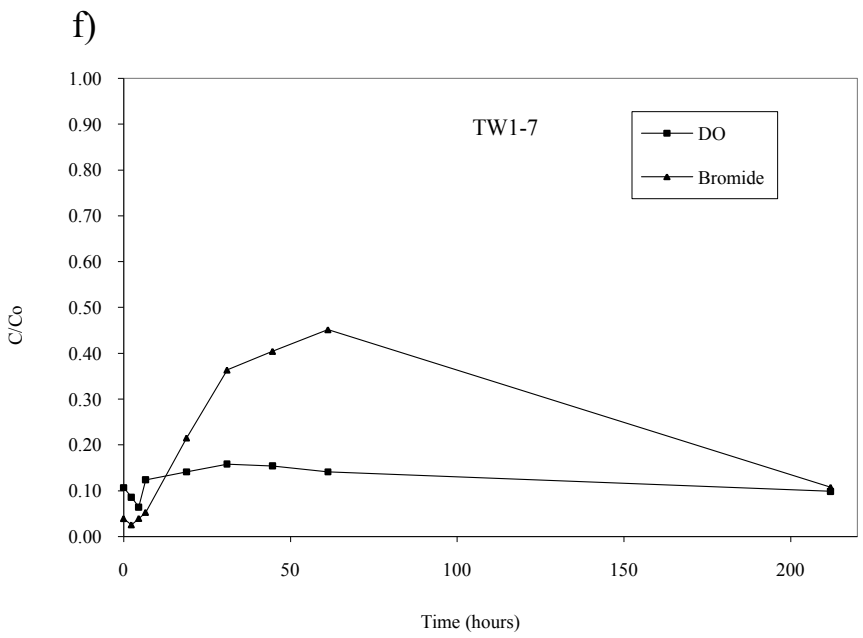

Figure 4-9 - Normalized concentration (C/Co) breakthrough plots for oxygen and bromide in a) TW1-1, b) TW1-2, c) TW1-3, d) TW1-4, e) TW1-6 and f) TW1-7.

4.4.3 Summary

Based on the results of the injection testing and the comparison between the oxygen and the bromide breakthrough curves, the mechanisms for transport of the solutes within the system were explained. The initial transport into the system was dominated by advective transport through the fractures and into the matrix and then transported down-gradient.

The main conclusion noted at several monitoring locations was that oxygen persisted somewhat longer than bromide. The persistence of oxygen was noted with the diffusive like tails seen on the breakthrough curves. The diffusive tails on the oxygen breakthrough curved could be attributed to a slower rate of back diffusion of the oxygen into the fractures.

The variation in diffusion rate of oxygen relative to bromide could be attributed to the variations in their diffusion coefficients. The bromide diffusion coefficient (D_o) is reported to be 1.1 x 10^{-11} m^2/s in water (Jardine et al., 1999), whereas the diffusion coefficient of oxygen is 5.0 x 10^{-9} m^2/s in water (Wilk et al., 1955). Neglecting the effects of tortuosity, tracers with larger molecular diffusion coefficients will be preferentially lost to the matrix porosity relative to tracers with smaller diffusion coefficients (Jardine et al., 1999).

Another factor that can contribute to the difference in shape between the oxygen and bromide breakthrough curves is oxygen utilization. Under conservative (non-reactive) conditions and advective-dominated transport, the normalized oxygen and bromide breakthrough curves would be similar in shape, as seen in TW1-2, -3 and -4. However, when the oxygen is utilized by microbial activity, the concentrations should decrease with respect to the (normalized) bromide concentrations (TW1-7). However in this field case, there is very little evidence of consumption of oxygen noted at the monitoring locations. This could be due to the high velocities in the fractures (measured at $8.7x10^{-4}$ and $1.37x10^{-3}$ m/s), relative to the rate of oxygen utilization (0.16 mg/L per hour, Johnston et

at., 1998). No additional work relating to the utilization of oxygen within the system was completed as part of this investigation.

4.4.4 Hydrocarbon Concentrations and Distribution

Prior to injection and for the duration of the monitoring period, samples were collected for analysis for BTEX and naphthalene, a PHC within the F1 range (Appendix C). The results are provided for reference purposes and not as an added objective of this thesis.

The variations in concentrations of the selected components analyzed prior to, during and after the injection, indicate that the injection created a slug of water that moved through the system to create a zone of treatment around the injection well and the down-gradient monitoring well.

4.4.5 Iron Concentrations and Distribution

The total iron concentrations within the monitoring points were measured prior to injection and for the duration of the monitoring period. The samples were collected to assess the potential change in oxidation conditions within the aquifer as a result of the addition of oxygen. The results are provided in Appendix E.

The concentration of iron at each of the monitoring points remained within the range of background concentrations with a standard deviation of less than 0.05 with the exception of concentrations at TW1-1. Concentrations at TW1-1 increased from a background concentration of 1.7 mg/L to 2.8 after 18.5 hours. The concentration fluctuated within 8% for the remainder of the monitoring period, peaking with a maximum above the method detection limits (>3 mg/L) after 212 hours. Similarly, the peak DO measurement was reported at 30.78 hours while the iron was within the elevated range.

5.0 Numerical Modelling

5.1 Introduction

The high-pressure oxygen injection experiment was simulated using the HEATFLOW/SMOKER model, a three-dimensional numerical model for groundwater flow and advective-dispersive transport within a discretely-fractured porous medium (Molson and Frind, 2009). The model was calibrated to the field conditions in order to reproduce the observed hydraulic pressure and distribution of dissolved oxygen within the system, and to predict the evolution of oxygen over time. The theoretical development and solution approach is detailed in Section 2.3 above.

The objectives of the modelling were to validate the conceptual model for the site, simulate the oxygen distribution within the fracture network and porous matrix (including long-term oxygen concentration levels during and after injection), and finally to test the sensitivity of key parameters in order to improve the focus and/or optimize field investigations at other sites.

To achieve the objectives of the modelling, a field-based model was first developed using the observed field site properties. Additional monitoring points were added to the model (within the matrix and along fracture number 2) to help evaluate the oxygen distribution within the system following the injection. The developed "field" model was then calibrated to the observed field conditions to obtain a best fit (base case), which required an increase in field-derived fracture apertures by a factor of approximately 3. The reason for the required increase in aperture to match the observed data is not well understood or well documented. Dickson and Thomson (2003) looked the variation in aperture obtained between a calculated hydraulic aperture (from field data) to a mass-balance aperture (based on tracer tests or in this case the model). They noted that calculated fracture apertures can vary up to three orders of magnitude depending on the field method used (hydraulic versus mass-balance). There study showed that the hydraulic fracture aperture

calculations to be sensitive to hydraulic head differences across the fracture plane and therefore the resulting apertures are often underestimated due to the tendency towards smaller apertures intercepted along the flow path. The calculations completed as part of this thesis used an average hydraulic head gradient, measured between two wells (TW1 and TW2) and not along a discrete fracture. This approach can potentially result in smaller fracture apertures and thus could explain the discrepancy between the field-calculated apertures and those required in the model.

The simulated base case flow system is shown by plotting the head distribution during injection as well as by plotting the velocities within the fractures and matrix. The transport behavior of oxygen in the base case simulation (and sensitivity runs) was also assessed using breakthrough curves at selected monitor points, as well as by plotting the oxygen distribution through the system (along the central vertical plane and within two transverse yz planes). A thermal simulation will be presented as an independent verification of the conceptual model used for the oxygen modelling.

Based on previous research (Chiang et al., 1989), it is assumed that any hydrocarbon biodegradation requires dissolved oxygen concentrations > 3.0 mg O_2/L. A concentration of 3.0 mg O_2/L was therefore used as a conservative base line to assess the distribution of oxygen within the system (lateral and transverse directions). However, it should be noted that all simulations herein assume oxygen is conservative, i.e. oxygen consumption by microbial hydrocarbon degradation is not considered. This assumption is supported by the lack of evidence of oxygen utilization in the field data. The conservative case thus provides the maximum potential extent of the oxygen within the system. It should also be noted that because the delivery of oxygen was the focus of the thesis, simulations for the conservative bromide tracer were not completed using the model.

Sensitivity analyses were completed to test the model and to assess the sensitivity of the model parameters on the distribution and transport of oxygen within the system. The need for the sensitivity runs stems from the uncertainty associated with measuring and estimating the parameters in the field. The calibrated (base case) model was varied by

adjusting the fracture apertures, hydraulic gradient, matrix hydraulic conductivity, diffusion coefficient and porosity. The sensitivity analyses are detailed in Section 5.5 below.

The model was also used to determine whether the system behaves as a discrete fracture network or as an equivalent porous medium. The effects of variable-aperture random fracture networks overlain onto a horizontal fracture network were also assessed to determine if a simplified horizontal fracture network was an accurate representation of the aquifer conditions. To further assess the effect of the bulk hydraulic conductivity on the system, a sensitivity run using a low matrix hydraulic conductivity and the random fracture network was completed.

The calibrated base-case model was then used to examine the potential for applying this oxygen delivery method for enhanced aerobic bioremediation and to help design further applications of the methods. Additional simulation runs with different injection scenarios were completed to assess the distribution and persistence of oxygen within the matrix (with no utilization) and within the zone of influence of the injection well (down-gradient and transverse).

5.2 Model Development

The numerical model was developed based on the site conceptual model and using the parameters measured in the field. The position of the model domain with respect to the field site is shown in Figure 5-1 and the position of the injection well (TW2) and the field monitoring well (TW1) with respect to the model domain is detailed in Figure 5-2.

The injection site was simulated using a 3D grid oriented parallel to the groundwater flow direction (Figure 5-3), and representing one-half of the full 3D domain. Symmetry was assumed about the y = 0 face containing the injection well, thus saving significant computational effort. The half-domain measured $15 \times 10 \times 10$ m in the x, y and z directions,

respectively, and was discretized with 78 x 40 x 62 (= 193,440) elements, being refined around the injection well and monitoring well.

The top of the model grid coincides with the top of the saturated rock (approximately 3 m bgs) and extends 10 m in depth (z); the model base is therefore at 13 m bgs. The injection well and the monitoring points were positioned on the grid relative to their position in the field and were assigned as breakthrough (monitoring) points in the model. The discrete fractures were positioned according to the site conceptual model (Figure 4-2) and the fracture apertures were adjusted based on the model response.

Flow boundary conditions were assigned using type 1 (Dirichlet) fixed heads at the up and down-gradient boundaries (left and right faces) and using a type 2 (Neumann) fluid flux boundary at the top boundary with a surface recharge rate of 1.0×10^{-9} m/s (3.2 cm/yr; Figure 5-4a). The remaining flow boundaries were assumed impermeable. For transport, depth-variable type 1 fixed oxygen concentrations were assigned along the up-gradient face according to the observed background concentrations. Zero-gradient (Neumann) conditions were assumed along all other transport boundaries (Figure 5-4b). Within the model, the input parameters and boundary conditions are assumed uniform in time, with the flow system assumed to reach steady state immediately after each change in injection rate. The effects of storage, temperature and fluid density are neglected.

The base-case model uses a simple set of horizontal planar fractures while more complex random fracture networks will also be assessed in the sensitivity analysis. The horizontal fractures were assumed to be continuous in the transverse (y) direction. Two upper fractures (8 and 9 in Figure 5-4) were added in the model to simulate the highly fractured upper zone (Zone 1). These upper fractures were needed to better match the bulk K of this zone and to be consistent with the site conceptual model (with $K = 1.0 \times 10^{-5}$ m/s as estimated from in the packer testing data). As will be shown, the addition of these upper fractures had little to no effect on the distribution of the injected oxygen, which occurred deeper within the system. The fracture aperture values detailed in Figure 5-4 are based on the calibrated base case (best fit) as detailed in Section 5.3.

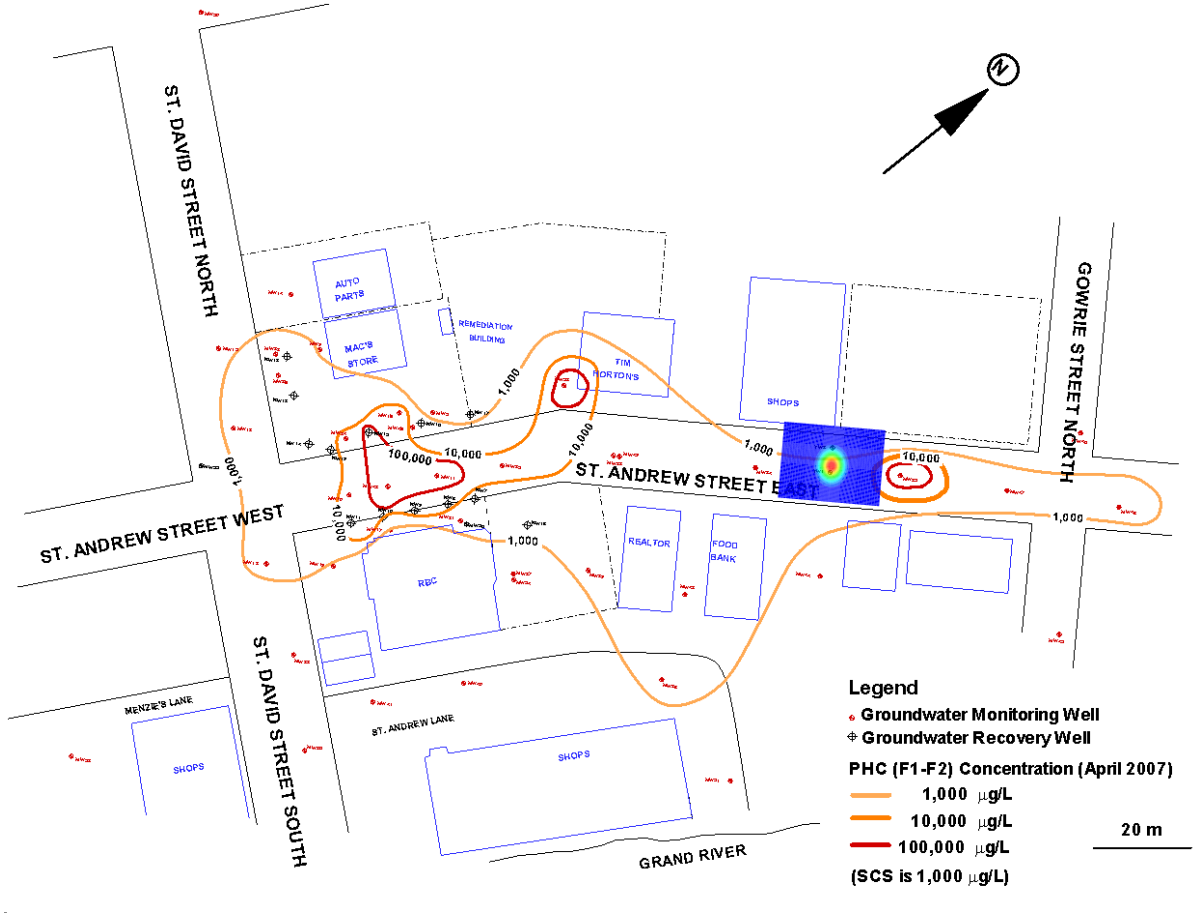

Figure 5-1 - Site location map with PHC (F1 + F2) groundwater plume delineated and model area defined.

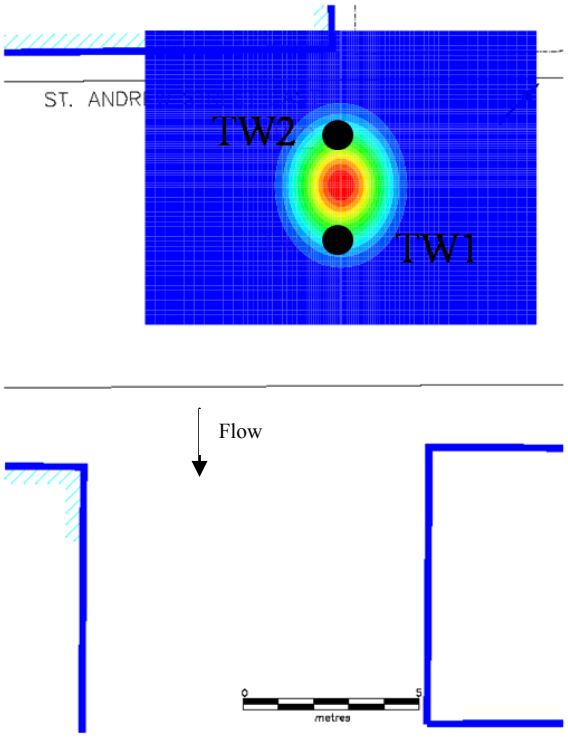

Figure 5-2 - Location of injection well TW2, down-gradient monitoring well TW1 and model domain.

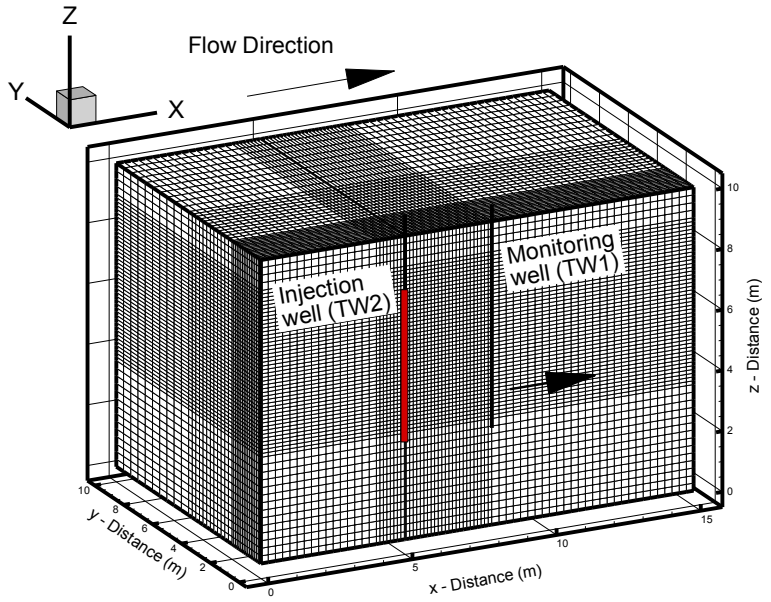

Figure 5-3 - Perspective plot showing the 3D model grid. The system is assumed symmetric about the y = 0 face.

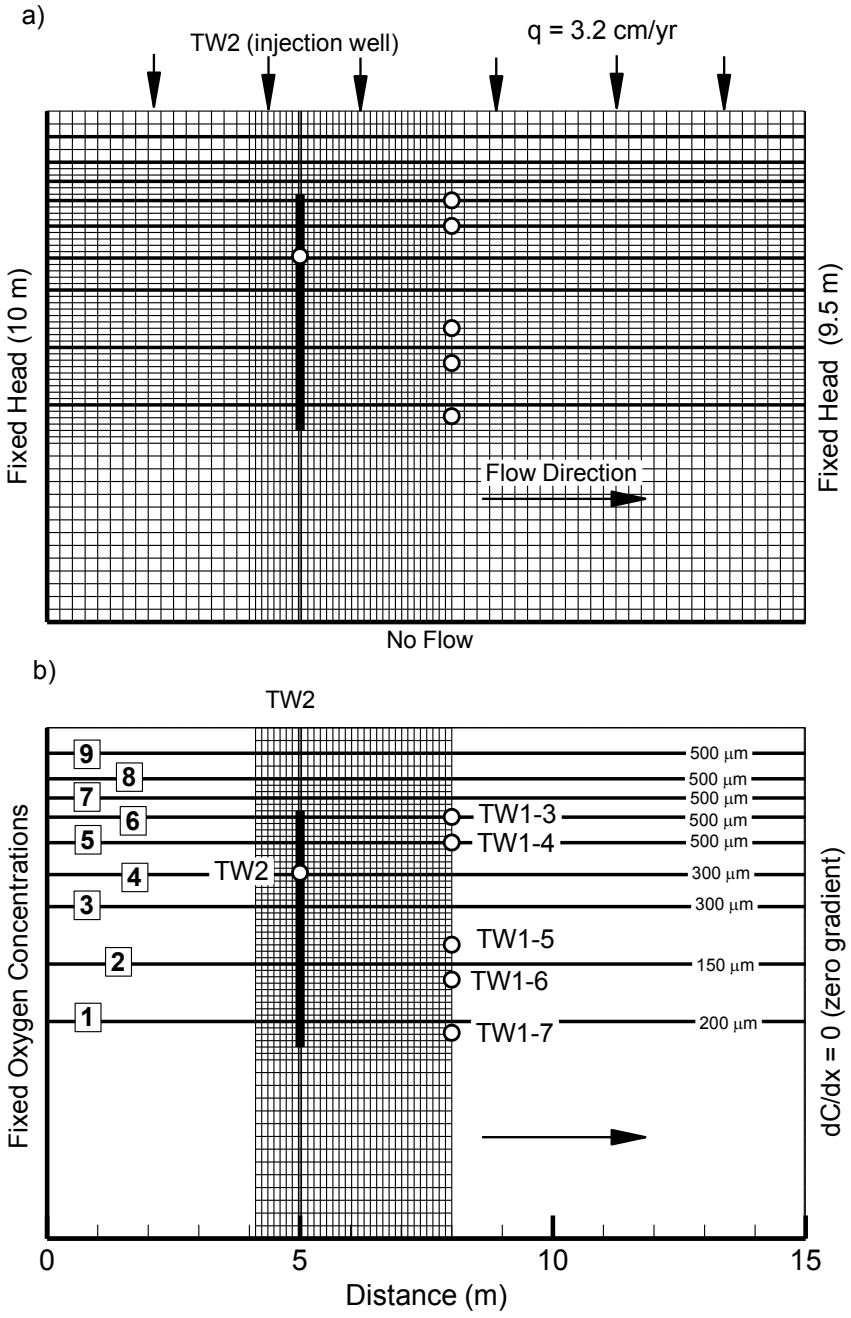

Figure 5-4 - Model layout and input parameters showing a) grid and flow boundary conditions and b) transport domain with monitoring points and fracture apertures identified. Fracture numbers are shown at left.

The initial oxygen concentrations were assumed horizontally uniform (vertically stratified corresponding to the fixed values along the up-gradient boundary face), varying from 0.004 to 0.0024 g O_2 / L based on background concentrations measured prior to the injection test on site.

The injection well was treated as a 6 cm diameter 1-D pipe element surrounded by a narrow high-K zone. The injected fluid was distributed uniformly along the 4-metre long well screen, together with the time-variable input concentrations determined from the field data. Injection conditions within the model were set to mirror those of the injection test with a two stage injection and a pause between injections (the injection rate was approximately 11 L/min for 44.2 minutes, then stopped for 29 minutes (to refill the tank), followed by another injection at 10.6 L/min for 37.8 minutes), as detailed in Section 3.2 above. The observed and model-input pressure curves during the injection periods are presented in Figure 5-5.

The physical parameters used in the model are detailed in Table 5-1.

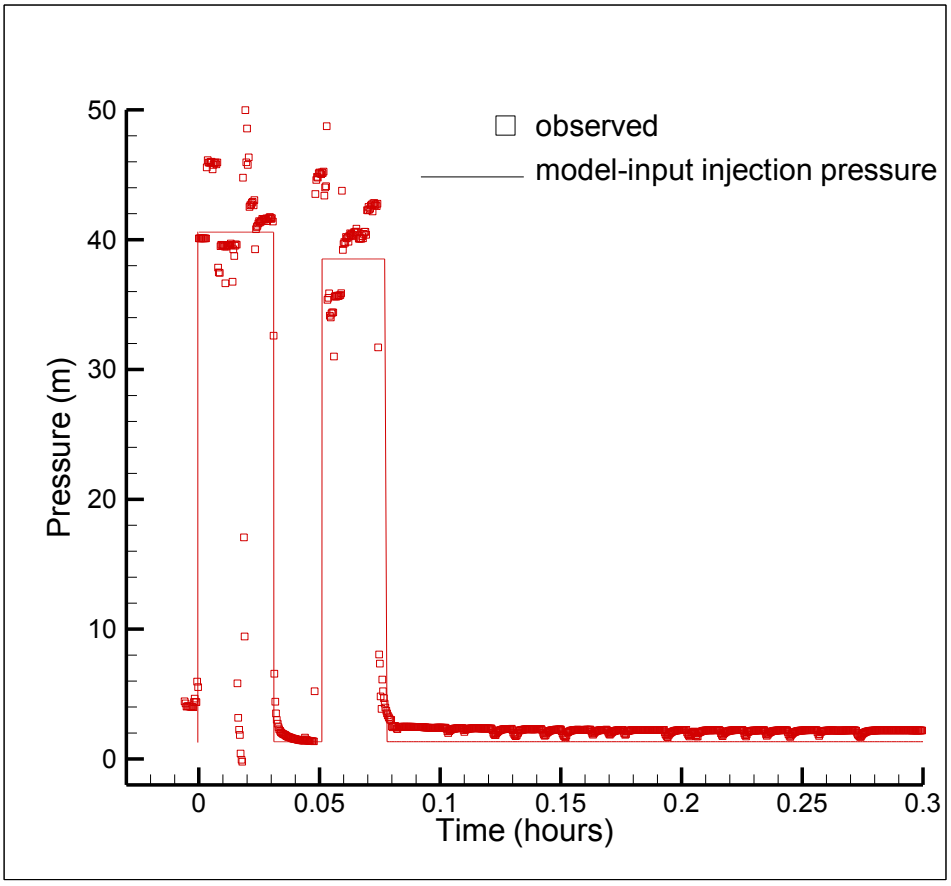

Figure 5-5 - Pressure curve comparison between observed and model-input injection pressures.

Table 5-1 - Base-case model input variables for the oxygen injection test.

Physical Variables	Value	Units
Longitudinal dispersivity (α_L)	0.2	m
Transverse horizontal dispersivity (α_{TH})	0.1	m
Transverse vertical dispersivity (α_{TV})	0.01	m
Retardation	1	
Matrix Porosity	0.15	
Hydraulic Conductivity	1.0×10^{-7}	m/s
Recharge	3.2	cm/yr
Hydraulic Gradient (between TW2 and TW1)	0.033	
Oxygen diffusion coefficient	5.0×10^{-10}	m^2/s

Model breakthrough (monitor) points were positioned to correspond with the monitoring points in the field (TW2, TW1-1 to -7). To further assess the behavior of the injected oxygen in the matrix and along the fractures, additional monitor points were added to the model. The first series of points (matrix points 8 to 12 in Figure 5-6) were positioned between fractures 2 and 3 to assess the conditions within the matrix and the oxygen breakthrough at various points along the flow path over time (one point at each of the following locations: up-gradient, in the injection well, between the injection well and the monitoring well, at the monitoring well and the end of the model domain). To monitor the same horizontal locations within the fractures, a second line of monitoring points was added to the model along fracture 2 (fracture points 13 to 17 in Figure 5-6).

The model was then calibrated to the field observations by adjusting the model parameters to obtain a best fit (base case).

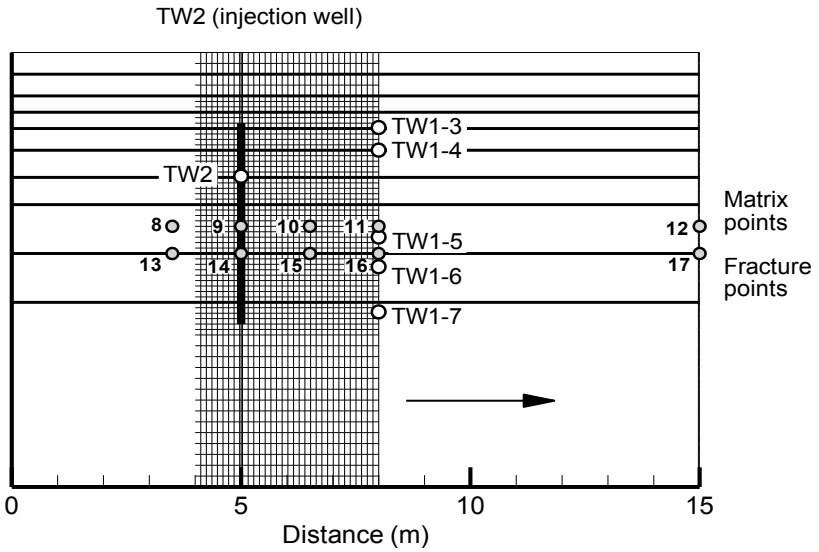

Figure 5-6 - Graphic showing layout of additional model monitoring points within the matrix (between fractures 2 and 3) and along fracture 2.

5.3 Base Case (Field-data)

Model calibration began by first selecting the estimated field parameters and simulating the oxygen injection test under these field-observed conditions. All model-input parameters for this field-data case are provided in Table 5.1. The field-data based simulated breakthrough curves are compared to the observed breakthrough curves in Figure 5-7. The flow simulation details for the field base case are consistent with that of the base case (best fit) and are therefore presented in Section 5.4.1 below.

Trends in the shape (peak and tails) of the breakthrough curves as well as the delay in the simulated peak arrival time of oxygen at the down gradient monitoring points (TW1-3 and 4) result in a clearly poor fit between the observed data and the field base case simulation. Although the peak concentrations are reasonable, the simulated decline in the oxygen concentrations within the injection well is significantly slower than observed, and there is a slight delay in the simulated arrival time of the peak concentrations at the down-gradient points TW1-3 and TW1-4, which are aligned with active fractures.

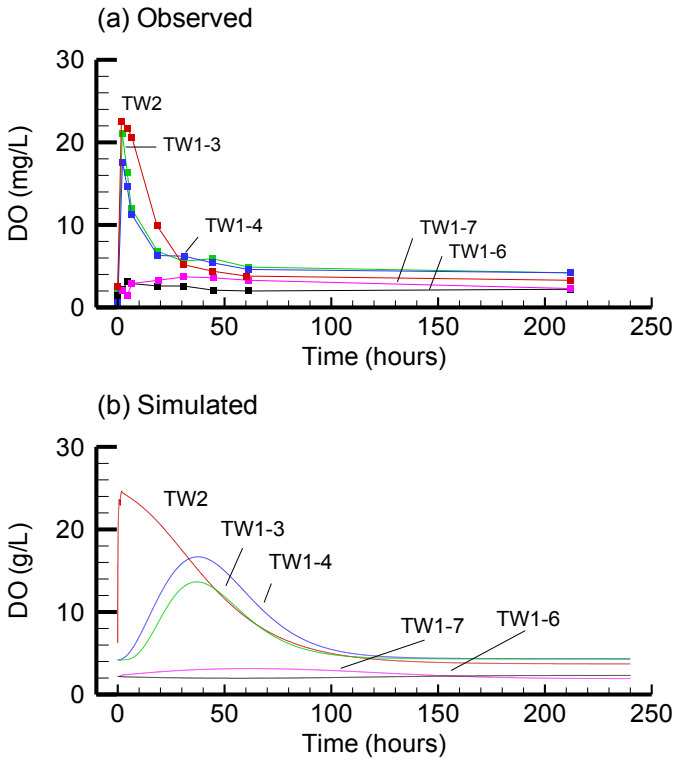

Figure 5-7 - Field case (un-calibrated) oxygen breakthrough curves a) observed and b) simulated.

Because of the poor initial fit, the field-based fracture apertures were modified during model calibration to obtain a best fit to the field observations. The calibration was completed by adjusting the fracture apertures and comparing the simulated and observed breakthrough curves at the injection well and down-gradient monitoring well. The simulated pressure distribution during injection was also compared to the observed injection pressures.

To obtain a reasonable fit to the breakthrough curves, the fracture apertures within the model had to be increased from those calculated using the cubic law and the given field data (Section 4.1.4). The apertures used in the best-fit model are compared to those calculated in the field in Table 5-2. The difference between the field-estimated and modeled best-fit apertures is at least in part due to the calculation of the hydraulic fracture apertures using general hydraulic head for the system (and not along the discreet fracture)

(Dickson and Thomson, 2003). Variations in aperture could also be a result of assumptions made in the cubic-law calculations.

Within the model, flow and transport is dominated by the horizontal fractures with some interaction with the matrix. In the field there are many small random fractures that are neglected in the model for simplicity. Therefore, a second argument for the field and model-derived aperture differences is that the model apertures must be larger to compensate for flow and transport in the neglected fractures. The transmissivity used to calculate the apertures in the field (equation 4) is derived from the packer testing completed on site. The hydraulic conductivity is then calculated based on the estimated transmissivity over the tested interval (in this case 1 m). The calculated hydraulic conductivity is a function of the bulk rock, taking into consideration the matrix and fractures. The calculated value underestimates the hydraulic conductivity of the fracture and therefore also underestimates the fracture aperture (directly proportional based on the cubic law).

During calibration, the uppermost limit of the injection interval was increased by ~ 1 m to extend above the packed-off interval in the field (~ 5.5 m bgs). This increase was required to provide a direct connection between the injection well and the fractures located at 4.55 and 5.2 m bgs (fractures 6 and 7; translating to monitoring points TW1-3 and TW1-4 down-gradient, respectively). Such a link was clearly required by the rapid arrival and decay of DO concentrations observed at TW1-3 and TW1-4. Although this observed behavior could also result from rapid but more circuitous pathways between the true deeper top of the injection screen and these down-gradient points, it is equally likely that some short-circuiting occurred directly along the well-bore into the overlying fractures. For simplicity, this latter case was assumed and the simulated injection interval was simply extended higher, resulting in the same effect.

5.4 Base Case (Best-Fit) Simulation

The calibrated base case model results were examined to provide insight into the oxygen distribution within the aquifer with a focus on the fracture network and porous matrix.

The HEATFLOW/SMOKER input file for the base case model run is provided in Appendix F.

5.4.1 Flow Simulation

The simulated steady state head distribution within the vertical cross section is shown in Figure 5-8. The calibrated model shows consistent head variations with the observed field conditions during and following the injections.

During injection a maximum pressure head of 40 m was reached within the injection well. The pressure is seen to dissipate along the discrete fractures and with distance from the well and is concentrated within the matrix between the fractures. Because storage is neglected, the heads within the system return to steady state conditions immediately following injection. The heads in the upper fractures are low because they are located above the injection zone (above the packer) and are thus isolated from the injection zone and are not influenced by the resulting injection pressures.

The velocities within both the matrix and fractures following injection are presented in Figure 5-9. Vectors showing the magnitude and direction of transport are detailed. High velocity vectors within the injection well were blanked in order to not interfere with the visual depiction of the matrix and fracture vectors. The vectors indicate that there is a significant component of advective transport into the matrix as well as through the fractures, but the matrix transport is limited compared to the fractures.

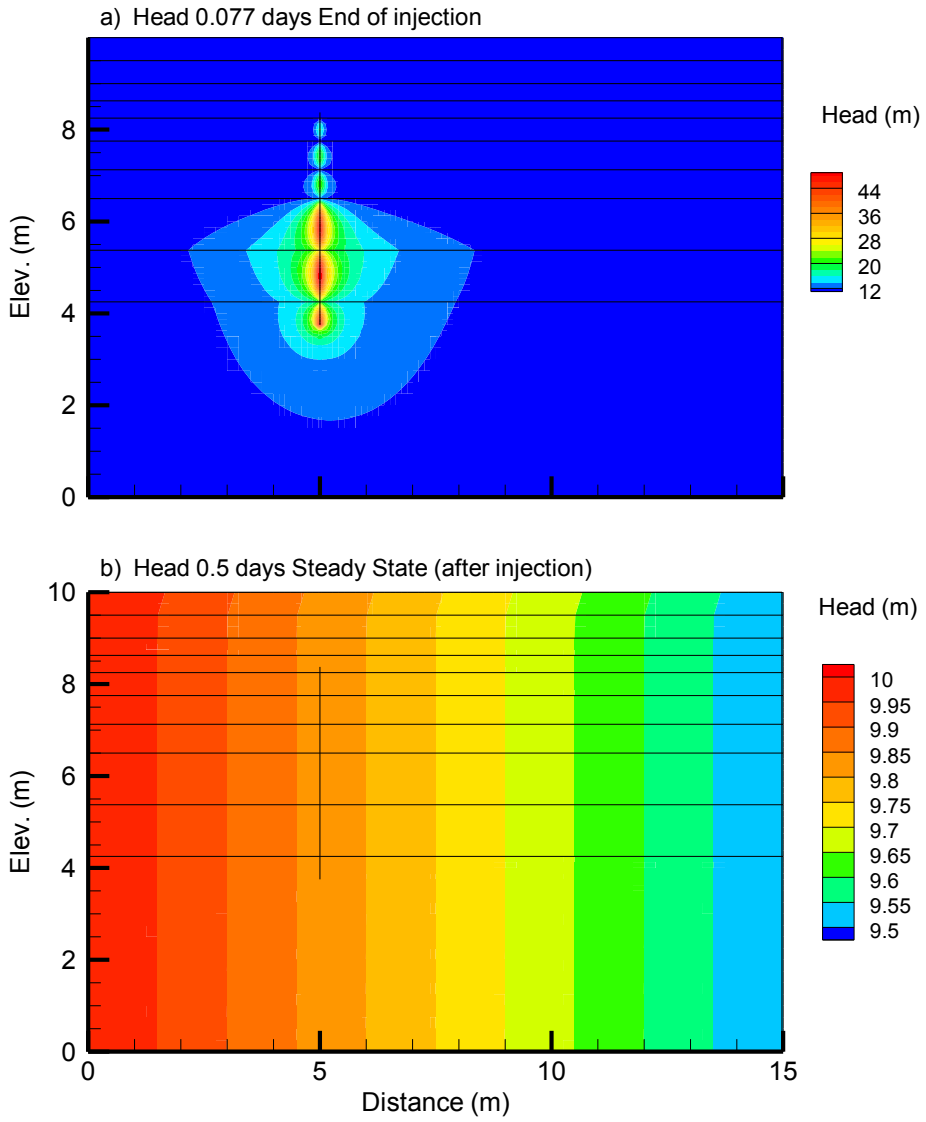

Figure 5-8 - Hydraulic head distribution a) during injection (end of second injection period) and b) steady state following injection.

Model-derived velocities within the fractures calculated based on the cubic law were compared to the field calculated velocities (Table 5-2). Model velocities are much higher than those calculated based on field parameters, which can be attributed to several factors. The higher simulated velocities are primarily due to the larger fracture apertures used in the model, as detailed in Section 4.1.4. The larger apertures were required to reproduce the observed oxygen breakthrough curves and were justified based on assumptions from the cubic law, including estimated transmissivity values and fracture

spacing. In addition, since the observed hydraulic gradient used to calculate the velocities was a local integrated gradient (measured between TW2 and TW1) and not a depth-discrete gradient measured within the discrete fractures, the field gradient may be underestimated. This would lead to an underestimation of the velocities.

Table 5-2 - Field and Model Variable Comparison (see Figure 5-4 for fracture positions).

Fracture Id	Fracture Depth (m bgs)	Field 2b (µm)	Field Velocity (m/s)	Model 2b (µm)	Model Velocity (m/s)
1	7.47	146	8.70E-04	200	1.63E-03
2	7.29	146	8.70E-04	150	9.20E-04
3	6.45	146	8.70E-04	300	3.68E-03
4	5.95	146	8.70E-04	300	3.68E-03
5	5.22	183	1.37E-03	500	1.02E-02
6	4.55	183	1.37E-03	500	1.02E-02
7	4.2	183	1.37E-03	500	1.02E-02

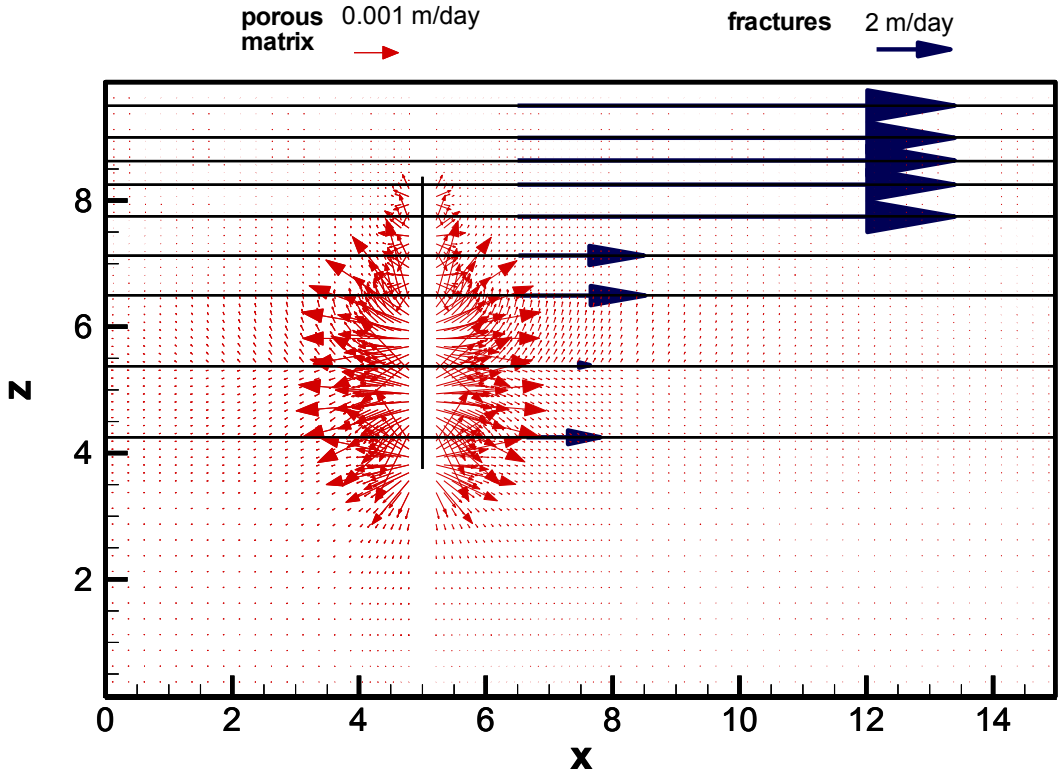

Figure 5-9 - Velocity vectors during injection within the matrix and the fractures.

The radial velocities within fracture 2 (identified in Figure 5-4b) are shown in Figure 5-10. An approximate 2 m radius of influence was noted within the fracture.

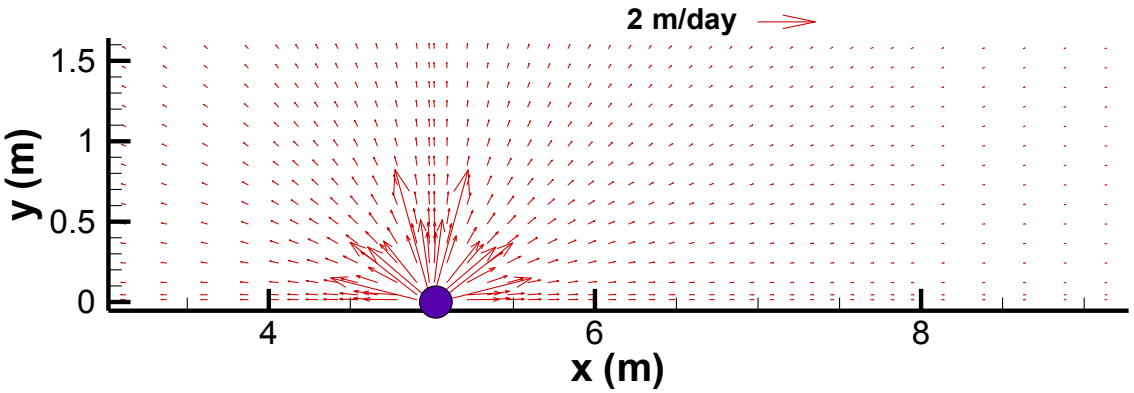

Figure 5-10 - Radial velocity vectors along fracture 2 in the horizontal (xy) plane.

5.4.2 Transport Simulation

The dissolved oxygen breakthrough curves from the calibrated base case (best-fit) model are consistent with those observed in the field (Figure 5-11).

The simulated results show similar trends to those observed with an initial sharp peak in the injection well (TW2) of 26 mg O_2/L, followed by a tailing with a decrease in concentration over time to background levels after approximately 50 hours. At the down-gradient monitoring locations TW1-3 and 4, similar trends were noted with simulated peak concentrations of 16 and 18 mg O_2/L, respectively; following injection, a rapid decline in concentration was noted before returning to background concentrations after approximately 20 hours. Small perturbations were noted in the simulated oxygen concentration at monitoring location TW1-6 and TW1-7. The response at TW1-6 was minimal with only a delayed gradual response over time to concentration above background. The concentration in TW1-7 also showed a delayed gradual response over time to a minimal peak concentration after approximately 50 hours.

Although the simulated responses at all monitor points provide a reasonably good match to the observed data (especially at the injection well), variations in trends between the observed and simulated breakthrough curves from the calibrated (best-fit) base model were noted. The most significant differences with the simulated results included a slightly delayed arrival time for the simulated peak DO concentrations at the down-gradient monitoring points (TW1-3 and 4) as well as a rapid, almost symmetrical decline (tail) at these points. The arrival curves here thus appear more pulse-like with limited evidence for diffusion-limited tailing. This could be the result, for example, of isolated highly-porous zones in the field that are not accounted for in the model. These zones would absorb oxygen, and then release it more slowly over time. On the other hand, the simulated oxygen concentrations within the injection well were an excellent match to those observed.

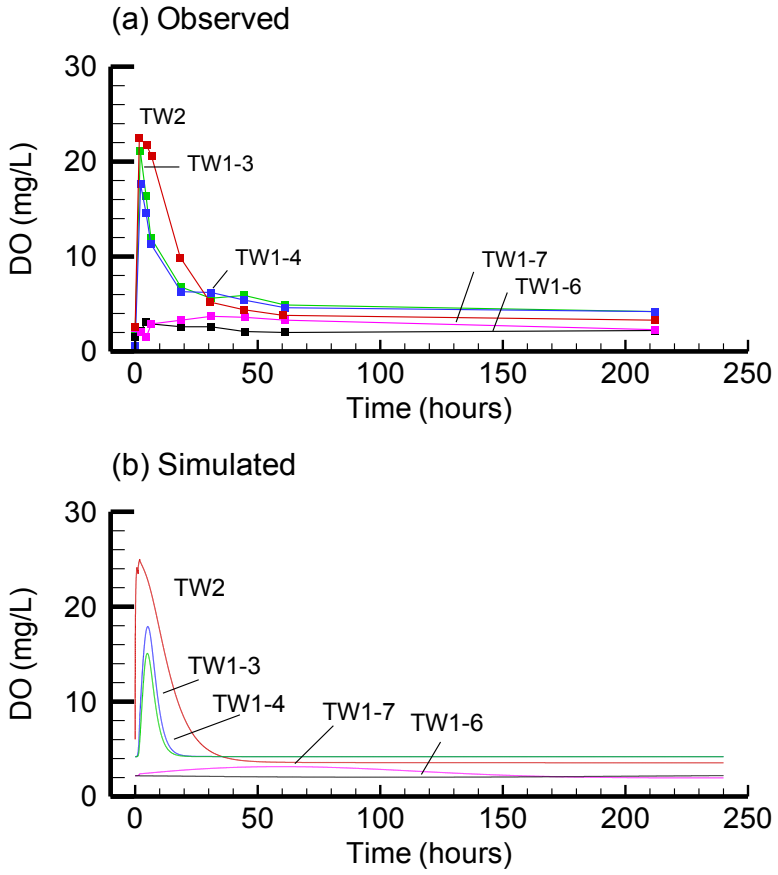

Figure 5-11 - Calibrated base case oxygen breakthrough curves a) observed and b) simulated.

The breakthrough of oxygen within the matrix can be observed by looking at the matrix monitoring points (points 8 to 12) that were added to the model (Figure 5-12b). Little to no oxygen above background levels was noted within the matrix in four of the five points (8, 10, 11 and 12). Additional oxygen was only noted at matrix point 9 within the injection well between fractures 2 and 3. The breakthrough curve for point 9 over the short term (during the injection test) shows a rapid increase in concentration to approximately 25 mg O_2/L with a gradual decrease to approximately 14 mg O_2/L over the 200 hours. The initial rapid decrease in concentration following injection is due to the flushing of the well with the slow decline in concentration and symmetrical tail over the 200 hours due to back diffusion of oxygen from the matrix. The shape of the breakthrough curve tail is indicative of transport and persistence of oxygen in the matrix over time.

Within the individual fractures (points 13 to 17) as seen in Figure 5-12c, the oxygen is initially forced up-gradient from the injection well (point 13) with a peak concentration during injection and then a gradual decline over time. At the injection well, the peak simulated concentrations within the fractures occurred during injection (point 14). Over time, the injected oxygen is transported down-gradient though the fractures, being flushed with clean groundwater as shown by the gradual increase and decrease of concentrations at the down-gradient points (15 and 16). No increase in oxygen above background concentrations was noted at the furthest down-gradient point (17).

The numerical model also allows for a visual depiction of the oxygen distribution over time and space. The oxygen distribution within the vertical xz symmetry plane is provided in Figure 5-13a showing oxygen concentrations at 0.077 days (end of injection), 0.5, 1 and 5 days.

The oxygen concentration contour plots show that during the injection period, the oxygen is transported rapidly by advection into the matrix surrounding the injection well and fills the local intersecting fractures. Peak concentrations of ~ 24 mg O_2/L were noted following injection. The transport of oxygen into the matrix around the injection well is

evident by the halo of oxygen concentrations (> 10 mg O_2/L) seen around the injection well (Figure 5-13a).

Following the 90-minute injection, the highest concentrations of oxygen are seen at the top of the injection interval (~30 mg O_2/L), but are quickly transported down-gradient through the fractures which are then rapidly flushed by the low-oxygen up-gradient water. Concentrations quickly decrease to background levels.

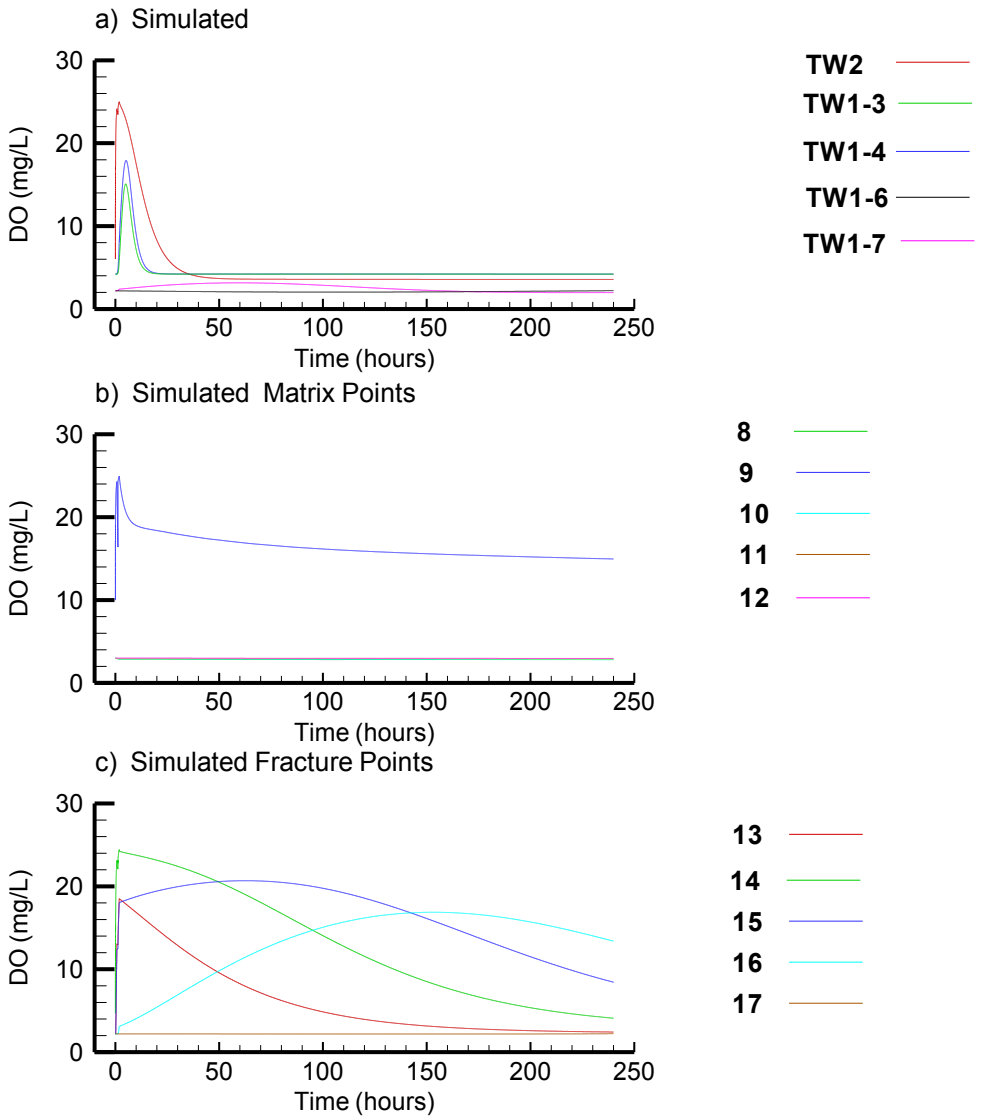

Figure 5-12 - Base Case oxygen breakthrough curves a) Simulated results at field observation points, b) matrix monitoring points and c) fracture monitoring points (see Figure 5-4 for monitor point locations).

Within the lower discrete fractures, the dissolved oxygen is transported primarily under advection, migrating with time down-gradient even after the injection stops. The rate of transport is slower in these lower fractures because of their smaller apertures and hence lower velocities. Transport into the matrix along the fractures can also be seen (e.g. at 5 days) with sharp concentration gradients into the matrix along the fracture surface interfaces. Evidence of transport into the matrix can be seen by observing the concentration halos that form above and below the fractures as the oxygen is transported down-gradient and the fractures are replaced with relatively oxygen-free water (Figure 5-13a). As the fractures are flushed with clean water, the oxygen in the matrix back-diffuses into the fractures (due to a reversal in the concentration gradients) which is likewise transported down-gradient.

With time, the oxygen is flushed from the injection well preferentially into the fractures. This can be seen by the layers of higher concentrations above and below the fractures within the injection well (Figure 5-13a) and by lower concentrations centered on the discrete fractures. Higher concentrations of oxygen, at ~26 mg O_2/L, persist within those intervals of the injection well which are not intersected by fractures since in these areas oxygen was not flushed as rapidly. The initial delivery of oxygen into the matrix surrounding the injection well was a result of pressure gradients, resulting in the initial deep oxygen penetration into the matrix around the injection well.

These trends are confirmed in the oxygen concentration profiles (g O_2/L) at two cross sections: AA' through the injection well and BB' at the down-gradient monitoring well (Figure 5-13b). Following injection, the oxygen concentration is uniform across the injection interval (AA') and small peaks of oxygen are seen at the down-gradient monitoring points (BB'). As time progresses, the oxygen is flushed through the fractures, causing dips in the concentration profile at the fracture intersections at AA' and peaks in concentrations at the fracture intersections in the down-gradient monitoring points (BB'). The persistence of oxygen in the matrix is apparent by the elevated oxygen concentrations between the dips in concentrations caused by the flushing of the fractures. As time progresses, the dips at AA' become wider as flushing of the fractures and back

diffusion of the oxygen from the matrix into the fractures continues. At the down-gradient monitor (BB'), the peaks in oxygen concentrations continue to increase (5 days).

The effects of transport into the matrix can be further examined by looking at the transverse distribution of oxygen within the system. For the base case, the transverse distribution of oxygen over time in the yz planes through the injection well and through the down-gradient monitoring points can be seen in Figure 5-13c.

The transverse advance of the oxygen plume (defined by the concentration contour of 3.0 mg O_2/L) into the matrix surrounding the injection well (between discrete fractures 2 and 3) is approximately 0.38 m after 5.0 days. Within the upper zone, the transverse distribution was limited to approximately 1 m following the injection (0.077 days) at the down-gradient monitoring location and did not persist with time or distance down-gradient (ie oxygen was not seen in the transverse direction within the upper zone at the down-gradient monitoring points following injection). With time, oxygen migrated down-gradient through the fractures, expanding in the transverse direction to approximately 1.5 m after 1 day. As time progressed, the transverse distribution at the injection well within the lower fracture after 1 day was approximately 1.7 m, therefore representing a 3.4 m diameter zone of influence transverse to the injection well.

To see the effect over time, the base case run was extended to 200 days. The results are presented in Figure 5-14 with views at 10, 50, 125 and 200 days. In the 200 day base case simulation (Figure 5-14a), the oxygen continues to be flushed from all the fractures over time (with no oxygen remaining after 50 days) but the oxygen persists in the matrix (concentrations >3.0 mg O_2/L) for the full 200 days. Oxygen is also flushed from the injection well (preferentially through the fractures and over time) where the oxygen had concentrated in the matrix and then back diffused to the open hole (Figure 5-14b).

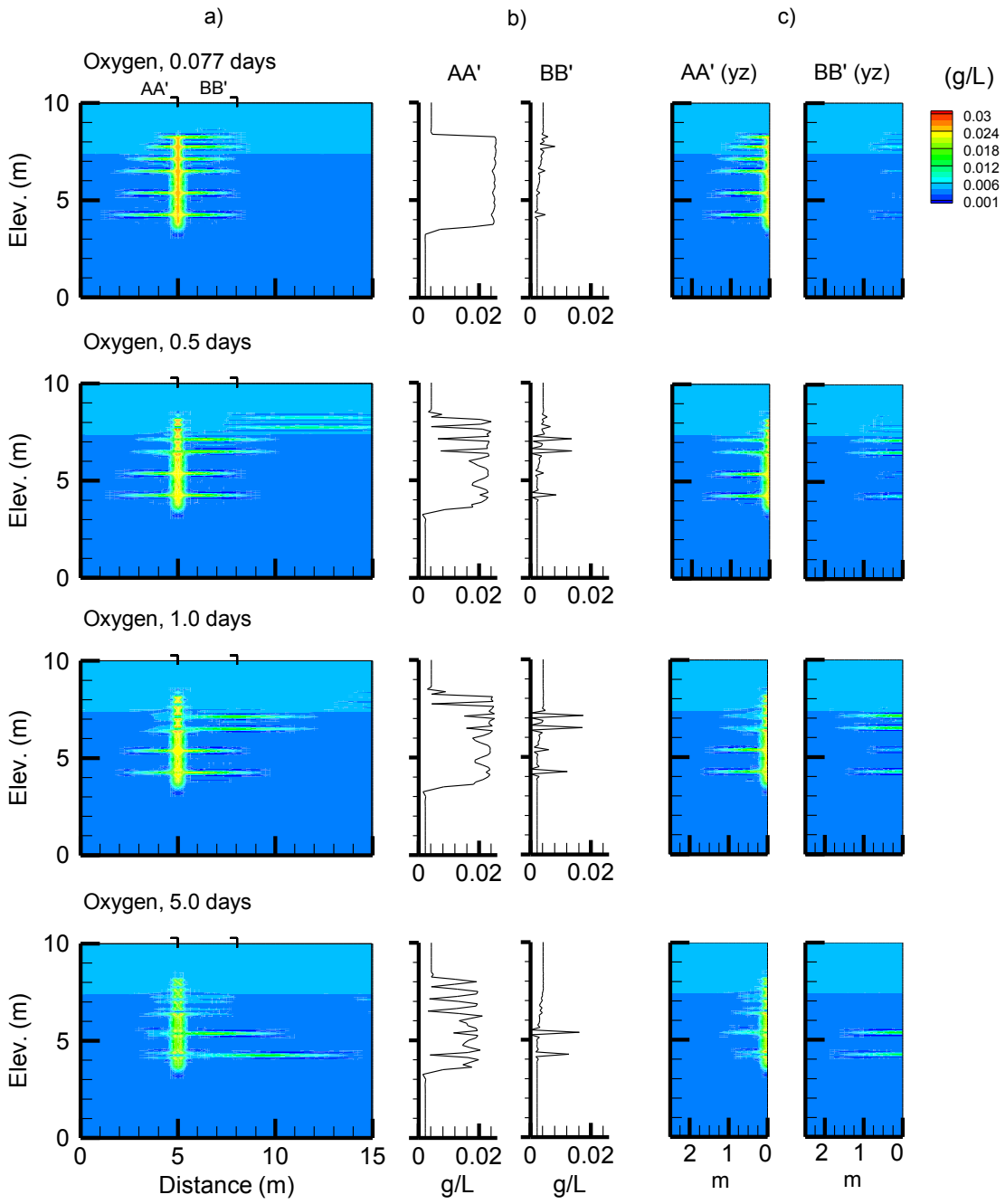

Figure 5-13 - Base case simulated oxygen distribution after 0.077, 0.5, 1.0 and 5.0 days a) plan view (xz), b) concentration profiles at AA' and BB' and c) transverse distribution (yz) at AA' and BB'.

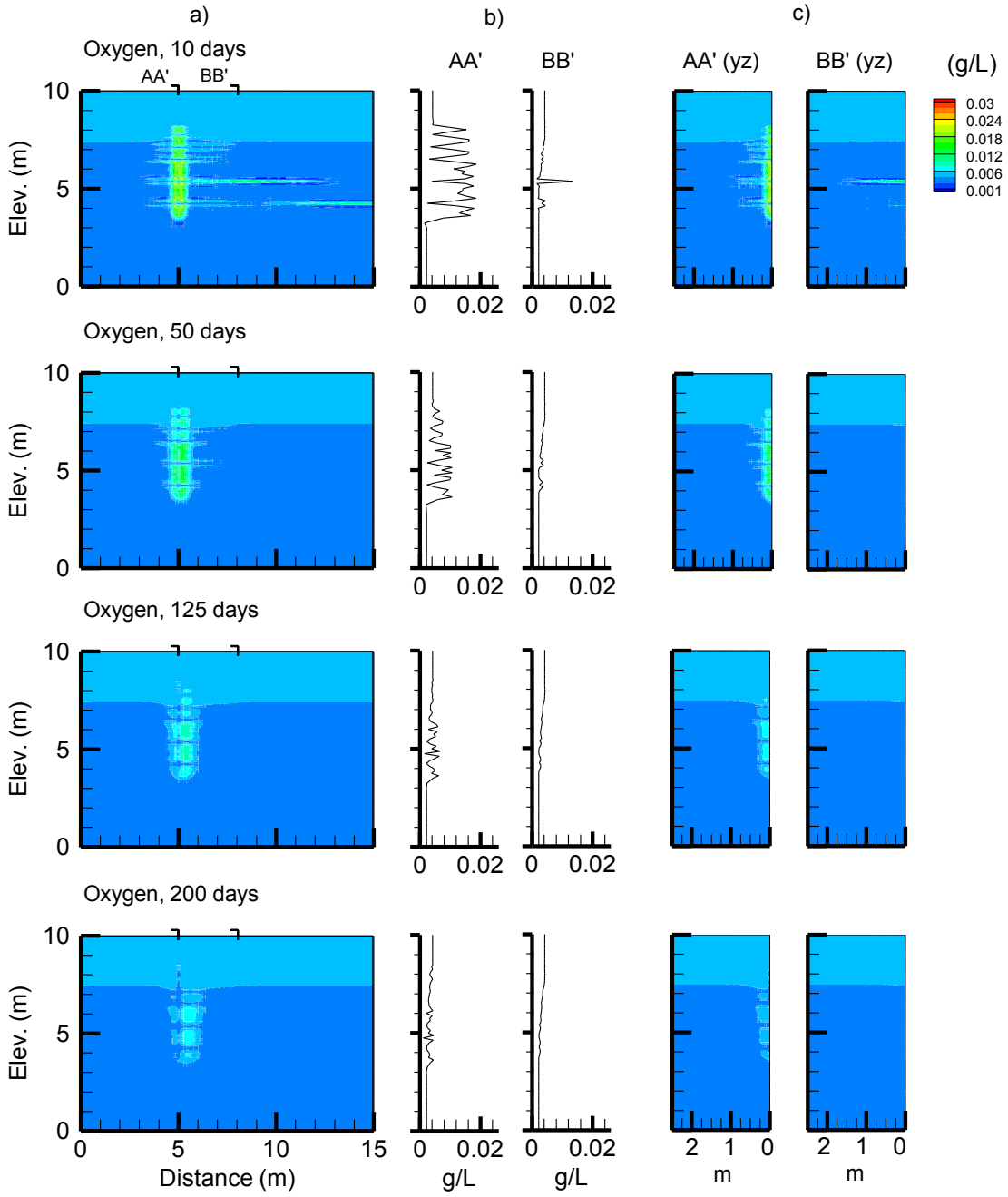

Figure 5-14 - Base case simulated oxygen distribution at 10, 50, 125 and 200 days showing a) vertical section (xz plane), b) concentration profiles at AA' and BB' and c) transverse distribution (yz) at AA' and BB'.

The transverse extent of the oxygen plume was found to decrease over time because the oxygen is flushed from the fractures and the oxygen stored in the matrix diffuses out. The transverse distribution is restricted to the oxygen in the matrix around the injection well (~1 m). The transverse distribution in the matrix persists around the injection well for the full 200 days with concentrations of ~ 3.0 mg O_2/L (Figure 5-14c). The transverse distance after 10 days within fracture 2 was limited to less than 1 m, as defined by an oxygen concentration of > 3.0 mg O_2/L. At the down-gradient monitoring point the transverse distribution in fracture 2 after 10 days was 1.7 m with concentrations of 3.0 mg O_2/L. No transverse distribution was noted down-gradient after 50 days.

Overall, the agreement between the simulated and observed breakthrough curves confirms that discrete factures play a defining role in the system behavior. It will be later shown in the sensitivity analysis that the observed system response cannot be reproduced using an equivalent porous media model.

5.4.3 Thermal Simulation

As an independent verification of the conceptual model used for the oxygen modelling, a thermal simulation was conducted using the same model developed for the oxygen injection simulations (HEATFLOW-SMOKER). The temperature data were obtained from a data logger positioned within the injection well (same logger which was used to log the pressure head during injection). The geometrical and physical conditions are identical in the thermal simulation to that of the base case (i.e. hydraulic gradient, fracture geometries and apertures, porosity, injection rates, etc.).

To simulate thermal transport, the hydrodynamic dispersion coefficient (D) in the input file was replaced by the thermal diffusivity κ (m^2s^{-1}), where : $\kappa = \lambda/C_o$, where λ is the thermal conductivity ($Jm^{-1}s^{-1}°C^{-1}$), and C_o is the heat capacity of the medium ($Jm^{-3}\,°C^{-1}$), defined as $C_o = \theta c_w \rho_w + (1-\theta) c_s \rho_s$, with θ being the porosity, and where c_w , ρ_w and c_s, ρ_s are the specific heats ($Jkg^{-1}\,°C^{-1}$) and densities (kgm^{-3}) of the water and solid phase, respectively (Molson et al., 1992; Molson and Frind, 2009). In this case, we use c_w =

4174 $Jkg^{-1}\,°C^{-1}$, ρ_w =1000 kgm^{-3}, c_s = 800 $Jkg^{-1}\,°C^{-1}$ and ρ_s =2630 kgm^{-3}. The base case value for the thermal conductivity of dolomite was chosen as λ=3.8 $Jm^{-1}s^{-1}°C^{-1}$ (Côté and Konrad, 2005), giving $\kappa=1.2\times10^{-6}$ m^2s^{-1}. In addition, the initial condition was fixed at a background temperature of 10 °C, and the water injection temperature was set to T=19°C for the first injection period and T=20°C for the second period. Temperature-dependent density (buoyancy) effects are also considered in the thermal transport model.

The observed and simulated temperature breakthrough within the injection well for three thermal conductivities (λ= 2, 3.8 and 5) are presented in Figure 5-15. While the λ=5 case is a somewhat better fit, this value is somewhat extreme and is shown only for sensitivity analysis purposes. The λ=3.8 case, derived from laboratory measurements on dolostone samples (Côté and Konrad, 2005), is considered the most realistic scenario.

All three simulated breakthrough curves show a slight deviation within the tail relate to the observed data. The early time deviations (following the injection) are indicative of greater thermal loss to the matrix due to the higher thermal conductivity values (Molson et al., 2007). The later time breakthrough curve tail shapes are a result of the rapid diffusion of heat stored within the matrix back into the fractures.

The thermal simulation shows that the observed temperature data collected in the field can be matched using the same conceptual model used for the oxygen modelling. The results provide an independent verification of the conceptual model used for the oxygen modelling.

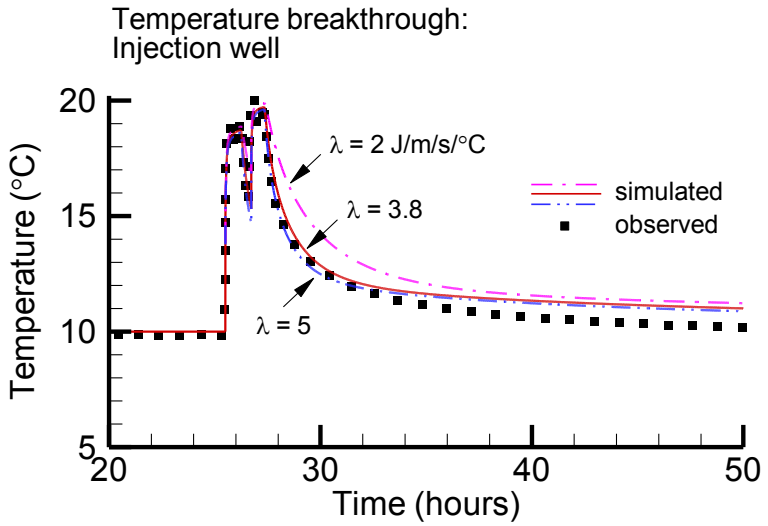

Figure 5-15 - Observed and simulated temperature evolution in the injection well, showing simulated results for thermal conductivities of λ=2, 3.8 and 5 $Jm^{-1}s^{-1}°C^{-1}$.

5.5. Sensitivity Analysis

Predictive simulations were run to validate the model parameters and to show their effect on oxygen distribution within the system. A summary of the runs completed is provided in Table 5-3. Key observations are summarized below and full graphical results are provided in Appendix G.

Equivalent porous medium

To first assess the applicability of the discrete fracture network model over an equivalent porous medium model (Scenario 1), a homogeneous non-fractured case was completed. The hydraulic conductivity of the rock matrix was increased to 1.0×10^{-5} m/s to simulate the bulk rock characteristics (including the unresolved fractures) but the remaining parameters were identical to the base case. The hydraulic conductivity value of 1.0×10^{-5} m/s was selected based on the results of the packer testing in which the bulk hydraulic conductivity (fracture and matrix) was calculated to be 1.0×10^{-5} m/s within the upper zones of rock.

Table 5-3 - Outline of sensitivity analyses performed with the model.

Scenario	Variable	Variation with respect to base case	Value
1	Equivalent porous medium bulk K	no fractures (homogeneous)	1.0 x 10^{-5} m/s
2a	Diffusion coefficient	10 × larger	5 x 10^{-9} m^2/s
2b		10 × smaller	5 x 10^{-11} m^2/s
3a	Apertures	2× larger	400, 300, 600 and 1000 μm
3b		2 × smaller	100, 75, 150 and 250 μm
4a	Gradient	Larger gradient	0.6
4b		Smaller gradient	0.01
5	Hydraulic Conductivity	Uniform low K	1.0 x 10^{-8} m/s
6a	Porosity	Lower n	0.075
6b		Higher n	0.3
7a	Random fractures	fracture sub set	mean aperture = 50 μm
7b		fracture sub set	mean aperture = 100 μm
7c		Uniform low K with random fractures	1.0 x 10^{-8}, 100 μm

The results show that the observed breakthrough of oxygen cannot be reproduced assuming a homogeneous system (Appendix G). Even with such a high K, the matrix cannot flush all the oxygen down-gradient rapidly enough and thus oxygen advances into the matrix surrounding the injection well with limited transport down-gradient (Figure 5-16). The discrete fractures are clearly needed to transport the oxygen rapidly down-gradient as the observed conditions show. An equivalent porous media model is thus not a valid approach in this type of system.

Diffusion coefficient

The diffusion coefficient was first increased by an order of magnitude (relative to the base case) to 5.0 x 10^{-9} m^2/s (Scenario 2a). The increase showed little to no effect on the breakthrough of the oxygen within the monitoring points or the matrix (Appendix G). Within the fractures, an increase in matrix diffusion (into the matrix along the fractures) was noted with time (Figure 5-17), resulting in less transport of oxygen down-gradient within the fractures (8 m down-gradient versus 9 m in the base case for concentration of

> 3 mg O_2/L). No significant difference in the transverse distribution of oxygen was observed (1.5 m after 1 day with concentration > 6 mg O_2/L). A decrease in the diffusion coefficient by an order of magnitude to 5 x 10^{-11} m^2/s also had no significant effect (Appendix G) (Scenario 2b) with breakthrough curves consistent with the base case. The oxygen distribution is also consistent with that of the base case.

Fracture apertures

The base case model has effectively shown that the dominant flow component is within the fractures. Fracture apertures were then varied (by factors of two larger and smaller) to evaluate their effect on the flow system. For these two cases, the background natural hydraulic gradient was kept constant at the base-case value. With an increase in aperture by a factor of two (Scenario 3a), the transport velocity of oxygen down-gradient within the fractures was significantly increased (Figure 5-18). With more rapid flushing and thus less time for diffusive losses into the matrix, the persistence of oxygen within the system decreased (concentrations greater than 3 mg O_2/L were not reached within the fractures after 5.0 days). The transverse distribution was also reduced due to the stronger component of advective transport down-gradient within the fractures (Appendix G). The transverse distance after 1 day within fracture 2 was limited to less than 1 m with an oxygen concentration of less than 3 mg/L. With a reduction in the fracture aperture by a factor of two (Scenario 3b), advective transport down-gradient within the fractures was reduced and diffusive transport of oxygen into the matrix increased, thus increasing the persistence of oxygen within the system (Appendix G). Concentrations > 3 mg O_2/L were noted 2 and 4 m down-gradient in fractures 2 and 1, respectively and after 5.0 days.

Hydraulic gradient

Variations in the hydraulic gradient had similar effects to the changes in fracture aperture. With an increased gradient (Scenario 4a), there is more rapid transport of the oxygen down-gradient within the fractures (Appendix G) (concentration of > 3 mg O_2/L 4 and 6 m down-gradient in fracture 2 and 1, respectively after 1 day). Little effect on the

transport into the matrix or on transverse transport was noted. Opposite effects were noted with a decrease in the hydraulic gradient (Appendix G) (Scenario 4b), in which transport through the fractures was delayed allowing more time for matrix diffusion and therefore increasing the persistence of oxygen within the system. Concentrations > 3 mg O_2/L only reached 3 and 4 m down-gradient in fracture 2 and 1, respectively after 1 day.

Hydraulic conductivity

In this scenario, the hydraulic conductivity of the un-fractured rock matrix was decreased by an order of magnitude relative to the base case (to 1.0 x 10^{-8} m/s) to assess its effects on oxygen transport within the system (Appendix G) (Scenario 5). The uniform decrease in hydraulic conductivity of the rock reduced the pressure-induced advective transport of oxygen into the matrix surrounding the injection well; oxygen was therefore forced more preferentially into the fractures and was then rapidly transported down-gradient (Figure 5-19). Concentrations of ~ 28 mg O_2/L were noted 1 and 1.5 m down-gradient in fractures 2 and 1, respectively after 1 day. The reduced hydraulic conductivity had the same effect on transport into the matrix as seen at the injection well, with less advective transport of oxygen from the fractures into the surrounding matrix and therefore less persistence in the matrix and more rapid transport of oxygen down-gradient.

Matrix porosity

In these scenarios, the porosity of the rock was increased and decreased by a factor of two. An increase in the porosity (Scenario 6a) allowed for more diffusion and less advective transport of the oxygen into the rock matrix, therefore causing less oxygen to be transported down-gradient within the fractures (Appendix G). Oxygen concentrations > 3.0 mg O_2/L were only noted 2.5 and 3.5 m down-gradient in fractures 2 and 1, respectively after 1 day. Opposite trends were noted with the decrease in porosity (Scenario 6b) (4.5 and 6.5 m transport down-gradient within fractures 2 and 1, respectively). With lower porosity, less oxygen was transported into the matrix and therefore more was transported down-gradient within the fractures (Appendix G).

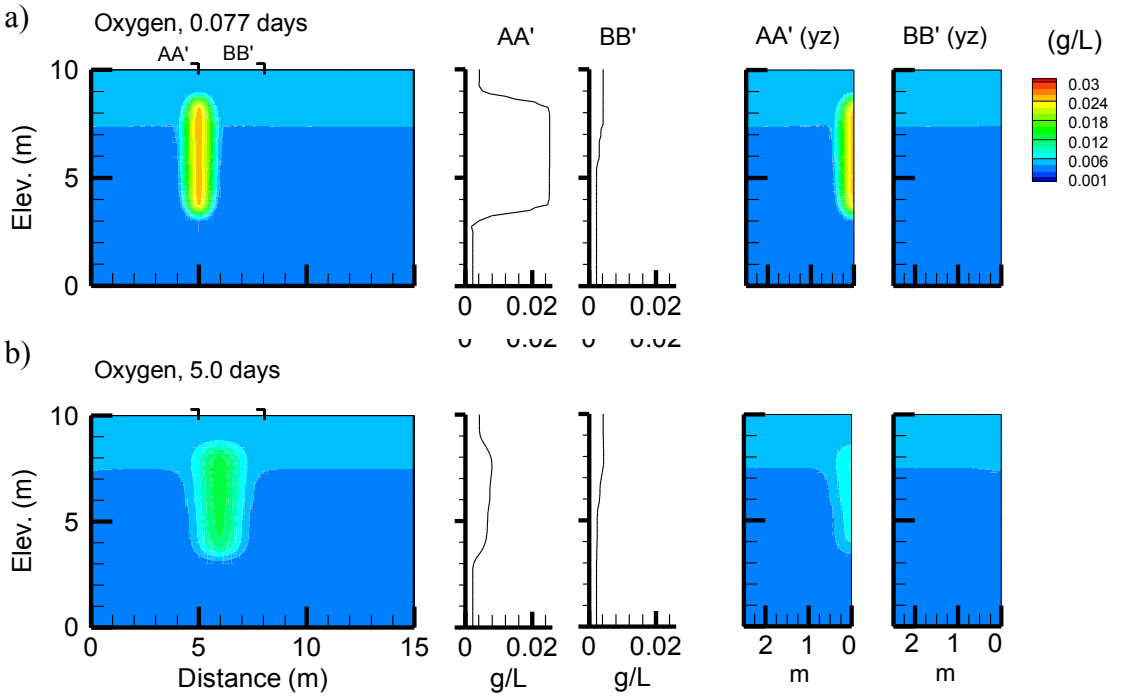

Figure 5-16 – Simulated oxygen distribution under homogeneous, non-fractured conditions (Scenario 1) after a) 0.077 days and b) 5.0 days.

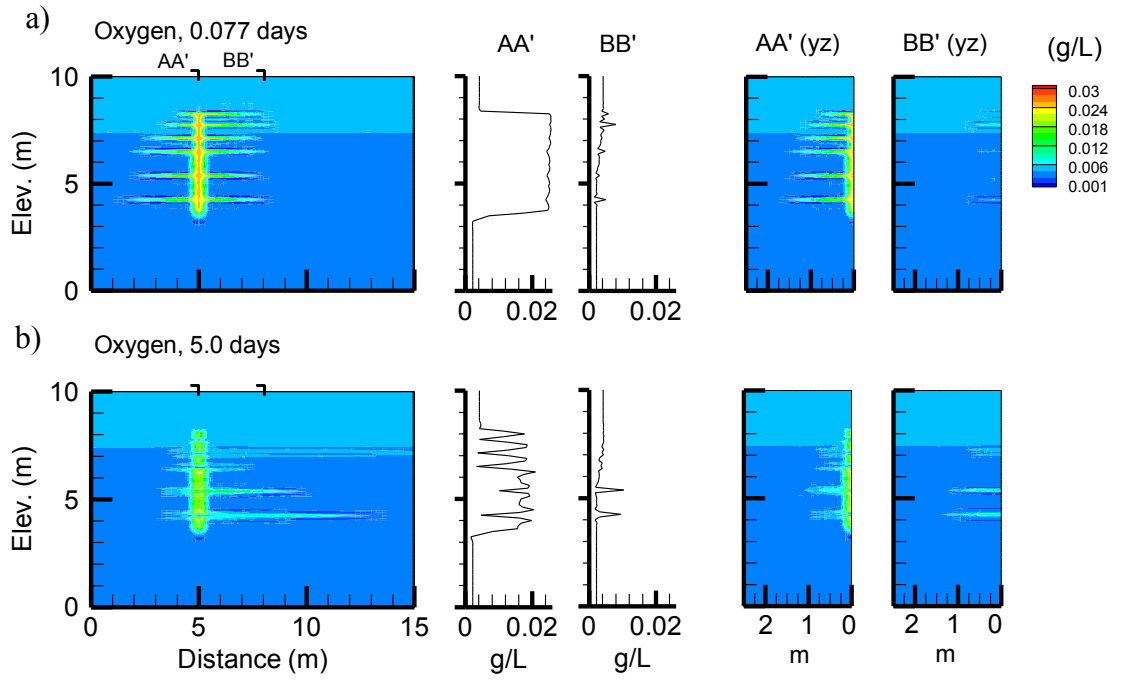

Figure 5-17 – Simulated oxygen distribution with 10 × higher diffusion coefficient (Scenario 2a) after a) 0.077 days and b) 5.0 days.

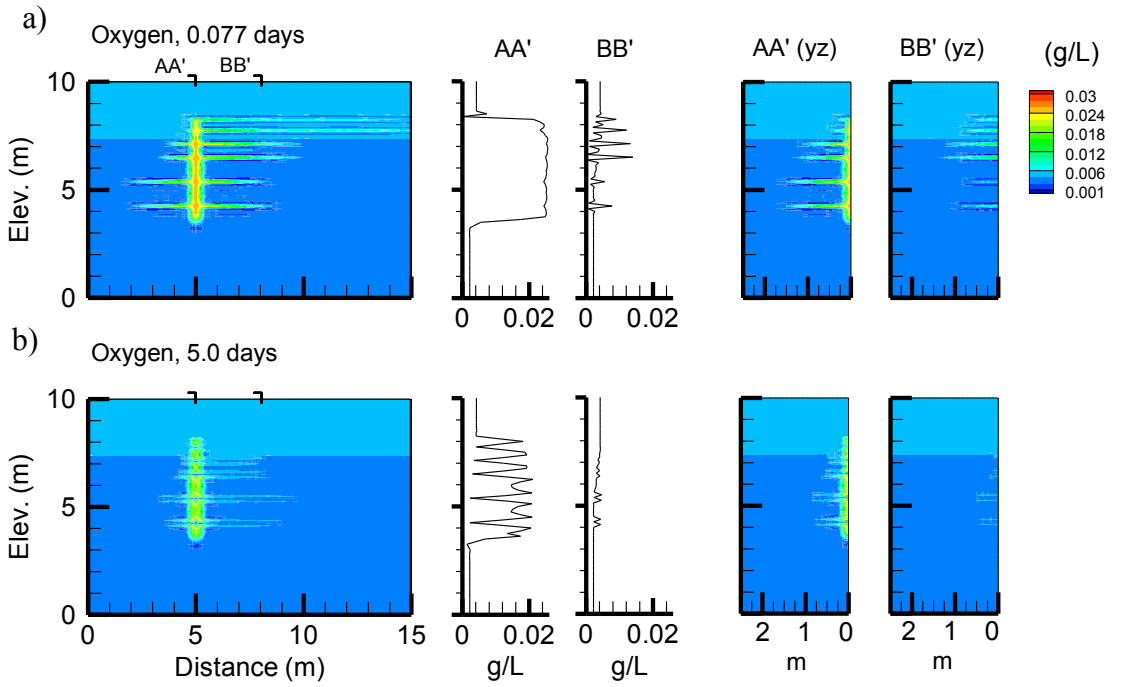

Figure 5-18 – Simulated oxygen distribution with 2 × larger fracture apertures (Scenario 3a) after a) 0.077 days and b) 5.0 days.

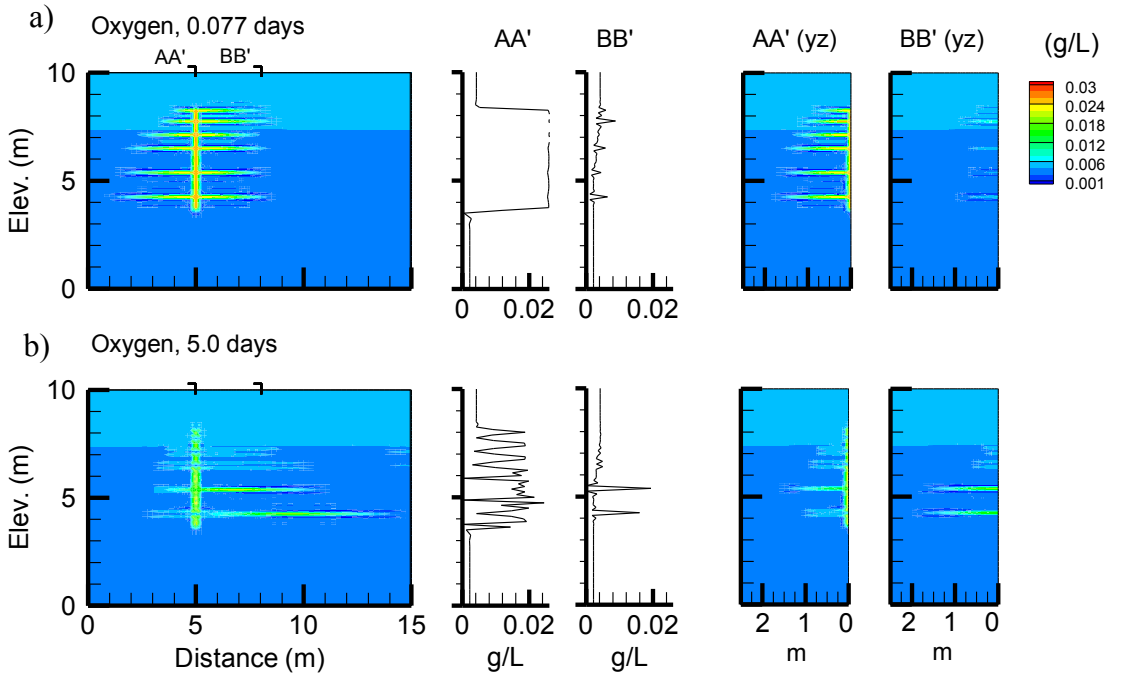

Figure 5-19– Simulated oxygen distribution with low hydraulic conductivity of 1.0 x 10^{-8} m/s (Scenario 5) after a) 0.077 days and b) 5.0 days.

5.5.1 Random Fracture Network

In these scenarios, two random fracture networks are superimposed onto the base case simplified set of nine horizontal fractures to determine if the match could be improved.

The two random fracture networks were developed with varying mean apertures of 50 and 100 μm. Each network considers two sets of fracture planes: one vertical (in the transverse yz plane) and one horizontal (in the xy plane). For simplicity, random fractures in the second vertical direction (xz plane) were not considered. The fracture networks are shown in Figures 5-19 and the statistics are provided in Table 5-4. The random fractures were assumed to be continuous in the transverse (y) direction.

Two cases were considered, as shown in Table 5-3: the base case with a superimposed random network of 50 μm mean fracture aperture (Scenario 7a), and the base case with a superimposed random network of 100 μm mean fracture aperture (Scenario 7b).

Table 5-4 - Random fracture network statistics

Variable/Plane	yz	xy
Mean Spacing (m)	1.8	0.5
standard deviation	0.25	0.25
Mean Apertures (μm)	50, 100*	50, 100*
Mean Length (m)	5	3
standard deviation	1	1
Mean Width (m)	3	15
standard deviation	1	1

* two cases

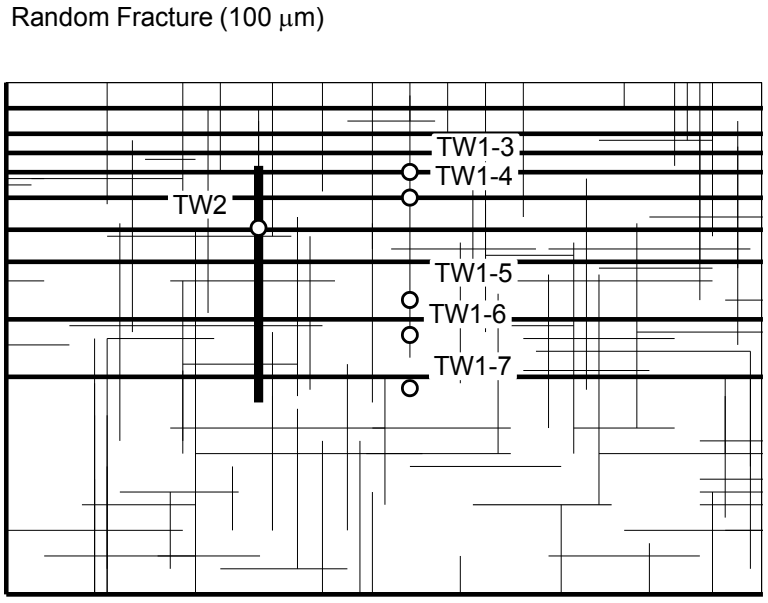

Figure 5-20 - Random fracture network, mean aperture of 100 μm.

Breakthrough curves with the random fracture networks showed little to no change from the simulated base case. The random fracture network causes somewhat more oxygen dispersion as the oxygen fills the intersecting fractures leaving less oxygen to enter the dominant horizontal fractures (Figure 5-21).

As a result, the peak concentrations along the fractures are slightly reduced (maximum concentration of ~ 18 mg O_2/L following injection). This affects the overall transport of oxygen down-gradient and results in less transport into the matrix around the injection well due to the oxygen being forced into a greater number of fractures. Less back diffusion was also noted with the random fracture network because with more fractures, there is more room for the oxygen to get flushed from the fractures before diffusing into the matrix. Similarly, the transverse distribution within the horizontal fractures is also significantly reduced.

The transverse distance after 1 day within fracture 2 was limited to less than 3 m with an oxygen concentration > 3.0 mg O_2/L and 4 m in fracture 1. In addition, the oxygen within

the random fractures creates a more uniform distribution of oxygen around the upper portion of the injection well between the upper horizontal fractures.

The random fracture network of mean aperture 50 µm had significantly less impact than with the increased mean aperture of 100 µm. Additional simulations with random network apertures greater than 100 µm (not shown) showed a clearly poor fit with the observed data.

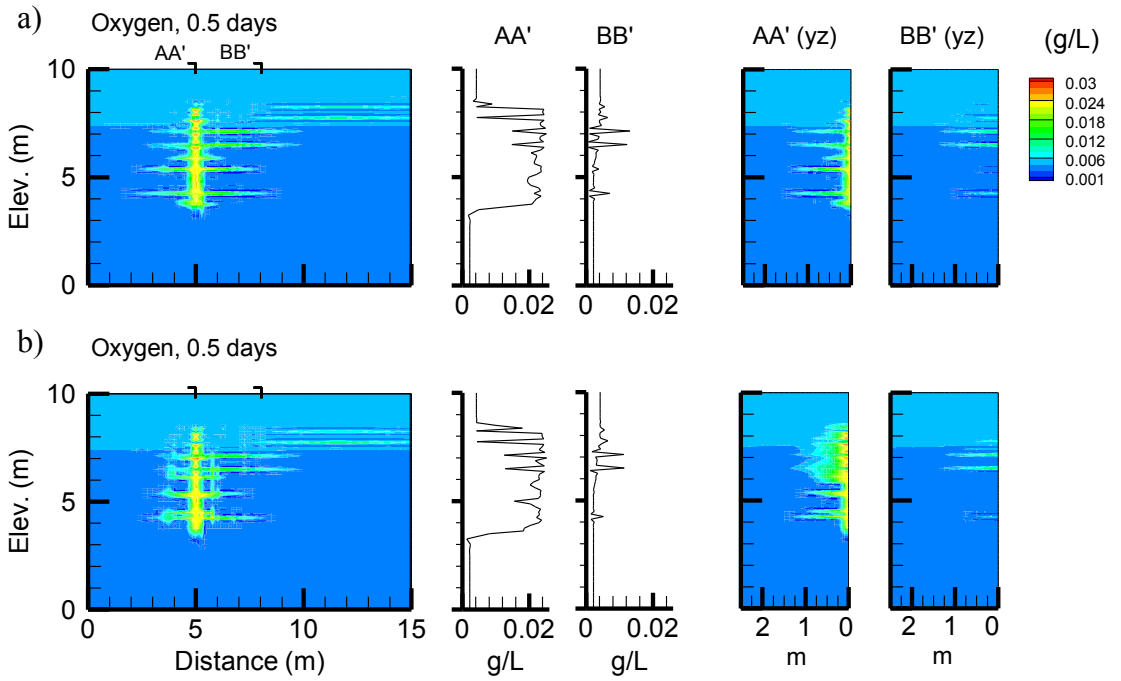

Figure 5- 21 - Simulated oxygen distribution assuming the base case conditions overlain by a random fracture network (Scenario 7) with: a) mean aperture 50 µm and b) mean aperture 100 µm.

Random network with lower matrix K

To assess the impacts of the bulk hydraulic conductivity on the transport of oxygen with the random fracture network, an additional sensitivity run was completed. The hydraulic conductivity of the rock matrix was reduced by an order of magnitude with respect to the base case to 1.0 x 10^{-8} m/s and the effect of the oxygen distribution with the random fracture network with a mean aperture of 100 µm was examined (Appendix G) (Scenario

7c). With the reduced hydraulic conductivity, there is no significant effect on the oxygen breakthrough within the monitoring points, matrix or fractures.

The distribution of oxygen is similar to that in Scenario 7a with the random fracture network (hydraulic conductivity of 1.0 x 10^{-7} m/s) but additional oxygen is noted within the fractures which are transported down-gradient (maximum concentration of ~ 26 mg O_2/L within the fractures). The low matrix hydraulic conductivity slows the mass transfer into the matrix which forces more oxygen into the fractures (Figure 5-22).

Higher concentrations were also noted to persist within the injection well over time (concentrations of ~ 30 mg O_2/L after 1.0 day). As seen with the random fracture network in Scenario 7a (hydraulic conductivity of 1.0 x 10^{-7} m/s), the transverse distribution within the dominant fractures is reduced due to more oxygen being concentrated in the random fractures and in the matrix around the injection well (1.1 and 1.3 m distribution in fractures 2 and 1, respectively after 1 day for concentration > 3.0 mg O_2/L).

This effect is compounded with the low hydraulic conductivity of the matrix. In addition, the uniform distribution of oxygen around the upper portion of the injection well between the upper horizontal fractures is also increased because higher concentrations of oxygen are forced into the random fractures and not into the matrix.

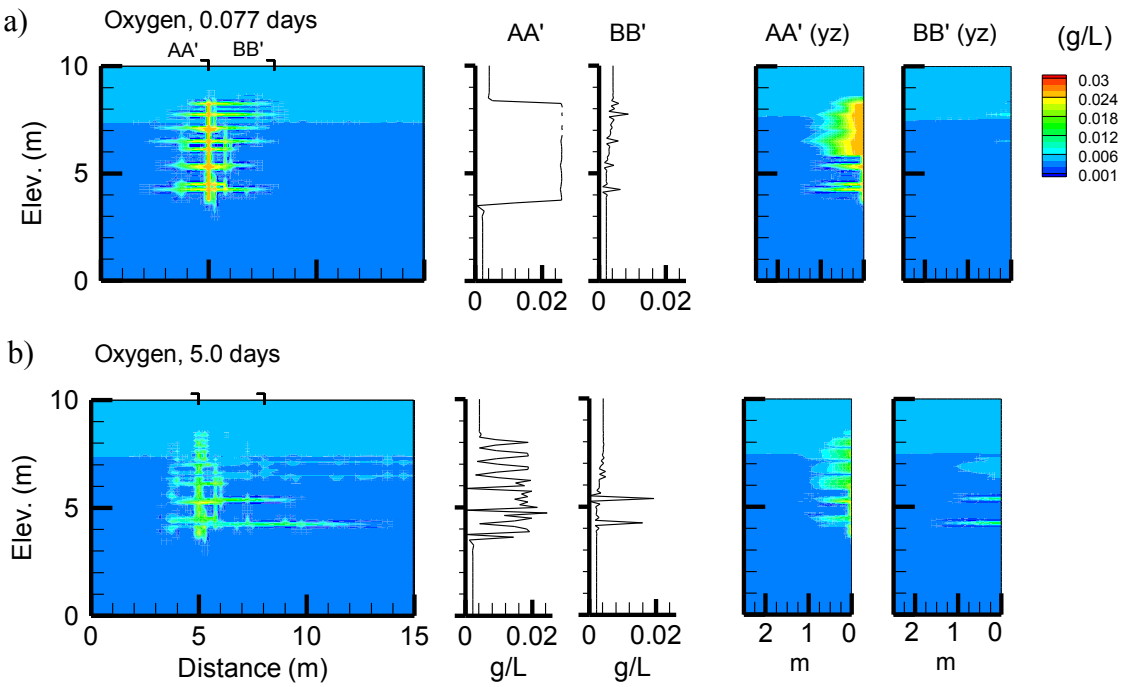

Figure 5-22 – Simulated oxygen distribution with low hydraulic conductivity and random fracture network (Scenario 7c) (mean aperture 100 μm) a) after 0.077 days and b) after 5.0 days.

6.0 Interpretation and Summary of Results

The results of the model, and in particular the good match between the observed and simulated breakthrough curves, confirms that fractures play a defining role in the system behavior.

Within the fractures, oxygen was shown to be transported from the injection zone as discrete pulses which caused rapid changes in the concentration gradients along the fracture/matrix interfaces. The pulses migrated at distinct velocities depending on the fracture apertures. Within the largest fractures, the simulated pulse migration was rapid with limited time for diffusion from the fractures to the matrix. Transport was slower through the smaller fractures which allowed more time for matrix diffusion. Transport within the fractures is dominated by advection which carries the injected oxygen down-gradient, resulting in sharp breakthrough curves at those monitoring points that are aligned with the major fractures (e.g. TW1-3 and TW1-4).

Transport into the rock matrix also occurs by diffusion and advective processes. Diffusive-like concentration tailing within the injection well persisted for several days following the injection, providing evidence that oxygen had rapidly penetrated the matrix under the high pressure gradients, followed by slow back diffusion into the open injection well. The transport mechanisms into the matrix may account for the variation in the breakthrough curve tails seen between the field and modelling results (TW1-3 and TW1-4).

Transport of oxygen into the matrix can explain the breakthrough of oxygen at the field observation point TW1-7 and to a lesser extent at TW1-6. The observed and simulated oxygen breakthrough at these locations must be a result of a diffusive pulse within the system.

Once the oxygen had entered the porous matrix and was flushed from the fractures, the concentration gradients reversed and oxygen then back diffused into the fractures. This

was best seen at point 9 within the model where there was a sharp peak concentration followed by a long diffusive tail. The concentrations decrease over 200 days to background levels due to the back diffusion of the oxygen from the matrix.

Observations from the sensitivity runs generally indicated that with variations to the input parameters such as aperture, hydraulic gradient and hydraulic conductivity, the distribution of oxygen within the system can be significantly different with varying degrees of advective transport within the fractures and diffusion into the rock matrix.

Results with the random fracture network overlay showed some limited differences from the base case (and perhaps gave a more realistic visual perspective) but were not significantly different from the original base case with the simple horizontal network. It is clear that the observed system is dominated by a few distinct fractures and thus can be reasonably reproduced with planar discrete fractures. A high hydraulic conductivity homogeneous equivalent porous medium modelling approach is not applicable in this case.

6.1 Effectiveness of Oxygen Injection

The degree of transport within the fractures and the matrix and ultimately the distribution of oxygen within the system is a function of the aquifer properties and was shown to vary based on the fracture aperture (and fracture network), hydraulic gradient, hydraulic conductivity and matrix porosity. For effective bioremediation, the delivery of the oxygen into the rock matrix is the key factor (Lipson et al., 2005). In this investigation, the controlling factors for the delivery of oxygen into the matrix were assessed. It was determined that under this short (1.5 hour) injection, oxygen can be effectively delivered into the matrix at concentrations conducive to aerobic biodegradation (> 3.0 mg O_2/L) along the injection well (transverse distribution of 0.5 m) and into the matrix along the fractures (10's of centimeters).

The results can be transferred to other sites if the aquifer conditions are determined to be similar. It should be noted that during this investigation, no significant utilization of the oxygen was observed in the field thus oxygen utilization was not taken into consideration by the model. In addition, it should be noted that the field injection was for a limited duration of about 80 minutes. These conditions therefore represent an idealized and simplified oxygen delivery environment.

Several unanswered questions remain with respect to the potential application of this oxygen delivery method on enhanced aerobic bioremediation, many of which were not addressed as part of this investigation. Some questions are addressed in the recommendation sections of this report. Those issues that can be addressed to help design further applications of the methods and to determine the implications for enhanced aerobic biodegradation include the persistence of oxygen within the matrix (with no utilization) and the zone of influence of the injections. To provide more information on these issues, two additional predictive simulations were conducted using the calibrated base model.

6.2 Predictive Simulations

6.2.1 Simulation 1 – Continuous Injection

For this first predictive simulation, a long term continuous injection was applied. The injection conditions were identical to the base case but the injection time interval was extended from 80 minutes to 7 days (168 hours at 26.4 mg O_2/L and at 11 L/min). The total mass injected was ~ 3 kilograms of oxygen.

The continuous injection saw a rapid rise in concentration in the injection well (TW2) and at the down-gradient monitoring points TW1-3 and 4, consistent with the breakthrough curves for the base case. The concentrations remained consistent at ~ 26 mg/L in TW2 and ~ 24 mg/L in TW1-3 and 4 for the duration of the injection (168 hours)

(Appendix H). Once the injection was turned off, the concentrations within the injection well decreased gradually before returning to background conditions after ~250 hours. In the down-gradient monitoring points TW1-3 and 4, the concentrations rapidly returned to background conditions (within several hours) after the injection was stopped. In the two additional monitoring points TW1-6 and 7, concentrations increased gradually until the end of injection (168 hours) when the concentration was ~ 6.0 mg O_2/L. The concentration in TW1-6 continued to increase over time and was ~12 mg O_2/L after 200 days. Within TW1-7 a similar trend was noted. Concentrations peaked after ~ 1400 hours (58 days) and then gradually declined to ~ 10 mg O_2/L after 200 days.

Within the matrix the concentrations at the points located up-gradient (point 8) and down-gradient (points 10 and 11) of the injection well showed a rapid increase in concentrations following the start of injection and remained above 20 mg O_2/L for the full 200 days. Concentrations within the injection well (point 9) also increased quickly following the start of injection but decreased quickly once the injection was stopped (168 days). Concentrations then declined gradually with time but remained above 16 mg O_2/L for the full 200 days.

Monitoring points within the fractures (points 13 -16) peaked at 26 mg O_2/L within ~ 50 hours then declined rapidly to ~10 mg O_2/L within 1000 hours (41.6 days) and then gradually declined to concentrations of ~ 6.0 mg O_2/L over the 200 days.

The oxygen distribution following injection (after 7 days) shows peak concentrations consistent with the injection fluid concentration within the injection well and extending 1 m into the matrix surrounding the well (Figure 5-24). The concentration within fracture 1 is ~ 24 mg O_2/L at the model boundary 10 m down-gradient and 7 m down-gradient in fracture 2. Oxygen is flushed from the injection well into the fractures over time with little remaining above 3.0 mg O_2/L after 50 days. With time the oxygen continues to be flushed from the fractures and concentrations within the matrix persists (> 3.0 mg O_2/L) for the full 200 days.

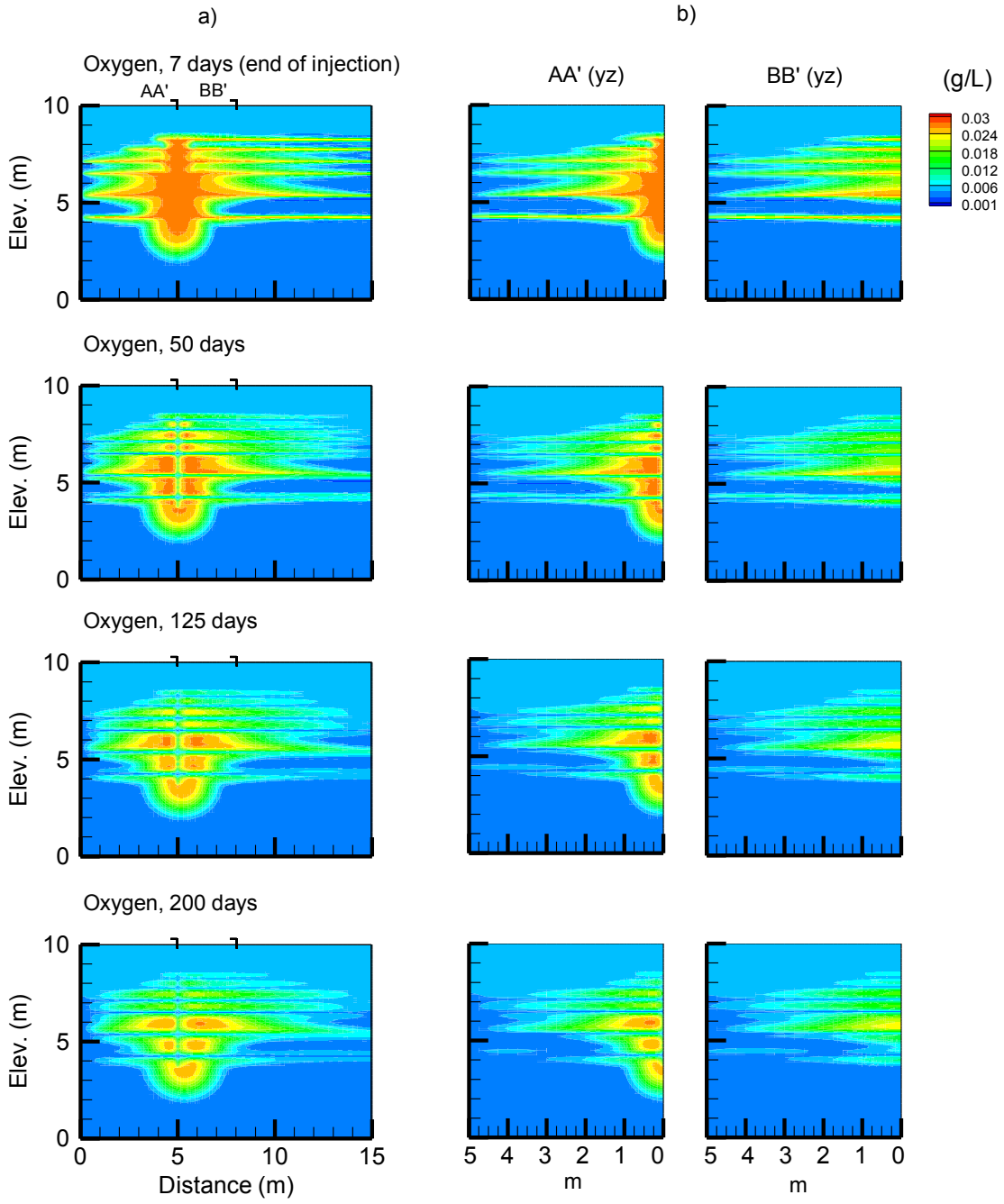

Figure 6-1 – Continuous 7-day injection simulation showing oxygen distribution at 7, 50, 125 and 200 days in the a) vertical (xz) and b) transverse (yz) sections at vertical profile locations AA' and BB'.

The flushing of the fractures following the injection results in limited diffusion of oxygen along the fractures into the matrix.

The transverse distribution of oxygen at the injection well and at the down-gradient monitoring well following injection (7 days) shows a greater than 5 m radius, at concentrations > 3.0 mg O_2/L and therefore a 10 m diameter zone of influence in the transverse direction was created. The increased concentrations within the fractures persisted for the full 200 days at the injection well and at the down-gradient monitoring point. Within the matrix between the fractures, the transverse distribution reached ~ 4 m from the injection well (concentrations > 3.0 mg O_2/L) and decreased only slightly over the 200 day period. The transverse distribution within the matrix around the injection well was therefore ~ 8 m. After 200 days a limited amount of oxygen remained within the fractures but concentrations persisted in the matrix within the injection well and down-gradient.

6.2.2 Simulation 2 – Cycle Injection

To mimic a series of injections, a simulation was completed with one injection every two days for 200 days. The injection conditions consisted of injecting every second day at 26.4 mg/L for 1.86 hours at 5.6 L/min for a total mass of ~3 kilograms of oxygen injected over the 200 day period (consistent with the continuous injection simulation above).

Breakthrough curves (Appendix H) within the injection well (TW2) and the down-gradient monitoring points (TW1-3 and 4) show increases and decreases in concentrations with each injection. Concentrations in monitoring points TW1-6 and 7 show gradual increases for the full 200 days. Monitoring point 9 (within the injection well) shows a rise and fall in concentration following each injection but the overall base-line concentration remains at ~ 20 mg O_2/L. Concentrations within the up-gradient point 8 and the down-gradient points 10 and 11 show small variations in concentration with each injection with an overall increasing trend to concentrations of ~ 20 mg O_2/L after

200 days. Within the fractures the variation in concentration with each injection is noted but the overall trend in concentration peaks after ~ 200 hours and remains constant at ~ 24 mg O_2/L for the full 200 days.

The cycle of injections creates an oxygen distribution similar to the base case with compound effects seen over time (Figure 5-25). The continuous supply of oxygen to the system over the 200 days creates a relatively uniform zone of high concentration oxygen within the matrix around the injection well while oxygen is being continuously transported down-gradient within the fractures. Maximum concentrations (equal to the injection concentration) are noted within the fractures 10 m down-gradient for the full 200 days. Concentrations within the matrix surrounding the injection well also persist at concentrations of ~ 24 mg O_2/L for the full 200 days. The zone of influence around the injection well is limited to less than 1 m following the first 10 injections but then increases with the number of injections to a maximum radius of 3 m after 200 (concentrations > 3.0 mg O_2/L). Due to the repetitive cyclic supply of oxygen into the fractures, the diffusion of oxygen into the matrix along the fractures has increased with respect to the equivalent 7-day injection simulation, resulting in less transport of the oxygen down-gradient and a more uniform distribution of oxygen within the fractures and the matrix.

The transverse distribution of dissolved oxygen is relatively consistent within the fractures at the injection well and within the monitoring points about 3 m down-gradient, thereby creating a zone of influence within the fractures in the transverse direction of ~ 6 m diameter at the injection well and down-gradient. Within the matrix the transverse distribution increases with the number of injections. A maximum distance of ~ 1.5 m was reached after 200 injections (concentrations ~ 3.0 mg O_2/L), corresponding to a zone of influence in the transverse direction of ~3 m.

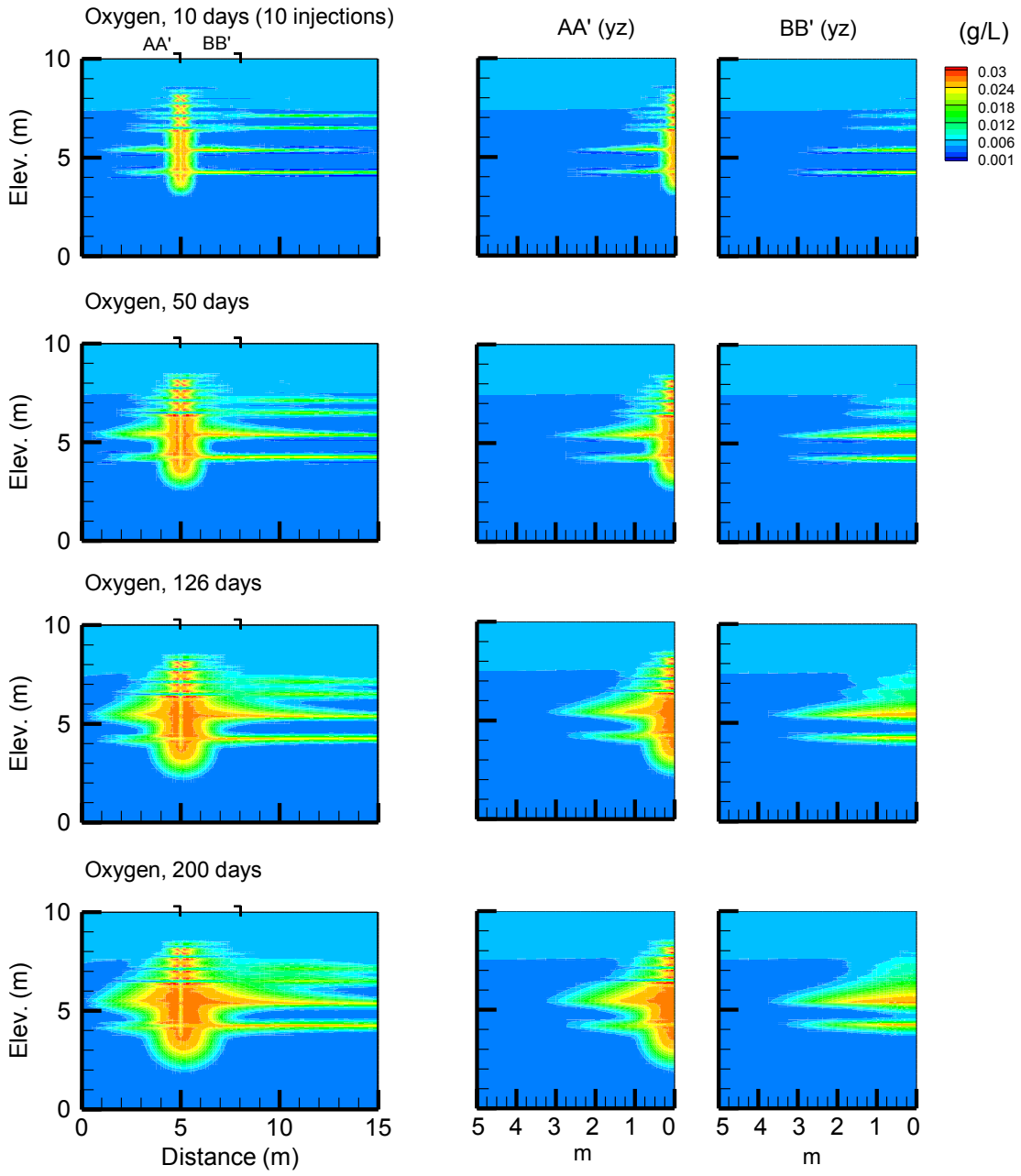

Figure 6-2 – Cycle injection showing oxygen distribution at 10, 50, 126 and 200 days in the a) vertical (xz), and b) transverse (yz) sections at AA' and BB' (plot times correspond to the end of each injection cycle).

6.2.3 Simulation Summary

Based on the results of the simulations, the persistence of oxygen within the system and the zone of influence based on injection conditions can be evaluated.

With continuous injection for 7 days, a maximum zone of influence (down-gradient and in the transverse direction) can be achieved while maintaining high levels of oxygen within the matrix. When injections are cycled, providing a more continuous supply of oxygen over time (in this case 200 days) to the system, the zone of influence is reduced but diffusion into the matrix along the fractures increases creating a more uniform zone of increased oxygen concentrations around the injection well and along the fractures.

The results of the predictive simulation scenarios demonstrate that the delivery of oxygen into the system (continuous or cyclic) can affect the advective transport of oxygen through the fractures and the diffusion of oxygen in to the matrix. The implications of the delivery method on the success of remediation cannot be evaluated at this time but recommendations for additional investigations are provided in Section 8 below.

7.0 Summary and Conclusions

The effectiveness of an oxygen delivery method in a fractured bedrock environment was assessed using a combined field and modelling approach. The fractured bedrock aquifer was characterized through drilling, packer testing, installation of monitoring points, visual interpretation (down hole camera), tracer testing and cross borehole testing.

An oxygen injection test was designed based on the aquifer characterization, and involved the injection of both dissolved oxygen and bromide (as a conservative tracer). The injection was completed using iTi's gPro® technology.

The injection test concluded that oxygen can be successfully delivered into a fractured bedrock aquifer. The effectiveness of the delivery is shown in the breakthrough curves resulting from the injection test and confirmed by the groundwater model which was developed and calibrated to the observed field conditions. The simulated distribution of oxygen within the system was consistent with the field conditions, with good agreement between the simulated and observed breakthrough curves.

The injection test and model demonstrated that oxygen propagated primarily through the discrete fractures in the system as seen in field monitoring points TW1-3 and 4 as well as in the fracture model monitoring points (13 to 17), but also by transport through the matrix (at field monitoring points TW1-6 and TW1-7 which correspond to model points 8 to 12). The results also indicate that under a non-reactive case, and once delivered to the formation, oxygen can potentially be sustained in the environment at levels required to enhance aerobic biodegradation. This can be seen with concentrations remaining above the levels required for aerobic biodegradation of petroleum hydrocarbons (~3 mg O_2/L) in the monitoring points after 200 hours.

Simulations using two different injection conditions (continuous and cyclic) were used to evaluate the sustainability of oxygen within the system and the zone of influence

achievable with the technology. The simulation runs determined that each method achieved somewhat different oxygen distributions and their possible advantages would need to be assessed on a site by site basis. Several remaining unanswered questions are noted in the recommendations below.

The results have generally demonstrated that oxygen can be effectively delivered into a fractured bedrock environment and maintained at concentrations which are potentially sufficient to enhance aerobic biodegradation. For efficient biodegradation throughout the fractured medium, a balance must be achieved between advective transport of oxygen through the fractures and the diffusion of oxygen into the matrix.

8.0 Recommendations

This study demonstrated that on a small scale, oxygen could effectively be delivered to a fractured bedrock system at levels potentially sufficient to enhance aerobic biodegradation. Additional investigations are required to fully assess the applicability of this technology.

The primary remaining questions relate to the behavior of oxygen when oxygen is being utilized within the system as a result of biodegradation or other factors. Oxygen consumption will affect its penetration and persistence within the fractures and matrix and will therefore affect the scale of the remediation zone. Competition for oxygen between inorganic reductants such as iron, non-target organics and targeted organics must also be considered.

To help assess the effects of utilization, more field work is required where higher rates of biodegradation and utilization can be observed over time and the effects evaluated. These factors can also be investigated using the groundwater model with a reactive transport component that can account for biodegradation and oxygen utilization by other factors within the system. Additional uses for a reactive groundwater model include plume simulation to help design the remediation system, including an assessment of the amount of oxygen required, remediation times and delivery scenarios (continuous/cycle etc.) to assess the effects of the balance of delivery to the fractures or the matrix.

In addition, the full scale implementation of the technology would allow for the assessment of the system under less controlled conditions and provide additional information with respect to the applicability of the technology to a real world environment. Other areas of investigation using this technology and or concepts to be investigated include the effects on biofilms and pore clogging, using both field and modelling approaches.

References

Aachib, M., M. Mbonimpa, M. Aubertin. 2004. Measurement and Perdiction of the Oxygen Diffusion Coefficiet in Unsaturated Media, with Applications to Soil Covers. *Water, Air and Soil Pollution. 156:* 163 – 193.

Arnon, S., E. Adar, Z. Ronen, A. Nejidat, A. Yakirevich and R. Nativ. 2005. Biodegradation of 2,4,6-tribromophenol during transport in fractured chalk. *Environmental Science and Technology. 39:* 748-755.

Azadpour-Keeley, A., M.J. Barcelona. 2006. Design of an MTBE Remediation Technology Evaluation. *Ground Water Monitoring and Remediation. 26:* 103-113.

Barcelona, M.J., T.R. Holm. 1991. Oxidation - Reduction Capacities of Aquifer Solids. *Environmental Science and Technology. 25 (9):* 1585-1572.

Bass, D.H., R.A. Brown, B.C. Alleman, A. Leeson. 1997. Performance of Air Sparging Systems; A Review of Case Studies; In-situ and On-site Bioremediation. *Bioremediation. 4:* 117-122.

Berkowitz, B. 2002. Characterizing Flow Transport in Fractured Geological Media: A Review. *Advances in Water Resources*. *25:* 861-884.

Brunton, F.R. 2008. Project Unit 08-004. Preliminary Revisions to the Early Silurian Stratigraphy of Niagara Escarpment: Integration of Sequence Stratigraphy, Sedimentology and Hydrogeology to Delineate Hydrogeologic Units. Summary of Filed Work and Other Activates 2008. *Ontario Geological Survey, Open File Report. 6226:* 31-1 to 31-18.

Brunton, F.R. 2007. Caprock Carbonate Stratigraphy and Bedrock Aquifer Character of the Niagara Escarpment- City of Guelph Region, Southern Ontario. In: Proc., 60th Annual CGS and 8th Joint IAH-CNC Groundwater Specialty Conference, Ottawa, 2007.

Canadian Council of Ministers of the Environment (CCME). 2001. Reference Method for the Canada-Wide Standard for Petroleum Hydrocarbons in Soil - Tier 1 Method. Publication No. 1310. (MOE DECPH-E3421/CCME).

Chapman L.J. and D.F. Putnam. 1984. The Physiography of Southern Ontario. *Ontario Geological Survey.*

Chapman, S.W., M.R. Vandergriendt, B.J. Butler, D.M. Mackay. 1998. Measurement of Oxygen Demand of Petroleum Hydrocarbon-Contaminated Groundwater. *Bioremediation Journal. 1(3):* 165-172

Chiang, C.Y. J.P. Salanitro, E.Y. Chai, J.D. Colthart, C.L. Klein. 1989. Aerobic Biodegradation of Benzene, Toluene and Xylene in a Sandy Aquifer – Data Analysis and Computer Modelling. *Ground Water. 27(6):* 823-834.

Côté, J., J.M Konrad. 2005. Thermal Conductivity of Base-Coarse Materials. *Canadian Geotechnical Journal. 42:* 61-78.

Day-Lewis, F.D., S.M. Gorelick. 2000. Identifying Fracture-zone Geometry Using Simulated Annealing and Hydraulic-connection Data. *Water Resources Research. 36:* 1707-1721.

Dickson, S.E., N.R. Thomson. 2003. Dissolution of Entrapped DNAPLs in Variable Aperture Fractures: Experimental Data and Empirical Model. *Environmental Science and Technology. 37:* 4128-4137.

Eaton, A.D., L.S. Clesceri, and A.E. Greenberg. (Eds). 1995. Standard Methods for the Examination of Water and Wastewater, 19th ed. American Public Health Association, American Water Works Association Water Environment Federation, Washington, DC.

Eckert. P., C.A.J Appelo. 2002. Hydrogeochemical Modelling of Enhanced Benzene, Toluene, Ethylbezene, Xylene (BTEX) Remediation with Nitrate. *Water Resources Research. 38 (8):* 5-1 – 5-11.

Eyles, N., Arnaud, E., Scheidegger, A.E., Eyles, C.H. 1997. Bedrock Jointing and Geomorphology in Southwestern Ontario, Canada: An Example of Tectonic Predesign. *Geomorphology*. *19:* 17-34.

Freeze, R.A., J.A. Cherry. *Groundwater*. Prentice Hall, Inc., New Jersey, 1979.

Gamlin, J.D., J.E. Clark, G.Woodside, R. Herndon. 2001. Large-Scale Tracing of Ground Water with Sulfur Hexafluoride. *Journal of Environmental Engineering. 127 (2):*171-174.

Geology of Ontario, *Ontario Geological Survey Special* Volume 4 part 2, 1992.

Grisak.G.E., J.F. Pickens. 1980. Solute Transport through Fractured Media 1. The Effect of Matrix Diffusion. *Water Resources Research. 16*: 719-730.

Grisak.G.E., J.F. Pickens. 1981. An Analytical Solution for Solute Transport Through Fractured Media with Matrix Diffusion. *Journal of Hydrology. 52*: 47-57.

Gwo, J.P., P.M. Jardine, W.E. Sanford. 2007. Modeling Field Scale Multiple Tracer Injection at a Low Level Waste Disposal Site in Fractured Rocks: Effects of Multi-scale Heterogeneity and Source Term Uncertainty on Conceptual Understanding of Mass Transfer Processes. *Journal of Contaminant Hydrology. 77:* 91-118.

Hutchins, S. R., G.W. Sewell, D.A. Kovacs, G.A. Smith. 1991. Biodegradation of Aromatic Hydrocarbons by Aquifer Microorganisms under Denitrifying Conditions. *Environmental Science and Technology 25*:68–76.

Illman,W.A., D.M. Tartakovsky. 2007. Asymptotic Analysis of Cross-hole Hydraulic Tests in Fractured Granite. *Ground Water. 44:* 555-563.

inVentures Technologies Incorporated. 2007. *gPro High Pressure System*. Promotional Material.

Jardine, P., W. Sanford. 1999. Quantifying Diffusive Mass Transfer on Fractured Shale Bedrock. *Water Resources Research. 35 (7):* 2015-2030.

Johnston, C.D., J.L. Rayner, B.M. Patterson, G.B. Davis. 1998. Volatilization and Biodegradation During Air Sparging of Dissolved BTEX-contaminated Groundwater. *The Journal of Contaminant Hydrology. 33:* 377-404.

Johnson, P.C. 1998. Assessment of the Contributions of Volatilization and Biodegradation to in Situ Air Sparging Performance. *Environmental Science and Technology. 32:* 276-281.

Kim, Y.C., K.K. Lee. 2002. Identification and Location of Transmissivity Fractures from Analysis of Tracer Test Data. *Quarterly Journal of Engineering Geology and Hydrogeology. 35:* 179-188.

Landmeyer, J.E., F.H. Chapelle, H.H. Herlong, P.M. Bradley. 2001. Methyl tert-butyl ether Biodegradation by Indigenous Aquifer Microorganisms under Natural and Artificial Oxic Conditions. *Environmental Science and Technology. 35:* 1118-1126.

Landmeyer, J.E., P.M. Bradley. 2003. Effect of Hydrologic and Geochemical Conditions on Oxygen-enhanced Bioremediation in a Gasoline-contaminated Aquifer. *Bioremediation Journal. 7:* 165-177.

Lapcevic.P.A., K.S. Novakowski, E.A. Sudicky. 1999. The Interpretation of a Tracer Experiment Conducted in a Single Fracture Under Conditions of Natural Groundwater Flow. *Water Resources Research. 35:* 2301-2312.

Lipson, D., B.H. Kueper, M. Gefell. 2005. Matrix Diffusion-derived Plume Attenuation in Fractured Bedrock. *Ground Water. 43:* 30-39.

Lovley, D.R., E.J.P. Phillips. 1988. Novel Mode of Microbial Energy Metabolism: Organic Carbon Oxidation Coupled to Dissimilatory Reduction of Iron and Manganese. *Applied and Environmental Microbiology 54*:1472–1480.

MacQuarrie, K.T.B., K.U. Mayer. 2005. Reactive Transport Modelling in Fractured Rock: A State of the Science Review. *Earth Science Review. 72:* 189-227.

Malard, F., F. Hervant. 1999. Oxygen Supply and the Adaptations of Animals in Groundwater. *Freshwater Biology. 41:* 1-30.

Molson. J.W., E.O. Frind, C. Palmer. 1992. Thermal Energy Storage in an Unconfined Aquifer 2. Model Development, Validation, and Application. *Water Resources Research. 28:* 2857-2867.

Molson, J.W., and E.O. Frind. 1994. Predicting the Behavior of Thermal Energy in Porous and Discretely Fractured Porous Media, In: Vol II of Proceedings: Eighth International Conference of the Association for Computer Methods and Advances in Geomechanics, (H.J. Siriwardane & M.M. Zaman, Eds.), A.A. Balkema, Rotterdam, p1237-1242, May 1994.

Molson, J.W., P. Pehme, J. Cherry, B. Parker. 2007. Numerical Analysis of Heat Transport in Fractured Sedimentary Rock: Implications for Thermal Probes, In Proceedings: 2007 NGWA/U.S. EPA Fractured Rock Conference: State of the Science and Measuring Success in Remediation (#5017), Portland, Maine, September 24-26, 2007.

Molson, J.W., E.O. Frind. 2009. HEATFLOW-SMOKER: Density Dependent Flow and Thermal Energy / Mass Transport Model in Three Dimensions, User Guide. Version 4.0, University of Waterloo & Université Laval.

Mulica, W.S., N. Mathis, J.F. Begley. 2004. Enhanced Natural Attenuation of MTBE and Benzene at a Low Permeability Site Using iSoc Technology. *Soil and Sediment Contamination. 12(2):* 208.

Mundel. K., D.A. Reynolds, M.R. West, B.H. Kueper. 2007. Concentration Rebound Following In Situ Chemical Oxidation in Fractured Clay. *Ground Water. 45 (6):* 692-702.

Novakowski. K., P. Lapcevic. 1994. Field Measurement of Radial Solute Transport in Fractured Rock. *Water Resources Research*. *30 (1):* 37-44.

Novakowski. K., P. Lapcevic, G. Bickerton. 1995. Preliminary Interpretation of Tracer Experiments Conducted in a Discrete Rock Fracture Under Conditions of Natural Flow. *Geophysical Research Letters. 22 (11):* 1417-1420.

Novakowski. K., G. Bickerton, P. Lapcevic. 2006. Measurement of Groundwater Velocity in Discrete Rock Fractures. *Journal of Contaminant Hydrology. 82:* 44-60.

Odling, N.E., J.E. Roden. 1997. Contaminant Transport in Fractured Rock with Significant Matrix Permeability, using Natural Fracture Geometries. *Journal of Contaminant Hydrology. 27:* 263-283.

Ontario Ministry of Environment (MOE). 2005. Soil, Groundwater and Sediment Standards for use Under Part XV.1 of the Environmental Protection Act.

Ontario Ministry of the Environment (MOE). 2007. Certificate of Approval – Air Number 4021-78HPN2. Water and Earth Science Associated Ltd. – Mobile Operation.

Parker, B. L., R.W. Gillham, J.A. Cherry. 1994. Diffusive Disappearance of Immiscible-Phase Organic Liquids in Fractured Geological Media. *Ground Water. 32(5):* 805-820.

Paillet. 1993. Using Borehole Geophysics and Cross-borehole Flow Testing to Define Hydraulic Connections between Fracture Zones in Bedrock Aquifers. *Journal of Applied Geophysics. 30:* 261-279.

Richard, F.A., N. van Walsum, K.D. Greer and K. Novakowski. 2004. *Continuous Downhole Hydraulic Testing of Fractured Bedrock Aquifers: Methodology and Field Example*. Proceedings of the 57th Canadian Geotechnical Conference/5th Joint IAH-CNC/CGS Conference, Québec City, Canada, Oct. 24-28, 2004.

Salanitro, J.P., P.C. Johnson, G.E. Spinnler, P.M. Maner, H.L. Wisniewski, C. Bruce. 2000. Field-scale Demonstration of Enhanced MTBE Bioremediation Through Aquifer Bioaugmentation and Oxygenation. *Environmental Science and Technology. 34:* 4152-4162.

Schafer, D., M. Ebert., R. Kober, V. Plagentz, A. Dahmke. 2006. Kinetics of Oxygen Release for ORC. *Biroremediation Journal. 10 (1-2):* 71-82.

Snow, D. 1968. Rock Fracture Spacings, Openings, and Porosities. *Journal of the Soil Mechanics and Foundations Division, Proceedings of the American Society of Civil Engineers. 94:* 73-91.

Sudicky, E.A., E.O. Frind. 1982. Contaminant Transport in Fractured Porous Media: Analytical Solution for a System of Parallel Fractures. *Water Resources Research. 18 (6):* 1634-1642.

Therrien, R., E.A. Sudicky. 1996. Three-dimensional Analysis of Variable-saturated Flow and solute Transport in Discretely-fractured Porous Media. *Journal of Contaminant Hydrology. 23:* 1-44.

Tsang, D.H., E.O. Frind, E.A. Sudicky. 1981. Contaminant Transport in Fractured Porous Media: Analytical Solution for a Single Fracture. *Water Resources Research. 17 (3):* 555-564.

Tsang, Y.W. 1984. The Effect of Tortuosity of Fluid Flow through a Single Fracture. *Water Resources Research. 20 (9):* 1209-1215.

Tsang C.F., Y.W. Tsang, F.V. Hale. 1991. Tracer Transport in Fractures: Analysis of Field Data Based on a Variable-Aperture Channel Model. *Water Resources Research. 27 (12):* 3095-3106.

United States Environmental Protection Agency. 1994. Method 200.8 Determination of Trace Elements in Water and Wastes by Inductively Coupled Plasma-Mass Spectrometry. Rev 5.4 *(EPA 200.8).* Cincinnati, Ohio.

United States Environmental Protection Agency (EPA). 1996. Low Stress (low flow) Purging and Sampling Procedure for the Collection of Ground Water Sampled from Monitoring Wells. Revision 2.

WESA. 2006. Remedial Action Plan Update, 101 St. Andrew Street East Fergus Ontario. July 2006.

WESA. 2007. Groundwater Monitoring Report, 101 St. Andrew Street East Fergus Ontario. October 2007.

Wilk, C.R., P. Chang. 1955. A.E.C.H.E. Journal 1: 264-270.

Wilson, R. D., D.M. MacKay. 1993. The Use of Sulphur Hexafluoride as a Conservative Tracer in Saturated Sandy Media. *Ground Water. 31:* 719.

Wilson, R.D., D.M. Mackay, K.M. Scow. 2002. In-situ MTBE Biodegradation Supported by Diffusive Oxygen Release. *Environmental Science and Technology. 36:* 190-199.

Yang, J., R.N. Edwards, J.W. Molson, E.A. Sudicky. 1996. Fracture-induced Hydrothermal Convection in the Oceanic Crust and the Interpretation of Heat-flow Data, *Geophysical Research Letters. 23 (9):* 929-932.

Appendix A

Methodology for Petroleum Hydrocarbons in Groundwater (CCME, 2001) with Modifications

Petroleum Hydrocarbon Analysis (PHC)

Organic Geochemistry Laboratory
Department of Earth and Environmental Sciences
University of Waterloo

Analyst: Marianne VanderGriendt
e-mail: mrvander@uwaterloo.ca phone: ext. 35180

PARAMETERS: F1 (C6 to C10), F2 (C10 to C16), F3 (C16 to C34), F4 (C34 to C50)

SCOPE AND APPLICATION: Although a national method is not available for water samples, analysis of PHC's was in accordance to applicable sections of the Canadian Council of Ministers of the Environment (CCME) method "Reference Method for the Canada-Wide Standard for Petroleum Hydrocarbons (CWS-PHC) in Soil – Tier 1 Method" (*MOE Method DECPH-E3421/CCME).* Modifications to the above method were employed to allow for PHC (F1,F2, F3,F4) assessment of groundwater samples during the analysis of BTEX, TMB, Naphthalene and PAH. Modifications to the above referenced method are listed below.

SAMPLE COLLECTION: In the field or laboratory, groundwater samples were collected before the pump to avoid contact with pump tubing. An in line, stainless steel screw cap sample head was fitted with a 25 ml (or 40 ml) glass vial. Several groundwater volumes were pumped through the vial before it was detached from the sample head. Care was taken to ensure that vials were filled full with no headspace. Sodium Azide was added as a preservative (0.25ml for 25ml size or 0.4ml for 40ml size, of a 10% W/V solution) and vials were quickly sealed with Teflon® lined screw caps. Samples were stored at 4°C and held for up to 14 days.

SAMPLE PREPARATION AND GAS CHROMATOGRAPHIC ANALYSIS: Samples and standards were equilibrated to room temperature before extraction. To solvent extract a sample (or standard), the Teflon® screw cap of the vial was quickly removed and 5.0 ml of sample was discarded with a glass/stainless syringe. This was followed immediately by the addition of 1.0 ml (or 2.0 ml for 40ml size) of methylene chloride (containing internal standards m-fluorotoluene (MFT) and fluorobiphenyl (FBP) at 25 mg/L). The vial was quickly resealed and agitated on its side at 350 rpm on a platform shaker for 20 min. After shaking, the vial was inverted and the phases were allowed to separate for 30 min. Approximately 0.7 ml (1.0 ml for 40 ml vial) of the dichloromethane phase was removed from the inverted vial with a gas tight glass syringe, through the Teflon septum. The solvent was placed in a Teflon sealed autosampler vial for injection into the gas chromatograph. Samples were analyzed with a HP 5890 capillary gas chromatograph, a HP7673A autosampler, and a flame ionization detector. Three microliters of methylene chloride was injected in splitless mode (purge on 0.5 min, purge off 10.0 min) onto a 0.25mm x 30M length, DB5 capillary column with a stationary phase film thickness of 0.25µm. Helium column flow rate was 2ml/min with a make-up gas flow rate of 30ml/min. Injection temperature was 275^{o}C, detector temperature was 325^{o}C and initial column oven temperature was 35 ^{o}C held for 0.5 min, then ramped at 15

^{o}C/min to a final temperature of 300 ^{o}C and held for 2 min. Chromatographic run time was 40 minutes. Data integration was completed with a HP 3396A integrator. F1 fraction included integration of all area counts beginning just after the end of the hexane (nC6) peak (hexane could not quite be resolved from the methylene chloride solvent peak) to the apex of the decane (nC10) peak, excluding the area of the internal standard (MFT). Standards containing nC6, nC10 and toluene were run. Toluene was used as the calibration standard. F2 (the integration of all area counts from the apex of the nC10 peak to the apex of the nC16 peak), F3 (the integration of all area counts from the apex of the nC16 peak to the apex of the nC34 peak) and F4 (the integration of all area counts from the apex of the nC34 peak to the apex of the nC50 peak) results were determined as per the referenced method, with the internal standard FBP area subtracted from the F2 range. The average response factor for nC10, nC16 and nC34 was used for calibration of these 3 ranges (F4 results were not detected in any samples).

CALIBRATION AND QUALITY ASSURANCE DATA:

Calibrations were made in internal standard mode and standards were run in triplicate at five (or more) different concentration, covering the expected sample range. Standards were prepared by spiking water with concentrated methanolic and/or toluene stock standards (purchased and certified from Ultra Scientific Analytical Solutions). Standards were extracted and analyzed by gas chromatography in the same way as samples. A multiple point linear regression was performed to determine the linearity and slope of the calibration curve. Quality control information on calibration curves (percent relative standard deviation and percent error) and blank information were included with reported data. Extraction duplicates were performed on samples and results were acceptable when they agreed within 10%. Matrix spikes were performed when necessary, by spiking a known amount of midrange standard into a duplicate field sample and then calculating the amount recovered after extraction. Method Detection Limits (MDL) for the F1,F2 fractions were less than 5 µg/L and less than 100 µg/L for the F3 fraction. The F4 range was not detected in any samples (baseline return after F3 range - no MDL was determined).

REFERENCES:

1. Canadian Council of Ministers of the Environment (CCME) method "Reference Method for the Canada-wide Standard for Petroleum Hydrocarbons (CWS-PHC) in Soil – Tier 1 Method" (*MOE Method DECPH-E3421/CCME)*

2. EPA Method 8011- 1,2 Dibromoethane and 1,2-Dibromo-3-chloropropane by Microextraction and Gas Chromatography, July 1992.

3. Glaze, William H., Lin, C.-C., Burleson, J. L., Henderson, J. E., Mapel, D., Rawley, R., Scott, D. R., "Optimization of Liquid-Liquid Extraction Methods for Analysis of Organics in Water", Project Report, Contract No's. CR-805472, CR-808561; USEPA/EMSL: Cincinnati, OH, 1983

4. Henderson, J.E., G.R. Peyton and W.H. Glaze (1976). A convenient liquid-liquid extraction method for the determination of halomethanes in water at the parts-per-billion level. IN: Identification and analysis of organic pollutants in water. Keith, L.H. Ed; Ann Arbor Science Publishers Inc., Ann Arbor, MI.

5. Longbottom, James E., Lichtenberg, James J., Ed. (1982). "Methods for Organic Chemical Analysis of Municipal and Industrial Wastewater", EPA-600/4-82-057, USEPA/EMSL: Cincinnati, OH, Appendix A – Definition and Procedure for the Determination of the Method Detection Limit.

Appendix B

Hydraulic Testing Results

Thiem Calculations of Transmissivity & Hydraulic Conductivity

Borehole # TW1	Date: August 23, 2006	Personnel: K. Greer
	Time: 8:23 AM	

Injection Zone Interval (m.b.g.s)

From	8.5
To	9.5

Field Data

Open Bore-Hole:

$h_{T.O.C}$	=	3.26	m.b.g.s
Casing stick up	=	0.00	m
$h_{static\ open\ borehole}$	=	3.26	m.b.g.s
D T.O.C. to manometer bottom	=	0.80	m.a.g.s
h initial in manometer (ruler)	1/2" =		m
	4" =	0.79	m
$h_{initial}$	=	4.850	m.a.g.s
$P_{transducer\ open\ borehole}$	=	3.1856	m

Calculating h_{static} (shut in):

$P_{transducer\ shut\ in}$	=	0.1268	m
$P_{bore\ hole} - P_{shut\ in}$	=	3.059	m H2O
$h_{shut\ in}$	=	0.20	m.b.g.s

Thiem Equation

$$T = (Q*\ln(r_e/r_w))/(\Delta h*2*\pi)$$

$$r_e = 2*((T/S)*t)^{1/2}$$

Variable Values

S	=	1.E-04	
$T_{estimated}$	=	4.0E-07	m^2/s
t	=	600	secs
r_w	=	0.10	m
$h_{initial}$	=	-4.85	m.b.g.s
h_{static}	=	0.20	m.b.g.s
Δh	=	5.05	m

Transmissivity Calculations

r_e = 3.10 m

T = 4.E-07 m^2/s

Hydraulic Conductivity Calculations

K = T/b

b = 1.0 m

K = 4.E-07 m/s

Injection Test Data

Borehole # TW1 Zone #1 **Date:** August 23, 2006 **Personnel:** K. Greer

Injection Interval	**Depth (m)**
From	8.5
To	9.5

Test Start Time: 8:23 AM

Injection Tube Diameter: 4 inch **X-Sec Area of tube =** 82.3 cm^2

Total Time t (secs)	**Hydraulic Head field (cm)**	**Hydraulic Head Calculated (cm)**	**Volumetric Flow Rate Q (cm^3/s)**	**Comments** Bottom packer was not attached
0	79	0		
5	78.5	0.5	8.23	
10	78	1	8.23	
15	77.8	1.2	3.29	
20	77.6	1.4	3.29	
30	77	2	4.94	
35	77	2	0.00	
40	76.8	2.2	3.29	
50	76.3	2.7	4.12	
60	76	3	2.47	
70	75.5	3.5	4.12	
75	75.3	3.7	3.29	
80	75	4	4.94	
100	74	5	4.12	
105	73.8	5.2	3.29	
110	73.6	5.4	3.29	
115	73.5	5.5	1.65	
120	73.3	5.7	3.29	
125	73	6	4.94	
130	72.8	6.2	3.29	
135	72.8	6.2	0.00	
145	72.3	6.7	4.12	
150	72	7	4.94	
155	71.8	7.2	3.29	
165	71.3	7.7	4.12	
175	71	8	2.47	
180	70.8	8.2	3.29	
190	70.4	8.6	3.29	
200	70	9	3.29	
210	69.8	9.2	1.65	
220	69.3	9.7	4.12	
230	69	10	2.47	
240	68.6	10.4	3.29	
250	68	11	4.94	
260	67.8	11.2	1.65	
270	67.5	11.5	2.47	
280	67	12	4.12	
290	66.7	12.3	2.47	
300	66	13	5.76	
330	65	14	2.74	
360	64	15	2.74	
390	63	16	2.74	
420	62	17	2.74	
450	61	18	2.74	
480	60	19	2.74	
510	59	20	2.74	
540	58	21	2.74	
570	57	22	2.74	
600	56	23	2.74	

Total Time of Test: = 600 secs

$Q_{average}$ = 3.40 cm^3/s

= 3.40E-06 m^3/s

Thiem Calculations of Transmissivity & Hydraulic Conductivity

Borehole # TW1	Date:	August 23, 2006	Personnel:	K. Greer
	Time:	9:03 AM		

Injection Zone Interval (m.b.g.s)

From	7.0
To	8.0

Field Data

Open Bore-Hole:

$h_{T.O.C}$	=	3.26	m.b.g.s
Casing stick up	=	0.00	m
$h_{static\ open\ borehole}$	=	3.26	m.b.g.s
D T.O.C. to manometer bottom	=	0.80	m.a.g.s
h initial in manometer (ruler)	1/2" =		m
	4" =	0.79	m
$h_{initial}$	=	4.850	m.a.g.s
$P_{transducer\ open\ borehole}$	=	1.9622	m

Calculating h_{static} (shut in):

$P_{transducer\ shut\ in}$	=	0.0000	m
$P_{bore\ hole} - P_{shut\ in}$	=	1.962	m H2O
$h_{shut\ in}$	=	1.30	m.b.g.s

Thiem Equation

$$T = (Q*\ln(r_e/r_w))/(\Delta h*2*\pi)$$

$$r_e = 2*((T/S)*t)^{1/2}$$

Variable Values

S	=	1.E-04	
$T_{estimated}$	=	5.0E-06	m^2/s
t	=	120	secs
r_w	=	0.10	m
$h_{initial}$	=	-4.85	m.b.g.s
h_{static}	=	1.30	m.b.g.s
Δh	=	6.15	m

Transmissivity Calculations

r_e =	4.90	m
T =	**5.E-06**	**m^2/s**

Hydraulic Conductivity Calculations

K = T/b

b =	1.0	m
K =	**5.E-06**	**m/s**

Injection Test Data

Borehole # TW1 Zone #2 **Date:** August 23, 2006 **Personnel:** K. Greer

Injection Interval	**Depth (m)**
From	7.0
To	8.0

Test Start Time: 9:03 AM

Injection Tube Diameter: 4 inch **X-Sec Area of tube =** 82.3 cm^2

Total Time t (secs)	**Hydraulic Head field (cm)**	**Hydraulic Head Calculated (cm)**	**Volumetric Flow Rate Q (cm^3/s)**	**Comments**
0	79	0		
5	75	4	65.84	
10	72.5	6.5	41.15	
15	70	9	41.15	
20	67	12	49.38	
25	63	16	65.84	
30	60	19	49.38	
35	57.5	21.5	41.15	
40	54.5	24.5	49.38	
45	51.5	27.5	49.38	
50	48.5	30.5	49.38	
55	45	34	57.61	
60	43	36	32.92	
65	40	39	49.38	
70	35.5	43.5	74.07	
80	30.5	48.5	41.15	
90	25.5	53.5	41.15	
100	19.5	59.5	49.38	
110	14	65	45.27	
120	9	70	41.15	

Total Time of Test: = 120 secs

$Q_{average}$ = 49.16 cm^3/s

= 4.92E-05 m^3/s

Thiem Calculations of Transmissivity & Hydraulic Conductivity

Borehole # TW1	Date: August 23, 2006	Personnel: K. Greer
	Time: 9:48 AM	

Injection Zone Interval (m.b.g.s)

From	5.3
To	6.3

Field Data

Open Bore-Hole:

$h_{T.O.C}$	=	3.26	m.b.g.s	
Casing stick up	=	0.00	m	
$h_{static\ open\ borehole}$	=	3.26	m.b.g.s	
D T.O.C. to manometer bottom	=	0.80	m.a.g.s	
h initial in manometer (ruler)	1/2" =		m	
	4" =	0.79	m	
$h_{initial}$	=	4.850	m.a.g.s	
$P_{transducer\ open\ borehole}$	=	0.7487	m	

Calculating h_{static} (shut in):

$P_{transducer\ shut\ in}$	=	-0.0782	m
$P_{bore\ hole} - P_{shut\ in}$	=	0.827	m H2O
$h_{shut\ in}$	=	2.43	m.b.g.s

Thiem Equation

$$T = (Q*\ln(r_e/r_w))/(\Delta h*2*\pi)$$

$$r_e = 2*((T/S)*t)^{1/2}$$

Variable Values

S	=	1.E-04	
$T_{estimated}$	=	2.0E-06	m^2/s
t	=	230	secs
r_w	=	0.10	m
$h_{initial}$	=	-4.85	m.b.g.s
h_{static}	=	2.43	m.b.g.s
Δh	=	7.28	m

Transmissivity Calculations

r_e = 4.29 m

T = 2.E-06 m^2/s

Hydraulic Conductivity Calculations

K = T/b

b = 1.0 m

K = 2.E-06 m/s

Injection Test Data

Borehole # TW1 Zone #3 **Date:** August 23, 2006 **Personnel:** K. Greer

Injection Interval	**Depth (m)**
From	5.3
To	6.3

Test Start Time: 9:48 AM

Injection Tube Diameter: 4 inch **X-Sec Area of tube =** 82.3 cm^2

Total Time t (secs)	**Hydraulic Head field (cm)**	**Hydraulic Head Calculated (cm)**	**Volumetric Flow Rate Q (cm^3/s)**	**Comments**
0	79	0		
5	76.5	2.5	41.15	
10	74	5	41.15	
15	71.5	7.5	41.15	
20	70	9	24.69	
25	68	11	32.92	
30	66.5	12.5	24.69	
35	64.5	14.5	32.92	
40	63.5	15.5	16.46	
45	61	18	41.15	
50	59	20	32.92	
55	57	22	32.92	
60	55	24	32.92	
65	53.5	25.5	24.69	
70	52	27	24.69	
75	50.5	28.5	24.69	
80	48.5	30.5	32.92	
85	47.5	31.5	16.46	
90	45.5	33.5	32.92	
95	44.5	34.5	16.46	
100	42.5	36.5	32.92	
110	39.5	39.5	24.69	
120	36.5	42.5	24.69	
130	33.5	45.5	24.69	
140	30	49	28.81	
150	27	52	24.69	
160	24.5	54.5	20.58	
170	22	57	20.58	
180	19	60	24.69	
190	16	63	24.69	
200	13	66	24.69	
210	10	69	24.69	
220	7	72	24.69	
230	4.5	74.5	20.58	

Total Time of Test: = 230 secs

$Q_{average}$ = 27.68 cm^3/s

= 2.77E-05 m^3/s

Thiem Calculations of Transmissivity & Hydraulic Conductivity

Borehole # TW1	Date: August 23, 2006	Personnel: K. Greer
	Time: 10:20 AM	

Injection Zone Interval (m.b.g.s)

From	4.3
To	5.3

Field Data

Open Bore-Hole:

$h_{T.O.C}$	=	3.26	m.b.g.s
Casing stick up	=	0.00	m
$h_{static\ open\ borehole}$	=	3.26	m.b.g.s
D T.O.C. to manometer bottom	=	0.80	m.a.g.s
h initial in manometer (ruler)	1/2" =		m
	4" =	0.81	m
$h_{initial}$	=	4.870	m.a.g.s
$P_{transducer\ open\ borehole}$	=	0.0352	m

Calculating h_{static} (shut in):

$P_{transducer\ shut\ in}$	=	-0.1310	m
$P_{bore\ hole} - P_{shut\ in}$	=	0.166	m H2O
$h_{shut\ in}$	=	3.09	m.b.g.s

Thiem Equation

$$T = (Q*\ln(r_e/r_w))/(\Delta h*2*\pi)$$

$$r_e = 2*((T/S)*t)^{1/2}$$

Variable Values

S	=	1.E-04	
$T_{estimated}$	=	1.0E-05	m^2/s
t	=	40	secs
r_w	=	0.10	m
$h_{initial}$	=	-4.87	m.b.g.s
h_{static}	=	3.09	m.b.g.s
Δh	=	7.96	m

Transmissivity Calculations

r_e = 4.00 m

T = 1.E-05 m^2/s

Hydraulic Conductivity Calculations

K = T/b

b = 1.0 m

K = 1.E-05 m/s

Injection Test Data

Borehole # TW1 Zone #4 **Date:** August 23, 2006 **Personnel:** K. Greer

Injection Interval	**Depth (m)**
From	4.3
To	5.3

Test Start Time: 10:20 AM

Injection Tube Diameter: 4 inch **X-Sec Area of tube =** 82.3 cm^2

Total Time t (secs)	**Hydraulic Head field (cm)**	**Hydraulic Head Calculated (cm)**	**Volumetric Flow Rate Q (cm^3/s)**	**Comments**
0	81	0		
5	71	10	164.60	
10	57	24	230.44	
15	47	34	164.60	
20	38	43	148.14	
25	29	52	148.14	
30	20	61	148.14	
35	12	69	131.68	
40	4	77	131.68	

Total Time of Test: = 40 secs

$Q_{average}$ = 158.43 cm^3/s

= 1.58E-04 m^3/s

Thiem Calculations of Transmissivity & Hydraulic Conductivity

Borehole # TW1	Date: August 23, 2006	Personnel: K. Greer
	Time: 10:51 AM	

Injection Zone Interval (m.b.g.s)

From	3.3
To	4.3

Field Data

Open Bore-Hole:

$h_{T.O.C}$	=	3.26	m.b.g.s
Casing stick up	=	0.00	m
$h_{static\ open\ borehole}$	=	3.26	m.b.g.s
D T.O.C. to manometer bottom	=	0.80	m.a.g.s
h initial in manometer (ruler)	1/2" =		m
	4" =	0.80	m
$h_{initial}$ **	=	4.860	m.a.g.s
$P_{transducer\ open\ borehole}$	=	-0.0521	m

Calculating h_{static} (shut in):

$P_{transducer\ shut\ in}$	=	0.0000	m
$P_{bore\ hole} - P_{shut\ in}$	=	-0.052	m H2O
$h_{shut\ in}$	=	3.31	m.b.g.s

Thiem Equation

$$T = (Q*\ln(r_e/r_w))/(\Delta h*2*\pi)$$

$$r_e = 2*((T/S)*t)^{1/2}$$

Variable Values

S	=	1.E-04	
$T_{estimated}$	=	1.0E-05	m^2/s
t	=	35	secs
r_w	=	0.10	m
$h_{initial}$	=	-4.86	m.b.g.s
h_{static}	=	3.31	m.b.g.s
Δh	=	8.17	m

Transmissivity Calculations

r_e = 3.74 m

T = 1.E-05 m^2/s

Hydraulic Conductivity Calculations

K = T/b

b = 1.0 m

K = 1.E-05 m/s

** head could not be measured due to the placment of the packer, head was assumed to be the same as measure for zone 4

Injection Test Data

Borehole # TW1 Zone #5 **Date:** August 23, 2006 **Personnel:** K. Greer

Injection Interval	**Depth (m)**
From	3.3
To	4.3

Test Start Time: 10:51 AM

Injection Tube Diameter: 4 inch **X-Sec Area of tube =** 82.3 cm^2

Total Time t (secs)	**Hydraulic Head field (cm)**	**Hydraulic Head Calculated (cm)**	**Volumetric Flow Rate Q (cm^3/s)**	**Comments**
0	80	0		
5	69	11	181.06	
10	60	20	148.14	
15	48	32	197.52	
20	38	42	164.60	
25	26	54	197.52	
30	17	63	148.14	
35	5	75	197.52	

Total Time of Test: = 35 secs

$Q_{average}$ = 176.36 cm^3/s

= 1.76E-04 m^3/s

Thiem Calculations of Transmissivity & Hydraulic Conductivity

Borehole # TW2	Date: August 22, 2006	Personnel: K. Greer
	Time: 10:54 AM	

Injection Zone Interval (m.b.g.s)

From	8.0
To	9.0

Field Data

Open Bore-Hole:

$h_{T.O.C}$	=	3.35	m.b.g.s
Casing stick up	=	0.00	m
$h_{static\ open\ borehole}$	=	3.35	m.b.g.s
D T.O.C. to manometer bottom	=	0.80	m.a.g.s
h initial in manometer (ruler)	1/2" =	0.82	m
	4" =	0.72	m
$h_{initial}$	=	4.870	m.a.g.s
$P_{transducer\ open\ borehole}$	=	2.8	m

Calculating h_{static} (shut in):

$P_{transducer\ shut\ in}$	=	0.0	m
$P_{bore\ hole} - P_{shut\ in}$	=	2.812	m H2O
$h_{shut\ in}$	=	0.54	m.b.g.s

Thiem Equation

$$T = (Q*\ln(r_e/r_w))/(\Delta h*2*\pi)$$

$$r_e = 2*((T/S)*t)^{1/2}$$

Variable Values

S	=	1.E-04	
$T_{estimated}$	=	6.0E-07	m^2/s
t	=	900	secs
r_w	=	0.10	m
$h_{initial}$	=	-4.87	m.b.g.s
h_{static}	=	0.54	m.b.g.s
Δh	=	5.41	m

Transmissivity Calculations

r_e = 4.65 m

T = 6.E-07 m^2/s

Hydraulic Conductivity Calculations

K = T/b

b = 1.0 m

K = 6.E-07 m/s

Injection Test Data

Borehole # TW2 Zone #1 **Date:** August 22, 2006 **Personnel:** K. Greer

Injection Interval	Depth (m)
From	8.0
To	9.0

Test Start Time: 10:54 AM

Injection Tube Diameter: 4 inch **X-Sec Area of tube =** 82.3 cm^2

Total Time t (secs)	Hydraulic Head field (cm)	Hydraulic Head Calculated (cm)	Volumetric Flow Rate Q (cm^3/s)	Comments
0	72	0		Bottom packer was removed
15	71	1	5.49	
20	70.5	1.5	8.23	
25	70	2	8.23	
30	69.8	2.2	3.29	
35	69.3	2.7	8.23	
40	69	3	4.94	
45	68.5	3.5	8.23	
55	68	4	4.12	
60	67.5	4.5	8.23	
65	67.5	4.5	0.00	
75	66.5	5.5	8.23	
80	66	6	8.23	
90	65.3	6.7	5.76	
100	64.5	7.5	6.58	
110	64	8	4.12	
120	63	9	8.23	
130	62.3	9.7	5.76	
140	61.5	10.5	6.58	
150	61	11	4.12	
160	60.3	11.7	5.76	
170	59.5	12.5	6.58	
180	58.8	13.2	5.76	
190	58	14	6.58	
200	57	15	8.23	
210	56.8	15.2	1.65	
220	56	16	6.58	
230	55.5	16.5	4.12	
240	54.5	17.5	8.23	
250	54	18	4.12	
260	53	19	8.23	
270	52.8	19.2	1.65	
280	52	20	6.58	
290	51	21	8.23	
300	50	22	8.23	
310	49.5	22.5	4.12	
320	49	23	4.12	
330	48.3	23.7	5.76	
360	46	26	6.31	
390	45	27	2.74	
420	43	29	5.49	
450	41	31	5.49	
480	39	33	5.49	
510	37	35	5.49	
540	35	37	5.49	
570	33	39	5.49	
600	31	41	5.49	
630	29	43	5.49	
660	27.5	44.5	4.12	
690	26	46	4.12	
720	24	48	5.49	
750	22	50	5.49	
780	20	52	5.49	
810	18	54	5.49	
840	16	56	5.49	
870	14	58	5.49	
900	12	60	5.49	

Total Time of Test: = 900 secs

$Q_{average}$ = 5.73 cm^3/s

= 5.73E-06 m^3/s

Thiem Calculations of Transmissivity & Hydraulic Conductivity

Borehole # TW2	Date: August 22, 2006	Personnel: K. Greer
	Time: 11:35 AM	

Injection Zone Interval (m.b.g.s)

From	7.0
To	8.0

Field Data

Open Bore-Hole:

$h_{T.O.C}$	=	3.35	m.b.g.s
Casing stick up	=	0.00	m
$h_{static\ open\ borehole}$	=	3.35	m.b.g.s
D T.O.C. to manometer bottom	=	0.80	m.a.g.s
h initial in manometer (ruler)	1/2" =		m
	4" =	0.74	m
$h_{initial}$	=	4.885	m.a.g.s
$P_{transducer\ open\ borehole}$	=	2.1	m

Calculating h_{static} (shut in):

$P_{transducer\ shut\ in}$	=	0.0	m
$P_{bore\ hole} - P_{shut\ in}$	=	2.060	m H2O
$h_{shut\ in}$	=	1.29	m.b.g.s

Thiem Equation

$$T = (Q*\ln(r_e/r_w))/(\Delta h*2*\pi)$$

$$r_e = 2*((T/S)*t)^{1/2}$$

Variable Values

S	=	1.E-04	
$T_{estimated}$	=	7.0E-07	m^2/s
t	=	900	secs
r_w	=	0.10	m
$h_{initial}$	=	-4.89	m.b.g.s
h_{static}	=	1.29	m.b.g.s
Δh	=	6.17	m

Transmissivity Calculations

r_e = 5.02 m

T = 7.E-07 m^2/s

Hydraulic Conductivity Calculations

K = T/b

b = 1.0 m

K = 7.E-07 m/s

Injection Test Data

Borehole # TW2 Zone #2 **Date:** August 22, 2006 **Personnel:** K. Greer

Injection Interval	**Depth (m)**
From	7.0
To	8.0

Test Start Time: 11:35 AM

Injection Tube Diameter: 4 inch **X-Sec Area of tube =** 82.3 cm^2

Total Time t (secs)	**Hydraulic Head field (cm)**	**Hydraulic Head Calculated (cm)**	**Volumetric Flow Rate Q (cm^3/s)**	**Comments** Bottom packer was removed
0	73.5	0		
5	72	1.5	24.69	
10	71.5	2	8.23	
15	71	2.5	8.23	
20	70	3.5	16.46	
30	69.5	4	4.12	
40	69	4.5	4.12	
50	67.5	6	12.35	
60	67	6.5	4.12	
65	66	7.5	16.46	
70	65.5	8	8.23	
80	65	8.5	4.12	
90	64.5	9	4.12	
100	63.5	10	8.23	
110	63	10.5	4.12	
120	62	11.5	8.23	
130	61.3	12.2	5.76	
140	61	12.5	2.47	
150	59.8	13.7	9.88	
160	59	14.5	6.58	
170	58.5	15	4.12	
180	57.8	15.7	5.76	
190	57	16.5	6.58	
200	56.3	17.2	5.76	
210	55.3	18.2	8.23	
220	54.3	19.2	8.23	
230	54	19.5	2.47	
240	53	20.5	8.23	
250	52	21.5	8.23	
260	51.2	22.3	6.58	
270	51	22.5	1.65	
280	50	23.5	8.23	
290	49	24.5	8.23	
300	48.5	25	4.12	
330	46.3	27.2	6.04	
360	44	29.5	6.31	
390	41.5	32	6.86	
420	39.3	34.2	6.04	
450	37	36.5	6.31	
480	35	38.5	5.49	
510	32.3	41.2	7.41	
540	30	43.5	6.31	
570	28	45.5	5.49	
600	25.8	47.7	6.04	
630	24	49.5	4.94	
660	21.5	52	6.86	
690	19	54.5	6.86	
720	17	56.5	5.49	
750	15	58.5	5.49	
780	12.8	60.7	6.04	
810	10.3	63.2	6.86	
840	8	65.5	6.31	
870	6	67.5	5.49	
900	4	69.5	5.49	

Total Time of Test: = 900 secs

$Q_{average}$ = 6.96 cm^3/s

= 6.96E-06 m^3/s

Thiem Calculations of Transmissivity & Hydraulic Conductivity

Borehole # TW2	Date: August 22, 2006	Personnel: K. Greer
	Time: 1:27 PM	

Injection Zone Interval (m.b.g.s)

From	6.4
To	7.4

Field Data

Open Bore-Hole:

$h_{T.O.C}$	=	3.35	m.b.g.s
Casing stick up	=	0.00	m
$h_{static\ open\ borehole}$	=	3.35	m.b.g.s
D T.O.C. to manometer bottom	=	0.80	m.a.g.s
h initial in manometer (ruler)	1/2" =		m
	4" =	0.76	m
$h_{initial}$	=	4.910	m.a.g.s
$P_{transducer\ open\ borehole}$	=	1.6	m

Calculating h_{static} (shut in):

$P_{transducer\ shut\ in}$	=	0.0	m
$P_{bore\ hole} - P_{shut\ in}$	=	1.621	m H2O
$h_{shut\ in}$	=	1.73	m.b.g.s

Thiem Equation

$$T = (Q*\ln(r_e/r_w))/(\Delta h*2*\pi)$$

$$r_e = 2*((T/S)*t)^{1/2}$$

Variable Values

S	=	1.E-04	
$T_{estimated}$	=	2.0E-07	m^2/s
t	=	900	secs
r_w	=	0.10	m
$h_{initial}$	=	-4.91	m.b.g.s
h_{static}	=	1.73	m.b.g.s
Δh	=	6.64	m

Transmissivity Calculations

r_e = 2.68 m

T = 2.E-07 m^2/s

Hydraulic Conductivity Calculations

K = T/b

b = 1.0 m

K = 2.E-07 m/s

Injection Test Data

Borehole # TW2 Zone #3 **Date:** August 22, 2006 **Personnel:** K. Greer

Injection Interval	Depth (m)
From	6.4
To	7.4

Test Start Time: 1:27 PM

Injection Tube Diameter: 4 inch **X-Sec Area of tube =** 82.3 cm^2

Total Time t (secs)	Hydraulic Head field (cm)	Hydraulic Head Calculated (cm)	Volumetric Flow Rate Q (cm^3/s)	Comments
0	76	0		
5	74	2	32.92	
10	73	3	16.46	
15	72.5	3.5	8.23	
20	72.3	3.7	3.29	
25	72.3	3.7	0.00	
30	72.3	3.7	0.00	
35	72	4	4.94	
40	71.8	4.2	3.29	
45	71.7	4.3	1.65	
50	71.6	4.4	1.65	
55	71.5	4.5	1.65	
60	71.3	4.7	3.29	
65	71	5	4.94	
70	70.8	5.2	3.29	
90	70.8	5.2	0.00	
100	70.8	5.2	0.00	
105	70.7	5.3	1.65	
110	70.7	5.3	0.00	
120	70.5	5.5	1.65	
150	70	6	1.37	
165	69.8	6.2	1.10	
180	69.5	6.5	1.65	
195	69.3	6.7	1.10	
210	69	7	1.65	
225	68.8	7.2	1.10	
240	68.5	7.5	1.65	
255	68.3	7.7	1.10	
270	68	8	1.65	
285	67.8	8.2	1.10	
300	67.5	8.5	1.65	
330	67	9	1.37	
360	66.5	9.5	1.37	
390	66	10	1.37	
420	65.5	10.5	1.37	
450	65	11	1.37	
480	64.5	11.5	1.37	
510	64.2	11.8	0.82	
540	63.8	12.2	1.10	
570	63.3	12.7	1.37	
600	62.8	13.2	1.37	
630	62.3	13.7	1.37	
660	62	14	0.82	
690	61.7	14.3	0.82	
720	61.3	14.7	1.10	
750	60.8	15.2	1.37	
780	60.4	15.6	1.10	
810	59.8	16.2	1.65	
840	59.3	16.7	1.37	
870	59	17	0.82	
900	58.7	17.3	0.82	

Total Time of Test: = 900 secs

$Q_{average}$ = 2.56 cm^3/s

= 2.56E-06 m^3/s

Thiem Calculations of Transmissivity & Hydraulic Conductivity

Borehole # TW2	Date: August 22, 2006	Personnel: K. Greer
	Time: 2:22 PM	

Injection Zone Interval (m.b.g.s)

From	5.4
To	6.4

Field Data

Open Bore-Hole:

$h_{T.O.C}$	=	3.35	m.b.g.s
Casing stick up	=	0.00	m
$h_{static\ open\ borehole}$	=	3.35	m.b.g.s
D T.O.C. to manometer bottom	=	0.80	m.a.g.s
h initial in manometer (ruler)	1/2" =		m
	4" =	0.77	m
$h_{initial}$	=	4.915	m.a.g.s
$P_{transducer\ open\ borehole}$	=	0.8	m

Calculating h_{static} (shut in):

$P_{transducer\ shut\ in}$	=	0.0	m
$P_{bore\ hole} - P_{shut\ in}$	=	0.785	m H2O
$h_{shut\ in}$	=	2.56	m.b.g.s

Thiem Equation

$$T = (Q*\ln(r_e/r_w))/(\Delta h*2*\pi)$$

$$r_e = 2*((T/S)*t)^{1/2}$$

Variable Values

S	=	1.E-04	
$T_{estimated}$	=	1.0E-07	m^2/s
t	=	900	secs
r_w	=	0.10	m
$h_{initial}$	=	-4.92	m.b.g.s
h_{static}	=	2.56	m.b.g.s
Δh	=	7.48	m

Transmissivity Calculations

r_e = 1.90 m

T = 1.E-07 m^2/s

Hydraulic Conductivity Calculations

K = T/b

b = 1.0 m

K = 1.E-07 m/s

Injection Test Data

Borehole # TW2 Zone #4 **Date:** August 22, 2006 **Personnel:** K. Greer

Injection Interval	Depth (m)
From	5.4
To	6.4

Test Start Time: 2:22 PM

Injection Tube Diameter: 4 inch **X-Sec Area of tube =** 82.3 cm^2

Total Time t (secs)	Hydraulic Head field (cm)	Hydraulic Head Calculated (cm)	Volumetric Flow Rate Q (cm^3/s)	Comments
0	76.5	0		
5	76.3	0.2	3.29	
10	76	0.5	4.94	
15	75.9	0.6	1.65	
20	75.8	0.7	1.65	
25	75.7	0.8	1.65	
30	75.5	1	3.29	
40	75	1.5	4.12	
45	74.8	1.7	3.29	
50	74.8	1.7	0.00	
55	74.7	1.8	1.65	
65	74.5	2	1.65	
70	74.3	2.2	3.29	
75	74.2	2.3	1.65	
80	74	2.5	3.29	
90	73.7	2.8	2.47	
100	73.5	3	1.65	
105	73.3	3.2	3.29	
115	73.2	3.3	0.82	
125	73	3.5	1.65	
130	73	3.5	0.00	
135	73	3.5	0.00	
140	73	3.5	0.00	
145	73	3.5	0.00	
180	72.8	3.7	0.47	
210	72	4.5	2.19	
240	71.5	5	1.37	
270	70.7	5.8	2.19	
300	70.5	6	0.55	
330	70	6.5	1.37	
360	69.7	6.8	0.82	
390	69	7.5	1.92	
420	68.7	7.8	0.82	
450	68	8.5	1.92	
480	67.7	8.8	0.82	
510	67.3	9.2	1.10	
540	67	9.5	0.82	
570	66.3	10.2	1.92	
600	65.8	10.7	1.37	
660	64.5	12	1.78	
720	64	12.5	0.69	
780	62.8	13.7	1.65	
840	62	14.5	1.10	
900	61	15.5	1.37	

Total Time of Test: = 900 secs

$Q_{average}$ = 1.66 cm^3/s

= 1.66E-06 m^3/s

Thiem Calculations of Transmissivity & Hydraulic Conductivity

Borehole # TW2	Date: August 22, 2006	Personnel: K. Greer
	Time: 3:22 PM	

Injection Zone Interval (m.b.g.s)

From	4.4
To	5.4

Field Data

Open Bore-Hole:

$h_{T.O.C}$	=	3.35	m.b.g.s
Casing stick up	=	0.00	m
$h_{static\ open\ borehole}$	=	3.35	m.b.g.s
D T.O.C. to manometer bottom	=	0.80	m.a.g.s
h initial in manometer (ruler)	1/2" =		m
	4" =	0.78	m
$h_{initial}$	=	4.928	m.a.g.s
$P_{transducer\ open\ borehole}$	=	0.1176	m

Calculating h_{static} (shut in):

$P_{transducer\ shut\ in}$	=	0.0958	m
$P_{bore\ hole} - P_{shut\ in}$	=	0.022	m H2O
$h_{shut\ in}$	=	3.33	m.b.g.s

Thiem Equation

$$T = (Q*\ln(r_e/r_w))/(\Delta h*2*\pi)$$

$$r_e = 2*((T/S)*t)^{1/2}$$

Variable Values

S	=	1.E-04	
$T_{estimated}$	=	4.0E-06	m^2/s
t	=	130	secs
r_w	=	0.10	m
$h_{initial}$	=	-4.93	m.b.g.s
h_{static}	=	3.33	m.b.g.s
Δh	=	8.26	m

Transmissivity Calculations

r_e = 4.56 m

T = 4.E-06 m^2/s

Hydraulic Conductivity Calculations

K = T/b

b = 1.0 m

K = 4.E-06 m/s

Injection Test Data

Borehole # TW2 Zone #5 **Date:** August 22, 2006 **Personnel:** K. Greer

Injection Interval	**Depth (m)**
From	4.4
To	5.4

Test Start Time: 3:22 PM

Injection Tube Diameter: 4 inch **X-Sec Area of tube =** 82.3 cm^2

Total Time t (secs)	**Hydraulic Head field (cm)**	**Hydraulic Head Calculated (cm)**	**Volumetric Flow Rate Q (cm^3/s)**	**Comments** Run # 2 for this zone
0	79.5	0		
5	70	9.5	156.37	
10	60	19.5	164.60	
15	51	28.5	148.14	
20	43	36.5	131.68	
25	38	41.5	82.30	
30	32	47.5	98.76	
35	29	50.5	49.38	
40	26	53.5	49.38	
45	24	55.5	32.92	
50	22	57.5	32.92	
55	21	58.5	16.46	
60	19.5	60	24.69	
65	19	60.5	8.23	
70	17.5	62	24.69	
80	15	64.5	20.58	
85	14.5	65	8.23	
90	13.5	66	16.46	
95	12.5	67	16.46	
100	11.5	68	16.46	
115	10.5	69	5.49	
120	9.5	70	16.46	
125	8.5	71	16.46	
130	6.5	73	32.92	

Total Time of Test: = 130 secs

$Q_{average}$ = 50.87 cm^3/s

= 5.09E-05 m^3/s

Thiem Calculations of Transmissivity & Hydraulic Conductivity

Borehole # TW2	Date: August 22, 2006	Personnel: K. Greer
	Time: 3:22 PM	

Injection Zone Interval (m.b.g.s)

From	4.4
To	5.4

Field Data

Open Bore-Hole:

$h_{T.O.C}$	=	3.35	m.b.g.s
Casing stick up	=	0.00	m
$h_{static\ open\ borehole}$	=	3.35	m.b.g.s
D T.O.C. to manometer bottom	=	0.80	m.a.g.s
h initial in manometer (ruler)	1/2" =		m
	4" =	0.78	m
$h_{initial}$	=	4.928	m.a.g.s
$P_{transducer\ open\ borehole}$	=	0.0401	m

Calculating h_{static} (shut in):

$P_{transducer\ shut\ in}$	=	0.0042	m
$P_{bore\ hole} - P_{shut\ in}$	=	0.036	m H2O
$h_{shut\ in}$	=	3.31	m.b.g.s

Thiem Equation

$$T = (Q*\ln(r_e/r_w))/(\Delta h*2*\pi)$$

$$r_e = 2*((T/S)*t)^{1/2}$$

Variable Values

S	=	1.E-04	
$T_{estimated}$	=	3.0E-06	m^2/s
t	=	120	secs
r_w	=	0.10	m
$h_{initial}$	=	-4.93	m.b.g.s
h_{static}	=	3.31	m.b.g.s
Δh	=	8.24	m

Transmissivity Calculations

r_e = 3.79 m

T = 3.E-06 m^2/s

Hydraulic Conductivity Calculations

K = T/b

b = 1.0 m

K = 3.E-06 m/s

Injection Test Data

Borehole # TW2 Zone #5 **Date:** August 22, 2006 **Personnel:** K. Greer

Injection Interval	**Depth (m)**
From	4.4
To	5.4

Test Start Time: 3:22 PM

Injection Tube Diameter: 4 inch **X-Sec Area of tube =** 82.3 cm^2

Total Time t (secs)	**Hydraulic Head field (cm)**	**Hydraulic Head Calculated (cm)**	**Volumetric Flow Rate Q (cm^3/s)**	**Comments** Run # 1 for this zone
0	77.8	0		
5	71	6.8	111.93	
10	63	14.8	131.68	
15	52	25.8	181.06	
20	44	33.8	131.68	
25	37	40.8	115.22	
30	31	46.8	98.76	
35	27	50.8	65.84	
40	23	54.8	65.84	
45	21	56.8	32.92	
50	19	58.8	32.92	
55	18	59.8	16.46	
60	17	60.8	16.46	
65	15.5	62.3	24.69	
70	15	62.8	8.23	
75	14	63.8	16.46	
80	13	64.8	16.46	
85	12	65.8	16.46	
90	11	66.8	16.46	
95	10	67.8	16.46	
100	9	68.8	16.46	
105	8.5	69.3	8.23	
110	7	70.8	24.69	
115	6.5	71.3	8.23	
120	6	71.8	8.23	

Total Time of Test: = 120 secs

$Q_{average}$ = 49.24 cm^3/s

= 4.92E-05 m^3/s

Thiem Calculations of Transmissivity & Hydraulic Conductivity

Borehole # TW2	Date: August 22, 2006	Personnel: K. Greer
	Time: 4:43 PM	

Injection Zone Interval (m.b.g.s)

From	3.4
To	4.4

Field Data

Open Bore-Hole:

$h_{T.O.C}$	=	3.35	m.b.g.s
Casing stick up	=	0.00	m
$h_{static\ open\ borehole}$	=	3.35	m.b.g.s
D T.O.C. to manometer bottom	=	0.80	m.a.g.s
h initial in manometer (ruler)	1/2" =		m
	4" =	0.80	m
$h_{initial}$ **	=	4.950	m.a.g.s
$P_{transducer\ open\ borehole}$	=	0.0000	m

Calculating h_{static} (shut in):

$P_{transducer\ shut\ in}$	=	0.0000 m
$P_{bore\ hole} - P_{shut\ in}$	=	0.000 m H2O
$h_{shut\ in}$	=	3.35 m.b.g.s

Thiem Equation

$$T = (Q*\ln(r_e/r_w))/(\Delta h*2*\pi)$$

$$r_e = 2*((T/S)*t)^{1/2}$$

Variable Values

S	=	1.E-04	
$T_{estimated}$	=	1.0E-05	m^2/s
t	=	35	secs
r_w	=	0.10	m
$h_{initial}$	=	-4.95	m.b.g.s
h_{static}	=	3.35	m.b.g.s
Δh	=	8.30	m

Transmissivity Calculations

r_e = 3.74 m

T = 1.E-05 m^2/s

Hydraulic Conductivity Calculations

K = T/b

b = 1.0 m

K = 1.E-05 m/s

** head could not be measured due to the placment of the packer, head was assumed to be the same as measure for zone 5

Injection Test Data

Borehole # TW2 Zone #6 **Date:** August 22, 2006 **Personnel:** K. Greer

Injection Interval	**Depth (m)**
From	3.4
To	4.4

Test Start Time: 4:43 PM

Injection Tube Diameter: 4 inch **X-Sec Area of tube =** 82.3 cm^2

Total Time t (secs)	**Hydraulic Head field (cm)**	**Hydraulic Head Calculated (cm)**	**Volumetric Flow Rate Q (cm^3/s)**	**Comments**
0	80	0		**Run # 2 for this zone**
5	70	10	164.60	
10	60	20	164.60	
15	48	32	197.52	
20	38	42	164.60	
25	28	52	164.60	
30	18	62	164.60	
35	8	72	164.60	

Total Time of Test: = 35 secs

$Q_{average}$ = 169.30 cm^3/s

= 1.69E-04 m^3/s

Thiem Calculations of Transmissivity & Hydraulic Conductivity

Borehole # TW2	Date: August 22, 2006	Personnel: K. Greer
	Time: 4:19 PM	

Injection Zone Interval (m.b.g.s)

From	3.4
To	4.4

Field Data

Open Bore-Hole:

$h_{T.O.C}$	=	3.35	m.b.g.s
Casing stick up	=	0.00	m
$h_{static\ open\ borehole}$	=	3.35	m.b.g.s
D T.O.C. to manometer bottom	=	0.80	m.a.g.s
h initial in manometer (ruler)	1/2" =		m
	4" =	0.79	m
$h_{initial}$ **	=	4.940	m.a.g.s
$P_{transducer\ open\ borehole}$	=	0.0000	m

Calculating h_{static} (shut in):

$P_{transducer\ shut\ in}$	=	0.0000 m
$P_{bore\ hole} - P_{shut\ in}$	=	0.000 m H2O
$h_{shut\ in}$	=	3.35 m.b.g.s

Thiem Equation

$$T = (Q*\ln(r_e/r_w))/(\Delta h*2*\pi)$$

$$r_e = 2*((T/S)*t)^{1/2}$$

Variable Values

S	=	1.E-04	
$T_{estimated}$	=	1.0E-05	m^2/s
t	=	30	secs
r_w	=	0.10	m
$h_{initial}$	=	-4.94	m.b.g.s
h_{static}	=	3.35	m.b.g.s
Δh	=	8.29	m

Transmissivity Calculations

r_e = 3.46 m

T = 1.E-05 m^2/s

Hydraulic Conductivity Calculations

K = T/b

b = 1.0 m

K = 1.E-05 m/s

** head could not be measured due to the placment of the packer, head was assumed to be the same as measure for zone 5

Injection Test Data

Borehole # TW2 Zone #6 **Date:** August 22, 2006 **Personnel:** K. Greer

Injection Interval	**Depth (m)**
From	3.4
To	4.4

Test Start Time: 4:19 PM

Injection Tube Diameter: 4 inch **X-Sec Area of tube =** 82.3 cm^2

Total Time t (secs)	**Hydraulic Head field (cm)**	**Hydraulic Head Calculated (cm)**	**Volumetric Flow Rate Q (cm^3/s)**	**Comments**
0	79	0		**Run # 1 for this zone**
5	65	14	230.44	
10	57	22	131.68	
15	44	35	213.98	
20	34	45	164.60	
25	23	56	181.06	
30	13	66	164.60	

Total Time of Test: = 30 secs

$Q_{average}$ = 181.06 cm^3/s

= 1.81E-04 m^3/s

Appendix C

Analytical Results

Petroleum Hydrocarbon Analytical Data

Parameter	TW1-1			TW1-2			TW1-3		
	8-Nov-06	25-Apr-07	25-Apr-08	8-Nov-06	25-Apr-07	25-Apr-08	8-Nov-06	25-Apr-07	25-Apr-08
benzene	159.12	77.7	1.15	0.41	0.2	<1.32	1.81	0.3	<1.32
toluene	14.28	30.8	<1.12	0.13	<1.0	<1.12	0.20	<1.0	<1.12
ethylbenzene	559.37	361.6	7.67	1.14	3.5	<1.50	1.24	2.2	<1.50
p+m-xylene	724.17	327.8	8.30	1.70	2.7	<2.63	2.13	1.7	<2.63
o-xylene	267.03	95.1	7.16	1.29	1.1	<1.79	1.29	<2.1	<1.79
Total Xylenes	991.19	422.97	15.46	3.00	3.86	<4.42	3.42	1.70	<4.42
1,3,5-trimethylbenzene	25.15	4.0	<1.05	<1.06	<1.1	<1.05	<1.06	<1.1	<1.05
1,2,4-trimethylbenzene	440.72	259.3	11.05	1.56	2.8	<0.96	2.31	1.6	<0.96
1,2,3-trimethylbenzene	138.13	73.7	5.74	<1.27	1.1	<1.19	1.52	<1.3	<1.19
naphthalene	170.80	101.8	20.08	<2.14	1.0	<2.21	0.88	<2.1	<2.21
indole+2-methyl naphthalene	65.32	5.5	-	<2.76	<2.8	-	<2.76	<2.8	-
1-methyl naphthalene	56.01	38.7	-	2.40	<1.4	-	<1.42	<1.4	-
biphenyl	17.10	7.0	-	<2.63	<2.6	-	<2.63	<2.6	-
acenaphthylene	10.13	5.4	-	2.31	<1.4	-	<1.40	<1.4	-
acenaphthene	<1.25	<1.3	-	<1.25	<1.3	-	<1.25	<1.3	-
dibenzofuran	22.59	15.3	-	<2.67	<2.7	-	<2.67	<2.7	-
fluorene	11.50	3.6	-	<1.56	<1.6	-	<1.56	<1.6	-
phenanthrene	<1.98	<2.0	-	<1.98	<2.0	-	<1.98	<2.0	-
anthracene	<2.57	<2.6	-	<2.57	<2.6	-	<2.57	<2.6	-
carbazole	<1.29	<1.3	-	<1.29	<1.3	-	<1.29	<1.3	-
fluoranthene	<3.01	<3.0	-	<3.01	<3.0	-	<3.01	<3.0	-
pyrene	<2.28	<2.3	-	<2.28	<2.3	-	<2.28	<2.3	-
B(A)anthracene	14.13	<2.6	-	<2.57	<2.6	-	<2.57	<2.6	-
chrysene	<7.42	<7.4	-	<7.42	<7.4	-	<7.42	<7.4	-
B(b+k)fluoranthene	<2.29	<2.3	-	<2.29	<2.3	-	<2.29	<2.3	-
B(a)pyrene	<1.55	<1.5	-	<1.55	<1.5	-	<1.55	<1.5	-
indeno(1,2,3,c,d)pyrene+dibenzo(a,h)anthracene	<4.45	<4.4	-	<4.45	<4.4	-	<4.45	<4.4	-
benzo(g,h,i)perylene	<1.78	<1.8	-	<1.78	<1.8	-	<1.78	<1.8	-
PHC F1 Fraction (minus BTEX)	554.13	347.2	-	3.85	4.0	-	4.96	9.1	-
PHC F2 Fraction (Minus Naphthalene)	3012.77	1385.6	-	108.81	22.8	-	45.64	23.0	-
PHC F3 Fraction (Minus 9 PAH's)	321.58	27.1	-	47.14	17.5	-	12.25	8.7	-

Notes

Units in µg/L

TW1-5 was dry screen located at 7.3 m

- not analysed

Petroleum Hydrocarbon Analytical Data (cont.)

Parameter	TW1-4						TW1-6		
	8-Nov-06	8-Nov-06 Field Dup	25-Apr-07	25-Apr-07 Field Dup	25-Apr-08	25-Apr-08 Field Dup	8-Nov-06	25-Apr-07	25-Apr-08
benzene	2.23	2.38	<0.8	0.2	1.26	1.35	20.08	0.3	<1.32
toluene	0.79	0.85	<1.0	<1.0	<1.12	<1.12	18.11	<1.0	<1.12
ethylbenzene	2.09	4.86	1.3	1.3	<1.50	<1.50	74.47	2.2	<1.50
p+m-xylene	4.45	7.42	0.8	0.7	1.61	<2.63	104.22	2.1	<2.63
o-xylene	2.96	3.21	<2.1	<2.1	1.42	1.44	36.73	1.4	<1.79
Total Xylenes	7.41	10.63	0.8	0.7	3.03	1.44	140.95	3.50	<4.42
1,3,5-trimethylbenzene	<1.06	<1.06	<1.1	<1.1	<1.05	<1.05	<1.06	<1.1	<1.05
1,2,4-trimethylbenzene	3.03	5.26	1.0	1.1	1.54	1.27	53.93	2.5	<0.96
1,2,3-trimethylbenzene	2.38	2.45	<1.3	<1.3	1.59	1.33	21.05	1.2	<1.19
naphthalene	2.67	3.86	<2.1	<2.1	1.79	1.47	24.21	1.0	<2.21
indole+2-methyl naphthalene	<2.76	<2.76	<2.8	<2.8	-	-	<2.76	<2.8	-
1-methyl naphthalene	<1.42	<1.42	<1.4	<1.4	-	-	<1.42	<1.4	-
biphenyl	<2.63	<2.63	<2.6	<2.6	-	-	<2.63	<2.6	-
acenaphthylene	<1.40	<1.40	<1.4	<1.4	-	-	<1.40	2.0	-
acenaphthene	<1.25	<1.25	<1.3	<1.3	-	-	<1.25	<1.3	-
dibenzofuran	<2.67	<2.67	<2.7	<2.7	-	-	<2.67	<2.7	-
fluorene	<1.56	<1.56	<1.6	<1.6	-	-	<1.56	<1.6	-
phenanthrene	<1.98	<1.98	<2.0	<2.0	-	-	<1.98	<2.0	-
anthracene	<2.57	<2.57	<2.6	<2.6	-	-	<2.57	<2.6	-
carbazole	<1.29	<1.29	<1.3	<1.3	-	-	<1.29	<1.3	-
fluoranthene	<3.01	<3.01	<3.0	<3.0	-	-	<3.01	<3.0	-
pyrene	<2.28	<2.28	<2.3	<2.3	-	-	<2.28	<2.3	-
B(A)anthracene	<2.57	<2.57	<2.6	<2.6	-	-	<2.57	<2.6	-
chrysene	<7.42	<7.42	<7.4	<7.4	-	-	<7.42	<7.4	-
B(b+k)fluoranthene	<2.29	<2.29	<2.3	<2.3	-	-	<2.29	<2.3	-
B(a)pyrene	<1.55	<1.55	<1.5	<1.5	-	-	<1.55	<1.5	-
indeno(1,2,3,c,d)pyrene+dibenzo(a,h)anthracene	<4.45	<4.45	<4.4	<4.4	-	-	<4.45	<4.4	-
benzo(g,h,i)perylene	<1.78	<1.78	<1.8	<1.8	-	-	<1.78	<1.8	-
PHC F1 Fraction (minus BTEX)	2.98	4.97	7.6	1.2	-	-	5.80	29.1	-
PHC F2 Fraction (Minus Naphthalene)	18.45	30.54	27.2	9.1	-	-	23.75	22.8	-
PHC F3 Fraction (Minus 9 PAH's)	5.58	6.79	12.7	5.7	-	-	13.80	12.4	-

Petroleum Hydrocarbon Analytical Data (cont.)

Parameter	TW1-7			TW2				Effluent
	8-Nov-06	25-Apr-07	25-Apr-08	8-Nov-06	25-Apr-07	25-Apr-07 Field Dup	25-Apr-08	25-Apr-07
benzene	38.44	2.7	3.11	26.25	3.2	3.1	4.95	0.2
toluene	5.98	<1.0	<1.12	10.03	0.3	0.2	<1.12	0.3
ethylbenzene	58.65	3.8	<1.50	61.13	2.3	2.2	<1.50	0.0
p+m-xylene	38.26	2.6	<2.63	67.04	0.3	<2.2	<2.63	<2.2
o-xylene	10.78	1.1	<1.79	25.97	<2.1	<2.1	<1.79	<2.1
Total Xylenes	49.04	3.72	<4.42	93.01	0.3	<2.0	<4.42	<2.0
1,3,5-trimethylbenzene	<1.06	<1.1	<1.05	1.29	<1.1	<1.1	<1.05	<1.1
1,2,4-trimethylbenzene	41.72	3.8	<0.96	14.07	<1.1	<1.1	<0.96	<1.1
1,2,3-trimethylbenzene	17.98	1.6	<1.19	9.99	1.3	1.4	<1.19	<1.3
naphthalene	24.07	1.7	<2.21	21.49	3.6	3.5	2.41	<2.1
indole+2-methyl naphthalene	<2.76	<2.8	-	14.12	<2.8	<2.8	-	2.7
1-methyl naphthalene	<1.42	<1.4	-	6.33	<1.4	<1.4	-	3.8
biphenyl	<2.63	<2.6	-	2.06	<2.6	<2.6	-	<2.6
acenaphthylene	<1.40	<1.4	-	2.07	1.5	2.4	-	<1.4
acenaphthene	<1.25	<1.3	-	<1.25	<1.3	<1.3	-	<1.3
dibenzofuran	<2.67	<2.7	-	4.80	3.1	3.0	-	<2.7
fluorene	<1.56	<1.6	-	2.67	<1.6	<1.6	-	<1.6
phenanthrene	<1.98	<2.0	-	<1.98	<2.0	<2.0	-	<2.0
anthracene	<2.57	<2.6	-	<2.57	<2.6	<2.6	-	<2.6
carbazole	<1.29	<1.3	-	<1.29	<1.3	<1.3	-	<1.3
fluoranthene	<3.01	<3.0	-	<3.01	<3.0	<3.0	-	<3.0
pyrene	<2.28	<2.3	-	<2.28	<2.3	<2.3	-	<2.3
B(A)anthracene	<2.57	<2.6	-	<2.57	<2.6	<2.6	-	<2.6
chrysene	<7.42	<7.4	-	<7.42	<7.4	<7.4	-	<7.4
B(b+k)fluoranthene	<2.29	<2.3	-	<2.29	<2.3	<2.3	-	<2.3
B(a)pyrene	<1.55	<1.5	-	<1.55	<1.5	<1.5	-	<1.5
indeno(1,2,3,c,d)pyrene+dibenzo(a,h)anthracene	<4.45	<4.4	-	<4.45	<4.4	<4.4	-	<4.4
benzo(g,h,i)perylene	<1.78	<1.8	-	<1.78	<1.8	<1.8	-	<1.8
PHC F1 Fraction (minus BTEX)	43.94	5.0	-	27.32	12.1	15.4	-	11.8
PHC F2 Fraction (Minus Naphthalene)	166.43	21.9	-	246.09	150.8	156.4	-	72.9
PHC F3 Fraction (Minus 9 PAH's)	12.25	11.4	-	7.84	19.4	11.3	-	23.0

Additional Analytical Results

Parameter	Units	TW1-1		TW1-2		TW1-3		TW1-4		TW1-6		TW1-7	
		8-Nov-06	25-Apr-07	8-Nov-06	25-Apr-07	8-Nov-06	25-Apr-07	8-Nov-06	25-Apr-07	8-Nov-06	25-Apr-07	8-Nov-06	25-Apr-07
pH		6.91	7.23	6.92	7.5	7.08	7.63	7.11	7.75	7.13	7.9	7.24	7.46
conductivity	µs	2070	3522	1488	1778	1490	1817	1600	1855	1930	>3999	2136	2411
Temperature	°C	13.3	-	13.6	-	13.5	-	13.5	-	13	-	12.4	-
DO	mg/L	1.6	1.3	9	3.1	8.2	2.8	8.1	2.5	8.8	7.3	2.1	6.2
BOD	mg/L	15.7	-	0.27	-	1.73	-	0.13	-	1.6	-	2.93	-
Iron (dissolved)	mg/L	2.78	-	0.34	-	0.3	-	0.3	-	0.48	-	6.21	-
Iron (total)	mg/L	3.45	-	0.36	-	0.34	-	0.34	-	8.08	-	6.33	-
Manganese (dissolved)	mg/L	0.132	-	0.019	-	0.064	-	0.098	-	0.083	-	0.12	-
Manganese (total)	mg/L	0.157	-	0.015	-	0.068	-	0.105	-	0.24	-	0.123	-

Parameter	Units	TW2	
		8-Nov-06	25-Apr-07
pH		6.97	7.6
conductivity	µs	1690	2128
Temperature	°C	13.9	-
DO	mg/L	2.2	5.2
BOD	mg/L	3.8	1.17
Iron (dissolved)	mg/L	0.39	-
Iron (total)	mg/L	0.59	-
Manganese (dissolved)	mg/L	0.046	-
Manganese (total)	mg/L	0.051	-

Notes
TW1-5 was dry screen located at 7.3 m
- not analysed

Appendix D

SF_6 Tracer Test Results and Cross Borehole Test Results

SF6 Tracer Test Results
Fergus
July 17 to 27, 2007

Sample Location	Well Depth (m)	Pre Test 16-Jul-07	Day 0 17-Jul-07	Day 1 18-Jul-07	Day 2 19-Jul-07	Day 3 20-Jul-07	Day 4 21-Jul-07	Day 5 22-Jul-07	Day 6 23-Jul-07	Day 7 24-Jul-07	Day 8 25-Jul-07	Day 9 26-Jul-07	Day 10 27-Jul-07
		Hours	0.3	18.0	36.0	54.0	69.0	93.0	103.0	114.8	138.8	162.8	186.8
TW2	9.05	0	1860.0	81.0	60.0	47.5	18.3	14.4	10.6	7.7	5.5	3.7	2.8
TW1-1	3.5	0	0	0.5	0.1	0.4	ns	0.1	<0.1	<0.1	<0.1	<0.1	<0.1
TW1-2	4.1	0	0	270.8	8.4	9.4	ns	0.9	0.2	0.1	0.4	0.1	0.1
TW1-3	4.7	0	0	354.9	14.1	8.5	ns	0.4	0.7	3.0	0.4	0.2	0.2
TW1-4	5.3	0	0	478.2	86.5	21.5	ns	2.9	3.5	9.7	2.1	1.2	0.7
TW1-6	7.9	0	ns	dry	dry	dry	ns	dry	dry	<0.1	dry	dry	dry
TW1-7	9	0	ns	<0.1	<0.1	<0.1	ns	<0.1	<0.1	<0.1	<0.1	<0.1	<0.1
MW44	5.85	0	ns	ns	ns	ns	ns	ns	<0.1	<0.1	<0.1	<0.1	<0.1

Notes:
results in ug/L
TW1-5 was dry
NS - Not sampled
dry - Not sampled because the well was dry
Tracer was injected into TW2 on July 17, 2007
500L of batch treated water with SF6 (bubbled for approximately 3 hr)
concentration on injected water was SF6 Co = 2473.0 ug/L
injection zone from 3.55 to 9 mbgs

Cross Borehole Test

TW1-1

Time (s)	Water level
0	2.99
376	2.99
705	2.99
1071	2.99
1370	2.99
1736	2.99
2302	2.99
2927	2.99
3480	2.99
4303	2.99
4853	2.99

TW1-2

Time (s)	Water level
0	2.99
285	2.96
660	2.96
1029	2.95
1325	2.95
1676	2.95
2257	2.965
2875	2.96
3421	2.96
4260	2.96
4784	2.96
5332	2.96

TW1-3

Time (s)	Water level
0	3.03
234	2.98
611	2.99
978	2.995
1298	2.98
1620	2.98
2233	2.98
2845	2.98
3380	2.98
4160	2.98
4723	2.98
5262	2.98

TW1-6

Time (s)	Water level
0	7.695
856	7.695
1492	7.695
2160	7.695
2526	7.695
3600	7.695

TW1-4

Time (s)	Water level
0	3.05
109	3.05
189	3.05
417	3.05
540	3.05
754	3.05
936	3.05
1140	3.05
1260	3.05
1535	3.05
1816	3.05
2187	3.05
2373	3.05
2666	3.05
2800	3.05
3341	3.05
4110	3.05
4664	3.05
5216	3.05

TW1-7

Time (s)	Water level
0	7.95
50	7.95
140	7.95
206	7.95
281	7.95
310	7.95
390	7.95
505	7.95
668	7.95
806	7.95
880	7.95
1092	7.95
1207	7.95
1370	7.95
1442	7.95
1645	7.95
1774	7.95
1880	7.95
1988	7.95
2101	7.95
2329	7.95
2490	7.95
2622	7.95
2813	7.95
2962	7.95
3157	7.95
3274	7.95
3540	7.95
3648	7.95
3730	7.95
3940	7.95
4403	7.95
4875	7.95
5262	7.95

Appendix E

Injection Test Results

Injection Test Data

Sample ID	Date	Time	Time (hr)	DO mg/L	c/co	Bromide mg/L	c/co	Benzene ug/L	Iron mg/L
TW2									
TW2- Background	22-Apr-08	0	0.00	2.60		4.47		4.95	0.01
TW2-1	23-Apr-08	13:42	1.70	23.4	1.00	306.11	1.00	0.00	0.09
	23-Apr-08	13:50	1.83	22.5	0.96	284.34	0.93		
	23-Apr-08	14:25	2.42	28.0	1.20	284.34	0.93		
	23-Apr-08	14:35	2.58	25.5	1.09	366.61	1.20		
	23-Apr-08	14:55	2.92	25.7	1.10	330.90	1.08		
	23-Apr-08	15:05	3.08	23.0	0.98	354.78	1.16		
	23-Apr-08	15:25	3.42	16.2	0.69	298.68	0.98		
	23-Apr-08	15:35	3.58	18.0	0.77	363.61	1.19		
	23-Apr-08	15:54	3.90	16.0	0.68	307.37	1.00		
	23-Apr-08	16:05	4.08	15.4	0.66	394.68	1.29		
	23-Apr-08	16:15	4.25	15.0	0.64	378.83	1.24		
TW2-2	23-Apr-08	16:40	4.67	21.7	0.93	276.30	0.90	0.00	0.09
TW2-3	23-Apr-08	18:40	6.67	20.6	0.88	217.84	0.71	7.75	0.02
TW2-4	24-Apr-08	8:25	18.42	9.9	0.42	156.94	0.51	9.36	0.07
TW2-5	24-Apr-08	18:35	30.58	5.2	0.22	116.36	0.38	1.92	0.01
TW2-6	25-Apr-08	8:15	44.25	4.4	0.19	58.69	0.19	2.50	0.08
TW2-7	26-Apr-08	12:20	60.33	3.8	0.16	44.05	0.14	0.00	0.01
TW2-8	02-May-08	8:00	212.00	3.3	0.14	16.5	0.05	0.00	0.01
TW1-1									
TW1-1- Background	22-Apr-08	0	0.00	1.8	0.08	6.18	0.0202	1.15	1.70
TW1-1-1	23-Apr-08	14:00	2.00	0.5	0.02	14.87	0.0486	1.12	2.27
TW1-1-2	23-Apr-08	16:20	4.33	0.4	0.02	7.78	0.0254	1.12	2.35
TW1-1-3	23-Apr-08	18:18	6.30	1	0.04	17.66	0.0577	13.20	2.56
TW1-1-4	24-Apr-08	8:30	18.50	0.6	0.03	14.10	0.0460	13.85	2.79
TW1-1-5	24-Apr-08	18:47	30.78	4.8	0.21	11.72	0.0383	0.00	2.50
TW1-1-6	25-Apr-08	8:20	44.33	0.5	0.02	15.11	0.0494	13.90	2.39
TW1-1-7	26-Apr-08	13:00	61.00	0.4	0.02	1.64	0.0054	14.01	2.41
TW1-1-8	02-May-08	8:00	212.00	4.7	0.20	1.70	0.0056	17.50	3.00
TW1-2									
TW1-2- Background	22-Apr-08	0	0.00	4	0.17	2.50	0.0082	0.00	0.01
TW1-2-1	23-Apr-08	14:04	2.07	21.8	0.93	277.43	0.9063	3.52	0.04
TW1-2-2	23-Apr-08	16:23	4.38	13.2	0.56	152.50	0.4982	3.52	0.05
TW1-2-3	23-Apr-08	18:21	6.55	7.9	0.34	71.15	0.2324	3.26	0.06
TW1-2-4	24-Apr-08	8:35	18.58	5.8	0.25	11.58	0.0378	0.00	0.04
TW1-2-5	24-Apr-08	18:50	30.83	6.1	0.26	13.42	0.0438	0.00	0.05
TW1-2-6	25-Apr-08	8:24	44.40	5.3	0.23	7.78	0.0254	0.00	0.01
TW1-2-7	26-Apr-08	13:05	61.08	4.8	0.21	7.53	0.0246	0.00	0.01
TW1-2-8	02-May-08	8:00	212.00	4.7	0.20	7.4	0.0243	0.00	0.00
TW1-3									
TW1-3- Background	22-Apr-08	0	0.00	2.2	0.09	3.33	0.0109	0.00	0.07
TW1-3-1	23-Apr-08	14:08	2.13	21.1	0.90	317.61	1.0376	3.45	0.06
TW1-3-2	23-Apr-08	16:25	4.42	16.4	0.70	194.22	0.6345	3.45	0.10
TW1-3-3	23-Apr-08	18:23	6.38	12	0.51	116.36	0.3801	4.08	0.02
TW1-3-4	24-Apr-08	8:39	18.65	6.8	0.29	18.17	0.0594	0.00	0.04
TW1-3-5	24-Apr-08	18:53	30.88	5.6	0.24	14.04	0.0459	0.00	0.00
TW1-3-6	25-Apr-08	8:28	44.47	5.9	0.25	7.97	0.0260	0.00	0.01
TW1-3-7	26-Apr-08	13:07	61.12	4.9	0.21	7.05	0.0230	0.00	0.01
TW1-3-8	02-May-08	8:00	212.00	4.2	0.18	5.7	0.0185	0.00	0.00
TW1-4									
TW1-4- Background	22-Apr-08	0	0.00	0.6	0.03	3.40	0.0111	1.26	0.08
TW1-4-1	23-Apr-08	14:13	2.22	17.6	0.75	284.34	0.9289	4.42	0.07
TW1-4-2	23-Apr-08	16:27	4.45	14.6	0.62	191.85	0.6267	4.42	0.07
TW1-4-3	23-Apr-08	18:26	6.43	11.3	0.48	118.77	0.3880	4.32	0.04
TW1-4-4	24-Apr-08	8:42	18.70	6.3	0.27	24.21	0.0791	1.13	0.05
TW1-4-5	24-Apr-08	19:06	31.10	6.2	0.26	22.86	0.0747	0.00	0.11
TW1-4-6	25-Apr-08	8:31	44.52	5.4	0.23	8.38	0.0274	0.90	0.04
TW1-4-7	26-Apr-08	13:10	61.17	4.6	0.20	7.14	0.0233	0.68	0.01
TW1-4-8	02-May-08	8:00	212.00	4.2	0.18	5.2	0.0170	0.00	0.02

Injection Test Data

Sample ID	Date	Time	Time (hr)	DO mg/L	c/co	Bromide mg/L	c/co	Benzene ug/L	Iron mg/L
TW1-6									
TW1-6- Background	22-Apr-08	0	0.00	1.5	0.06	7.02	0.0229	0.00	0.07
TW1-6-1	23-Apr-08	14:16	2.27	2.2	0.09	13.15	0.0429	0.00	0.04
TW1-6-2	23-Apr-08	16:30	4.50	3.1	0.13	22.68	0.0741	0.00	0.09
TW1-6-3	23-Apr-08	18:29	6.48	2.9	0.12	13.59	0.0444	0.00	0.04
TW1-6-4	24-Apr-08	8:47	18.78	2.6	0.11	17.30	0.0565	0.00	0.02
TW1-6-5	24-Apr-08	18:56	30.93	2.6	0.11	12.72	0.0416	0.00	0.05
TW1-6-6	25-Apr-08	8:36	44.60	2.1	0.09	8.31	0.0271	0.00	0.01
TW1-6-7	26-Apr-08	13:14	61.23	2	0.09	8.01	0.0262	0.00	0.03
TW1-6-8	02-May-08	8:00	212.00	2.2	0.09	5.9	0.0194	0.00	0.03
TW1-7									
TW1-7- Background	22-Apr-08	0	0.00	2.5	0.11	11.92	0.0389	3.11	0.09
TW1-7-1	23-Apr-08	14:20	2.33	2.0	0.09	7.75	0.0253	3.14	0.12
TW1-7-2	23-Apr-08	16:33	4.55	1.5	0.06	12.01	0.0392	3.14	0.16
TW1-7-3	23-Apr-08	18:35	6.58	2.9	0.12	16.07	0.0525	4.02	0.14
TW1-7-4	24-Apr-08	8:53	18.88	3.3	0.14	65.82	0.2150	1.94	0.06
TW1-7-5	24-Apr-08	19:01	31.02	3.7	0.16	111.23	0.3634	1.50	0.03
TW1-7-6	25-Apr-08	8:40	44.67	3.6	0.15	123.74	0.4042	1.21	0.01
TW1-7-7	26-Apr-08	13:17	61.28	3.3	0.14	138.22	0.4515	0.00	0.07
TW1-7-8	02-May-08	8:00	212.00	2.3	0.10	32.8	0.1071	0.00	0.04

Appendix F

Base Case Smoker Input File

```
THERMAL HEAT FLOW MODEL: O2 Injection
79x41x57 nodes
Dec. 2008 -
   1    0    0    0    0    0    1   1        ;KPRT,KCN,KWT,KINT,KINTV,KGO,ksat,kmass
   5    4    3                      ;ngx,ngy,ngz
  4. 4.97  5.03  8.  15.            ;xlim (m)
  0.06  2.  5.   10.              ;ylim
  3.5  9.  10.               ;zlim
  16  8  2  24  28            ;nlx
  2  16  12  10            ;nly
  14   44  4                ;nlz
   10     0.                      ;nwtl, DATUM (flow)
   26   1    39    39    +1              ;breakthrough point 1
   26   1    44    44    +1              ;breakthrough point 2
   51   1    19    19    +1                   ;breakthrough point 3
   51   1    27    27    +1                      ;breakthrough point 4
   51   1    33    33    +1              ;breakthrough point
   51   1    49    49    +1              ;breakthrough point 6
   51   1    53    53    +1              ;breakthrough point 7
   15   1    34    34    +1                   ;breakthrough point 8   - matrix - upgradient
   26   1    34    34    +1                   ;breakthrough point 9   - matrix - middle of
injection well - between fractures
   39   1    34    34    +1                   ;breakthrough point 10  - matrix - between injection
& monitor
   51   1    34    34    +1                   ;breakthrough point 11  - matrix - monitor well
   79   1    34    34    +1                   ;breakthrough point 12  - matrix - exit boundary
   15   1    30    30    +1    13   on fracture
   26   1    30    30    +1    14   on fracture
   39   1    30    30    +1    15   on fracture
   51   1    30    30    +1          16   on fracture
   79   1    30    30    +1    17   on fracture
   51   1    21    21    +1          18              -fracture 21 at TW1
   79   1    21    21    -1          19              -fracture 21 at exit
  26  26    1    1   17   53       1       1  0.000250   +1      ;injection well pipe  17-53 =37
nodes
   1  78    1   40   21   21       2       5  0.000200  +1     ;
   1  78    1   40   30   30       2       5  0.000150  +1    h
   1  78    1   40   39   39       2       5  0.000300  +1    h
   1  78    1   40   44   44       2       5  0.000300  +1    h
   1  78    1   40   49   49       2       5  0.000500  +1    h
   1  78    1   40   53   53       2       5  0.000500  +1          horizontal to end
   1  78    1   40   56   56       2       5  0.000500  +1    h
   1  78    1   40   59   59       2       5  0.000500  +1    h
   1  78    1   40   61   61       2       5  0.000500  -1    h
   1    1    0    0    0    2                  ;B.C.'S (FLOW)      -
   1   41    1   63     10.       -1              ;H AT FACE 1
```

```
  1   41    1   63      9.50      -1              ;H AT FACE 2     -
  1   79    1   41     1.0E-09   -1               ;nodal RECHARGE ON TOP(m/s)
  1  193440          1.0E-7  1.0E-7  1.0E-7  2. 2. 2. 0.15  -1   ;elements, KX,KY,KZ (m/s)
  1   78  1  40  49 62 1.0e-7  1.0e-7  1.0e-7  2. 2. 2. 0.15  +1 ;indexed K (m/s)
  1   78  1  40  25 48 1.0e-7  1.0e-7  1.0e-7  2. 2. 2. 0.15  +1 ;indexed K (m/s)
  25  26  1   1  17 53 5.e-5   5.e-5  5.e-5    2. 2. 2. 0.15  -1 ;high K well
 .000                                  ;SS
  0   10.0                              ;INIT,H0 (READ FLOW I.C.)
  1    0    0    0    0    0            ;B.C.'S (TRANSPORT) -
  1   41    1   31    0.0022   +1             ;left
  1   41   32   33    0.0025   +1
  1   41   34   41    0.0030   +1
  1   41   42   45    0.0035   +1
  1   41   46   46    0.0040   +1
  1   41   47   63    0.0042   -1
 1.00     1.00       .30               ;top: TCON,BZ,SAT (m,s)
  -11.4    19.    365.      0.    -11.          ;surfat min,amp,per,phase,cutoff;  Guelph
data
   0     0.       0.       0.              ;IVEL,VX,VY,VZ (m/s)
   0.2       .10      0.02        5.e-10      1.  0.   ;AL,ATH,ATV,(m) DD(m^2/s),retard,decay
 4174.     1000.     800.         2630.          ;THERMAL PROPS (m,s)
 0.00E+05   .10       5.                ;L. HEAT,P,Q FOR WU
1   79    1   41   1   63    0.002    0.002    +1       ;TEMP.I.C.(END WITH -1)
1   79    1   41   1   31    0.0022 0.0022  +1
1   79    1   41  32   33    0.0025 0.0025  +1
1   79    1   41  34   41    0.0030 0.0030  +1
1   79    1   41  42   45    0.0035 0.0035  +1
1   79    1   41  46   46    0.0040 0.0040  +1
1   79    1   41  47   63    0.0042 0.0042  -1
 .0001       .01      .0001      10   10          ;CCP,CCT,CCW,MAXIT1,MAXIT2
  1.0    1.00       .96                ;OVER-RELAX HEADS,TEMP.,TSA
  26  51                               ;KNOX(1),(2)TRANSV. SECTION
  1    0                              ;KNOY(1),(2)LONG.  SECTION
  0    0                              ;knoz
 0.077    0.1     1.0    5.0     0.     0.      ;five 3d print times (days)
  0.      0.031     0.0001     310  310  +1      ;T0,T1,DT,KPLOT(days) time info        ;on -
1st interval
   0.0     1.                           ;hinc,rinc
  10    12    1    1   5.            -1          ;surface temp patch
  0  0   0  0   00  00   0.   0.  -1             ;internal heat source, fluxin, decay
 26    1    17   53  +2.5e-6  0.0264 -1               ;SOURCE flow rate per node
  0.031    0.051    0.0001     100   100   +1      ;T0,T1,DT,KPLOT(days) time info
```

```
;off
    0.0    1.                          ;hinc,rinc
   10   12   1   1   5.          -1        ;surface temp patch
   0  0   0  0   00  00   0.   0.  -1          ;internal heat source, fluxin, decay
  26   1   17   53  +0.00E-06  0.000   -1              ;SOURCE
   0.051   0.077   0.0001   260  260   +1     ;T0,T1,DT,KPLOT(days) time info
;2nd interval
    0.0    1.                          ;hinc,rinc
   10   12   1   1   5.          -1        ;surface temp patch
   0  0   0  0   00  00   0.   0.  -1          ;internal heat source, fluxin, decay
  26   1   17   53  2.37E-06  0.0264  -1              ;SOURCE
   0.077  0.1      0.001    23 23    +1     ;T0,T1,DT,KPLOT(days) time info        !off
    0.0    1.                          ;hinc,rinc
   10   12   1   1   5.          -1        ;surface temp patch
   0  0   0  0   00  00   0.   0.  -1          ;internal heat source, fluxin, decay
  26   1   14   47  +0.0E-06  0.    -1             ;SOURCE
   0.10  1.0      0.001    100  900    +1     ;T0,T1,DT,KPLOT(days) time info
    0.0    1.                          ;hinc,rinc
   10   12   1   1   5.          -1        ;surface temp patch
   0  0   0  0   00  00   0.   0.  -1          ;internal heat source, fluxin, decay
  26   1   14   47  +0.0E-06  0.    -1             ;SOURCE
   1.0  10.0      0.001    500  900    -1     ;T0,T1,DT,KPLOT(days) time info
    0.0    1.                          ;hinc,rinc
   10   12   1   1   5.          -1        ;surface temp patch
   0  0   0  0   00  00   0.   0.  -1          ;internal heat source, fluxin, decay
  25   1   14   47  +0.0E-06  0.    -1             ;SOURCE
```

Appendix G

Sensitivity Analysis Modelling Results including Random Fracture Network

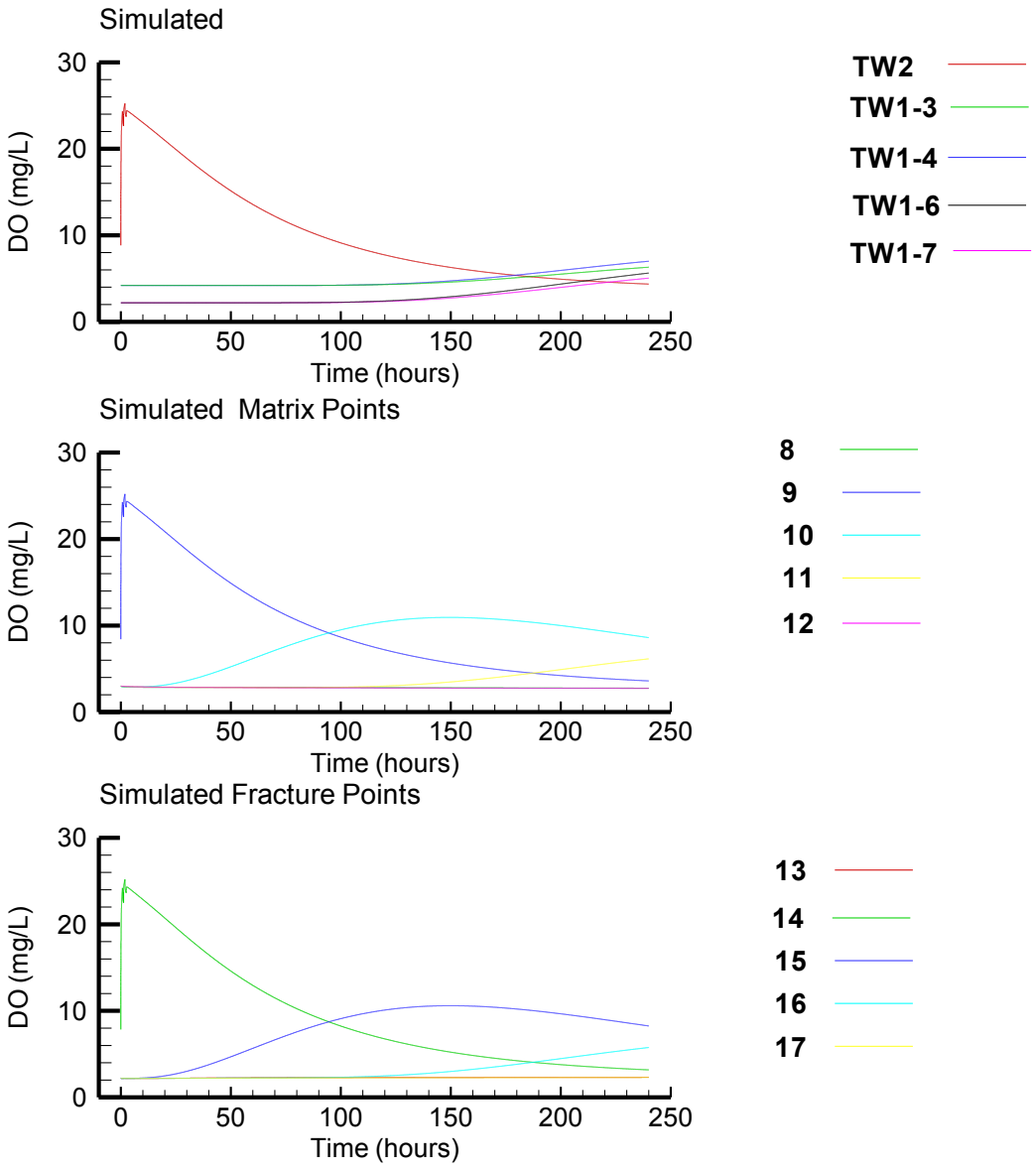

Appendix G- Senario 1 Eqivalent Porous Media with no Fractures

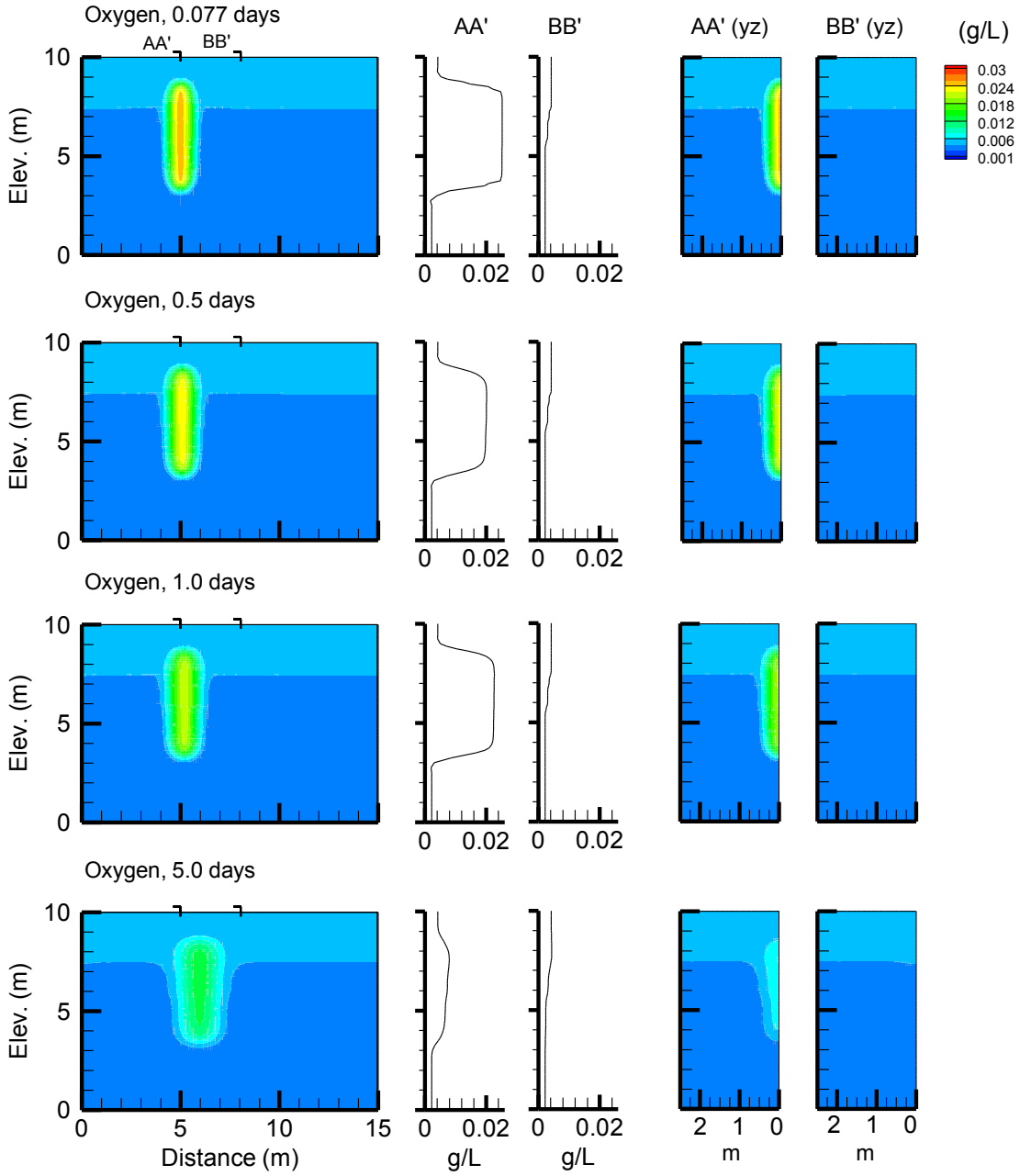

Appendix G- Senario 1 Eqivalent Porous Media with no Fractures

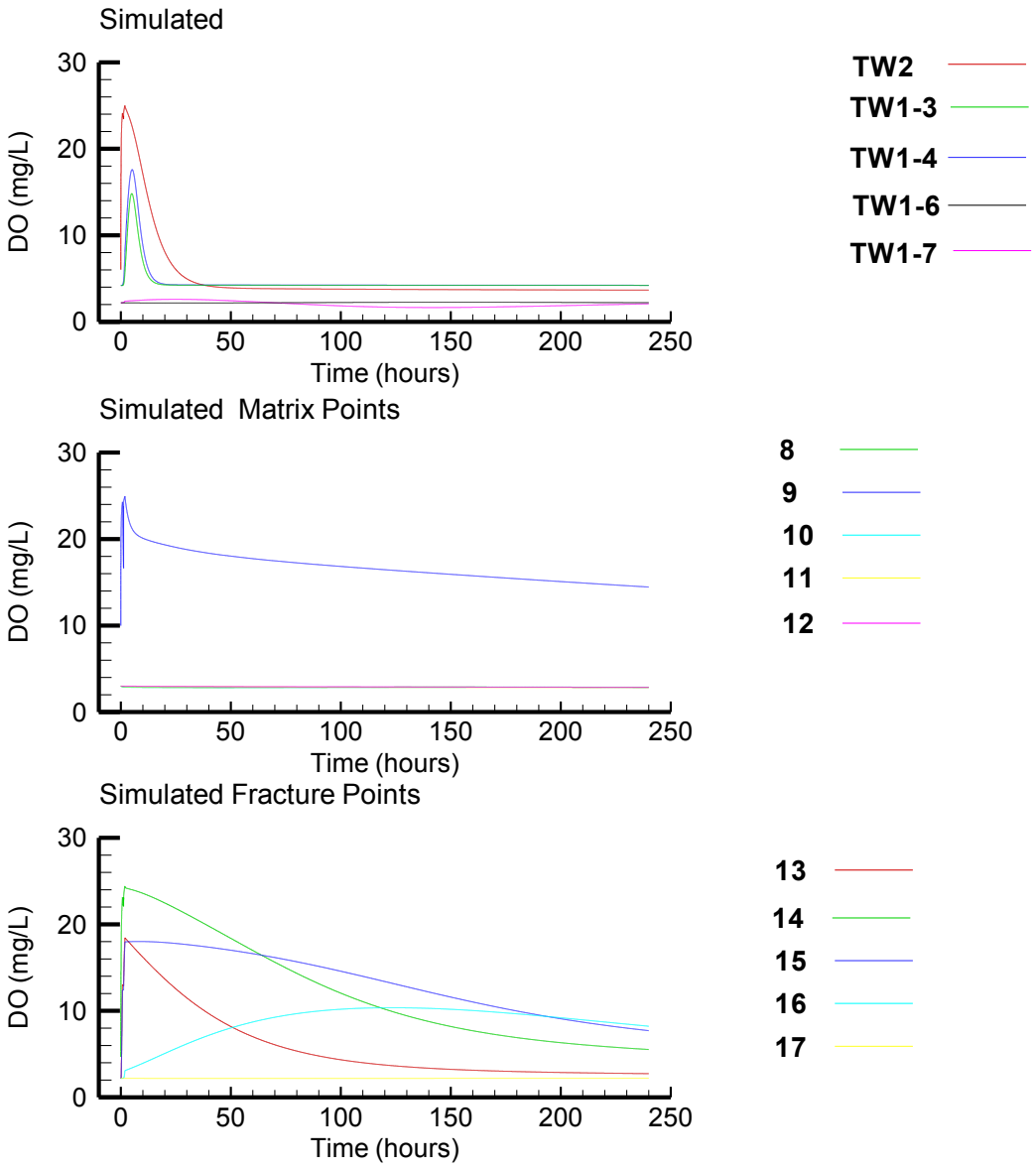

Appendix G- Senario 2a 10 × Larger Diffusion Coefficient

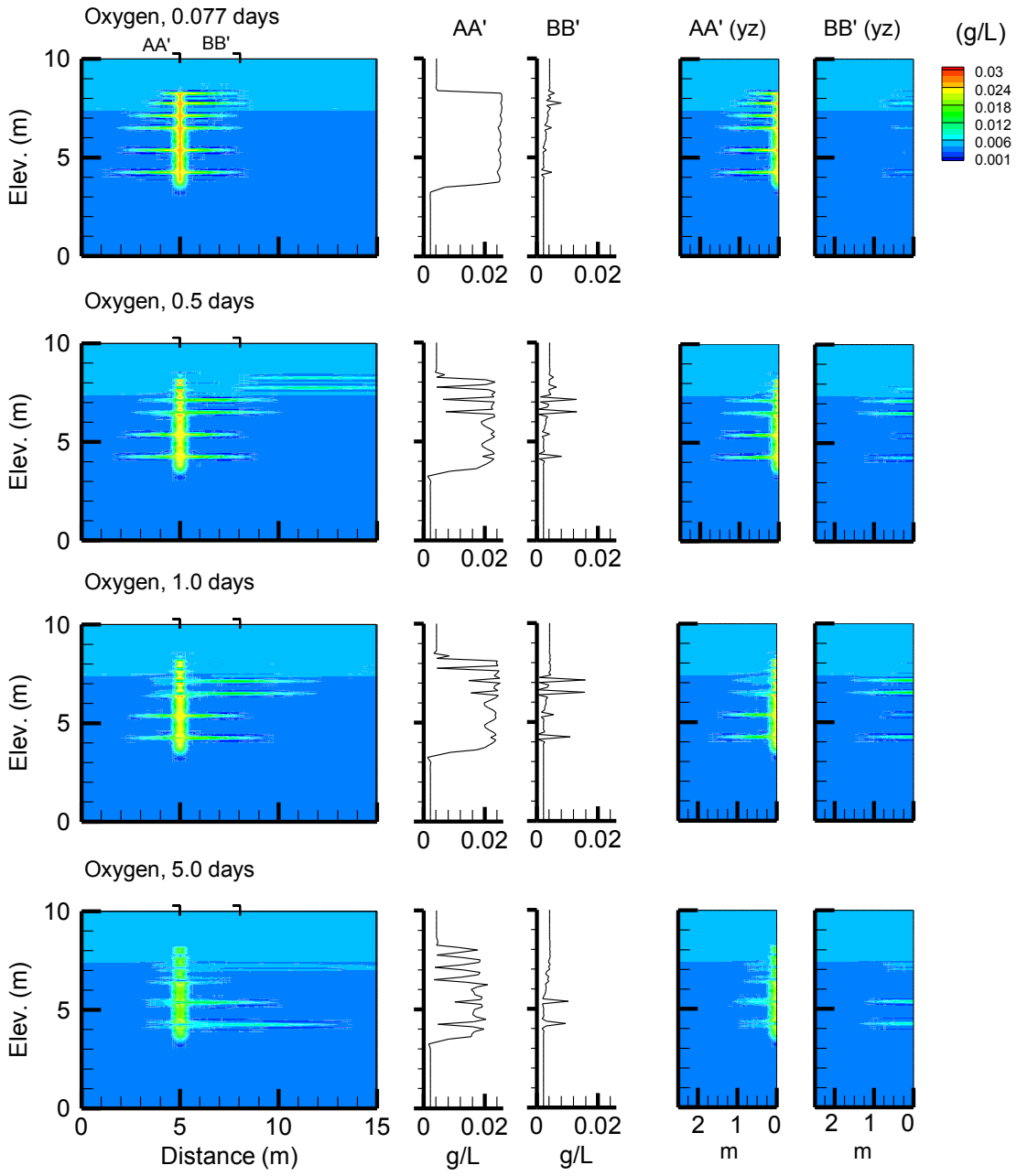

Appendix G- Senario 2a 10 × Larger Diffusion Coefficient

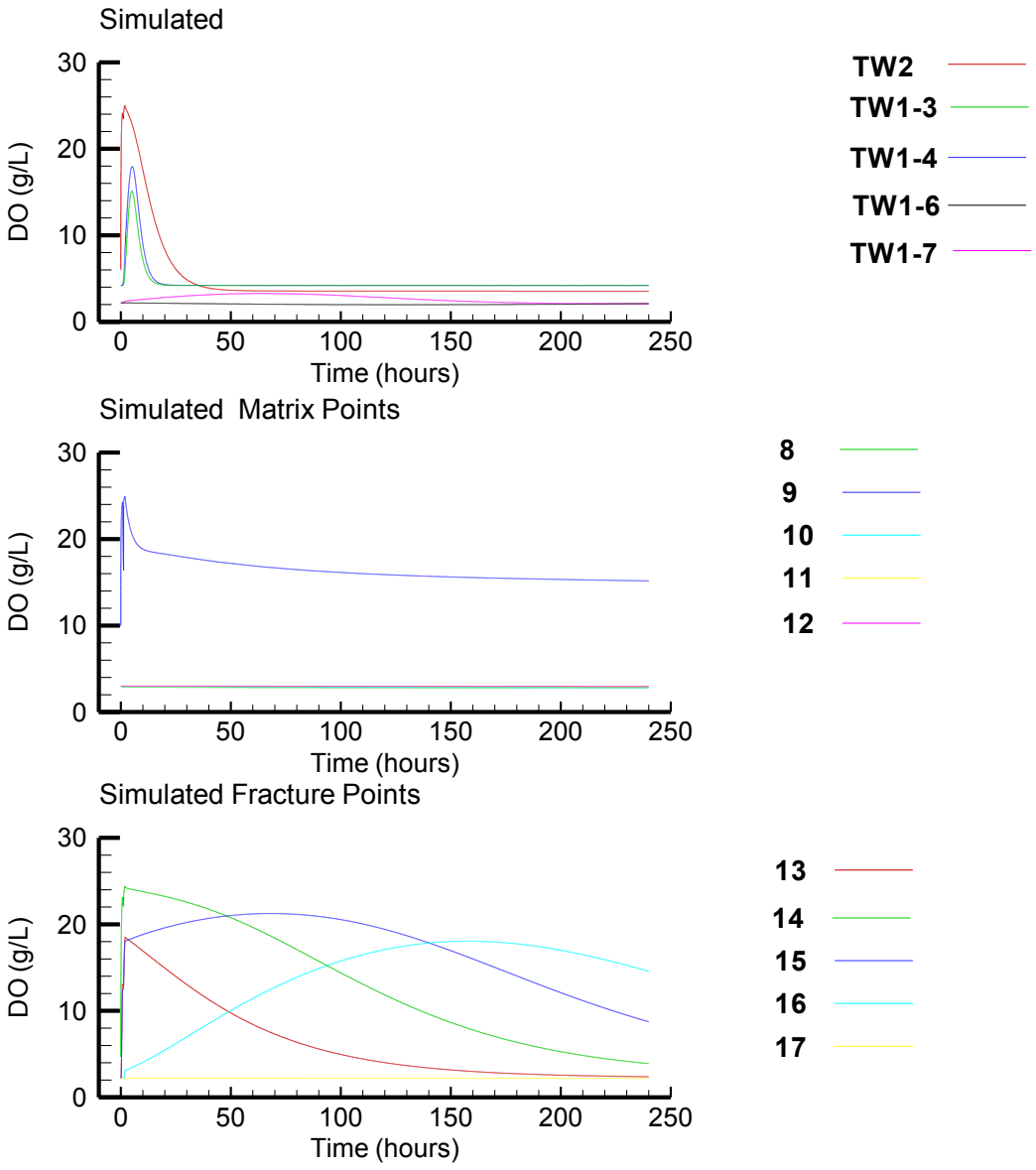

Appendix G- Senario 2b 10 × Smaller Diffusion Coefficient

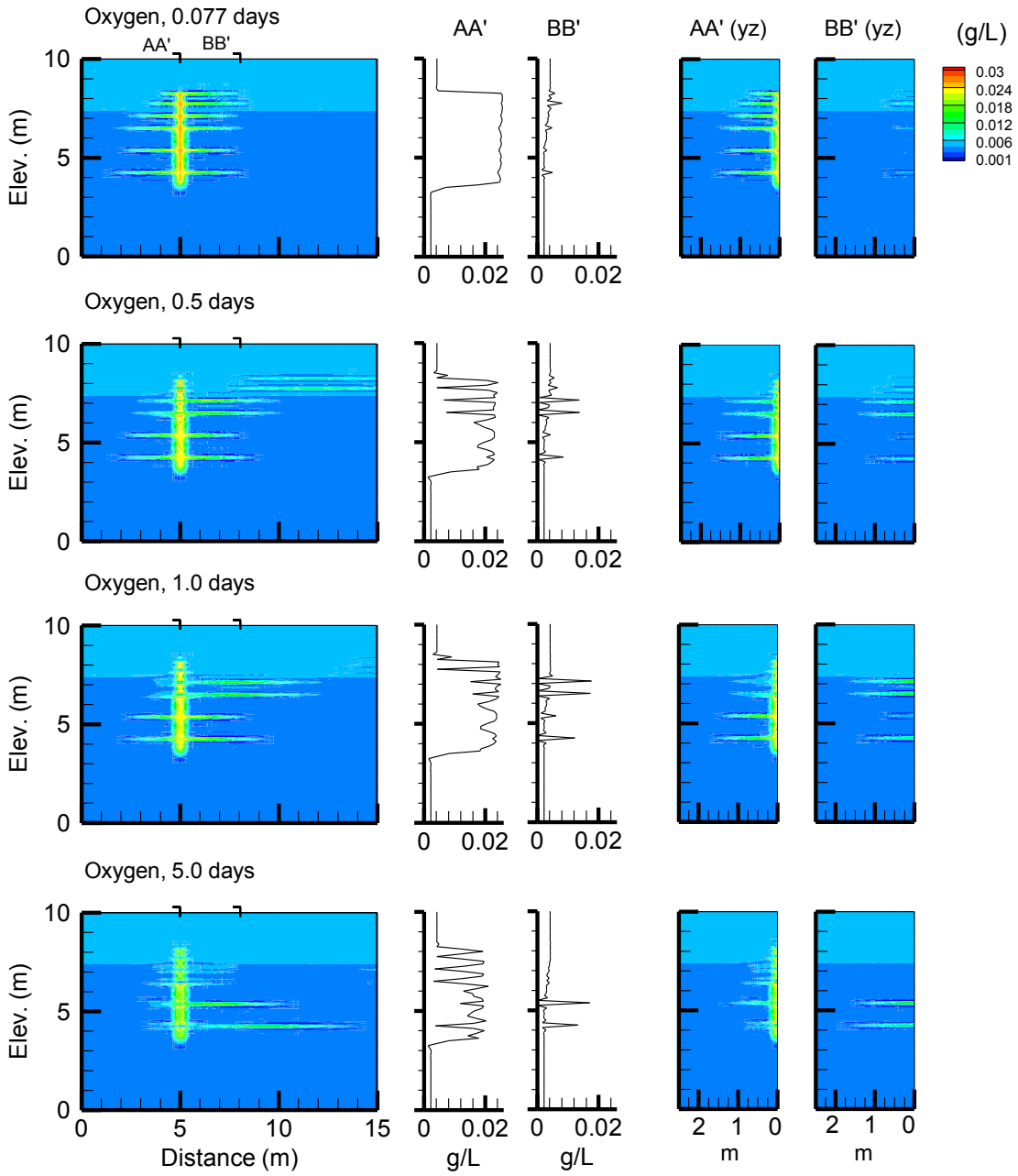

Appendix G- Senario 2b 10 × Smaller Diffusion Coefficient

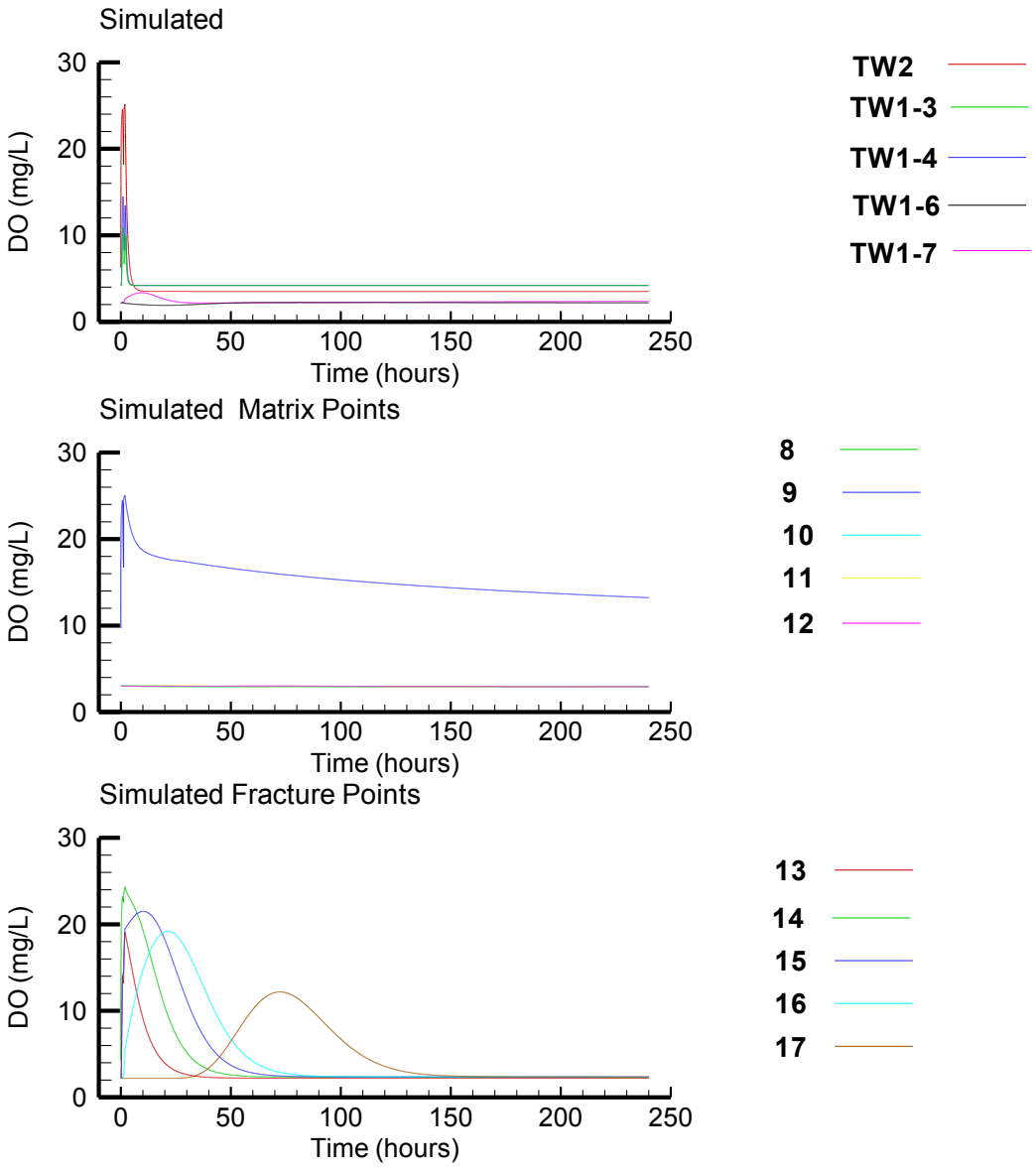

Appendix G- Senario 3a 2 × Larger Apertures

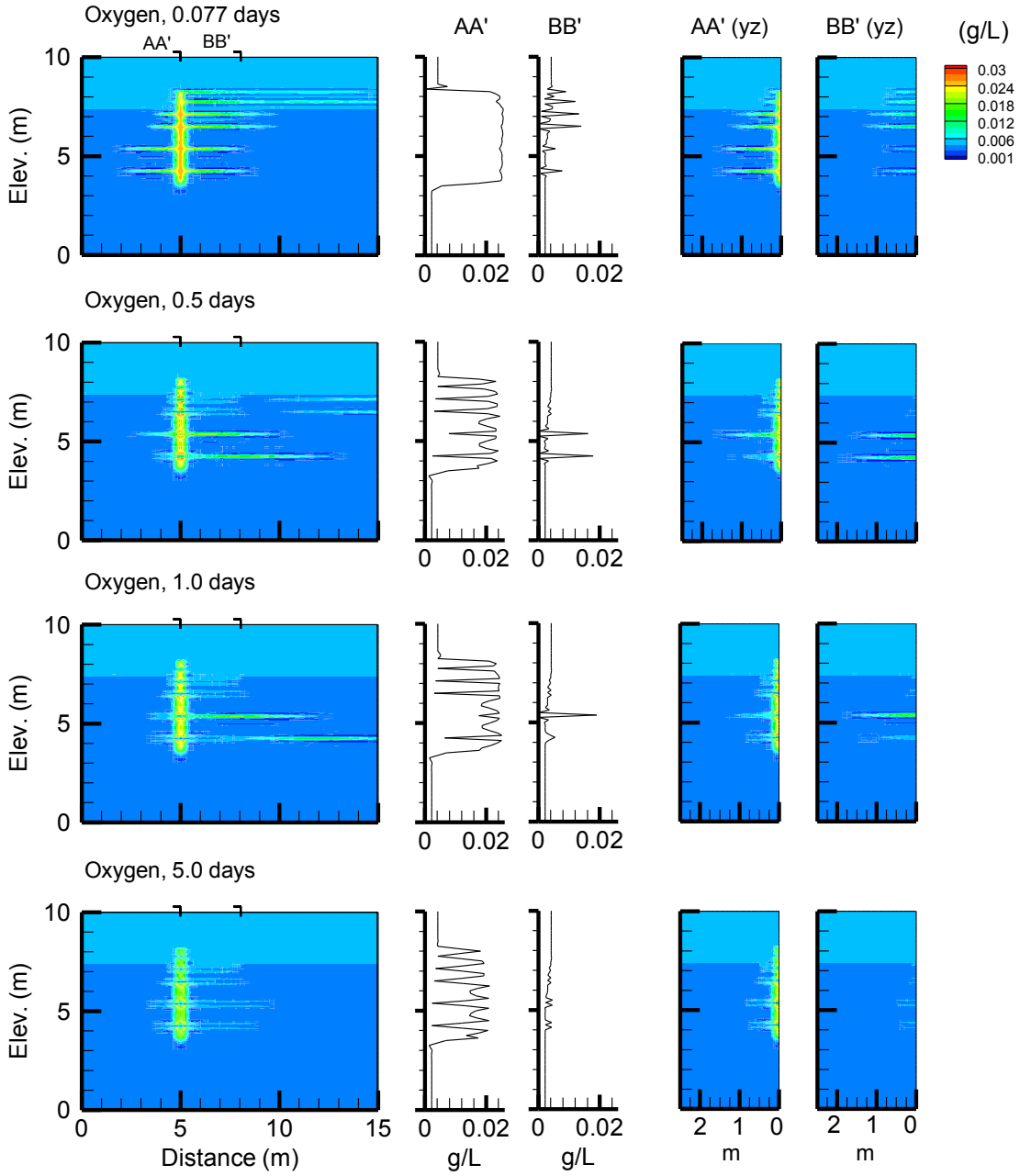

Appendix G- Senario 3a 2 × Larger Apertures

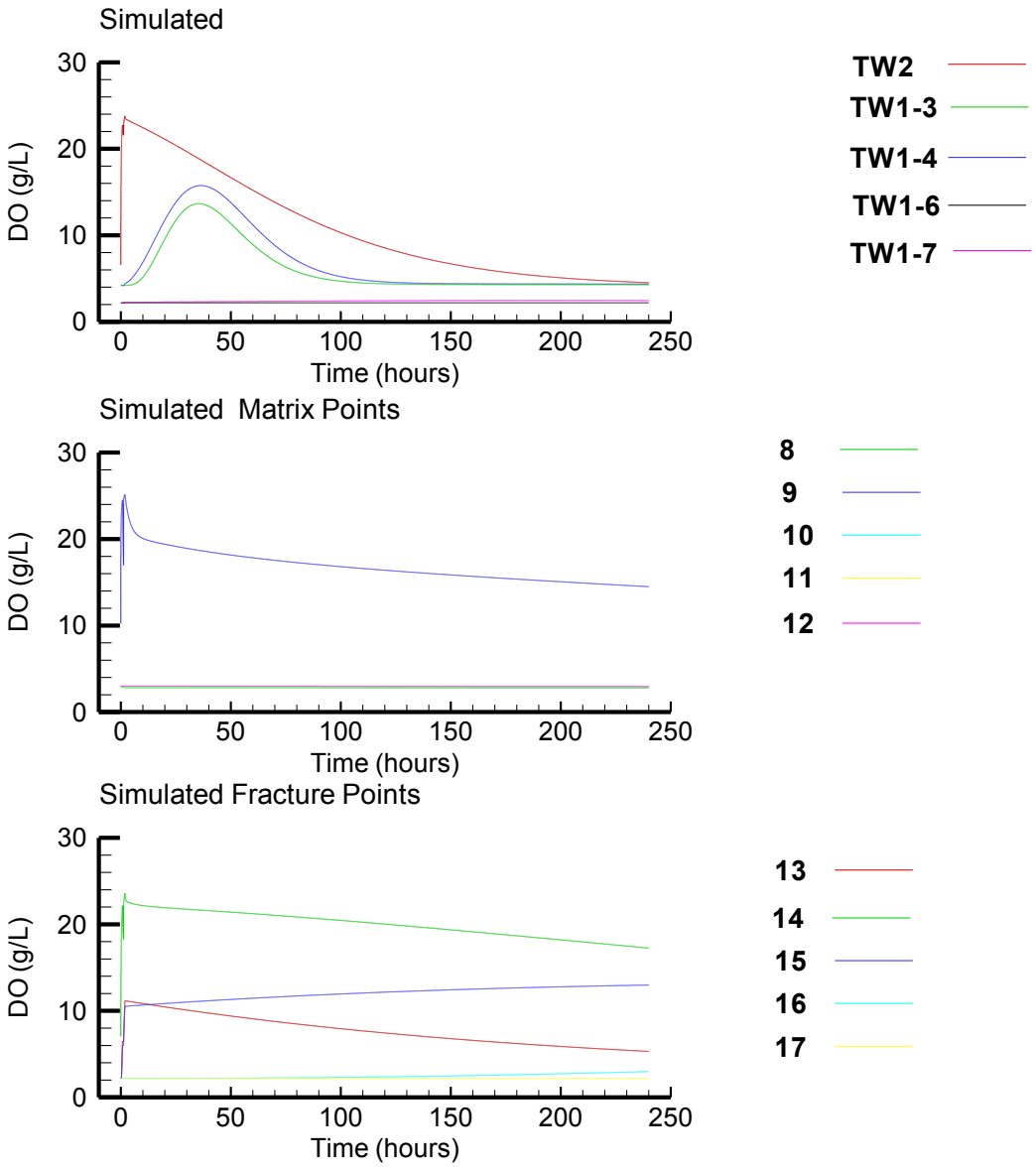

Appendix G- Senario 3b 2 × Smaller Apperture

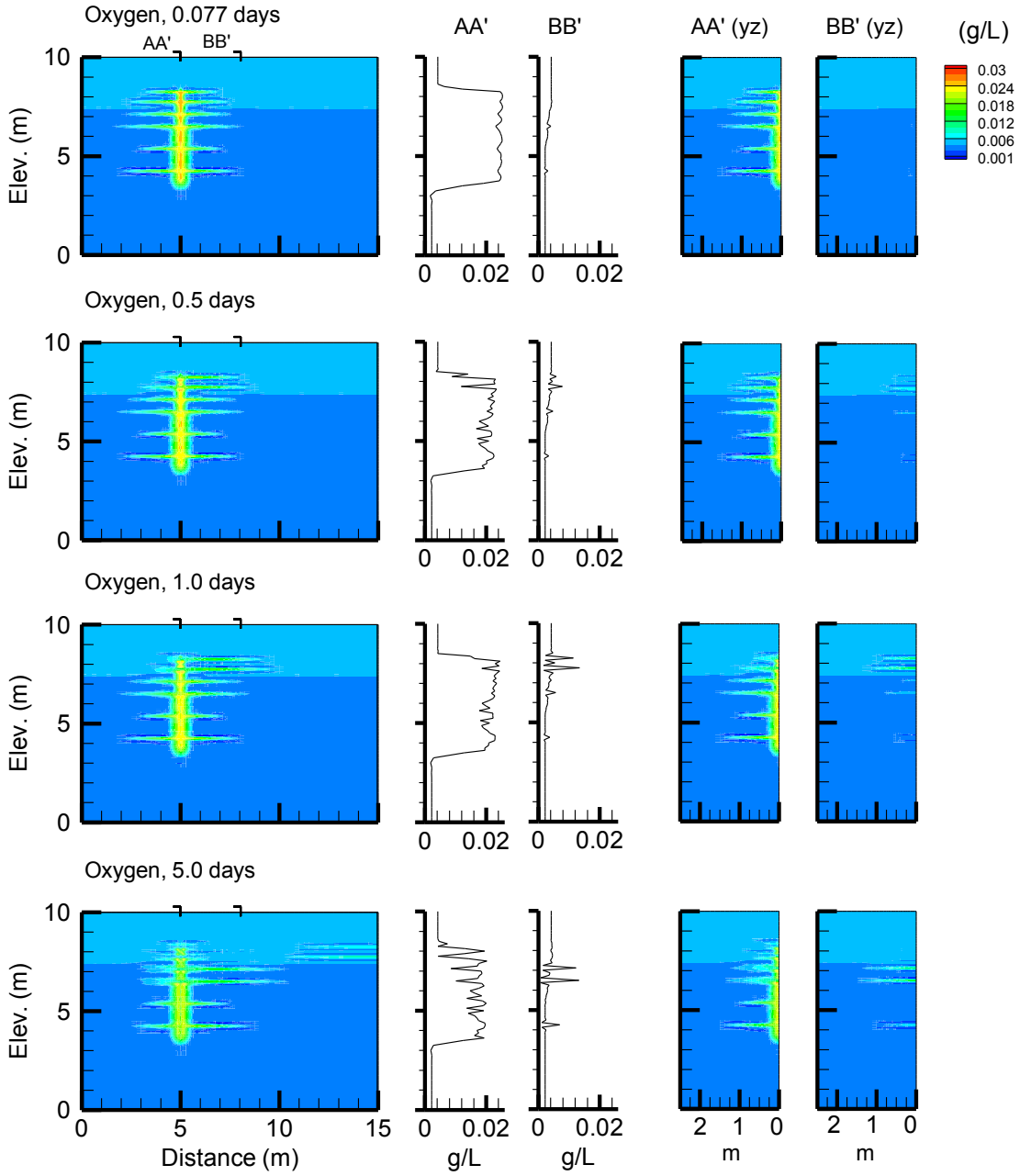

Appendix G- Senario 3b 2 × Smaller Apperture

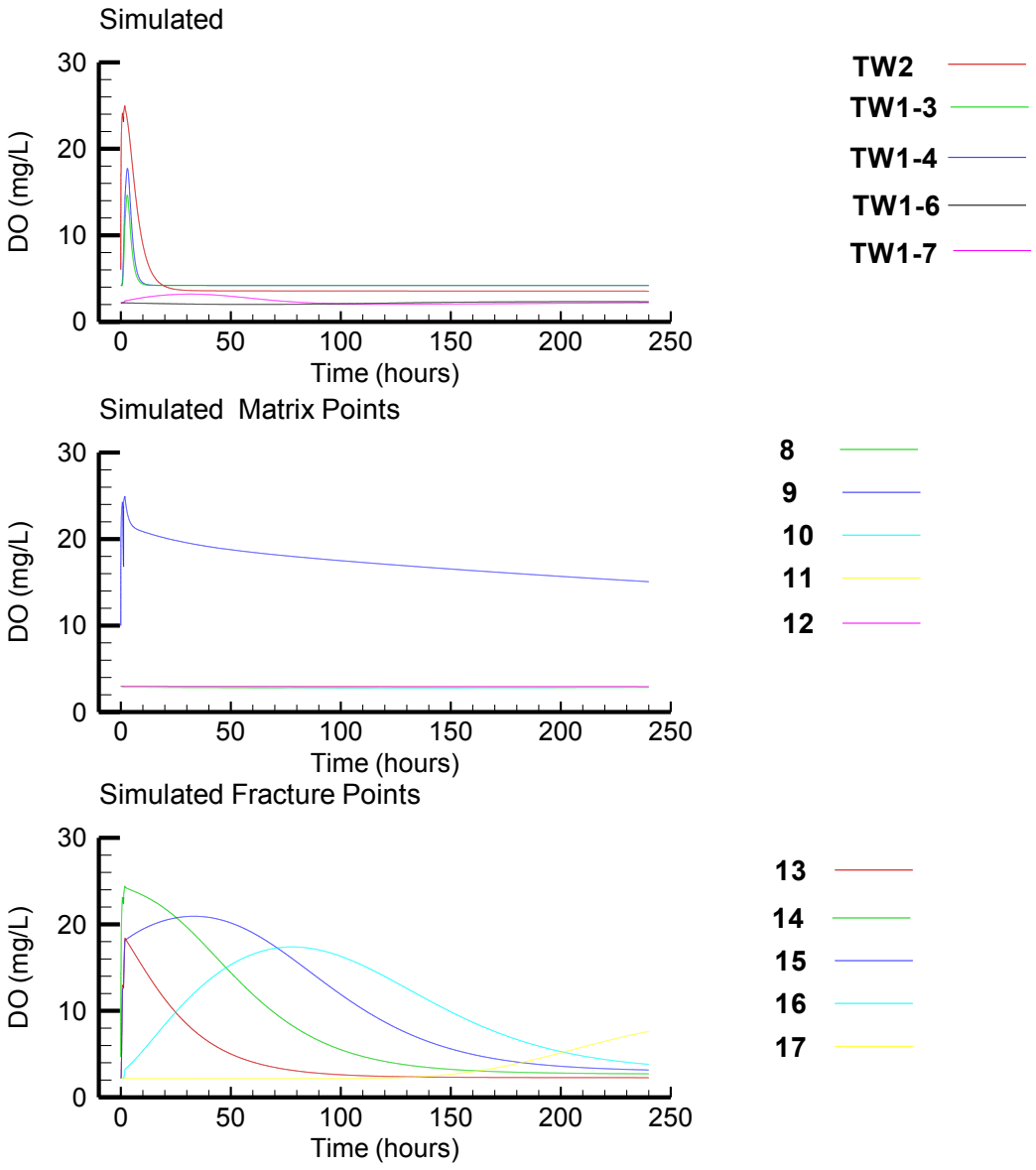

Appendix G-Senario 4a Larger Gradient

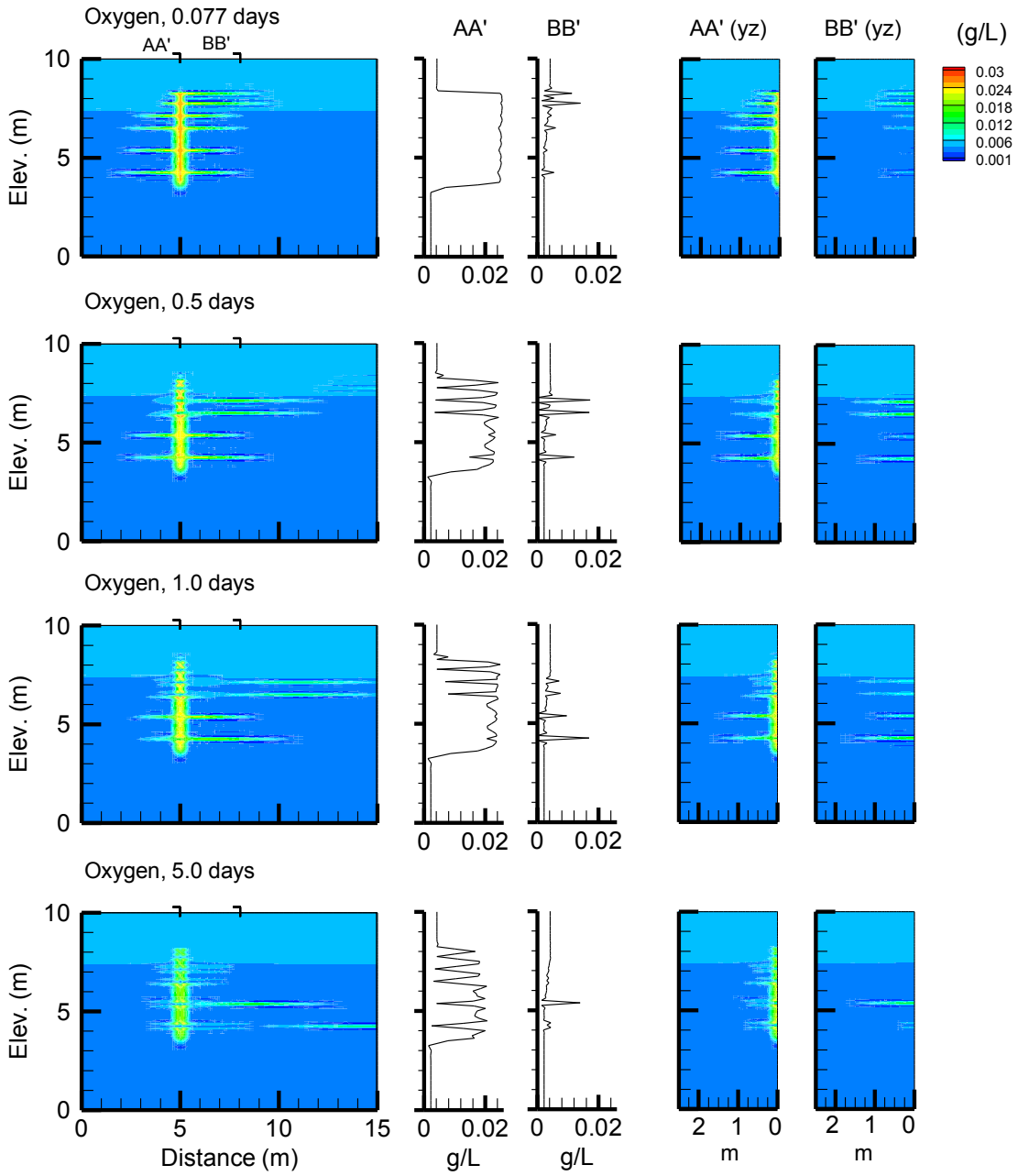

Appendix G-Senario 4a Larger Gradient

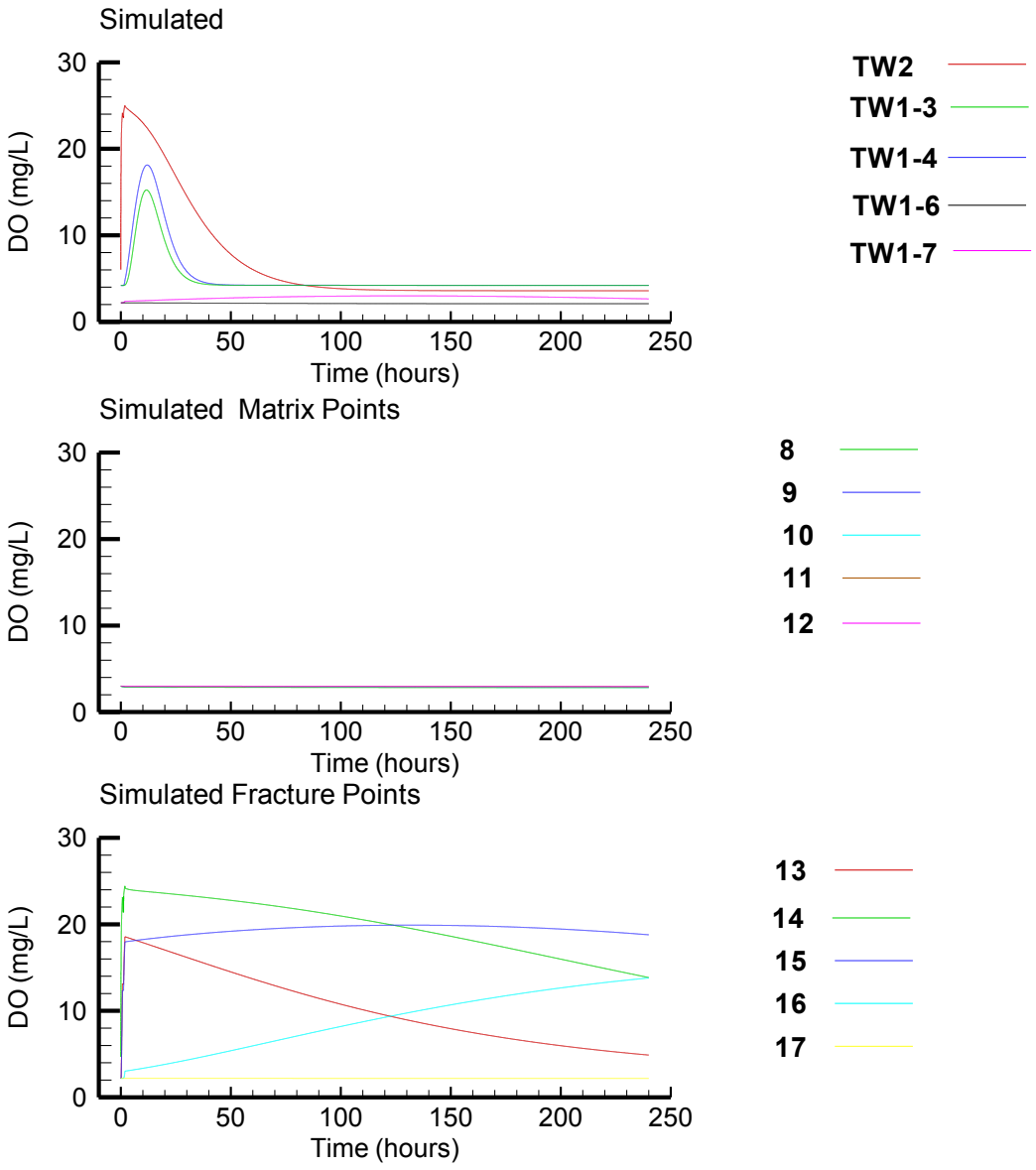

Appendix G- Senario 4b Smaller Gradient

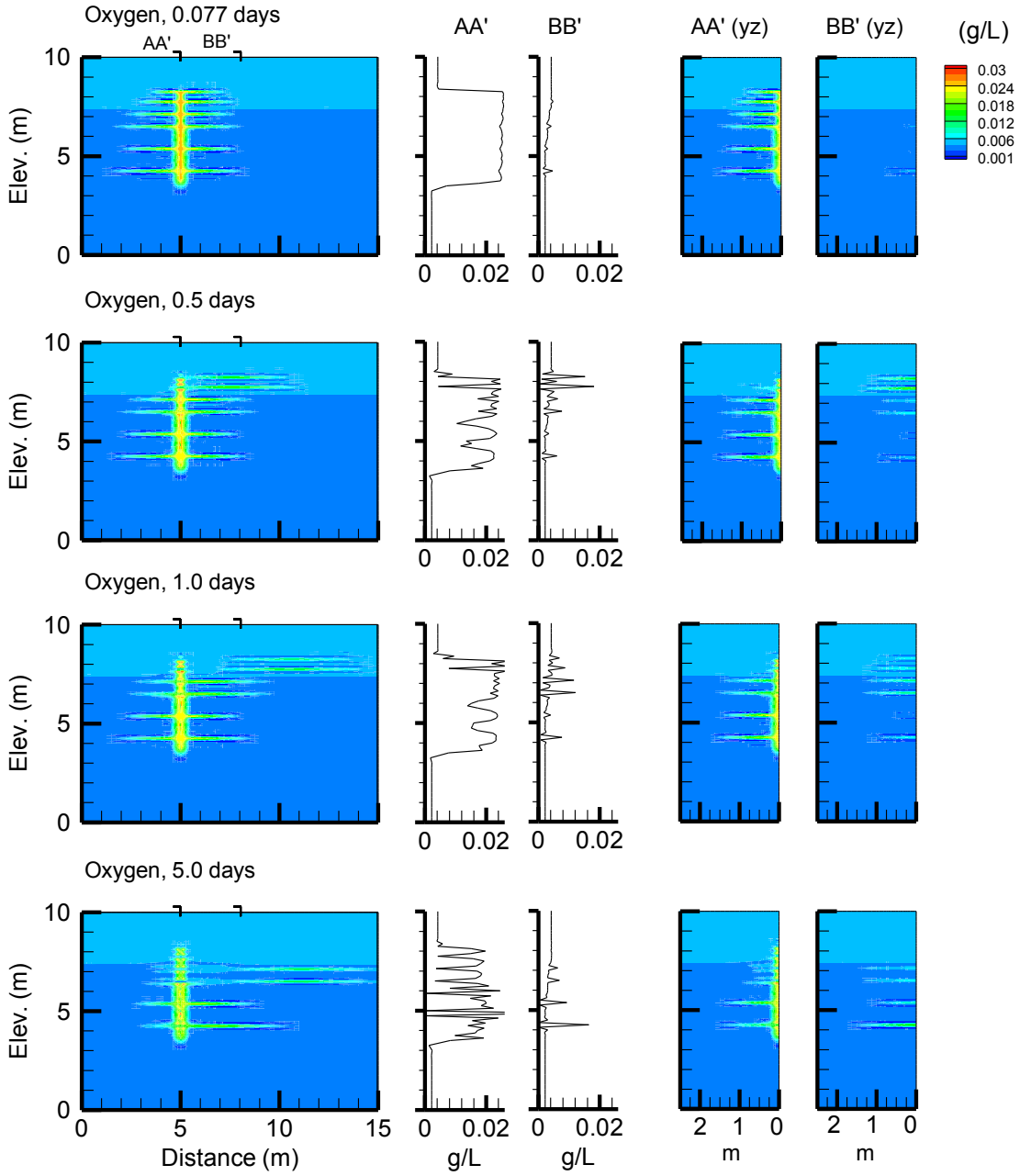

Appendix G- Senario 4b Smaller Gradient

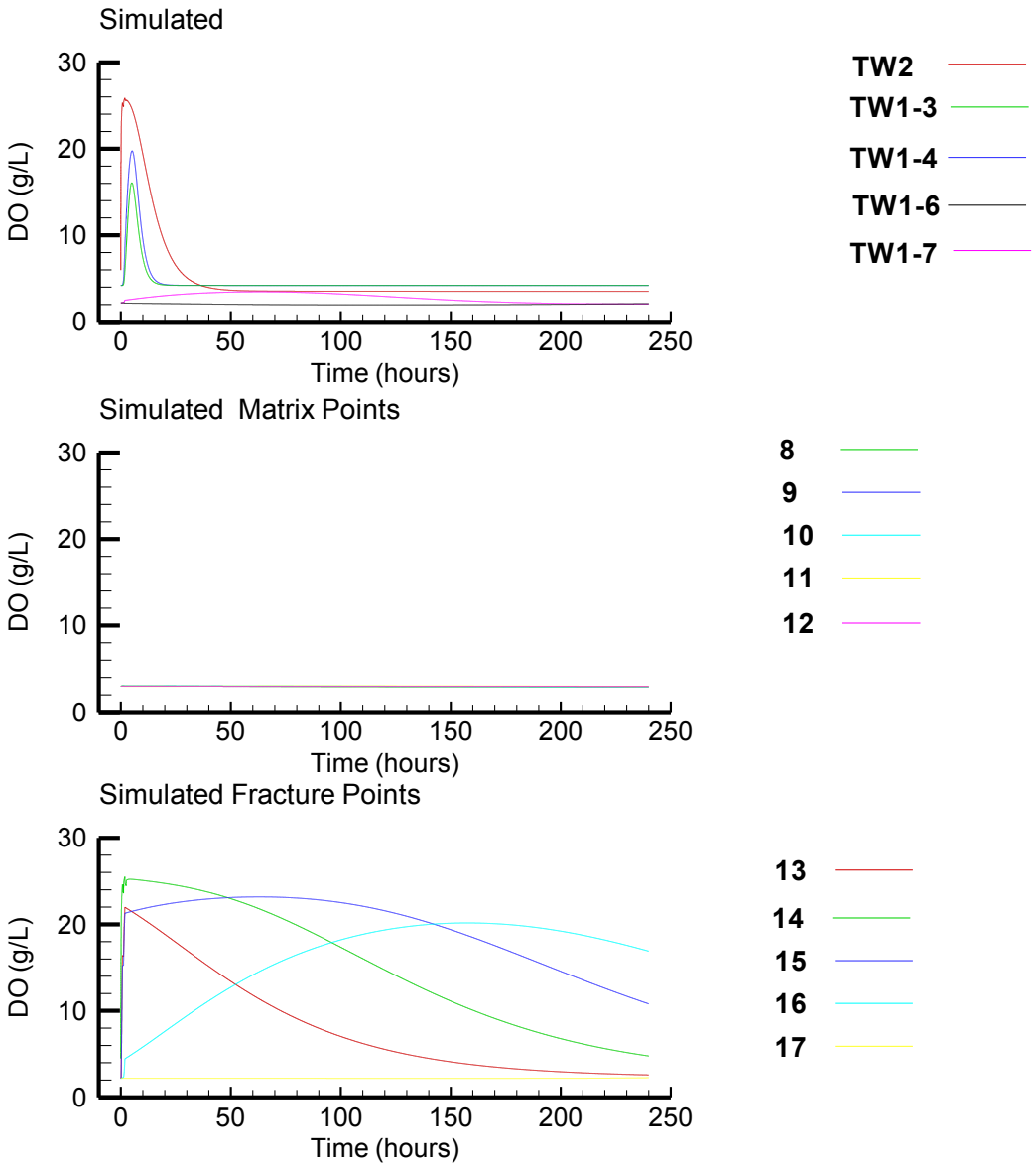

Appendix G - Senario 5 Uniform Low Hydraulic Conductivity

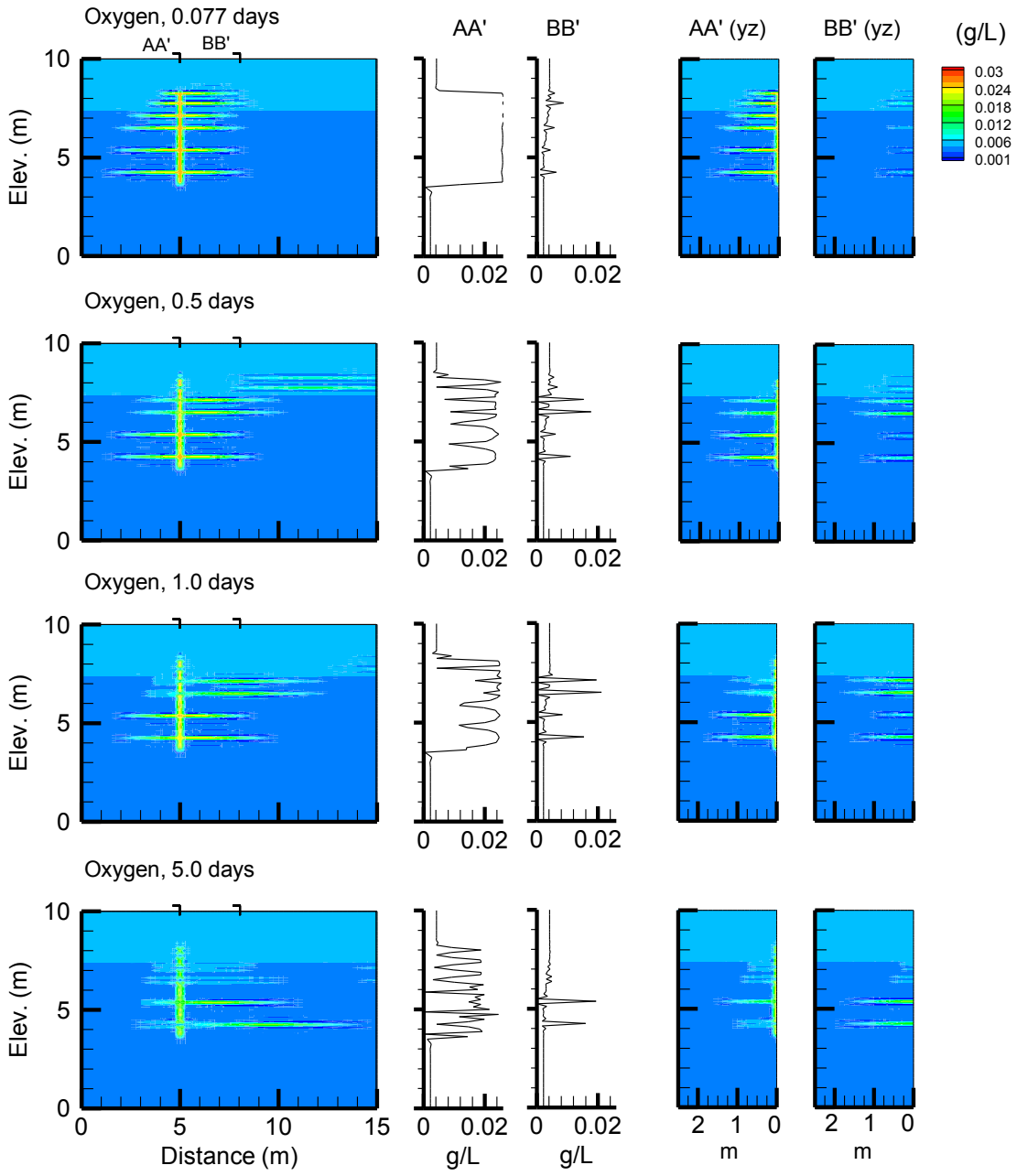

Appendix G - Senario 5 Uniform Low Hydraulic Conductivity

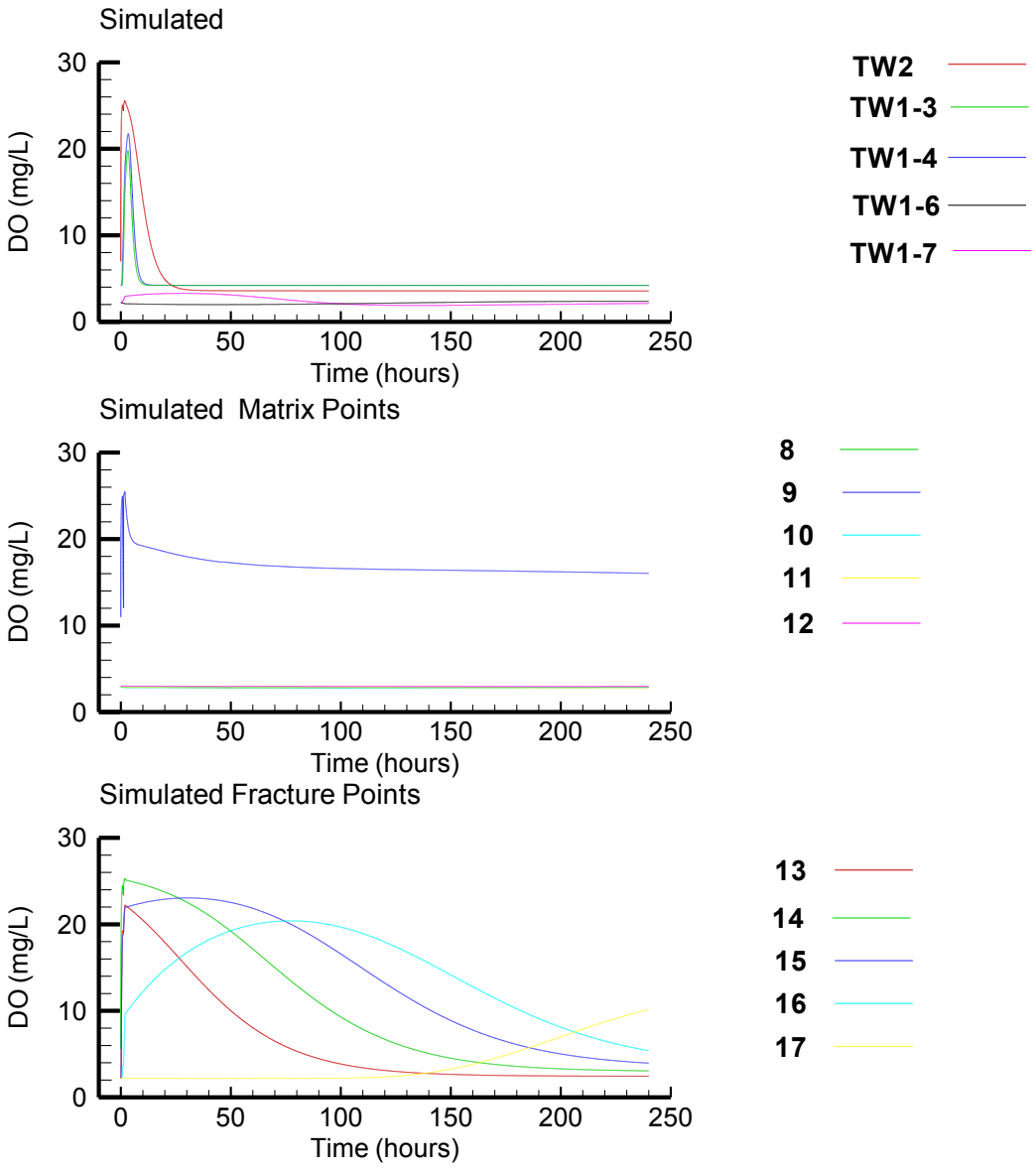

Appendix G- Senario 6a Lower Porosity (0.075)

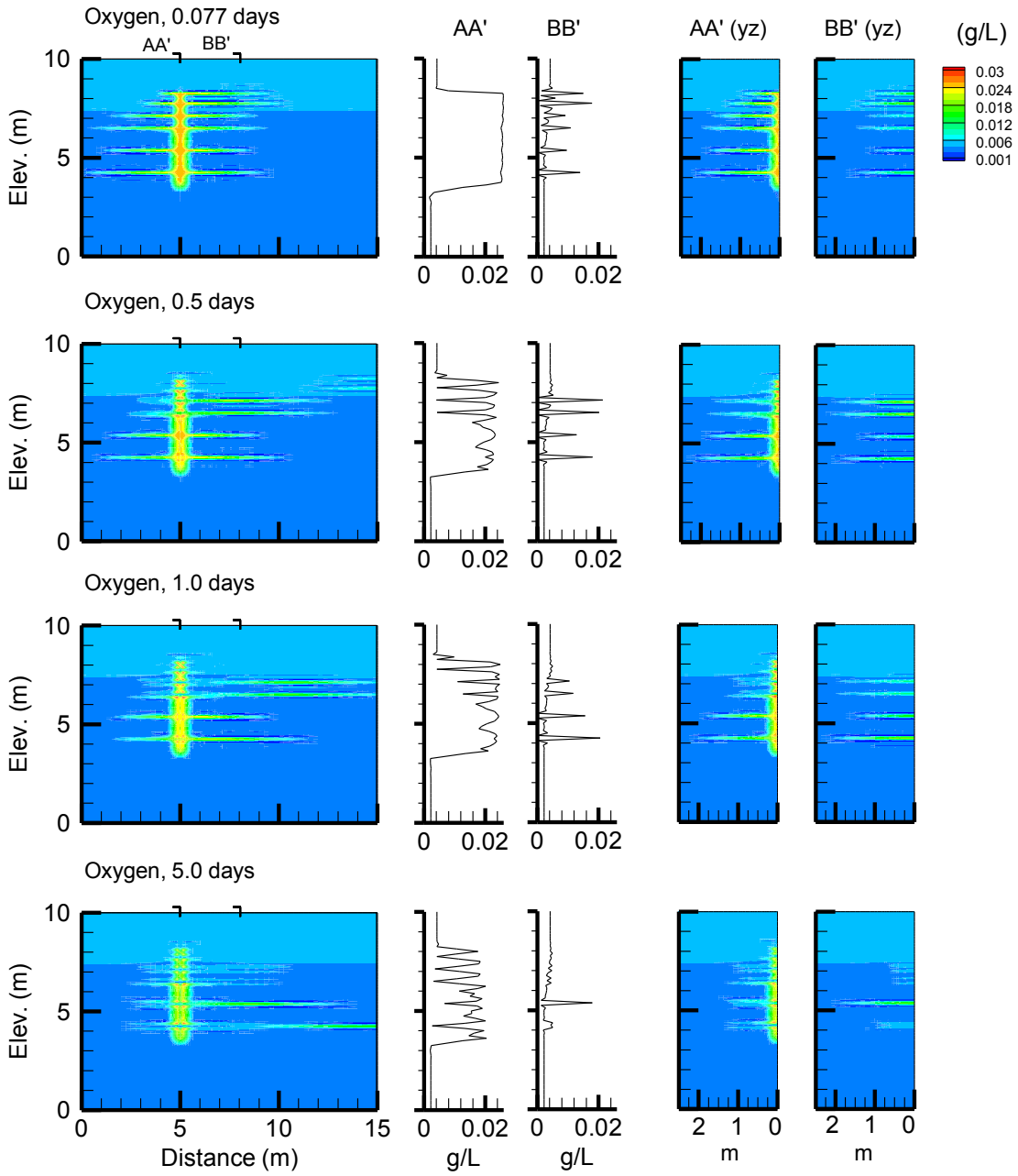

Appendix G- Senario 6a Lower Porosity (0.075)

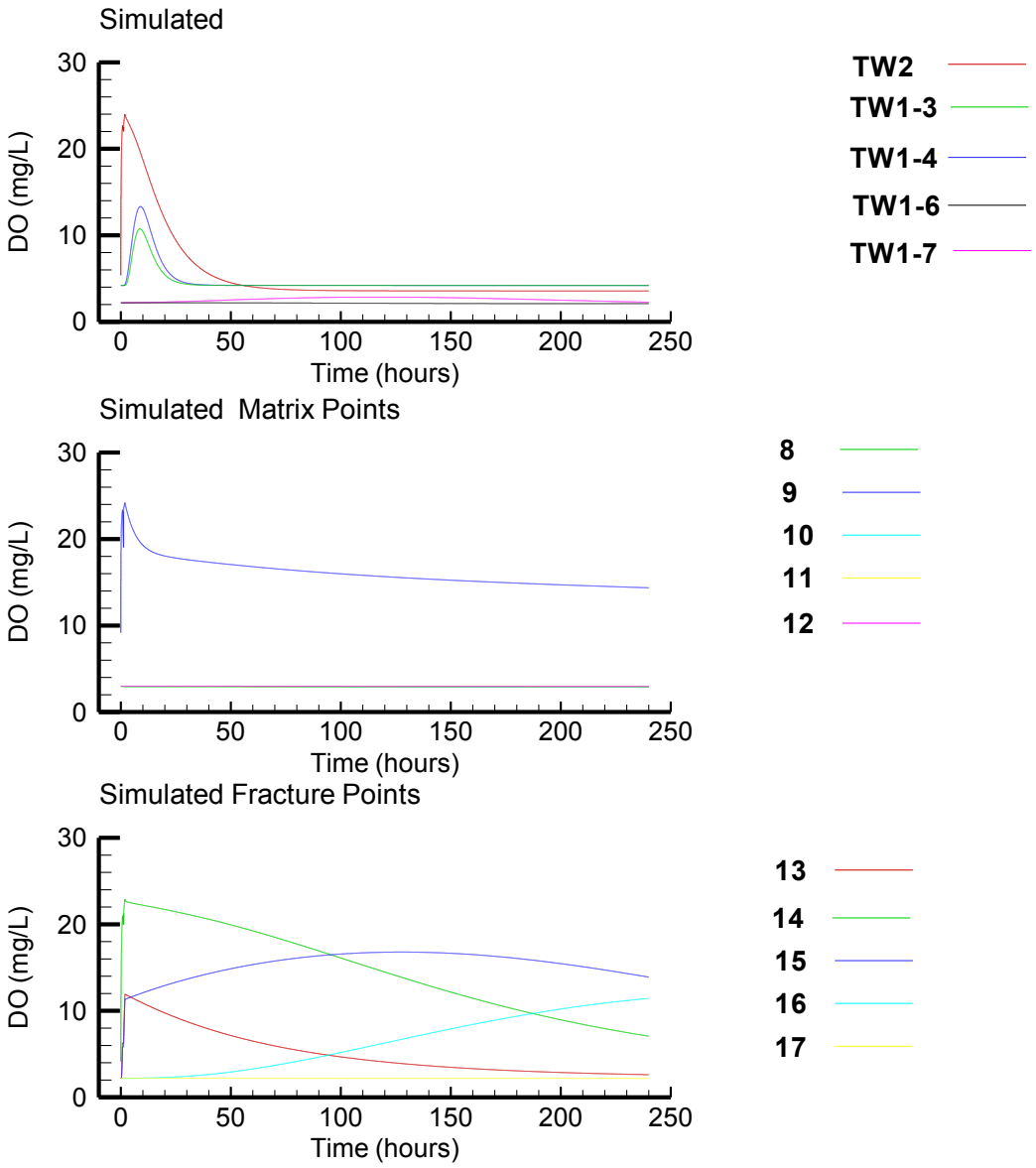

Appendix G- Senario 7b Higher Porosity (0.3)

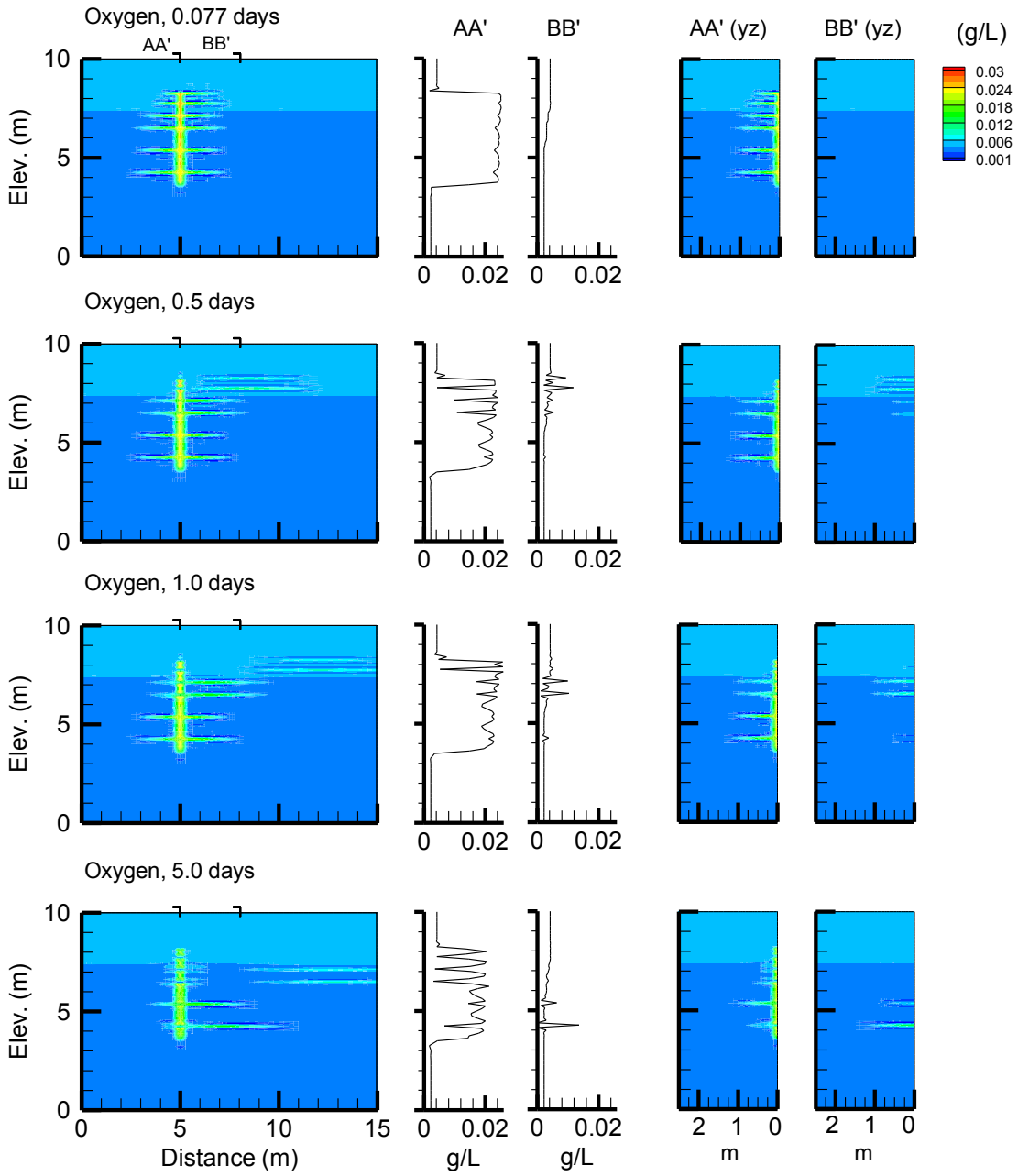

Appendix G- Senario 7b Higher Porosity (0.3)

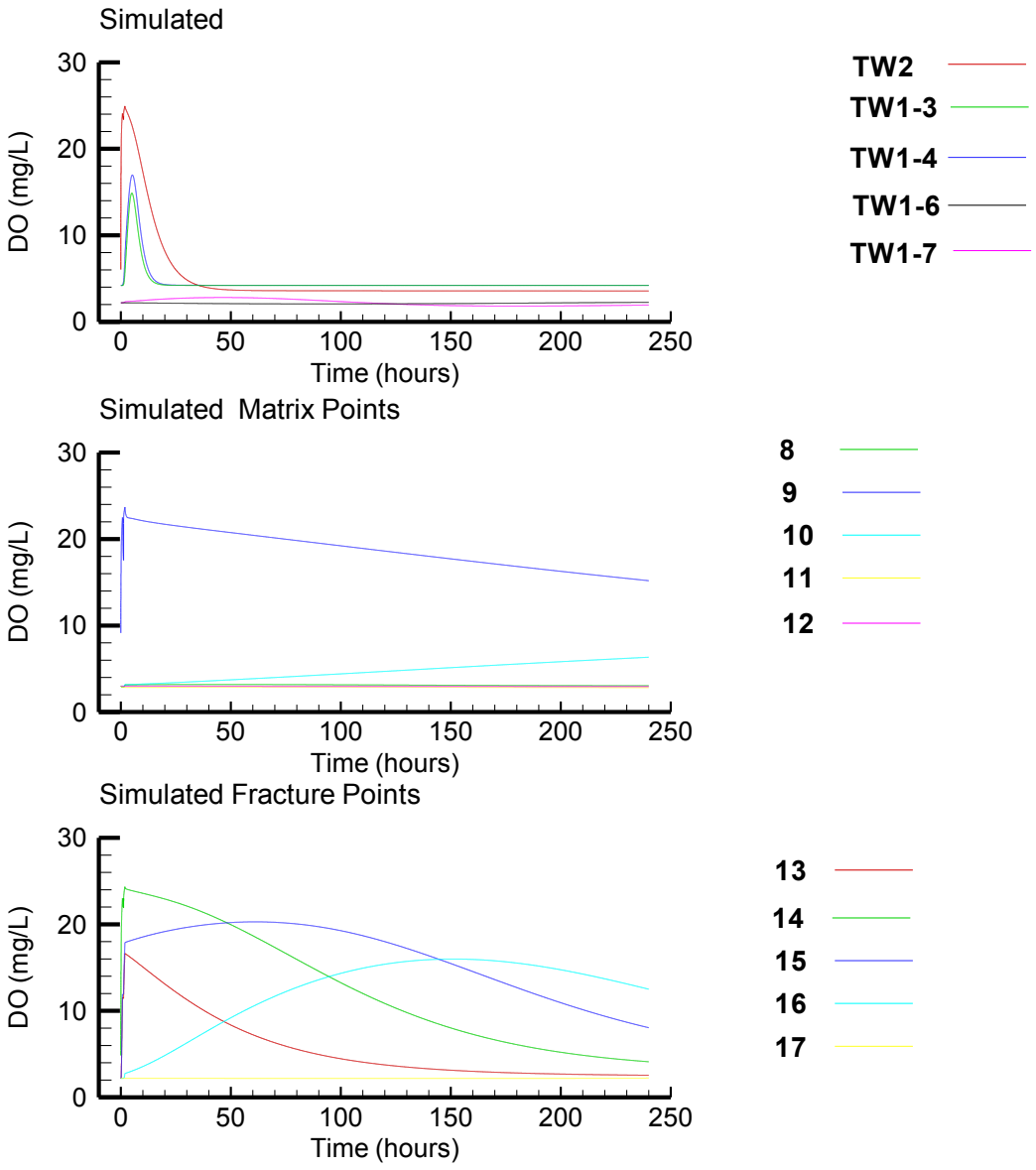

Appendix G- Senario 7a Random Fracrture Set (mean aperture = 50 µm)

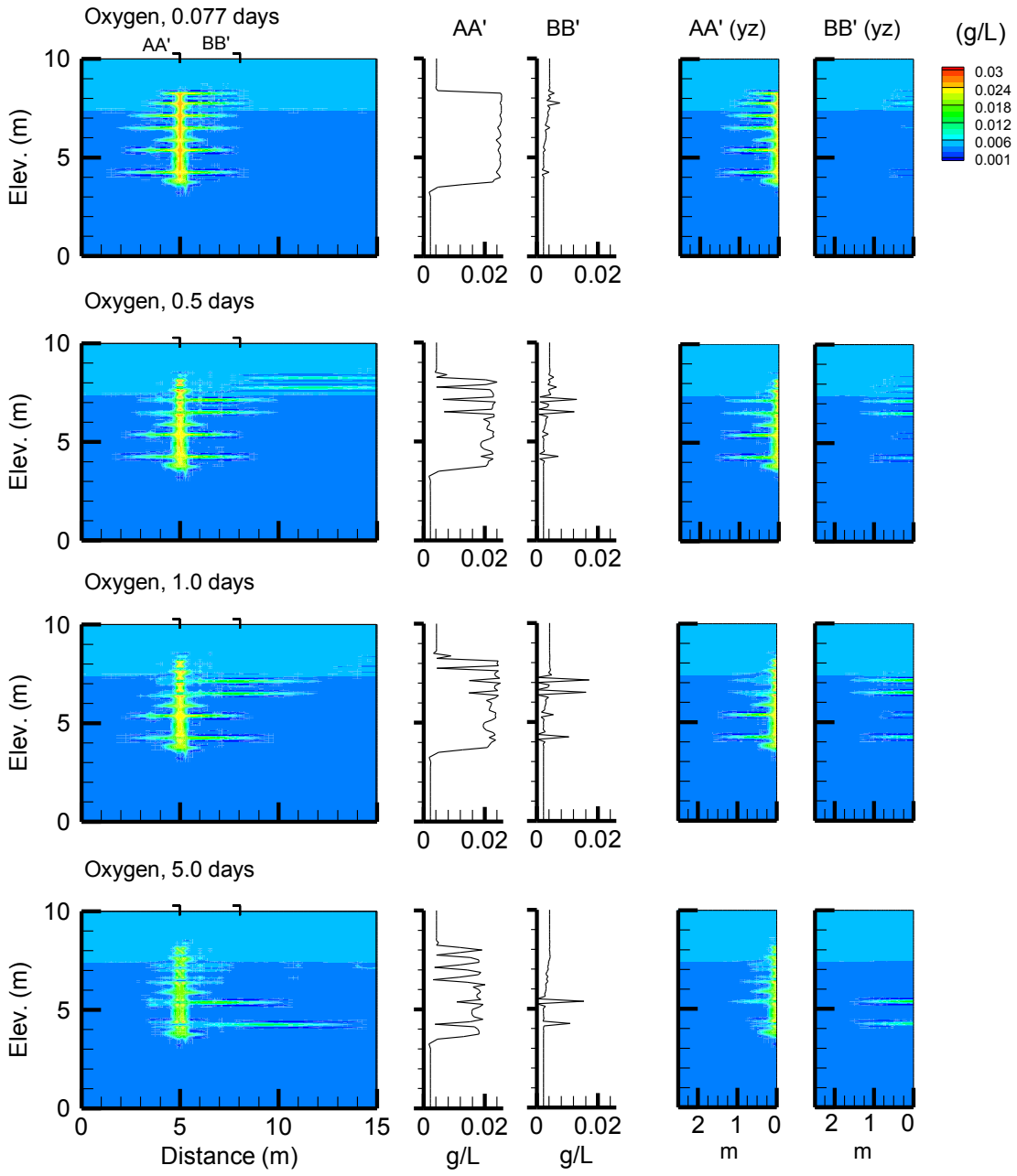

Appendix G- Senario 7a Random Fracrture Set (mean aperture = 50 μm)

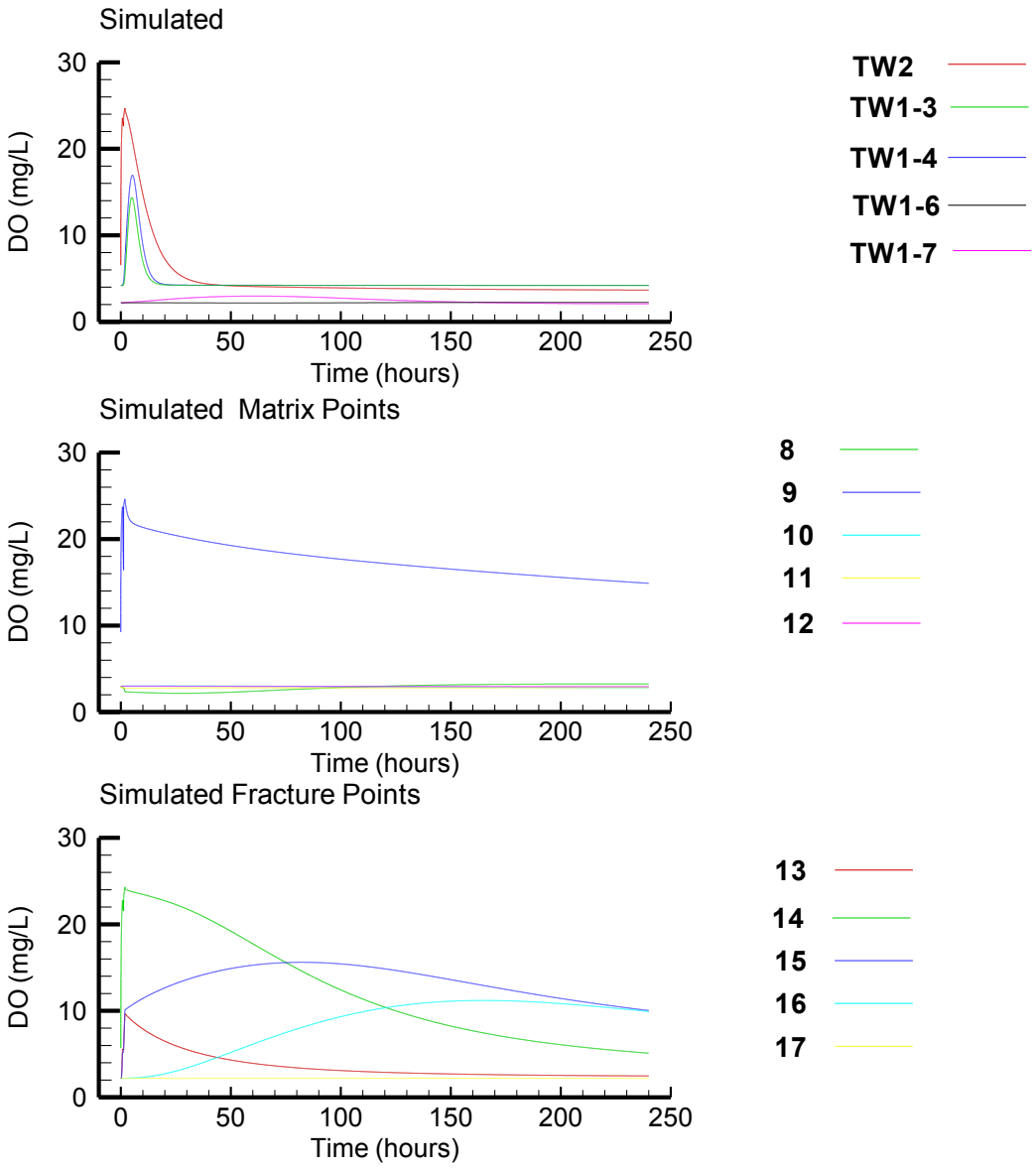

Appendix G- Senario 7b Random Fracrture Set (mean aperture = 100 μm)

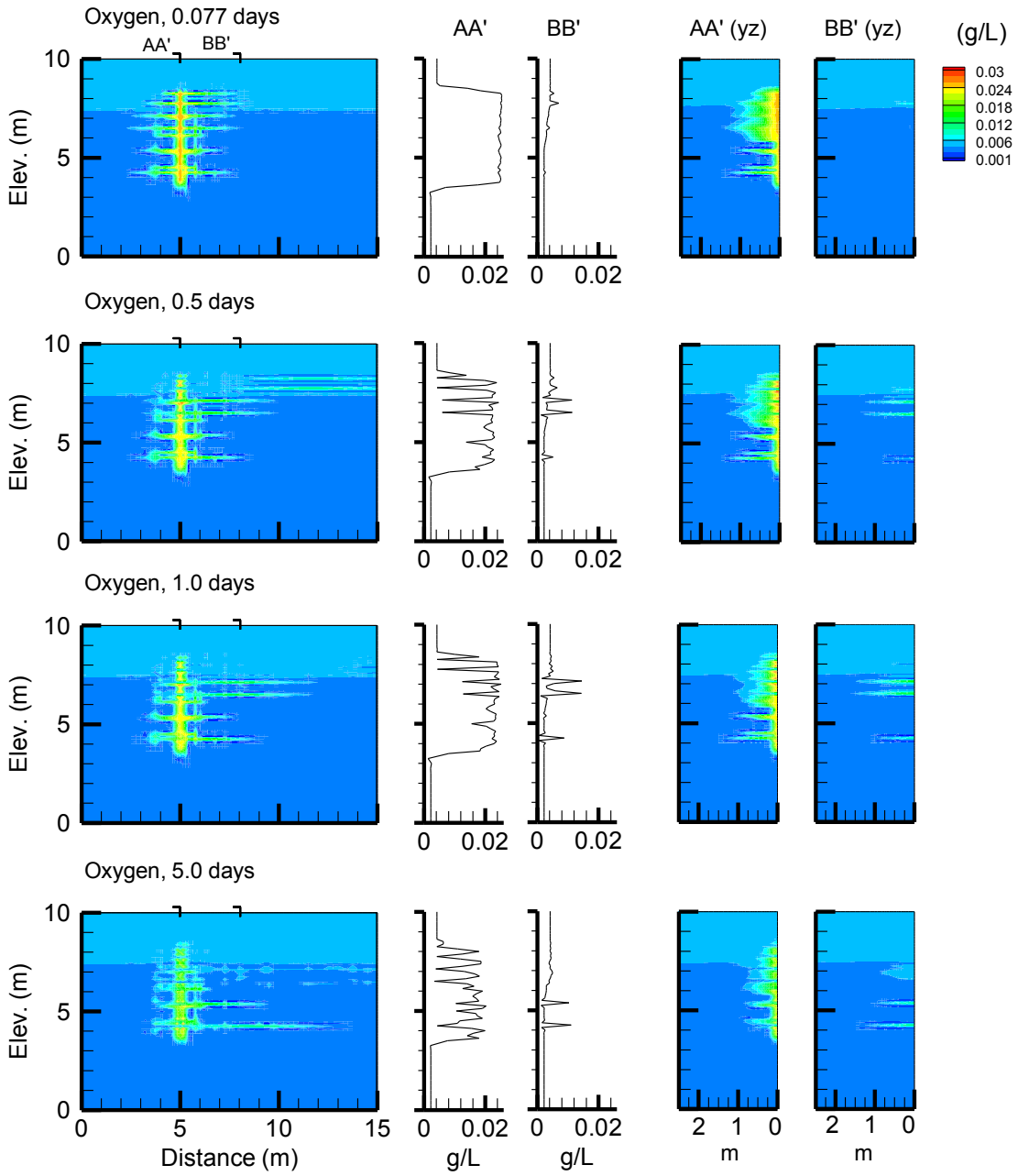

Appendix G- Senario 7b Random Fracrture Set (mean aperture = 100 μm)

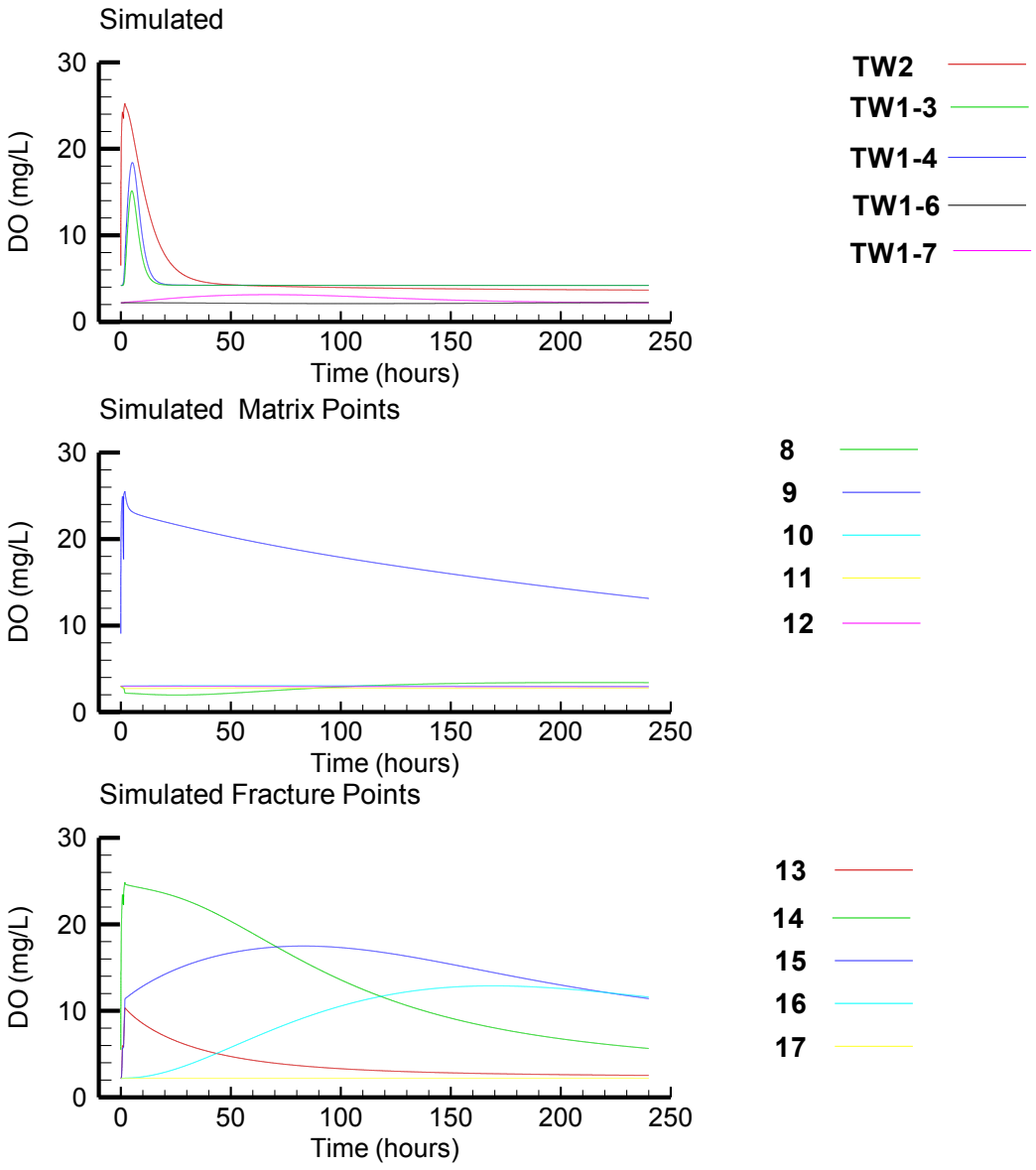

Appendix G- Senario 7c Low hydraulic conductivity (1.0 x 10-8 m/s) and random fracture network (mean aperture = 100 um)

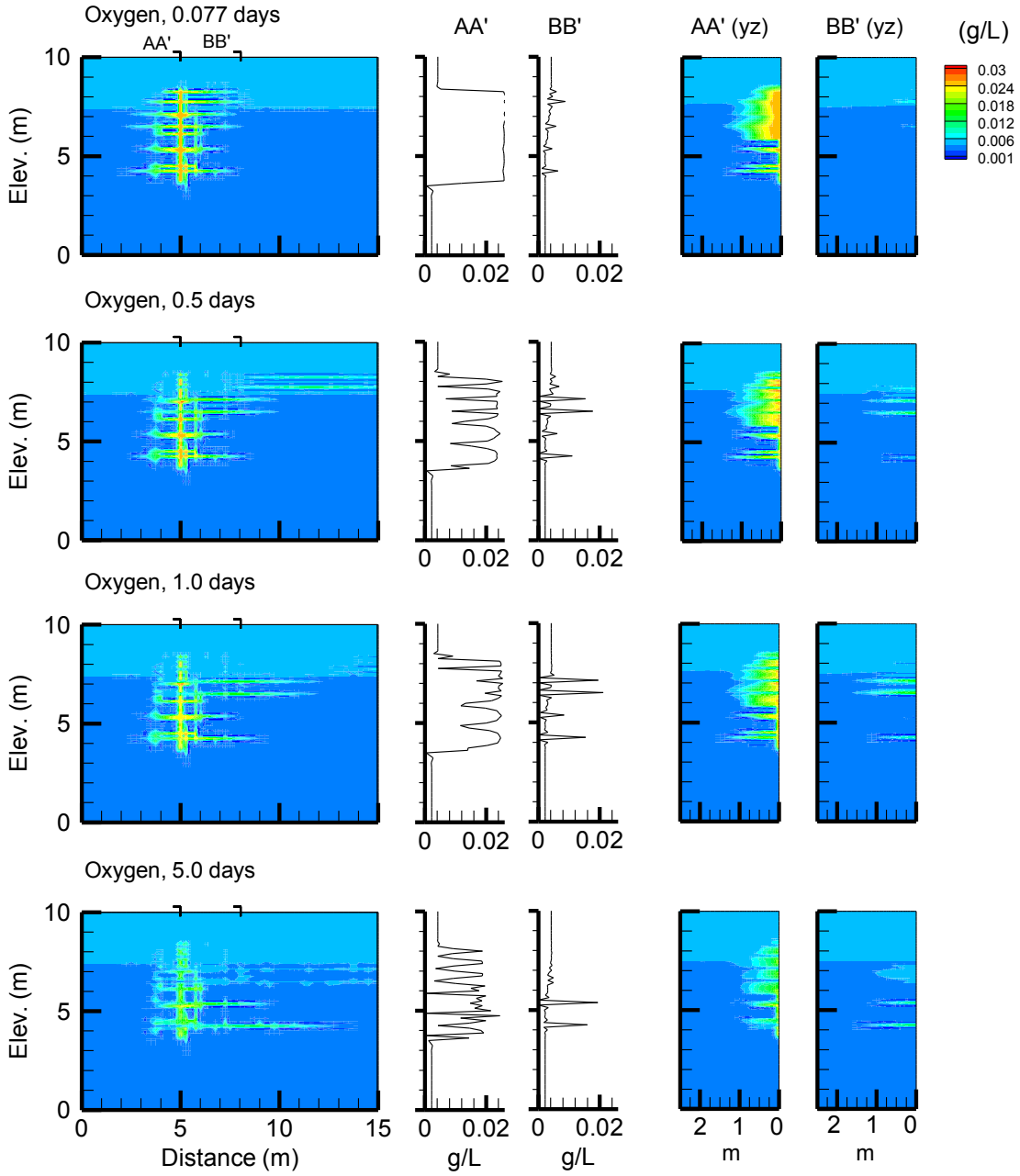

Appendix G- Senario 7c Low hydraulic conductivity (1.0 x 10-8 m/s)
and random fracture network (mean aperture = 100 um)

Appendix H

Simulation Modelling Results

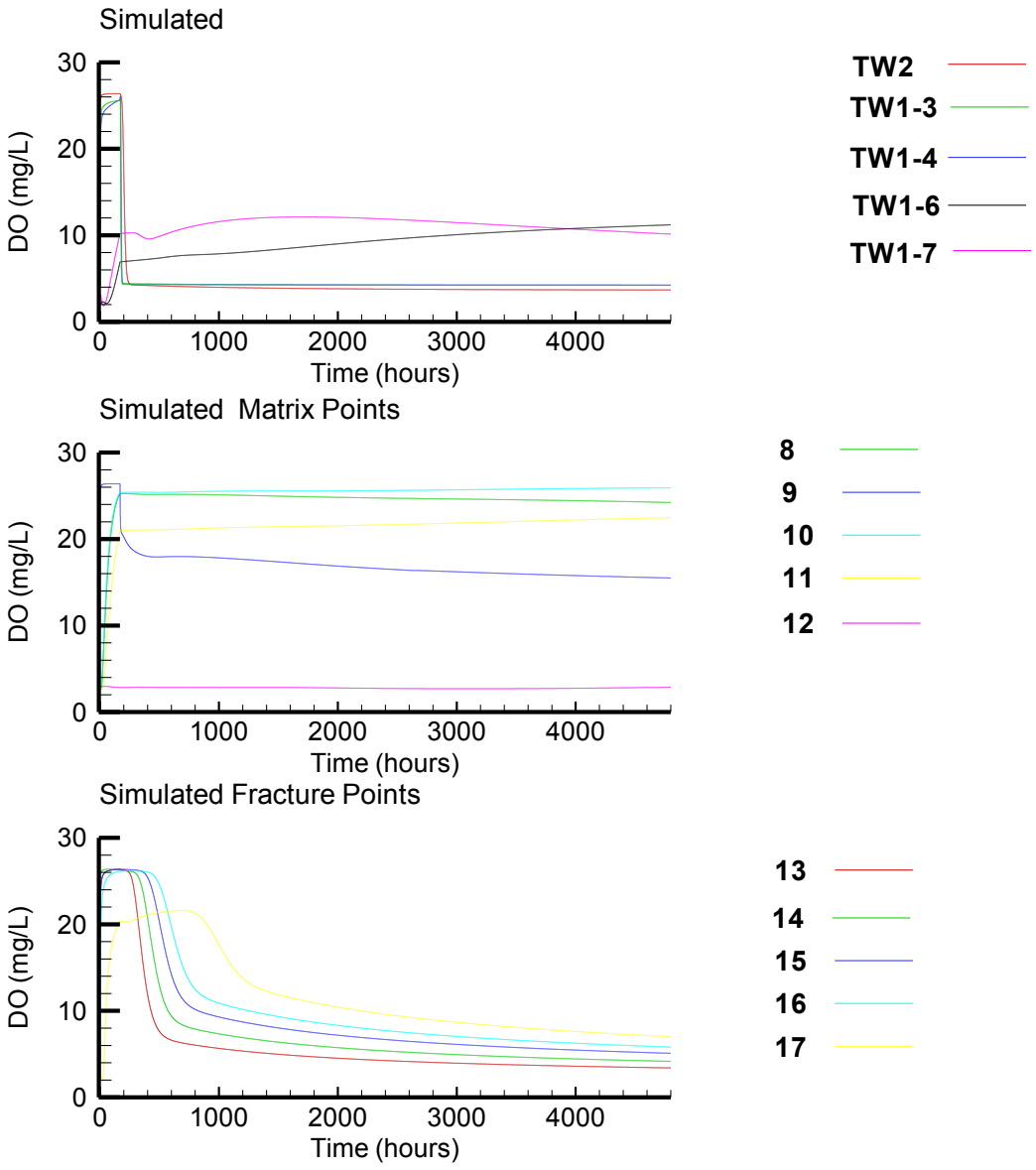

Appendix H - Simulation 1 Continuous Injection

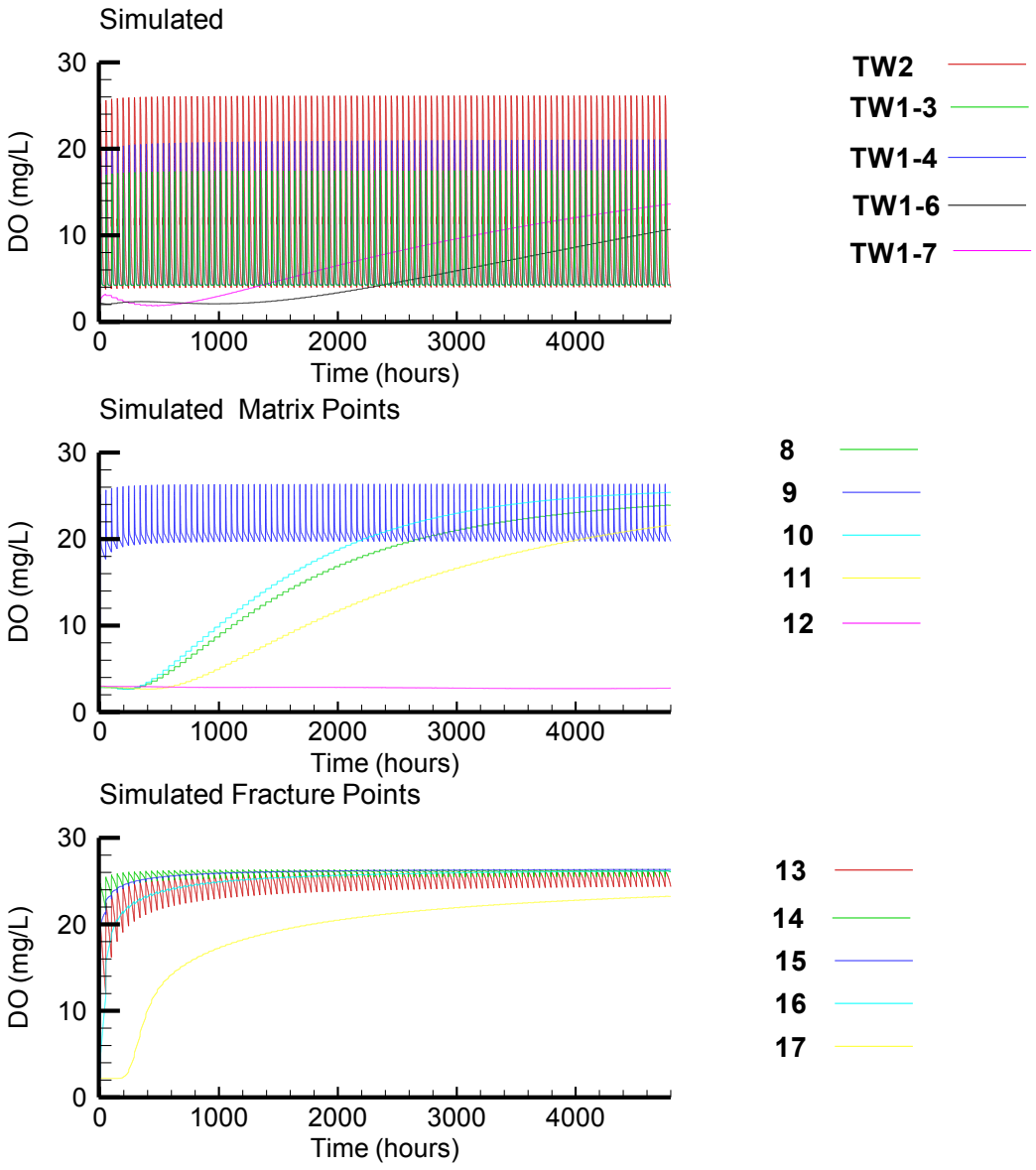

Appendix H - Simulation 2 Cycle Injection